THE UNIVERSITY
of EDINBURGH

Molecular mechanisms of oncolytic properties of Newcastle disease virus (NDV) in human cancer cells

Archana Chandrabhan Jadhav

Submitted for the degree of Doctorate of Philosophy

27th February 2020

I want to dedicate this thesis to my beloved late brother Nitish.

"I felt it shelter to speak to you."
Emily Dickinson

Declaration

I, the author of this thesis, declare that the work generated herein is my own unless stated otherwise. The work or part of the work produced in this thesis has not been submitted for any other degree or professional qualification.

Archana Chandrabhan Jadhav

Abstract

Newcastle disease virus (NDV) is a single-stranded, non-segmented, negative-sense enveloped RNA virus, which belongs to the *Orthoavulavirus* genus of Paramyxoviridae family. It is a well-known, economically important poultry pathogen worldwide. Over the last five decades, NDV is known to have oncolytic properties based on its tumour-selective replication sparing the healthy cells and immunostimulation affirming potential candidate for oncovirotherapy.

In this PhD project, the efficacy of naturally occurring and genetically modified GFP expressing non-pathogenic NDV strains investigated in various human cancer cell lines as an oncolytic virus. This study has demonstrated that the heterogeneous colorectal cancer cell line Caco-2 was the most susceptible to the cytotoxicity induced by avirulent NDV strains amongst the panel of diverse cell lines tested. Despite the high levels of cell cytotoxicity induced by NDV in Caco-2 cells, a small population of surviving cells was isolated from NDV superinfected Caco-2 cells 12 days post infection and named VR Caco-2 cells (virus-resistant Caco-2 cells). The persistent infection with avirulent strains of NDV was demonstrated in VR Caco-2 cells for the first time.

An integrated approach of cellular, transcriptomic, and proteomic data was used to study differences between persistently NDV-infected VR Caco-2 cells,and acutely NDV-infected and uninfected Caco-2 cells. This study has shown that persistent NDV-infection resulted in slower cell proliferation of VR Caco-2 cells than parental Caco-2 cells, and production of recoverable and replicating virus at lower titres. VR Caco-2 cells have demonstrated resistance to NDV re-infection. In contrast, VR Caco-2 cells were susceptible to other viruses such as avian influenza virus (H9N2) and vesicular stomatitis virus (VSV). Persistent NDV infection in VR Caco-2 cells resulted in reduced NDV-induced cytotoxicity, although VR Caco-2 cells were still sensitive to the increased cell cytotoxicity induced by the VSV infection. This would suggest that a combination of oncolytic viruses could be used to overcome the effects of NDV persistent infection.

Potential mechanisms of persistence of NDV in Caco-2 cells were explored. Both Caco-2 and VR Caco-2 cells demonstrated the lack of efficient induction of *IFN-β* and *ISG15* mRNAs, which could be a potential reason for the establishment of NDV persistent infection. RNA-seq data analysis demonstrated extensive regulation of thousands of genes and hundreds of cellular pathways in VR Caco-2 cells while maintaining 50-times lower viral load compared to acute NDV-infection (in Caco-2 cells). Fluctuation in SQSTM1/p62, a multifunctional and multidomain signalling adapter protein required in

selective autophagy, was also demonstrated suggesting the induction of autophagy in NDV-infected Caco-2 cells.

The results generated in this PhD project strongly suggest that NDV not only establishes persistent infection but that too reduces NDV-induced cytotoxicity while regulating thousands of genes in Caco-2 cells. It also suggests the need for detailed investigation of persistent NDV-infection *in vitro* and *in vivo* models of Caco-2 cells before and after developing the NDV as an oncolytic therapeutic vaccine for cancer.

Acknowledgements

I want to acknowledge my supervisors: Prof Venugopal Nair, Prof Lonneke Vervelde, Dr Luca Ferretti, Dr Muhammad Munir and Dr Madhuri Subbiah for their expert advice and endless support throughout the four years of scientific training during this PhD project.

I must also thank The Pirbright Institute (UK) for providing a productive environment to carry out my research, the National Institute of Animal Biotechnology (India) for allowing me to join this project, and The University of Edinburgh (UK) for enabling me to fulfil my dream of pursuing a PhD degree.

I express my sincere thanks to Dr William Mwangi, Dr Manoja Rasamanikkam, Angila Gurung, Dr Joshua Sealy, and the lab members of Avian Oncogenic Viruses group along with many other friends and colleagues at The Pirbright Institute. They shared their vast knowledge and engaged guidance unreservedly with me, as well as their immense support and encouragement, have been critical during my journey. I have been fortunate to work in the company of world-class researchers as my guides and friends, and I am forever grateful for this experience. It enabled me to meet many wonderful people from all walks of life from many different countries who honoured me with their friendship.

I want to express my earnest gratitude to Dr Luca Ferretti (Big Data Institute, Oxford) for providing his expertise in transcriptomic and proteomic data analysis. I am forever grateful for his valuable time spent in our discussions and understanding of my data. I want to thank Prof Chan Ding (Shanghai Veterinary Research Institute, China) for kindly providing us with the RNA-seq data from LaSota or Herts/33 infected chicken embryonic fibroblasts (CEF) cells and chicken tissues.

I cannot thank my family enough; my parents, my brothers Nitish, Mayank, and my grandparents, for their immense support, love, and the confidence, not only during this PhD project but also for raising me into a strong independent woman. Without their help, I wouldn't be able to do this on my own. Thank you so much.

Lastly, I would like to acknowledge the Newton Fund, BBSRC, and The Pirbright Institute for the provision of financial support without which this work would not have been possible.

Table of contents

Author's declaration..... 1
Abstract..... 2
Acknowledgements..... 4
Content of thesis chapters..... 5
List of Figures..... 9
List of Tables..... 13
Abbreviations..... 15
Chapter 1 Introduction..... 21
1.1. General introduction to cancer 21
1.2. Types and stages of cancer 26
1.3. Oncovirotherapy as a cutting-edge treatment for cancer 27
1.4. Commercially approved OVs for cancer treatment 30
1.4.1. Rigvir 30
1.4.2. Oncorine 31
1.4.3. T-VEC (Imlygic™) 32
1.5. Mouse models used in the study of oncovirotherapy 33
1.6. General mechanism of oncolytic viruses 34
1.7. Potential limitations of oncovirotherapy 38
1.8. NDV as an oncolytic virus 39
1.8.1. Introduction to NDV 39
1.8.2. NDV genotypes 41
1.8.3. NDV life cycle 41
1.9. Oncolytic NDV strains 43
1.10. Important oncolytic properties of NDV 44
1.10.1. Tumour selective replication 44
1.10.2. Safety profile 45
1.10.3. Immuno-stimulatory properties 46
1.11. Mechanisms of NDV-induced oncolysis 47
1.11.1. The direct mechanism of NDV-induced oncolysis 47
1.11.2. Indirect mechanism of NDV-induced oncolysis 51
1.12. Genetically modified NDV strains used in oncovirotherapy 55
1.13. Clinical NDV trials 57
1.14. Potential for oncolytic NDV to break resistance to therapy 61
1.15. Projections for NDV as oncolytic viruses 62
1.15.1. Improving tumour-specific targeting and systemic delivery 63
1.15.2. Enhancement of NDV-mediated immunomodulation and bypassing NDV neutralising immune responses 65
1.16. Aims and objectives of the thesis 67

Chapter 2 Materials and Methods..... 68
2.1. Materials 68
2.1.1. Cells 68
2.1.2. Viruses 69
2.1.3. Primers 70
2.1.3.1. Amplification primers 70
2.1.3.2. Cloning primers 70

2.1.3.3. NDV cDNA synthesis, amplification, and sequencing primers 71
2.1.3.4. SYBR Green qRT-PCR primers 73
2.1.3.5. TaqMan qRT-PCR probe and primers 73
2.1.4. Antibodies 74
2.1.4.1. Primary antibodies 74
2.1.4.2. Secondary antibodies 74
2.1.5. Media and Buffers 75
2.1.5.1. Media and solutions 75
2.1.5.2. Buffers 77
2.5.1.3. Commonly used reagents 78
2.2. Methods 78
2.2.1. Cell culture techniques 78
2.2.1.1. Culturing, passaging, and storage of adherent cells 78
2.2.1.2. Cell counting and cell seeding in culture vessels 79
2.2.1.3. Transfection 79
2.2.1.4. Cell viability and cell toxicity assay 81
2.2.1.5. Caspase-3/7 activity assay 83
2.2.1.6. Luciferase assay 83
2.2.1.7. Cell proliferation assay 84
2.2.1.8. Indirect immunofluorescence (IF) assay 84
2.2.1.9. siRNA mediated to knockdown 85
2.2.1.10. CRISPR/Cas9 Knockout (KO) 86
2.2.2. Virology techniques 87
2.2.2.1. Propagation of virus 87
2.2.2.2. Confirmation of virus by hemagglutination (HA) assay 88
2.2.2.3. Receptor binding avidity assay 88
2.2.2.4. Virus infection 90
2.2.2.5. Virus titration using plaque assay 90
2.2.2.6. Multiplicity of infection (MOI) calculation 91
2.2.2.7. Use of flow cytometry to quantify virus infection 92
2.2.3. Molecular techniques 92
2.2.3.1. DNA Extraction 92
2.2.3.2. Polymerase chain reaction (PCR) amplification 92
2.2.3.3. Agarose gel electrophoresis 93
2.2.3.4. PCR product purification and Gel extraction 93
2.2.3.5. Gene cloning 93
2.2.3.5.1. Restriction digestion 93
2.2.3.5.2. T4-DNA ligation 94
2.2.3.5.3. E. coli transformation 94
2.2.3.5.4. Plasmid DNA screening 95
2.2.3.6. Large-scale plasmid DNA preparation 95
2.2.3.7. Plasmid DNA and PCR product sequencing 96
2.2.3.8. RNA Extraction 96
2.2.3.8.1. Total RNA Extraction 96
2.2.3.8.2. MicroRNA extraction 97
2.2.3.8.3. RNA Quantification 97
2.2.3.8.4. DNase Treatment 97
2.2.3.8.5. cDNA synthesis 98

2.2.3.9. Quantitative real-time (qRT)-PCR 98
2.2.3.9.1. One-step SYBR Green qRT-PCR 98
2.2.3.9.2. TaqMan qRT-PCR 99
2.2.3.10. Protein analysis 101
2.2.4. Sample preparation for RNA-seq analysis 102
2.2.5. Sample preparation for Mass spectrometry analysis 102
2.2.6. RNA-seq data analysis 105
2.2.7. Statistical analysis 105

Chapter 3 Establishment of a model system to study oncolytic properties of lentogenic strains of Newcastle disease virus (NDV)…… 106
3.1. Introduction 106
3.1.1. Chapter objectives 107
3.2. Results 107
3.2.1. Cell line screening for *in vitro* NDV-induced oncolysis study 107
3.2.2. Caco-2 cells response to different lentogenic strains of NDV 110
3.2.3. Isolation of NDV-resistant VR Caco-2 cells 112
3.2.4. Characterisation of VR Caco-2 cells 114
3.2.5. NDV re-infection study in VR Caco-2 cells 121
3.2.6. Confirmation of NDV-specific resistance in VR Caco-2 cells 123
3.2.7. IFN-β induction study in Caco-2 cells 126
3.2.8. Role of miR-155 in VR Caco-2 cells 128
3.3. Discussion 129

Chapter 4 An integrated analysis of persistently NDV-infected VR Caco-2 cells using transcriptomic and proteomic approaches…… 133
4.1. Introduction 133
4.1.1. Chapter objectives 134
4.2. Results 134
4.2.1. RNA-seq datasets 134
4.2.2. Transcriptomics Data Analysis 135
4.2.3. Comparative transcriptomics and proteomics data analysis 151
4.2.4. Comparative data analysis 155
4.2.4.1. NDV and Coxsackievirus infection in Caco-2 cells 155
4.2.4.2. NDV infection in Caco-2 and CEF cells 158
4.3. Discussion 165

Chapter 5 Newcastle disease virus (NDV)-mediated p62/SQSTM1 degradation……... 169
5.1. Introduction 169
5.1.1. Chapter objectives 173
5.2. Results 173
5.2.1. Confirmation of mitophagy in Caco-2 cells 173
5.2.2. p62/SQSTM1 degradation study using the IF assay 174

5.2.3. Time-course study of p62/SQSTM1 degradation in Caco-2 cells using IF and western blot assay 175
5.2.4. Investigation of each NDV protein in p62/SQSTM1 degradation 178
5.2.5. CRISPR/Cas9 based p62/SQSTM1 Knockout approach in HEK-293 cells 180
5.3. Discussion 185

Chapter 6 Genomic diversity and evolution of quasi-species in Newcastle Disease Virus (NDV) infections…… 188
6.1. Introduction 188
6.1.1. Chapter objectives 190
6.2. Results 191
6.2.1. Genetic diversity 191
6.2.2. The frequency spectrum of mutations of NDV cultured in Caco-2 and CEF cells 195
6.2.3. Selection on polymorphisms in coding sequences 197
6.2.4. Comparison between phylogenetic divergence and within-sample polymorphisms divergence between different NDV sequences from the same genotype 199
6.3. Conclusion 203

Chapter 7 General Discussion…….. 205
Chapter 8 Appendix…… 210
References…….. 229

List of Figures

Sr. No.	Figure name	Page No.
Figure 1.1.	Dagram illustrating cell cycle regulation.	22
Figure 1.2.	The principal hallmarks, which characterise the malignancy of abnormal neoplastic cells.	24
Figure 1.3.	The mechanisms of action of oncolytic viruses.	36
Figure 1.4.	Schematic diagram of NDV structure and its genomic make-up.	40
Figure 1.5.	Schematic representation of NDV replication.	42
Figure 1.6.	An illustration of apoptotic signalling pathways.	48
Figure 1.7.	An illustration of the oncolytic mechanisms of action of NDV.	53
Figure 2.1.	The schematic representation of the NDV genome fragmentation for Sanger sequencing.	71
Figure 2.2.	Viable cells metabolically convert resazurin to resorufin.	82
Figure 2.3.	The strategy of lentiviral vector-based CRISPR/Cas9 KO of SQSTM1.	87
Figure 2.4.	Standard curve of miR-223-3p mimic microRNA used for absolute quantification of miR-155 in all cells used in the assay.	100
Figure 3.1.	Time and NDV dose-dependent CellTiter-Blue® Cell Viability Assay in different human cancer cells.	109
Figure 3.2.	Time and NDV dose-dependent CellTiter-Blue® Cell Viability Assay in Caco-2 cells infected with different avirulent NDV strains.	110
Figure 3.3.	Tumour selective NDV replication in Caco-2 cells.	112
Figure 3.4.	Schematic representation of Virus Resistant Caco-2 cells isolation from B1-GFP infected Caco-2 cells.	113
Figure 3.5.	Loss of GFP expression in VR Caco-2 cells.	114
Figure 3.6.	Confirmation of persistent NDV infection in VR Caco-2 cells using IF and qRT-PCR assays.	115
Figure 3.7.	Confirmation of persistent NDV infection in VR Caco-2 cells using HA and plaque assays.	117
Figure 3.8.	Analysis of NDV-HN protein.	118
Figure 3.9.	Cell proliferation assay.	120
Figure 3.10.	Microscopic observation of Caco-2 and VR Caco-2 cells.	121

Figure 3.11.	Resistance to NDV re-infection demonstrated in VR Caco-2 cells.	122
Figure 3.12.	VR Caco-2 cells showed susceptibility to H9N2, and VSV infections only	123
Figure 3.13.	Validation of NDV-specific resistance in VR Caco-2 cells	124
Figure 3.14.	VSV replication and cell death assay in VR Caco-2 cells	125
Figure 3.15.	Inefficient IFN-β induction in Caco-2 cells and VR Caco-2 cells	127
Figure 3.16.	miR-155 expression and NF-kB activity in Caco-2 cells	129
Figure 4.1.	Scatter plots representing the gene expression profile in Caco-2 cells across different conditions.	136
Figure 4.2.	The relative account of differential genes expression in pairwise comparisons across all conditions in Caco-2 cells.	138
Figure 4.3.	Venn diagram summarising distribution pattern of differentially expressed genes (DEGs).	144
Figure 4.4.	Quantile-quantile distribution of log2-fold changes across different pairwise conditions.	145
Figure 4.5.	Cluster analysis of gene expression profiles.	147
Figure 4.6.	Dynamic classification of the functional profile of GOs (gene ontologies) and pathways in differentially regulated pathways in uninfected, acutely, and persistently NDV-infected Caco-2 cells.	149
Figure 4.7.	Clustering of the time profile of pathways from the Ingenuity Pathway Analysis (IPA).	151
Figure 4.8.	Quantile-quantile distribution of fold changes in mRNA abundance (RNA-seq) and protein abundance between VRCaco-2 and uninfected Caco-2 cells.	152
Figure 4.9.	Comparison of pathways/GOs detected by proteomics and RNA-seq in persistently NDV-infection VR Caco-2 cells compared to the uninfected Caco-2 cells.	153
Figure 4.10.	Quantile-quantile distribution of log2-fold changes between infected and uninfected Caco-2 cells.	156
Figure 4.11.	Comparative analysis of RNA-seq data from NDV-infected, persistently NDV-infected VR Caco-2 and uninfected Caco-2 cells with CVB-infected or uninfected Caco-2 cells grown in 2D and 3D cultures.	158
Figure 4.12.	Comparative analysis of the effects of NDV infection in Caco-2, VR Caco-2, and CEF cells.	160
Figure 4.13.	Expression analysis of NDV genes and P mRNA editing in infected Caco-2, VR Caco-2, and CEF cells.	162
Figure 4.14.	Assessment of acute NDV infection in Caco-2 and CEF cells.	163
Figure 5.1.	Schematic representation of the autophagic process.	169
Figure 5.2.	Cellular mechanism of p62/SQSTM1.	171
Figure 5.3.	Confirmation of NDV-induced mitophagy in Caco-2 cells.	174

Figure 5.4.	NDV-induced p62/SQSTM1 degradation in Caco-2 cells.	175
Figure 5.5.	Time-course study for p62/SQSTM1 degradation in NDV-infected Caco-2 cells using indirect immunofluorescence (IF) assay.	176
Figure 5.6.	Time-course study for P62/SQSTM1 degradation in NDV-infected Caco-2 cells using western blotting.	177
Figure 5.7.	The investigation of the role of individual NDV protein in p62/SQSTM1 degradation.	178
Figure 5.8.	Prediction of signal peptide cleavge site in fusion protein sequence of NDV B1 strain.	179
Figure 5.9.	p62/SQSTM1 siRNA silencing in Caco-2 cells.	181
Figure 5.10.	The strategy of lentiviral vector-based CRISPR/Cas9 KO of SQSTM1 in Caco-2 and HEK-293 cells.	183
Figure 5.11.	Identification of p62/SQSTM1 protein KO in Caco-2 and HEK-293 cells.	184
Figure 5.12.	Confirmation of p62/SQSTM1 protein KO in HEK-293 cells.	184
Figure 6.1.	Read depth per position along the NDV genome.	192
Figure 6.2.	Diversity measurements per base across different samples.	193
Figure 6.3.	Local SNP density estimation along the NDV genome across all samples.	194
Figure 6.4.	Measures of nucleotide diversity along the NDV genome across all the samples.	194
Figure 6.5.	Mutation site frequency spectrum for SNPs across all samples.	196
Figure 6.6.	Tajima's D (a measure of the relative abundance of common versus rare alleles) across all samples.	197
Figure 6.7.	Location, frequency and classification of all SNPs across all samples.	198
Figure 6.8.	Measures of selection related to comparison of nonsynonymous to synonymous variants ratio.	199
Figure 6.9.	Neighbour-joining tree of avirulent NDV strains (genotype II, including LaSota and B1) and highly pathogenic strains (genotype IV, including Herts/33) used for the estimates of within-genotype divergence.	200
Figure 6.10.	Comparison between patterns of divergence (scale on the left) and polymorphisms (nucleotide diversity, right) along the NDV genome for all samples in genotype II.	201
Figure 6.11.	Comparison between patterns of divergence (scale on the left) and polymorphisms (nucleotide diversity, right) along the NDV genome for all samples in genotype IV.	201
Figure 6.12.	The ratio between polymorphisms (pairwise nucleotide diversity) or divergence estimated across the 1st and 2nd base of each codon versus the same quantities estimated for the 3rd base.	202

Figure 8.1. The sets and subsets of highly overexpressed proteins in VR Caco-2 cells. 211

Figure 8.2. The sets and subsets of highly underexpressed proteins in VR Caco-2 cells. 212

List of Tables

Sr. No.	Table Name	Page No.
Table 1.1	TNM based cancer categorisation	27
Table 1.2	List of oncolytic viruses	29
Table 1.3	Recently completed combinational oncovirotherapy list	33
Table 1.4	Summary of NDV-induced cell death in different cell lines	51
Table 1.5	Summary of NDV clinical trials	60
Table 2.1	List of cells/cell lines used in this study	68
Table 2.2	List of viruses used in this study	69
Table 2.3	p62/SQSTM1 primer used to study CRISPR/Cas9 Knockout	70
Table 2.4	List of cloning primers used in this study	70
Table 2.5	List of primers used for NDV cDNA synthesis and PCR amplification	71
Table 2.6	List of sequencing primers used to sequence NDV fragment	71
Table 2.7	List of SYBR-Green qRT-PCR primers used in this study	73
Table 2.8	TaqMan primers and probes used in this study	73
Table 2.9	List of primary antibodies used in this study	74
Table 2.10	List of secondary antibodies used in this study	74
Table 2.11	List of media and solutions used in this study	75
Table 2.12	List of buffers used in this study	77
Table 2.13	List of common reagents used in this study	78
Table 2.14	List of plasmids used in this study	80
Table 2.15	siRNA transfection mixture preparation	85
Table 2.16	Two-fold dilutions α2-3,6,8 Neuraminidase enzyme in PBSa	89
Table 2.17	α2-3,6,8 Neuraminidase enzyme in units used for cRBCs treatment	89

Table 2.18	MicroRNA-specific cDNA synthesis reaction mixture	100
Table 2.19	Sample TMT Labels	103
Table 3.1	PFU/ml count in different passages of VR Caco-2 cell supernatant	116
Table 4.1	Number of reads from Caco-2 cells (with or without NDV) and VR Caco-2 cells RNA-seq data	135
Table 4.2	Number of reads from RNA-seq samples from two different projects	135
Table 4.3	Number of DEGs across all conditions in Caco-2 cells	136
Table 4.4	Most relevant under or overexpressed genes in acutely NDV-infected Caco-2 cells in comparison with uninfected Caco-2 cells	139
Table 4.5	Most relevant under or overexpressed genes in persistently NDV-infected VR Caco-2 cells in comparison with uninfected Caco-2 cells	140
Table 4.6	Most relevant under or overexpressed genes in persistently NDV-infected VR Caco-2 cells in comparison with acutely NDV-infected Caco-2 cells	141
Table 4.7	Summary of Biological processes regulated in VR Caco-2 cells compared to Caco-2 cells from a relative account of proteomics and transcriptomics data	154
Table 4.8	Reactome pathway analysis of VR Caco-2 cells compared to Caco-2 cells from a relative account of proteomics and transcriptomics data	154
Table 4.9	Biological processes commonly shared by NDV-infected Caco-2 and CEF cells	164
Table 4.10	Reactome pathways commonly shared by NDV-infected Caco-2 and CEF cells	164
Table 6.1	Number of reads of different samples generated from two different deep sequencing projects	190
Table 8.1	List of significantly underexpressed or overexpressed proteins in VR Caco-2 cells in comparison with uninfected Caco-2 cells	213

Abbreviations

2D	2-Dimensional
3D	3-Dimensional
5-FU	5-fluorouracil
Ad	Adenoviruses
ADA	Adenosine deaminase
AIV	Avian influenza virus
ALB	Albumin
APCs	Antigen-presenting cells
aPKC	Atypical protein kinase C
APMV-1	Avian paramyxovirus type-1
APOA1	Apolipoprotein A1
ARE	AU-rich elements
ATV-NDV	Autologous tumour vaccine with NDV
BC	Beaudette C
BH-3	Bcl-2 homology-3
BHK	Baby Hamster Kidney fibroblasts
BID	BH3-interacting domain death agonist
BUGT	Bilirubin-UDP-glucuronosyltransferase
C3	Complement component 3
CAM	Cell adhesion molecules
CASP1	Caspase-1/Interleukin-1 converting enzyme (ICE)
CCCP	Carbonyl cyanide m-chlorophenyl hydrazone
CDC42	Cell division control protein 42
CDK	Cyclin-dependent kinase
cDNA	Complementary DNA
CEF	Chicken embryo fibroblast
CHK	Checkpoint serine/threonine kinase
CMV	Cytomegalovirus
COX VIII	Cytochrome c oxidase VIII
cRBCs	Chicken red blood cells
CT	Chemotherapy
CTLA-4	Cytotoxic T Lymphocyte antigen 4
CTLs	cytotoxic T lymphocytes
CVB	Coxsackievirus B
Cyt-c	Cytochrome-c
DAF	Decay accelerating factor
DAMPs	Damage-associated molecular patterns
DDR	DNA damage response
DDX60	DExD/H-Box Helicase 60
DE	Differential expression
DEGs	Differentially expressed genes
DMEM	Dulbecco’s modified eagle's medium
DMSO	Dimethyl sulfoxide
dpi	Days post-infection
DS	Dermatan sulfate
DSBs	Double-stranded breaks
DTH	Delayed-type hypersensitivity

DTT	Dithiothreitol
DVGs	Defective viral genomes
ECHO-7	Enteric Cytopathogenic Human Orphan type 7
ED-B	Extradomain B
EGFP	Enhanced green fluorescent
EGFR	Epidermal growth factor receptor
EID50	50 percent Embryo Infectious Dose
eIF2	Eukaryotic Initiation Factor 2
ELAM-1	Endothelial cell-leukocyte adhesion molecule 1
eNOS	Endothelial NOS
EPN3	Epsin 3
ER	Endoplasmic reticulum
ERK1/2	Extracellular signal-regulated kinases 1/2
F	Fusion protein
FADD	Fas-associated death domain
FBS	Foetal bovine serum
FDR	False-discovery rate
FGF1/2	Fibroblast growth factors 1/2
Fv	Variable fragment
G0	Gap 0 phase
G1	Gap 1 phase
G2	Gap 2 phase
GABARAP	Gamma-aminobutyrate receptor-associated protein
GBM	Glioblastoma multiforme
GE	Gene end
GFP	Green fluorescent protein
GM-CSF	Granulocyte-macrophage colony-stimulating factor
GMP	Good Manufacturing Procedure
GO	Gene Ontology
gRNA	guide-RNA
GS	Gene start
h	hour/hours
HA	Hemagglutination assay
HAU	Hemagglutinating unit
HCC	Hepatocellular carcinoma
HCV	Hepatitis C virus
HEK-293	Human embryonic kidney cells-293
HIF	Hypoxia-inducible factor
HIF-α	hypoxia-inducible factor-alpha
HMGB1	High-mobility group box 1
HMW	High molecular weight
HN	Haemagglutinin-neuraminidase protein
HNSCC	Head and neck squamous cell carcinoma
hpi	Hours post-infection
HSPs	Heat-shock proteins
HSV-1	HSV-1
hTERT	Human telomerase reverse transcriptase
HTLV-1	Human T-cell lymphotropic virus 1
HuR	Human antigen R

HVEM	Herpesvirus entry mediator
IAP	Inhibitor of apoptosis
IARC	International Agency for Research on Cancer
IAV	Influenza A virus
ICAM-1	Intercellular adhesion molecule-1
ICD	immunogenic cell death
ICIs	Immune checkpoint inhibitors
ICP	Infectious cell protein
IF	Indirect immunofluorescence
IFIT1	Interferon-induced protein with tetratricopeptide repeats 1
IFNs	Interferons
IFN-β	Interferon beta
IGS	Intergenic sequence
IL-1	Interleukin-1
IL-12	Interleukin-12
IL-15	Interleukin 15
IL-17A	Interleukin-17A
indels	insertions/deletions
iNOS	Inducible nitrous oxide synthase
IP	Intraperitoneal
IP-10	IFN-γ-inducible protein-10
IPA	Ingenuity Pathway Analysis
IRF	IFN-regulated factors
IRF3	IFN regulatory factor-3
IRF7	IFN regulatory factor-7
ISG12a	IFN-stimulated gene (ISG) 12a
ISG15	Interferon-stimulated gene 15
ISGs	IFN-stimulated genes
IT	Intratumoral
IV	Intravenous
JAK-STAT	Janus kinase–signal transducer and activator of transcription
JNKs	Jun amino-terminal kinases
K63	Lysine 63
KO	Knock-out
KRT17	Keratin 17
L	Large RNA-dependent RNA polymerase
L1CAM	L1 Cell Adhesion Molecule
Lag-3	Lymphocyte activation gene-3
LAS	Leica application suite
LB	Luria Broth
LC3	Microtubule-associated protein 1 light chain 3
LFCs	Log2 fold changes
LGP2	Laboratory of Genetics and Physiology 2
LHT	Local hyperthermia
LIR	LC3 interacting region
LN	Lymph node
LPS	Lipopolysaccharide
LXR	Liver X receptors
M	Matrix protein

mAbs	Monoclonal antibodies
MAPK	Mitogen-activated protein kinases
MDA5	Melanoma differentiation-associated protein 5
MDSC	Myeloid-derived suppressor cells
mEHT	Moderate local electrohyperthermia
MEM	Minimum essential medium
MHC-II	Major histocompatibility complex class II
miR	MicroRNA
MOI	Multiplicity of infection
MOMP	Mitochondrial outer membrane permeabilization
MS	Mass spectrometry
MS4A10	Membrane Spanning 4-Domains A10
MSCs	Mesenchymal stem cells
MTD	Maximum tolerable dose
MUC 1/13/17	Mucins 1/13/17
MuV	Mumps virus
MV	Measles virus
NADPH	Nicotinamide adenine dinucleotide phosphate
NBR1	Neighbour of Brca1 gene
NDV	Newcastle disease virus
NF-kB	Nuclear Factor kappa-light-chain-enhancer of activated B cells
NGF	Nerve growth factor
NHEJ	Non-homologous end joining
NK	Natural killer cells
NLS	Nuclear localisation sequence
NO	Nitrous oxide
NOS	Nitric oxide synthase
NOX2/4	NADPH oxidases2/4
NP	Nucleocapsid protein
NRF2	Nuclear factor erythroid-2-related factor 2
NS3	Non-structural protein 3
NSCs	Neural stem cells
OASL	2'-5'-Oligoadenylate synthetase-like protein
Orm1	Orosomucoid 1
Orm2	Orosomucoid 2
OVs	Oncolytic viruses
P	Phosphoprotein
p62/ SQSTM1	Sequestosome 1
PAC	Puromycin N-acetyltransferase
PAGE	Polyacrylamide gel electrophoresis
PAGE4	P Antigen Family, Member 4 (Prostate Associated)
PAMPs	Pathogen-associated molecular patterns
PB1	Phox and Bpem1
PBMCs	Peripheral blood mononuclear cells
PBS	Phosphate buffer saline
PBSa	Ca+2/Mg+2 free Phosphate buffer saline
PCR	Polymerase chain reaction
PD-1	Programmed cell death protein-1
PDGF	Platelet-derived growth factor

PDGFRA	Platelet-derived growth factor receptor alpha
PD-L-1	Programmed cell death ligand -1
PERK	PKR-like endoplasmic reticulum kinase
PFA	Paraformaldehyde
PFU	Plaque-forming unit
PI3K/AKT	Phosphoinositide 3-kinases/RAC-alpha serine/threonine-protein kinase
PIV5	Parainfluenza virus type 5
PKR	Protein kinase RNA-activated
PMEL17	Premelanosome protein 17
poly(I:C)	Polyinosinic-polycytidylic acid
PRRs	Pattern associated receptors
RANKL	Receptor activator of nuclear factor kappa-B ligand
RANTES	Regulated on activation, normal T cell expressed and secreted
Rb	Retinoblastoma
RCC	Renal cell carcinoma
RE	Restriction enzymes
RFP	Red fluorescent protein
RGCC	Regulator Of Cell Cycle
RIG-1	Retinoic acid-inducible gene-1
Rigvir	Riga virus
RIP1	Receptor-interacting serine/threonine-protein kinase 1
RIPA	Radio-Immuno precipitation assay
RLR	RIG-I like receptor
RLU	Relative light units
RNAi	RNA interference
rNDVs	Recombinant NDVs
ROS	Reactive oxygen species
RPKM	Reads Per Kilobase of transcript per Million reads
RPMI	Roswell Park Memorial Institute
RSV	Respiratory syncytial virus
RT	Radiotherapy
RXRs	Retinoid X receptors
S	DNA synthesis phase
SCCHN	Squamous cell carcinoma head and neck
scFv	single-chain Fv
SDF-1	Stromal cell-derived factor-1
SDS	Sodium dodecyl sulfate
SeV	Sendai virus
siRNA	small interfering RNA
SLC10A1	Solute Carrier Family 10 Member 1
SLC38A4	Solute Carrier Family 38 Member 4
SMAC	Second mitochondria-derived activator of caspases
SNPs	Single nucleotide polymorphisms
SP100	Speckled 100 KDa Nuclear Antigen
STAT-1	Signal transducer and activator transcription factor 1
STR	Short tandem repeat
TAAs	Tumour associated antigens
TBE	Tris/borate/EDTA
TBS	TRAF6-binding site

TCA	Tricarboxylic acid cycle
TCID50	Median Tissue Culture Infectious Dose
TFBS	Transcription factor binding sites
TGFB1	Transforming growth factor beta 1
TGF-α	Transforming growth factor-alpha
TIM3	T-cell immunoglobulin and mucin domain 3
TK	Thymidine kinase
TLR	Toll-like receptor
TMT	Tandem Mass Tag
TMZ	Temozolomide
TNF	Tumour necrosis factor
TNFR2	Tumor necrosis factor receptor 2
TRADD	TNFR-1 associated death domain
TRAF3	TNF associated factor 3
TRAF6	Tumour necrosis-associated factor 6
TRAIL	TNF-related apoptosis-inducing ligand
TTP	Tristetraprolin
T-VEC	Talimogene laherparepvec
UBA	Ubiquitin-associated
uPA	Urokinase plasminogen activator
UPR	Unfolded protein response
VEGF	Vascular endothelial growth factor
VGF	Vaccinia growth factor
VHL	Von Hippel-Lindau
VR Caco-2	Virus-Resistant Caco-2
VSV	Vesicular stomatitis virus
VV	Vaccinia viruses
WB	Western blot
WT	Wild-type
XIAP	X-linked inhibitor of apoptosis protein
ZZ	ZZ-type zinc finger

Chapter 1

1 Introduction

1.1. General introduction to cancer

Cancer is the second most leading cause of death worldwide followed by cardiovascular diseases, and according to the International Agency for Research on Cancer (IARC) report, 9.6 million deaths have been recorded, and 18.1 million new cases have escalated internationally, in 2018. The cancers of lung, colorectum, stomach, liver, and breast are the most common causes of cancer deaths and ranking first to fifth from the lung to mammary glands.

Cancer is generic terminology used for malignancies of diverse tissues leading to the severe life-threatening diseases consequential of the complex process of tumorigenesis. Cancer is resulted from fundamental abnormalities in the regulation of the cell cycle (1). Under normal condition, cellular homeostasis maintained by cell proliferation, cell growth arrest, and apoptosis regulated by precise control of cell cycle checkpoints (1). The cell cycle is a tightly regulated process of cellular division achieved by intricate sequences divided into interphase and mitotic phase (M) controlled by various checkpoint regulators (illustrated **in Figure 1.1.**) (2, 3). The interphase comprises gap 1 phase (G1), DNA synthesis phase (S), and gap 2 phase (G2). The G1 and G2 phases corresponds to obvious gaps in the cell cycle that occur between S phase and M phase. In G1 phase cell undergoes duplication of cellular constituents before DNA replication in S phase, whereas in G2 phase cell undergoes final protein synthesis and cellular growth preparation before M phase (4). The M phase constitutes of 4 different sub-phases [prophase (Pro), metaphase (Met), anaphase (Ana), and telophase (Tel)] of karyokinesis where cell divides into two daughter cells followed by cytokinesis. The gap 0 phase (G0) phase represents cell cycle arrest, where cells are reversibly reserved from cell division cycle in response to elevated cell density and mitogen deficiency (5). Cell cycle checkpoints are regulatory mechanisms of cell growth and proliferation governed by complex array regulatory proteins interactions (1). Checkpoints of the cell cycle confirm orderly succession of cell cycle, are crucial in the maintenance of genomic stability and deregulation of these checkpoints often result in carcinogenesis in the majority of cancers (2). Oncogenes (such as Her2/neu, Ras, c-Myc, etc.) and tumour suppressor genes (such as Rb, p53, Bcl-2, SWI/SNF etc.) are important two gene types play vital role in cycle and cancer development (1).

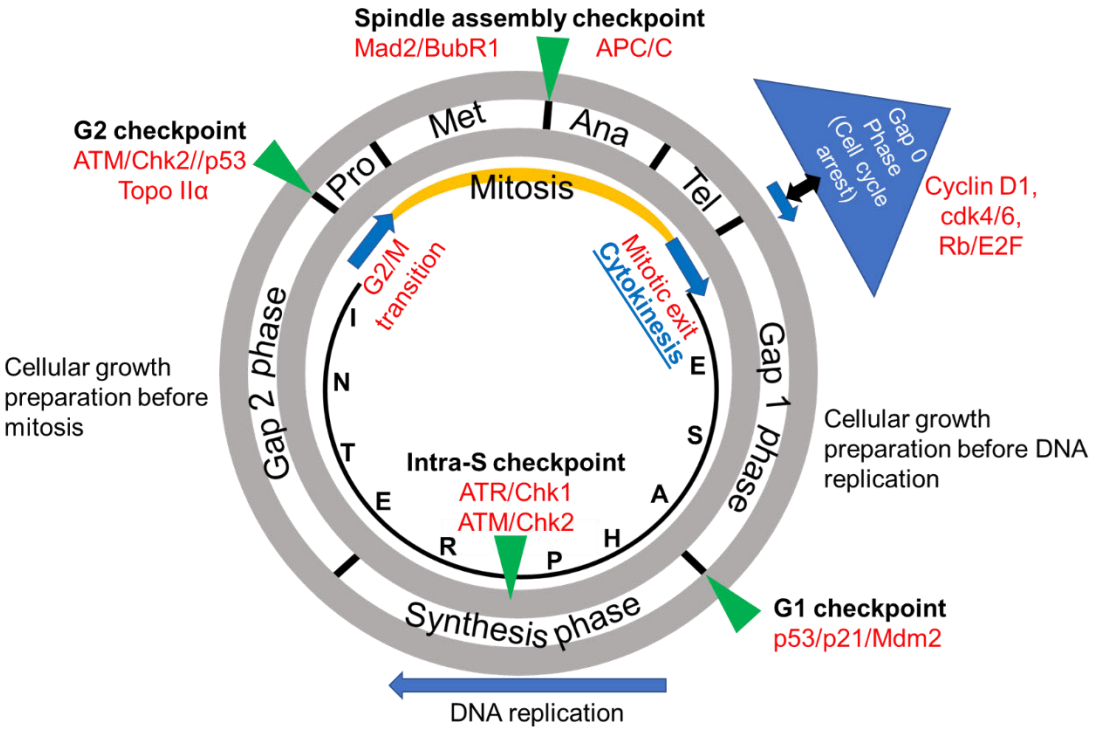

Figure 1.1. Dagram illustrating cell cycle regulation, adapted from Bower et al. (2). The cell cycle phases [Interphase covering gap 1 (G1), synthesis (S), and gap 2 (G2); Mitosis (M) which consists of several sub-phases: prophase (Pro), metaphase (Met), anaphase (Ana), and telophase (Tel), and the gap 0 phase (G0)]are shown in the grey circle. The interphase is the longer phase of the cell cycle that consists of growth phases where cellular constituents grows before (G1) and after (G2) synthesis of DNA replication phase. The mitosis is a shorter phase consisting of subphases of karyokinesis followed by shortest cytokinesis phase. The G0 phase is a restriction point where cell cycle arrest designated by blue triangle with a black dual headed arrow to show changeable nature of cell cycle entry and dormancy. The cell cycle progression is activated by several checkpoints triggered by external factors while cell transitions from phases. Major cell checkpoint regulators are designated in red font at green triangle. Cell checkpoints regulation is important for accurate DNA replication and cell division.

There are at least 4 different cell cycle checkpoints which are deregulated in cancer cells: the cell cycle arrest point (G0/G1), the G1 checkpoint, the G2 checkpoint, and the mitosis-associated spindle assembly checkpoint (SAC) (2). In the G0/G1 cell cycle arrest point, the transition from G1 constrains the induction of cell dormancy reversion due to lack of growth factors and regulates cell division (2). The Rb/E2F signalling pathway mainly controls G0/G1 checkpoint, where release of E2F transcription factors from Rb activates genes involved in the initiation of DNA repictaion at the start of S phase. Cyclin D1 and cyclin-dependent kinases (cdk) 4/6 are upstream regulators of Rb and overexpression or mutation in these regulators can lead to dysregulation of G0/G1 checkpoint that results into early activation of DNA replication (2). The p53/p21/Mdm2 pathway controls G1 checkpoint and regulates DNA damage in the cell. DNA damage

postpones the initiation of DNA replication which often resulted from inactivation or mutation of wild-type p53 and leads to error-prone synthesis of DNA in S phase (2). Two types of G2 checkpoints are identified: G2 DNA damage checkpoint and decatenation G2 checkpoint. DNA damage delays initiation of mitosis by sequestering cyclin B1/cdk 1 in the cell cytoplasm. The catalytic inhibition of topoisomerase IIα (topo IIα) without explicit DNA damage activates decatenation G2 checkpoint. The ATM/Chk2/p53 pathway play major role controlling both G2 checkpoints and inactivation of either of G2 checkpoints lead to chromosomal instability (2). Lastly, SAC regulates mitosis at the onset of anaphase by controlling bipolar attachment of chromosomes to mitotic spindle. Regualtors such as APC/C, BubR1, and Mad2 play important role in SAC and impairment of SAC signalling result into multipolar spindles or inadequate separation of sister chromatids into daughter cells (2). Defects in any of these checkpoints lead to progression of tumorigenesis in a tumour.

The complexity of tumorigenesis is fundamentally characterized by six principal hallmarks proposed by Hanahan and Weinberg (6, 7) which are self-containment of growth signals and unresponsiveness to anti-growth stimuli, unregulated cell proliferation, defective anti-survival pathways, constant genetic instability, enhanced angiogenesis, and activation of tissue invasion with metastasis (illustrated in **Figure 1.2**). Unlike healthy cells, neoplastic cells proliferate in a disorderly and uncontrolled manner due to the aberrant growth stimuli regulations and responses. Cancer cells become self-contained in growth signal production; such growth signals include platelet-derived growth factor (PDGF), transforming growth factor-alpha (TGF-α) and by overexpression of receptors like epidermal growth factor receptor (EGFR) which are hyper-responsive to the ambient growth factors. Cancer cells become insensitive to anti-growth factors as a result of a disruption in anti-survival pathways, retinoblastoma (Rb) pathway is one such example. In human cancers, disruption of the Rb/E2F pathway results from a mutation in p16, a cdk inhibitor 2A, which is responsible for the control of cyclin D/cdk4 kinase activity. The absence of p16 elevates cyclin/cdk4 kinase activity leading to Rb phosphorylation and release of E2F transcription factors which leads to uncontrolled cell proliferation (8). Cancer cells lose homeostasis by acquiring defects in anti-apoptotic and other cell death pathways via several mechanistic manipulations of regulatory molecules. For example, genetic alteration in anti-apoptotic Bcl-2 family of molecules disrupts mitochondrial apoptotic pathway in most of the cancers like melanoma, leukaemia and others (9). The expression of vascular endothelial growth factor (VEGF), acidic and basic fibroblast growth factors (FGF1/2) governs the escalation in angiogenesis which accomplishes self-dependency of oxygen and

nutrients of neoplastic cells. The switch in angiogenesis inducers and inhibitors upsets the balance resulting in exponential tumour growth as a result of new vasculature supplementing nutrients to the hypoxic tumour microenvironment (6, 7). In the advanced phase of malignancy, cancer cells migrate from tumour origin to distant locations and establish new tumorigenic colonies. The establishment of tissue invasion and metastasis in cancer cells becomes plausible due to alterations in expressions of cell adhesion molecules (CAM) and E-cadherin molecules (6, 7).

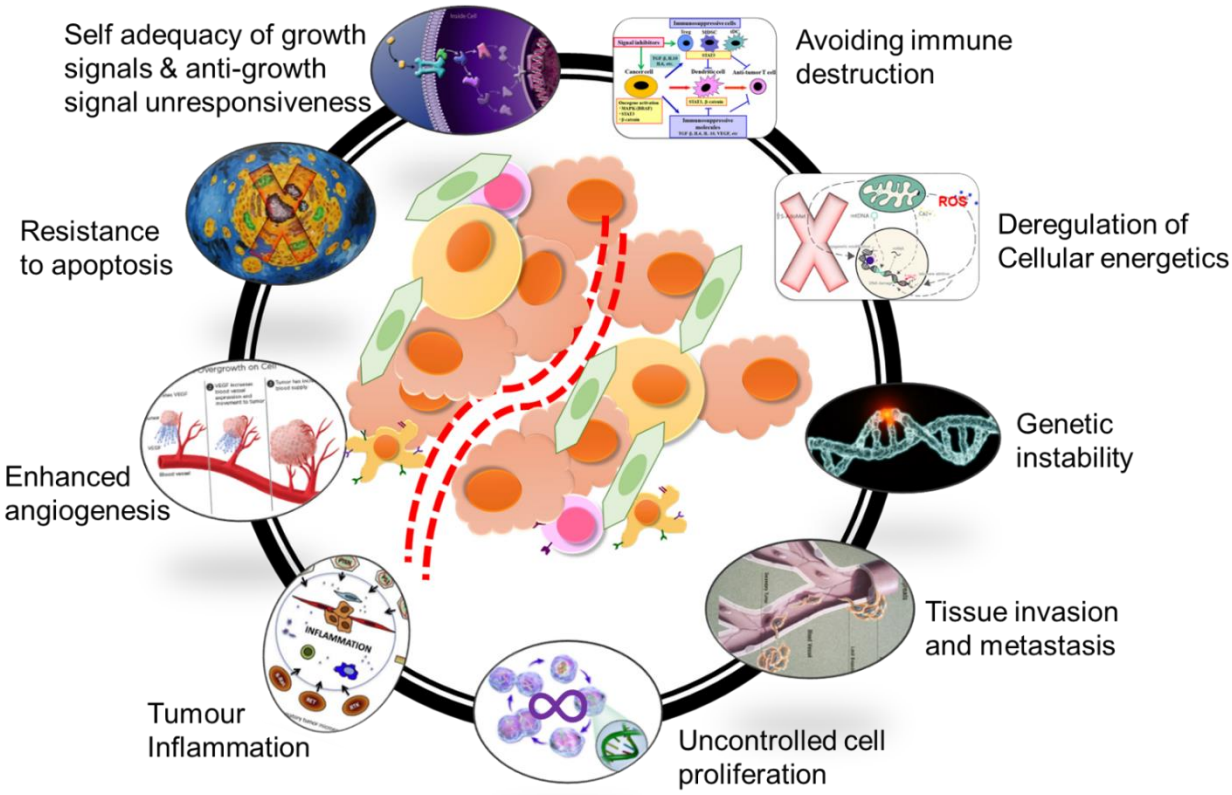

Figure 1.2. The principal hallmarks, which characterise the malignancy of abnormal neoplastic cells, adapted from Hanahan & Weinberg, 2000 (6) and Hanahan & Weinberg 2011 (7). A large group of diseases grouped under the category of cancer signifies these core hallmarks as a characterisation marker under malignancy umbrella. Cancer and its progression can be identified by self-sustenance by growth signals or receptors adequacy and insensitivity to anti-growth factors, uncontrolled cell proliferation, defects in cell death pathways, self-sustainable angiogenesis, activation of tissue invasion and metastasis, and genetic instability.

The instability in the genetic makeup of cancer cells stands out as a critical feature for recognition of the status of the various cancers, which results from mutations in the DNA-repair genes in the form of either chromosomal instability or microsatellite instability or karyotypic instability as a result of telomerase depletion. The genomic instability plays roles in both hereditary and non-hereditary types of cancers. The genomic instability

modifies cancer cells by reprogramming and deregulating cellular energetics to adapt with the continually changing complex tumour microenvironment for the supply of nutrients, oxygen, and growth stimulants under the metabolic stress (10). Tumour inflammation is evident in most of the neoplastic microenvironment due to infiltration of immune cells and release of inflammatory cytokines such as tumour necrosis factor (TNF), interleukin-1 (IL-1) and release of reactive oxygen species (ROS) at the site of inflammation. However, in some cancer cells modulation of immune checkpoints results in the evasion of the immunosurveillance; for example, overexpression of programmed cell death ligand -1 (PD-L-1), cytotoxic T lymphocyte-associated antigen-4-B7 (CTLA4-B7), and T-cell immunoglobulin and mucin domain 3 (TIM3) on cancer cells inactivates or negatively regulates cytotoxic T lymphocytes (CTLs) activation and lead to CD4+ and CD8+ T-cells tolerant tumour microenvironment (7). Immune checkpoints are regulatory pathways of the immune system to modulate the extent and time of immune responses to maintain self-tolerance of the immune cells and prevent tissue damage in case of the pathogenic invasion in healthy cells. Tumour cells manipulate immune checkpoints to avoid the immune system. T-cell mediated cytotoxicity plays an inevitable role in tackling the rejection of tumours because of selective antigen presentation, direct CD8+ effector T-cell-mediated cytotoxicity in response to antigens, and dual functionality in the innate and adaptive immune system. T-cell mediated immune responses implicate multiple steps and complex array of molecules at each stage starting from antigen-specific clonal selection, activation, maturation, and proliferation in lymphoid organs, to interactions with APCs. Hence, each of these steps is regulated by counteracting co-stimulatory and co-inhibitory molecules to govern the normal functioning of T-cells (11). Tumour cells over-express inhibitory signals as membrane-bound receptors such as B7, programmed cell death ligand -1 (PD-L-1), and high mobility group box protein 1 (HMGB1) which interacts with their membrane-bound and soluble ligands such as CTLA4-B7, PD-1: PD-L1/L2, and TIM3-HMGB1, which limit T-cells activation. The interactions mentioned above are the potential targets for currently used ICIs (12). ICI mainly comprises of CTLA-4 and PD-1. FDA approved targets as of prime importance are discussed below in relation with oncovirotherapy.

CTLA-4 (also known as CD152) is an inhibitory molecule expressed on the activated T-cell surface which prevents binding of B7 to CD28 molecules and leads to unfavourable regulatory T-cell functions. Prevention of B7-CD28 interaction results in disruption of naïve T-cell activation and ultimately decreased T-cell-mediated immune responses. Ipilimumab is a commercially available anti-CTLA-4 antibody used as ICI and its

improved antitumour activity facilitated by NK cells and CTL activation is reported in a murine melanoma model.

PD-1 is a checkpoint immunoglobulin molecule expressed on activated T-cells, B-cells and NK cells for the extended time frame than CTLA-4 (13). The PD-1 signalling inhibits T-cell activation in a late stage of activation of the immune response to tumours and tissues, whereas CTLA-4 inhibits T-cell activation occurs in early stages. PD-1 has appeared as a most promising target of ICI which can promote antitumor immune reactions. PD-1 is overexpressed on regulatory T-cells; hence, blockade therapy might help in enhancing the T-cell activation of the immune response by reducing the suppressor activity of regulatory T-cells. PD-1 mainly interacts with PD-L-1 and PD-L-2 ligands. In many cancers such as lung, ovarian, and melanoma, PD-L-1 upregulation is very common; moreover, it is also usually overexpressed on myeloid cells in the tumour microenvironment, perhaps an adaptation to the immune response development in the tumour microenvironment. Numerous anti-PD-1 and anti-PD-L1 inhibitors have been developed for blockade therapy, and in 2014 FDA approved the first PD-1 inhibitor pembrolizumab for the melanoma treatment.

1.2. Types and stages of cancer

More than 100 types of cancers are identified and named for the organs or tissues of origins. Most of cancers are grouped into one of 3 main categories: carcinoma, sarcoma, and lymphoma or leukemia. Carcinomas are most common types of cancers and include ≥ 90% of human cancers derived from malignancies of epithelial cells. Carcinomas have specific names based on types of epithelial cells such as adenocarcinoma (epithelial cells producing mucus or fluids in tissues e.g. colon, breast, prostate etc.) and squamous cell carcinoma (epithelial squamous cells from skin, lung, thyroid, vagina etc.). Sarcomas are rare form of cancers comprising solid tumours of connective tissues, including cartilage, bone (osteosarcoma), muscles, and fibrous tissues. Lymphomas and leukemias are malignancies derived from immune cells and blood forming cells, which comprises ≥ 8% of human cancers (14).

Tumorigenesis is a complex multistep process of cancer cell development including mutation and clonal selection of cells with uncontrolled cellular proliferation, survival, invasion, and metastasis (14). Stages of cancer are defined by the American Joint Committee on Cancer (AJCC) (15), and are based on clinical, pathological, and post-therapy identification. The cancer staging is dependent on various elements such as

location of primary tumour, size of tumour, involvement of lymph node, and presence or absence of metastasis at distant sites in the body. TNM staging is widely used cancer staging system and regulated by the AJCC and the Union for International Cancer Control (UICC). TNM system of cancer stage classification based on the level of the tumour (T), the degree of spread to lymph nodes (N), and the evidence of metastasis (M). TNM staging further categorised in different groups as shown in **Table 1.1**.

Table 1.1: **TNM based cancer categorisation**

Categorization based on primary tumour (T)	
TX	Primary tumour evaluation is impossible
T0	No evidence for primary tumour
Tis	Abnormal cells/tissue in situ
T1-T4	size and extent of tumour
Categorization based on lymph node (N)	
NX	Evaluation of regional N is impossible
N0	No evidence of regional N involvement
N1-N3	Involvement of regional N
Categorization based on distant metastasis (M)	
M0	No distant metastasis
M1	Evidence of distant metastasis

Once the status of the T, N, and M are determined, cancer is broadly classified in 5 broad stages. The classification of cancer vary based on the type of cancer and each stage further subdivided based on type of cancer using letters e.g., IA, IIB, IIIC etc. These broad stages of cancer are described as below.

Stage 0: abnormal cells growing *in situ*.

Stage I: cancers localised to one specific part of body.

Stage II: locally advanced cancer without any sign of spread to other tissue or organs.

Stage III: locally advanced cancer with the evidence of invasion of neighboring tissues and regional spread.

Stage IV: advanced cancer with metastasis at distant sites in the body.

1.3. Oncovirotherapy as a cutting-edge treatment for cancer

From the early 19th-century, surgery followed by radiation therapy has been employed to treat cancers. The first successful surgical partial mastectomy was performed under general anaesthesia for a breast cancer patient in 1804 by Seishu Hanaoka (16). After the discovery of X-ray by Wilhelm Roentgen in 1895 and the radioactive radium and polonium discovery by Marie and Pierre Curie in 1898 led to the use of radioisotopes in

radiation therapy as a new avenue for cancer treatment (17). In 1903, S.W. Goldberg and Efim London demonstrated the use of radiation to treat 2 patients with basal cell skin carcinoma with complete eradication of cancer cells. Surgery is still used today to remove localised tumours if recognised in early stages of diagnosis and remain essential backbone treatment for cancers of various tissues. Radiotherapy also has dominated since its emergence until the discoveries in the field of anti-metabolites, e.g. methotrexate and alkylating agents such as nitrogen mustard, potential cytotoxic chemicals which cause inhibition of DNA synthesis and a cascade of other cytotoxic effects in cells (18, 19). Despite the success of nitrous oxide and methotrexate in lymphoma and leukaemia cancer patients, by 1950 physicians noticed limitations and were disappointed with chemotherapy as a result of failed durability and remission of tumours leading to the advanced stage.

Conventional methods have significant drawbacks and enormous side effects because of poor specificity. The need of target-specific cancer treatment became promising with everyday scientific advancements in molecular biology, immunology, cancer biology, and virology to manage cancer. Targeted therapy included novel approaches to tackle cancer, such as monoclonal antibodies, antibody-drug conjugates, tyrosine kinase inhibitors, immune checkpoint inhibitors, hormonal agents, antitumor vaccines and oncolytic viruses (OVs). The extensive study of OVs in recent times has resulted from inquisitive and vigilant observations of the last century in cancer patients where remission of tumours was linked to patients contracting infectious diseases. The first such instance was presented in 1910 at the International Cancer Congress, Paris, by Italian clinician, N. G. De Pace where the dramatic remission documented in rabies virus vaccinated uterine cervical cancer patients and likewise similar effects documented in African Burkitt's lymphoma positive children with measles virus infections (20, 21). There are historical accounts of oncolytic activity accredited to replicating viruses available in the scientific domain as published case reports as early as 1912, where sporadic but dramatic reactions in cancer patients recovered from viral vaccinations have been recorded (22, 23). In the 1950s–1970s, live viruses were injected into cancer patients and presented promising cytotoxic activity, notably Egypt 101 West Nile virus (4/34 transient regressions), adenovirus lysates (26/40 showing localised tumour necrosis), and Urabe strain of mumps virus (37/90 complete remission or partial responses) (23). In contrast, virus-induced oncolysis noted in these early studies are principally from naturally occurring wild type Egypt 101 strain of West Nile virus injected in immune-suppressed patients with leukaemia or lymphoma. Virus-infected 5 of 8 patients were sensitised by a viral infection and experienced severe encephalitis (23).

Oncolytic viruses include naturally occurring or genetically engineered non-pathogenic and replication-competent viruses that favourably replicate in tumour cells sparing the healthy cells resulting in tumour cell lysis (24). Viruses inclusive of both DNA and RNA genomic classes are identified to have oncolytic properties, e.g. adenoviruses (Ad), herpes simplex virus type-1 (HSV-1), vaccinia viruses (VV), poxviruses, Newcastle disease virus (NDV), Measles virus (MV), Mumps virus (MuV), Sendai virus (SeV), Marba virus, parvovirus, reovirus, vesicular stomatitis virus (VSV) and Coxsackievirus etc. The details of identified OVs are listed in **Table 1.2**.

Oncolytic viruses are usually administered either locally via intra-tumoural route or systemically via intravenously and intraperitoneally into test animals and/or paitients (25). Local administration of OV through inntra-tumoural route ensures direct entry of viral particles to tumour. Systemic administration of OV provides few benefits such as introduction of viral particles to distant tumour sites as well as the site of primary leison. However, the efficacy of administration of OV via either of the routes depend upon various factors e.g., type of cancer, type of OV, dose of OV etc. (25).

Table 1.2: **List of oncolytic viruses, adapted from Kaufman et al. (26)**

Virus	**Baltimore classification**	**Genome size (~in kb)**	**Family**	**Virion**	**Cell receptor**	**Replication Site**
Adenovirus	Group-I: dsDNA	35	Adenoviridae	Naked	Coxsackie-adenovirus receptor	Cytoplasm
Vaccinia virus	Group-I: dsDNA	190	Poxviridae	Complex coated	Unknown	Cytoplasm
Herpes virus	Group-I: dsDNA	154	Herpesviridae	Enveloped	Herpesvirus entry mediator, Nectin 1, and Nectin 2	Nucleus and cytoplasm
Parvovirus H1	Group-II: ssDNA	5	Parvoviridae	Naked	Sialic acid residues	Nucleus and cytoplasm
Reovirus	Group-III: dsRNA	23	Reoviridae	Naked	Unknown	Cytoplasm
Coxsackievirus	Group-IV: ssRNA	28	Picornaviridae	Naked	Coxsackie-adenovirus receptor /Decay accelerating factor/ICAM-1	Cytoplasm
Seneca Valley Virus	Group-IV: (+) ssRNA	7	Picornaviridae	Naked	Unknown	Cytoplasm
Poliovirus	Group-IV: (+) ssRNA	7.5	Picornaviridae	Naked	CD155	Cytoplasm

Virus	Baltimore classification	Genome size (~in kb)	Family	Virion	Cell receptor	Replication Site
Measles virus	Group-V: (-) ssRNA	16	Paramyxoviridae	Enveloped	SLAM and CD46	Cytoplasm
Newcastle disease virus	Group-V: (-) ssRNA	15	Paramyxoviridae	Enveloped	Sialic acid residues	Cytoplasm
Sendai virus	Group-V: (-) ssRNA	15	Paramyxoviridae	Enveloped	Sialic acid residues	Cytoplasm
Maraba virus	Group-V: (-) ssRNA	11	Rhabdoviridae	Enveloped	Low-density lipoprotein receptor LDLR	Cytoplasm
Vesicular stomatitis virus	Group-V: (-) ssRNA	11	Rhabdoviridae	Enveloped	Low-density lipoprotein receptor LDLR	Cytoplasm

1.4. Commercially approved OVs for cancer treatment

Noteworthy progress has been accomplished in the field of oncovirotherapy, from naturally occurring viruses to genetically engineered viruses. Recombinant viruses include improved tumour-specificity, where virus replication is mediated through target-oriented cell entry and transcription. Additionally, expression of reporter genes for noninvasive monitoring, and insertion of immunomodulating genes have enhanced OV-induced cytotoxicity and provide superior immunostimulation. To date, three oncolytic viruses are commercially available for cancer treatment; Rigvir (picornavirus) was approved in Latvia, Georgia, and Armenia; Oncorine H101 (adenovirus) was approved in China; talimogene laherparepvec (T-VEC) (herpesvirus) was approved in the USA and Europe.

1.4.1. Rigvir

Rigvir (Riga virus) is natural Enteric Cytopathogenic Human Orphan type 7 (ECHO-7) picornavirus. Rigvir became the first approved oncovirotherapy worldwide in 2004 with regulatory approvals internationally; in Latvia from 2004, in Georgia from 2015, and Armenia as of 2016 (27). Despite being the first-ever approved OV, there are minimal data available in the English language, including the one review on the clinical trial of three patients with advanced stage cancers: melanoma (stage IV M1c), small cell lung cancer (stage IIIA), and histiocytic sarcoma (stage IV) (28) and other study from Lativian clinical trial on 79 patients in early stage melanoma (27).

In pioneering study in Latavia, melanoma patients at various stages of cancer (early stages with different subclasses based on tumour thickness, spread, and ulceration IB, IIA, IIB, and IIC) received surgical resection and Rigvir. Patients who received surgical resection and Rigvir (n=52) survived significantly longer than patients from control surgical resection only group (n=27). Rigvir was injected intramuscularly in localized tumours in patients (surgical resection+OV group) postoperatively when surgical wounds were healed; patients showed remarkable disease-free survival. Rigvir was postoperatively injected intramuscularly in locoregional tumours with a minimum median tissue culture infectious dose (TCID50) level of 1 x 10^6/ml in 2 ml volume without any dose optimisation in patients under the study. Each patient received about 33 doses over 3 years: first dose of 2 ml was administered at localised tumour for 3 successive days, then after 4 weeks, same dose was repeated for 3 successive days and repeated 4 weeks later. Later, a single dose was administered at monthly intervals throughout first year. In second year, dose was administered at 6 weeks interval for first 6 moths and in last 6 months repeated after 2 months. In third year, dose was administered at every 3 months until end. The effects of Rigvir, are reported only from low-grade melanoma, whereas the status in high-grade aggressive melanoma remains unclear. Nevertheless, future studies are required to be done in the non-resectable melanoma in advanced stage to get a clear understanding of the mechanism and efficacy of Rigvir-mediated oncolysis for a potential future oncovirotherapy (27, 29).

1.4.2. Oncorine

Oncorine is a genetically modified adenovirus H101 which has been approved by the China Food and Drug Administration for the treatment of advanced head and neck cancer with a combination of chemotherapy in 2005 (30, 31). Oncorine is previously known as Onyx-015, which is an attenuated serotype 5 adenoviral vector modified by deletion of E1B-55k along with four other deletions in the viral E3 unit. It is hypothesised that Oncorine selectively replicates in p53 deficient tumours, as E1B-55k is a potent p53 repressor. The E1B-55k inhibits infection-induced apoptosis and allows viral replication in p53-normal cells.

Nevertheless, adenoviruses with E1B-55k deletion have been shown to infect and replicate in p53 positive tumours indicating an alternate mechanism of tumour-selective viral replication (32-34). A patient-approved clinical trial of Oncorine was performed comprising of an extensive, multi-centre, open, randomised use of Oncorine in combination with chemotherapy against chemotherapy alone in head and neck

squamous cell carcinoma (HNSCC) or oesophagal cancer patients. Patients who received a combination of cisplatin and 5-fluorouracil (5-FU) with or without Oncorine at 5 x 10^{11} to 1.5 x 10^{12} viral particles/day for 5 successive days every 3 weeks and repeated every 3 weeks while all patients received minimum 2 cycles of chemotherapy. Combinational Oncorine and chemotherapy arm had a significant 78.8% (41/52) response rate compared with a 39.6% (21/53) response rate of chemotherapy alone patients (35).

There is a practical limitation to deliver Oncorine intravenously to treat highly metastatic disease due to high antibody occurrence against several adenovirus serotypes, including the backbone of Oncorine, serotype 5. Some clinical trials (VCN-01 NCT02045602, Enadenotucirev NCT02028442) are ongoing to circumvent pre-existing immunity against existing adenoviral vectors and focusing on the reduced seroprevalence or modified adenoviral knob proteins to test its safety and efficacy via intravenous Oncorine delivery. Although oncolytic adenoviruses have been in development for over 20 years, Oncorine remains the only approved adenovirus for cancer therapy and administer with combinational chemotherapy only (35-37).

1.4.3. T-VEC (Imlygic™)

IMLYGIC™ (T-VEC/Talimogene Laherparepvec), a genetically engineered live-attenuated HSV-1, was approved in 2015 by the United States Food and Drug Administration and European Union to treat cutaneous, subcutaneous and unresectable lesions intratumorally post-operation in advanced melanoma patients (38-41). T-VEC is a recombinant human HSV-1 deleted for both copies of the viral gamma 34.5 and viral ICP47, which elevates the expression of US11, and encodes two copies of human granulocyte-macrophage colony-stimulating factor (GM-CSF) under cytomegalovirus (CMV) promoters (42). Since February 2018, 23 clinical trials are ongoing, evaluating the safety and efficacy of T-VEC as a single agent or as a combination with checkpoint inhibitors, chemotherapy, or radiation therapy in melanoma and other indications in patients with liver, pancreatic, and advanced non-central nervous system solid tumours. A phase II trial has revealed encouraging results in late-stage melanoma patients treated with a combination of T-VEC and programmed cell death protein-1 (PD-1) inhibitor pembrolizumab published in 2017 (43). The combination therapy of T-vec with pembrolizumab had confirmed complete response in 21% (7/33) patients with advanced melanoma with metastases (43).

Amongst the plethora of OV families, recently finished clinical trials of successful candidates are listed in **Table 1.3**. Herein the thesis focus is on the NDV and development of NDV as an oncovirotherapy.

Table 1.3: **Recently completed combinational oncovirotherapy list**

Virus	Name	Route of administration and stage of cancer		Tumour	Combination	References
Adenovirus	ONYX-015	IT	III	Squamous cell carcinoma head and neck (SCCHN)	Cisplatin	(44)
		IT	I/II	Pancreatic cancer	Gemcitabine	(45)
		IT	I/II	Advanced sarcoma	Mitomycin-C, doxorubicin, cisplatin	(46)
	Oncorine (H101)	IT	III	SCCHN or oesophageal cancer	5-fluorouracil + cisplatin or adriamycin	(47)
	Ad5-CD/Tkrep	IT	I	Prostate cancer	5-fluorocytosine, valganciclovir, radiation	(48)
	ONCOS-201	IT	I	Solid tumours	Cyclophosphamide	(49)
Herpes simplex virus	Talimogene laherparepvec	IT	I/II	SCCHN	Radiation, cisplatin	(50)
		IT	Ib	Melanoma	Ipilimumab (CTLA-4 inhibitor)	(51)
	G207	IT	I	Glioma	Radiation	(52)
Reovirus	RT3D	IV	I/II	Advanced cancers	Carboplatin/ paclitaxel	(53)
Vaccinia virus	GL-ONC1	IV	I	Head and neck carcinoma	Cisplatin, radiotherapy	NCT01584284
	JX-594 (Pexa-Vec)	IV	I/IIa	Colorectal cancer	Irinotecan	NCT01394939
Note: IT- intratumoral; IV-intravenous; CTLA-4 –Cytotoxic T Lymphocyte antigen 4						

1.5. Mouse models used in the study of oncovirotherapy

Mouse models are widely used in the field of cancer therapy to conduct *in vivo* studies in pre-clinical trials to study the efficacy of type of the therapy used in the study. Mouse models provide relative similarities in genetic and physiological make-up of tumour biology between humans and mice (54).

Conventionally, immunocompetent immunocopromised mice are used to study cancer biology. Based on the origin of tumour and host used, there are two widely used tumour mouse models: syngeneic and xenograft tumour models. In syngeneic models, murine cancer cell lines or tumour tissues are used for transplantation in inbred animals with same genetic make-up. Syngeneic mouse models provide advantages of tumour

tissues, tumour microenvironment, and host are from the same species e.g., Leukemia1210 (L1210) cell line derived from L1210 of DBA/2 mouse transplanted in animals of same species (55). In xenograft models, athymic (nude) or severe combined immunodeficiency (SCID) mice are injected with the tumour cell lines or tissues derived from humans, e.g. human non-small cell lungcancer cells (A549) injected in Balb/c nude mice (55). Genetically engineered mouse models are also used commonly, where immunocompetent mice with genetic defects are introduced using RNA interference, inducible gene expression, viruses, DNA recombination techniques, or CRISPR/Cas9 methods are used (56).

Transplantaion of tumours are achieved by using either orthotopic or heterotopic methods. Orthotopic tumour transplantation refers to introduction of tumour cells into the organ of origin (anatomic location from where cells or tissues are derived) in immunocompromised mice. Orthotopic transplantation is achieved either by surgery at the original location or by direct injection of tumour cells (55, 56). Whereas, the heterotropic transplantation refers to introduction of tumour cells to the sites other than its origin. Heterotropic tumour transplantation is accomplished by transplantation under the skin (subcutaneous) and in the abdominal cavity (intraperitoneal) of the athymic host (55, 56).

1.6. General mechanisms of oncolytic viruses

The mechanisms of how OVs mediate tumour cell lysis are not entirely understood. The majority of OVs directly kill tumours cells by infecting, replicating, burdening the host cell machinery, and invoking the antiviral responses. The oncolytic efficacy of a virus depends upon multiple factors like efficiency of infection in cancer cells, type of virus, natural and induced viral tropisms leading to the kind of cell deaths (apoptosis, necrosis, necroptosis, pyroptosis and autophagy). OV characterises oncotropism due to defective mechanisms of cell death and weaker antiviral responses in cancer cells compared to the healthy cells. In healthy cells, the virus does not proceed beyond infection because of intact and effective antiviral mechanisms in play comprising various pathways participating in clearing the virus.

Primary infection in healthy cells stimulates type-I interferons (IFNs) secreted after pathogen-associated molecular patterns (PAMPs) such as viral proteins, and nucleic acids are recognised by pattern associated receptors (PRRs) like toll-like receptor (TLR) family (TLR-TLR 3/5/7/9). TLR signalling then activates antiviral elements and systemic

innate immune mediators in the infected host cells including tumour necrosis factor (TNF) associated factor 3 (TRAF3), IFN regulatory factor-3 (IRF-3), IRF-7 and retinoic acid-inducible gene-1 (RIG-1). These elements then consecutively activate the JAK-STAT (Janus kinase–signal transducer and activator of transcription) pathway, which in response collaborates with a complex array of antiviral molecules and enzymes such as kinases -protein kinase RNA-activated (PKR). PKR recognises PAMPs in the infected host cells and activates transcription factors, terminates host cell protein synthesis, induces response type-I IFNs to clear the virus by killing the infected cancer cells (57).

Based on the type of OV, viruses can manipulate different abnormal signalling factors to block apoptosis in the tumour cells, which favours more time for the virus to complete its life cycle. Most oncolytic viruses induce cell death by active virus replication and burdening host cell machinery as well as activation of the immune system. Activation of host cell immunity significantly happens due to cell death and release of danger signals from dying cells (apoptotic, necrotic, autophagic, and pyroptotic cell deaths) (58). For efficient OV-mediated clearance of tumours, virus critically needs to activate both innate and tumour-specific adaptive immune molecules to participate in the oncolysis. Following the cancer cell demise exposure of tumour associated antigens (TAAs) along with viral proteins, can play a crucial role in interlinking the innate and adaptive immune systems leading to the abscopal effect regressing the distant untreated tumours.

Along with PAMPs, dying cancer cells also release damage-associated molecular patterns (DAMPs) such as DNA, RNA, or metabolic products (ATP, and uric acid), proteins, such as calreticulin, high-mobility group box 1 (HMGB1), heat-shock proteins (HSPs), and proteins in the intracellular matrix generated following injury, such as hyaluronan fragments (58) and secretes several cytokines (type-I IFNs, TNFα, IFNγ, and interleukin-12 (IL-12)), and chemokines (RANTES, IP-10, CCL22 and CXCL12). All these different types of danger signals promote maturation of natural killer cells (NK) and antigen-presenting cells (APCs) such as dendritic cells (DC), which then activate antigen-specific CD4+ and CD8+ T-cells. Activated CD8+ T-cells can expand to CTLs, which migrate to the tumour and diminish tumour cells via antigen-specific cytotoxicity. Type-I IFNs are also known to activate NK cells and DC cells and connect the innate and adaptive immune systems. Viruses naturally induce host antiviral immune responses, which result in the clearance of the virus by invoking neutralising antiviral antibodies and CTL-mediated immune responses. However, the extent of neutralising antiviral antibody production and its effect on anti-tumour immunity is complex and can

depend on many variables, especially on the characteristics of the virus and the tumour microenvironment (26).

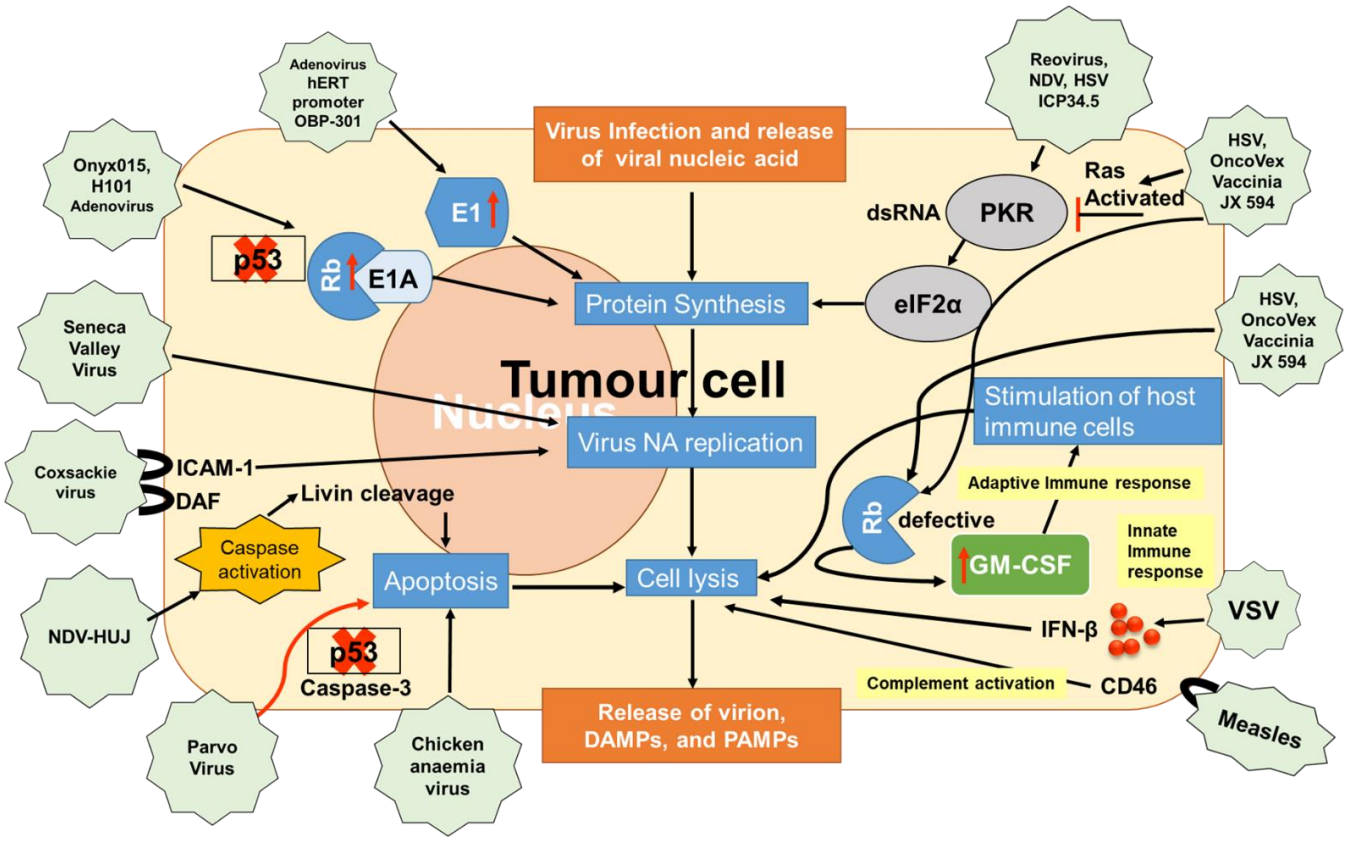

Figure 1.3. The mechanisms of action of oncolytic viruses adapted from Fountzilas et al., 2017 (59). Oncolytic viruses (natural or genetically modified) exploit favourable conditions provided within tumour cells to promote viral genome replication, transcription, and egress of viral particles. Viruses such as Seneca valley virus, Coxsackie virus, NDV etc. induce cancer cell death by active viral replication leading to substantial stress on host cellular machinery and caused direct cell death. Genetically engineered viruses such as Onyx015, HSV1 etc. use specific pathways like the p53 pathway and induce cell death. Virus replication and release result in activation of pathogen-associated molecular patterns (PAMPs) like viral DNA, ss RNA, ds RNA, and viral glycoproteins which are recognised by pattern associated receptors (PRRs) such as RIG-I, TLR3, and TLR5, which then activate type-I IFN pathways. Stimulation of IFNs induces caspases and cause cell death. Damage-associated molecular patterns (DAMPs) like calreticulin and heat shock proteins (HSPs) also released as a result of viral replication. PAMPs and DAMPs together activate innate immune responses and adaptive immune responses, ultimately resulting in immunogenic cell death. By and large, all oncolytic viruses-mediate tumour cell lysis by first direct cell death pathways activated by caspases and second by indirectly enabling the immune system.
NA-Nucleic acid, DAF–Decay accelerating factor, GM-CSF-Granulocyte monocyte-colony stimulating factor, HSV – Herpes Simplex Virus, hTERT–Human telomerase, ICAM-1–Intercellular adhesion molecule-1, ICP–Infectious cell protein, IFN-β-Interferon beta, NDV–Newcastle Disease Virus, VSV–Vesicular Stomatitis Virus.

A distinct characteristic of an OV is to establish a lytic cycle either by naturally manipulating inherent tumour weaknesses or by genetic modification. Different OVs utilise various ways to enter the cancer cell, determining the targeted tumour-selective replication. For example, measles virus uses CD46 surface receptor, NDV-HN protein binds to sialic acid conjugates, Coxsackievirus uses intercellular adhesion molecule 1 (ICAM-1; also known as CD54) and decay-accelerating factor (DAF; also known as CD55), HSV-1 uses the herpesvirus entry mediator (HVEM) and selected nectins for cell entry **(Table 1.2)**. Also, tumour-specific oncotropism precisely can be achieved by means of genetic modifications for instance adenovirus Ad5/3-Δ24 was modified to bind to the integrins that are overexpressed on ovarian cancer cells (60), and ICP 34.5 deleted HSV-1 expressing a 68-amino acid fragment of US11 containing a novel proline-rich basic RNA binding domain, which inhibits PKR activation and results in cell death of tumour cells (61). **Figure 1.3** and **Figure 1.7** illustrate the mechanisms of action of oncolysis broadly shared by most oncolytic viruses on a primary basis. The mechanisms of NDV-induced oncolysis are discussed in length in **section 1.11.** of this chapter.

Genetically engineered replication restrictive ICP34.5 deleted HSV-1, modified adenoviruses, such as Onyx015, H101, and naturally occurring parvovirus exploit pro-apoptotic p53 tumour suppressor protein. Modified viruses developed by eliminating p53 binding viral proteins such as E1B in case of adenoviruses, preferentially replicate in p53-deficient tumour cells (26). Adenovirus KH901 express E1A (a viral protein that inhibits the cell cycle) regulated under the human telomerase reverse transcriptase (hTERT) promoter. The hTERT abundantly expresses on cancer cells, which assures selectively higher virus replication in the cancer cells (26). Another example of promoter-controlled virus replication is CG0070 oncolytic mutant of adenovirus, where E1A expression is regulated under E2F1 promoter, which favours viral replication in Rb-defective cells. In healthy cells, E2F1 inhibits Rb expression results in the inhibition of viral E1A expression restricting to the cancer cells only (26). Vaccinia growth factor (VGF) protein of vaccinia virus binds to EGFR receptors to induce RAS signalling pathways, which results in the activation of cell proliferation increase in thymidine kinase (TK) production; which promote virus replication in infected cells. However, deletion of VGF restricts vaccinia virus replication only to the cancer cells showing anomalous EGFR-RAS regulation (26).

1.7. Potential limitations of oncovirotherapy

A plethora of natural as well as genetically modified viruses has been reported as potential OV candidates. However, genetically modified HSV-1, adenoviruses, and VV are in most ongoing clinical trials. Genetically modified viruses have significant advantages in providing efficient oncolysis and stronger antitumour immune responses than their natural wild-type counterparts. However, there are disadvantages of genetically engineered viruses in terms of the spread of virus compromised as a result of the deletion of pathogenic elements in mutant viruses. For example, HSV-1 does not spread from cell to cell naturally to cause viraemia. Hence, oncolytic HSV-1, like T-VEC and G47Δ, are best administered intratumorally, and intravenous delivery may not be preferred. However, the phase III study of T-Vec in melanoma patients at advanced stages, with local intralesional injections of oncolytic HSV-1 have shown promotion of abscopal antitumour immunity at remote untreated lesions through induction of systemic antitumor immunity and prolonged survival (62). It has also been demonstrated that GM-CSF expression does not increase the efficacy of oncolytic HSV-1, except IL-12 expression, in immunocompetent mouse tumour models. So, it could be possible that the systemic effect via antitumor immunity is the outcome of HSV-1 infection itself and not GM-CSF effect (63).

Another main concern of oncolytic virus therapy has been the presence of pre-existing immunity against OVs, which can reduce the efficacy of oncovirotherapy. Naturally occurring viruses producing viraemia are likely to be inactivated by neutralising antibodies; thus, intravenous administration for such viruses may be inadequate in previously OV vector vaccinated patients. An adverse effect of circulating neutralising antiviral antibodies has been reported in an oncolytic measles virus (MV-NIS) clinical trial with multiple myeloma patients (64). In this dose-escalation study, a very high dose of 10^{11} TCID50 was required for intravenous infusion to show efficiency with MV-NIS (64). Preclinical research in the tumour-bearing immunocompetent murine model, reovirus intravenous administration has resulted in recurrence of tumours within three weeks after injection, which is explained by augmented anti-reovirus antibody titres in the serum. In the phase-I clinical trial, data have shown the presence of maximum neutralising anti-reovirus antibody titres were attained by 7^{th} day in 36% (12/33) of patients, and by 14^{th} day in 75% (20/33) of patients (64).

However, this problem has been addressed by other researchers in case of modified adenoviruses; it is reported that well-tolerated oral doses of adenovirus permitted the repeated adenovirus-directed gene transfer despite the presence of a residual antibody titer from previous adenoviral exposure (65). Ricca et al. have reported that intratumoral administration of LaSota augmented the antitumoral immune response despite the preexisting neutralising antibodies in NDV immunised syngeneic mouse tumour models (66). Moreover, use of cell carriers can also improve the antitumour efficacy not only fighting the pre-existing immunity but also improves systematic delivery of OV at the distant metastatic site. Cancer stem cells such as NSCs and MSCs have demonstrated better candidates for packaging the OV because for their abilities such as intrinsic tumour-homing ability, supporting viral replication and protecting it from peripheral antiviral immunity, ability to migration towards tumour based on various chemoattractants produced in the tumour microenvironment like hypoxia-inducible factor (HIF), stromal cell-derived factor-1 (SDF-1), VEGF and urokinase plasminogen activator (uPA) in glioma cells (67). Above mentioned approaches have explained the strategies of enhancing the efficiency of OV-mediated cancer therapy in various types of cancers and viruses.

1.8. NDV as an oncolytic virus

1.8.1. Introduction to NDV

Newcastle disease virus (NDV) is an economically important poultry pathogen causing Newcastle disease (ND), which is prevalent in many countries. NDV is an avian pathogen and known to infect over 250 bird species (68). Doyle named NDV in 1926 as a highly pathogenic disease in chickens at a farm near Newcastle-upon-Tyne in England (69). NDV was previously known as avian paramyxovirus type-1 serotype (APMV-1). Now it is classified as a member of genus *Orthoavulavirus* in the order Mononegavirales, family Paramyxoviridae, subfamily Avulavirinae (70). NDV, like other paramyxoviruses, has a non-segmented, single-stranded, negatively-charged, 15.186 kb long RNA genome encoding six essential genes expressing nucleocapsid protein (NP), phosphoprotein (P), matrix protein (M), fusion protein (F), haemagglutinin-neuraminidase protein (HN), and large RNA-dependent RNA polymerase (L) (71) **(Figure 1.4)**.

Virions of paramyxoviruses range from 150 to 250 nm in diameter and are pleomorphic, often filamentous in shape (72). Virions are enveloped within a lipid membrane derived

from the host cell plasma membrane. Two transmembrane glycoproteins are expressed on the viral envelope; the HN and F proteins. A non-glycosylated membrane M protein lies underneath the envelope. The ribonucleotide protein (RNP) replication complex comprises viral nucleocapsid that includes the NP, P and L proteins encapsidating the (-) ssRNA genome. Each gene in NDV genome is tagged by conserved gene start (GS), and gene end (GE) sequences and two genes split by a conserved intergenic sequence (IGS), which regulates mRNA transcription (73).

NDV has been classified into three pathotypes based on the clinical signs of the disease in chickens: avirulent or non-pathogenic (lentogenic), moderately pathogenic (mesogenic), and highly pathogenic or virulent (velogenic) (74). The velogenic strains of NDV have polybasic amino acids (R-X-K/R-R↓F) in the F protein cleavage site, which is a preferred recognition site for furin and furin-like proteases. Cleavage of F0 protein into F1 and F2 subunits, by the ubiquitous intracellular host cell proteases, and is is an essential event in NDV replication to facilitate the virus replication in the tumour microenvironment (75).

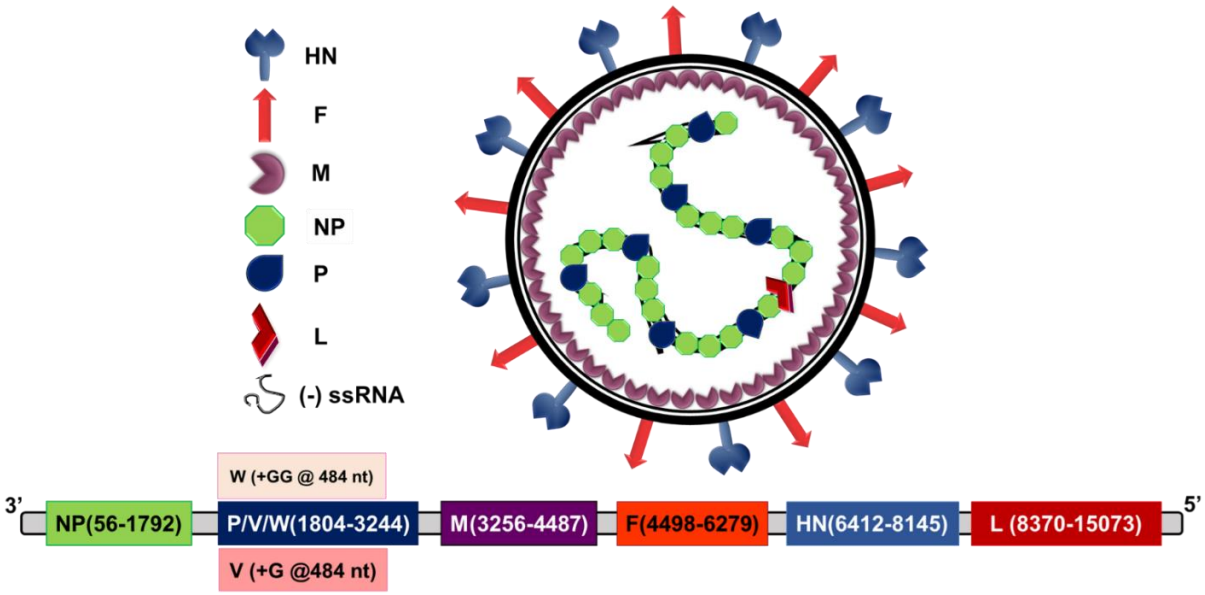

Figure 1.4. Schematic diagram of NDV structure and its genomic make-up, adapted from Ganar et al., 2014 (73). The viral envelope contains two transmembrane glycoproteins; the haemagglutinin-neuraminidase (HN) and the fusion (F) proteins. Beneath the envelope lies a non-glycosylated membrane protein called matrix (M) protein. The viral nucleocapsid consists of viral RNA and the replication complex proteins that include the nucleocapsid (N), phosphoprotein (P) and large RNA-dependent RNA polymerase protein (L). NDV genome comprises different transcriptional units encoding six essential proteins; NP, P, M, F, HN and L proteins. The RNA genome contains flanking 55 nucleotides long leader at 3 prime and 114 nucleotides long 5 prime trailer extragenic regions. Two accessory proteins V and W are derived from mRNA editing at 484th position of the P mRNA by adding non-template G residues.

1.8.2. NDV genotypes

There are two classifiaction systems are used worldwide: first one is suggested by Aldous, where he groups NDV into 6 lineages and 13 sublineages and later addition of 3 more sublineages (76). Second classifiaction system divides NDV into two clades: class I and class II. Class I clade is further is divided into 9 genotypes (1-9). Class II clade is divided into 11 genotypes (I-XI), and genotypes I, II, VI, and VII sub-divided Ia and Ib, II and IIa, VIa through VIf, and VIIa through VIIh (77). There is no consensus on classification of NDV and both systems are used for classification and generates confusion (77). All NDV strains are classified into genotypes/lineages based on NDV genome size and sequences of F and L gene sequences (78).

1.8.3. NDV life cycle

NDV infects cells and replicates in the host cell cytoplasm, where NDV genome completes replication and transcription. NDV proteins and genomic RNA are packaged into virion particles and egress from cells by a budding mechanism, and upon release, NDV virions infect neighbouring cells. NDV shares common lifecycle with other paramyxoviruses such as sendai virus, measles, mumps, canine distemper virus etc. (79).

NDV entry into host cells: NDV enters inside host cells with the help of two glycoproteins, HN and F, are expressed on NDV envelope. NDV-HN proteins bind to sialyl glycoconjugate receptors on the host cells (80, 81). NDV-HN protein interacts efficiently with α-2, 3 and α-2, 6 N-linked sialic acid conjugates (82, 83). The HN protein and cell receptor tethering activate the F protein, which facilitates fusion activity for viral entry into host cells (84). NDV also is known to exploit alternate caveolae-mediated endocytic pathways (85) and clathrin-mediated micropinocytosis routes (86) to enter host cells through pH-dependent mechanisms. Once NDV attached to host cells, RNP complex is released into the host cell cytoplasm and negative-sense RNA gets transcribed into positive-sense mRNA, which translates all viral proteins utilising the host cell machinery.

NDV transcription and replication: The RNP complex is required for NDV transcription and replication, which consists of three different stages of viral RNA synthesis by viral RNA polymerase. First, in the early infection stage, transcription results in the synthesis of 3 prime leader untranslated region followed by transcription of the NP gene. The NP mRNA translated into protein, NP accumulation switches from

transcription to the replication. Secondly, viral RNA polymerase recruits NP proteins to encapsidate nascent genomic RNA (-vRNA). Viral RNA polymerase aborts transcription of encapsidated -vRNA, and synthesise antigenomic RNA (+vRNA), which serves as a template for replication viral RNA (87). Finally, secondary transcription of progeny genome results in abundant mRNA transcription of viral genes (88). Viral RNA polymerase modifies all six mRNAs to have a 5 prime methyl cap and 3 prime polyA tail (89). Viral RNA polymerase uses conserved GS sequence to start translation of 5 prime capped RNA and terminates at conserved GE sequence of 3 prime polyadenylated site of all viral mRNAs encoding proteins (89). The viral RNA polymerase uses start and stop mechanism to transcribe all NDV genes and maintain the abundance of all mRNA in a gradient manner from 3 prime NP gene to last 5 prime L gene (90). Both genomic (-vRNA) and antigenomic (+vRNA) viral RNA contains cis-acting regulatory untranslated 3 prime leader (55 nucleotides) and 5 prime trailer (114 nucleotides) sequences, which are involved in transcription, replication, and packaging of genomic and antigenomic RNA (90). The NDV replication briefly illustrated in **Figure 1.5**.

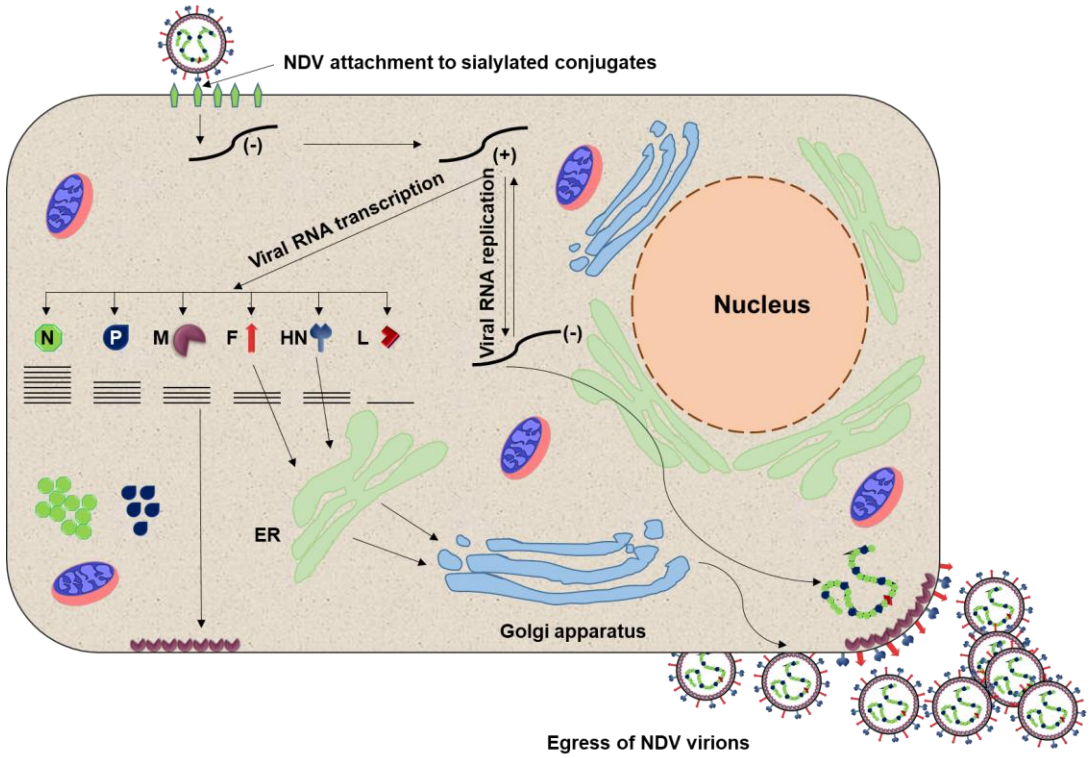

Figure 1.5. Schematic representation of NDV replication, adapted from Ganar et al., 2014 (73). NDV enters the host cell via sialic acid receptors tethering to NDV HN protein and fusion facilitated by F protein. The ribonucleotide complex of N, P, and L proteins with negatively charged RNA released inside the cell cytoplasm, where viral RNA genome gets transcribed and replicated by viral RNA-dependent RNA polymerase (L) protein, where exploiting host cellular machinery all viral genes get translated. Once NP protein transcribed, it activates the anti-genome gets transcribed in the negatively charged RNA genome followed by RNP complex formation and virion packaging resulting in the NDV virion egress from host cells.

mRNA editing of the NDV P gene: NDV expresses two non-structural accessory proteins by mRNA editing of the P gene at nucleotide position 484 in the preserved editing site (3 prime-UUUUUCC-5 prime). P gene uses non-template guanine residues (G) viz. V (+G) and W (+GG) during transcription, resulting in a shift of the respective open reading frame, where P, V, and W proteins share the amino-terminal but have a distinctive carboxy-terminal end. Mebatsion et al. (2001) have reported the proportions of P and edited P mRNAs in NDV-infected chicken cells: 68% of P-encoding mRNA, 29% of V-encoding mRNA, and 2% of W-encoding mRNA (91). Sometimes more than two G residues insertions leading to the supplementary amino acid insertion reported in chicken cells (60, 61). The V protein plays roles in NDV virulence as it antagonises IFN responses (62, 63). The carboxy-terminal of V protein inhibits type-I IFNs (IFN-α/β) signalling by targeting signal transducer and activator transcription factor 1 (STAT-1). The C-terminal domain of V protein interacts with melanoma differentiation-associated protein 5 (MDA5) to impede IFN-β response (64). However, the function of the W protein remains unclear.

Egress of NDV from infected cells: Transcribed viral mRNAs translate to the proteins; NP, P, L proteins and genomic RNA forms RNP complex and translocate to the site of packaging in the host cells. M proteins bind to the host cell membrane and promote cell membrane deformation. M proteins serve as an adapter link between viral proteins and assembly in the host cell. NDV glycoproteins HN and F translocate through host cell plasma membrane using their transmembrane domains and promotes complete viral packaging. NDV virions egress from the site of packaging by a budding mechanism and use neuraminidase activity of HN protein to cleave virion particles from the host cell receptors **(Figure 1.5)** (88, 92).

1.9. Oncolytic NDV strains

In 1957, J. Sinkovics first time reported the oncolytic potential of NDV, where NDV coated ascitic cancer cells inoculated in the abdominal cavity of mice lost their viability (93), stating the non-pathogenicity and oncolytic possibility of naturally occurring NDV. Soon after in 1965, Cassel and Garrett used mesogenic strain 73T of NDV. The 73T had been attenuated by 73 passages *in vitro* and 13 passages *in vivo* in murine Ehrlich ascites tumour cells. The antineoplastic nature of 73T was confirmed in Ehrlich ascites carcinoma of the mouse and HeLa, human cervical cancer cells (94). In 1980, Hungary licensed attenuated NDV-H (referred to as MTH-68/H-more than hope/Hungarian strain)

to treat cancer patients for the very first time (21). Many other lentogenic (non-pathogenic) strains such as Hitchner B1, LaSota, Ulster, V4UPM, MTH-68/H, and NDV-HUJ (Hebrew University Jerusalem) and mesogenic (moderately pathogenic) strains suh as PV701, and 73T and velogenic (highly pathogenic) AF2240 have been used in various preclinical and clinical studies.

1.10. Important oncolytic properties of NDV

1.10.1. Tumour selective replication

Tumours provide a favourable environment for NDV and other virus replication and spread due to the crippled antiviral responses, weaker IFN sensitivity, weaker expression of IFN receptors, and resistance to cell death pathways (95). Tumour selective replication and cell death induction by various strains of NDV conclusively demonstrated in many human and murine cancer cells (96, 97). NDV-HN protein interacts efficiently with α-2, 3 and α-2, 6 N-linked sialic acids conjugates (82, 83) expressed by most of the cells to infect and replicate, which make it easy to target all types of cancer cells. Fusion activation occurs after F protein interaction with the stalk region of HN protein of NDV while egressing new virions resulting in syncytium formation in infected cells, which helps viral spread within the tumour. Enhanced NDV-mediated cell lysis and up to two-log fold improved virus replication was reported in anti-apoptotic Bcl-xL protein-expressing A549 and 293T cells. Overexpression of Bcl-xL protein strikingly increased NDV-induced apoptosis as an outcome of better NDV replication with the induction of type-I IFN in A549 cells, proving selective tumour replication in apoptosis-resistant cells (98).

Similarly, Lazar et al. confirmed that Livin, an inhibitor of apoptosis (IAP) family protein-expressing chemo-resistant primary melanoma cells overcame the resistance by non-lytic NDV-HUJ virus replication. NDV-induced apoptosis in melanoma cells was associated with the cleavage of anti-apoptotic Livin to pro-apoptotic tLivin protein independent of type-I IFN pathways (99).

Type-I IFNs are known to diminish viral replication, and their antiviral action lead to activation of a complex array of cellular processes. Cellular response to IFN launches antiviral eminence through the expression of IFN-stimulated genes (ISGs) against numerous family of viruses (100, 101). Like many other viruses, NDV evades the immune system using its accessory V protein in its natural hosts, where V protein

interferes with JAK-STAT mediated type-I IFN signalling pathways (102, 103). However, in mammalian and rodent cells, the escape mechanism does not work. The expression of ssRNA and dsRNA intermediates of NDV is recognised (as PAMPs) by TLR3 and also by RIG-I like receptor (RLR), and activates IRF-3, IRF-7, and IFN-β antiviral products to diminish viral replication in healthy cells (104-106). Most cancer cells lack strong antiviral signalling responses and have resistance to the IFN-stimulated apoptosis. Krishnamurthy et al. investigated the differential response of NDV in primary human fibroblast cells and HT1080 fibrosarcoma cells. NDV replicated better in HT1080 cells than human skin fibroblast cells regardless of the IFN-β pre-treatment confirming the role of unresponsive antiviral system, where the decrease in phosphorylation of STAT-1 and STAT-2 proteins along with downregulation of ISG3 gene was reported (104). NDV showed improved susceptibility to IRF-3, and IRF-7 genes deleted murine macrophages. However, IRF-3 knockout (KO) cells supported better viral replication than in IRF-7 KO and normal macrophages. IRF-3 KO cells expressed lower levels of basal NDV-induced RIG-I expression than IRF-7 KO and normal murine macrophages (107).

NDV-73T had shown thousand-fold increased susceptibility to HT1080 cells overexpressing N-Ras and H-Ras oncogenes (108). The elevated expression of these oncogenes potentially related to sialyl glycoconjugate expression, and hence the sensitivity to NDV can be explained (109, 110). The investigation of NDV sensitivity in HaCaT multistage skin carcinogenesis model revealed the requirement of oncogenic Rho GTPase Rac1 protein expression to sustain viral replication (111). The dynamic relationship between the actin cytoskeleton and Rho GTPases, including Rac1, Cdc42, and Rho, have been associated within the establishment of cell-cell contacts and cell-matrix interactions (112), which is known to be exploited by different DNA and RNA viruses including paramyxoviruses such as SeV and NDV to promote virus replication, assembly and egress (113).

1.10.2. Safety profile

The high levels of safety profile is explained in NDV-infected patients by various factors NDV being avian pathogen: e.g. an absence of pre-existing antibodies against NDV in human, absence of recombination for gene exchange, cytoplasmic viral replication, lack of viral RNA integration into host cell genome, non-pathogenic nature in humans, higher tolerable doses tested in phase I/II clinical trials, and mild side effects observed in immunocompromised patients.

Recombination has not been detected in NDV. In last 50 years, study has revealed the difference in the NDV strains are typically results of point mutations in the F, HN, and M genes (114). NDV replicates in the cell cytoplasm **(Figure 1.5)**, the viral genome does not integrate into the host genome, and it replicates regardless of host genome replication. Unlike conventional chemotherapy and radiotherapy, NDV can replicate in non-dividing, resting, radiation and drug-resistant, hypoxic cancer cells. Pecora et al. demonstrated tolerance of intravenously administered PV701 attenuated mesogenic strain of NDV up to 1.2 x 10^{10} PFU/m^2 in advanced solid tumours in phase I clinical study, where patients displayed mild flu-like symptoms developed only after first injection (115).

Further, the PV701 intravenous dose optimised for administration, where maximum tolerable dose (MTD) is reported up to 12 x 10^{10} PFU/m^2 of solid tumours in advanced cancers and dose as high as 4 x 10^{12} PFU/m^2 tolerated via the intratumoral route (115-117). NDV being an avian pathogen cause only mild flu-like disease symptoms such as eye infections, usually consisting of unilateral or bilateral reddening, excessive lachrymation, and oedema of the eyelids, conjunctivitis and sub-conjunctival haemorrhage in high risk and immunocompromised individuals only. Most of the human population are reported to be NDV seronegative (116, 118).

1.10.3. Immuno-stimulatory properties

NDV infection and replication in favourable tumour microenvironment forms syncytium due to the expression of viral HN and F glycoproteins and have domino effects, inducing cell death in tumour cells. For instance, NDV causes immunogenic cell death which leads to translocation of danger signals like HSPs, calreticulin, and viral glycoproteins HN/F to the plasma membrane. Damage-associated molecular patterns((DAMPs) and pathogen associated molecular patterns (PAMPs) then activate the antiviral responses post oncolytsis by triggering the innate immune system, cytokines, and adaptive immune responses. NDV activates innate immune responses as 5 prime phosphate of viral ss RNA and ds RNA intermediates recognised by RIG-I (105, 119) and TLR3 (120). NDV-HN proteins are known to have immunostimulatory properties such as induction of IFN-α and tumour necrosis factor-related apoptosis-inducing ligand (TRAIL) in human blood mononuclear cells (121) as well as increase the adherence of cancer cells to leukocytes and induce adaptive immune response participation by T-cell co-stimulation (122-124).

1.11. Mechanisms of NDV-induced oncolysis

NDV induces cancer cell death by two mechanisms (direct and indirect), as discussed in detail below. The mechanisms of NDV-induced oncolysis are also schematically represented in **Figure 1.7**.

1.11.1. The direct mechanism of NDV-induced oncolysis

NDV kills cancer cells as a direct consequence of virus replication followed by the hijacking of host cellular machinery, causing stress leading to the ultimate cell death. NDV proteins are known to play a crucial role in participating activation of programmed cell death in natural host (avian) cells as well as in mammalian cancer cells. NDV is reported to induce cytotoxicity in chicken embryos by activating the apoptotic pathways (125), and studies in chicken embryo fibroblast (CEF) cells have confirmed that HN protein causes programmed cell death (126). Characterisation of AF2240 NDV strain protein sequences revealed the pro-apoptotic Bcl-2 homology-3 (BH-3) domain-like homology with M, F, and L proteins. HeLa cells transfected with plasmids expressing AF2240-M and AF2240-F proteins showed apoptotic cell death (127). The interaction of AF2240-M protein with BH-3 domain of Bax protein was confirmed by co-immunoprecipitation. Moreover, deletion of BH-3 like region in M protein obliterated the M interaction with the Bax protein and revealed that M protein of AF2440 strain played a role in triggering cell death in HeLa cells. However, AF2240-F protein have not demonstrated any interaction with Bcl-2 family proteins such as Bax, Bad, or Bcl-XL (127).

Furthermore, NDV-induced apoptosis has been reported in several studies of various mammalian cell cultures such as Vero, HeLa, and PC12 cells (128-131). In 2006 Elankumaran et al. confirmed that human cancer cells originated from ecto, meso, and endodermal sites, were prone to NDV-induced oncolysis due to activation of both mitochondrial/intrinsic apoptotic pathway and death receptor/extrinsic apoptotic pathway (132). Apoptosis is a type of programmed cell death and can be triggered by two signalling pathways: extrinsic (death receptor) pathway and intrinsic (mitochondrial) pathway, illustrated in **Figure 1.6**. The extrinsic pathway is initiated by oligomerisation of death receptors such as FAS, CD95 ligand (CD95L), or tumor necrosis factor receptor (TNFR) by death signals such as CD95, TNF-α, or TRAIL. Death receptor activation lead to the recruitment of adaptor proteins (Fas-associated death domain (FADD)/TNFR-1 associated death domain (TRADD)) and pro-caspase-8/10, which activates initiator caspase-8/10. Initiator caspase-8/10 activates executioner caspase-3/7 to execute apoptotic cell death (133).

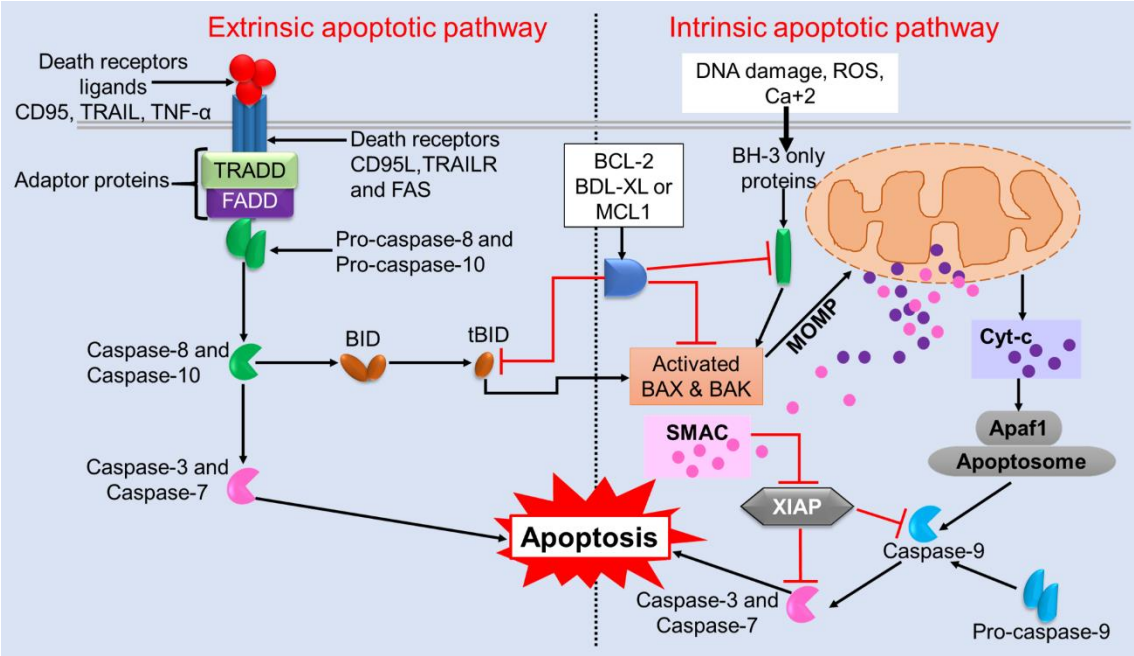

Figure 1.6. An illustration of apoptotic signalling pathways, adapted from Galluzzi et al. (133) and Baig et al. (134). Apoptosis can be induced by two patways: extrinsic (death receptor) pathway and intrinsic (mitochondrial) pathway. The extrinsic apoptotic pathway is induced by the activation of death receptors of the tumor necrosis factor (TNF) receptor (TNFR) superfamily such as CD95 (APO-1/Fas) or TNF-related apoptosis-inducing ligand (TRAIL) receptors (TRAILR) by CD95 ligand (CD95L) or TRAIL. Activation of death receptors result to recruitment of adaptor proteins e.g. Fas-associated death domain (FADD)/TNFR-1 associated death domain (TRADD) and pro-caspase-8/10, which activates pro-caspase-8/10 to caspase-8/10 to initiate apoptosis. In contrast, the intrinsic apoptotic pathway is induced mitochondrial outer membrane permeabilization (MOMP) and release of cytochrome-c (Cyt-c), inducing factor (AIF), or second mitochondria-derived activator of caspases (SMAC) in the cytoplasm. Release of Cyt-c in cytoplasm initiates activation of caspase-3/7 via formation of the apoptosome complexcontaining Cyt-c/Apaf-1/caspase-9. The SMAC promotes caspase activation by blocking X-linked inhibitor of apoptosis protein (XIAP). Both pathways are interconnected by BH3-interacting domain death agonist (BID) BH3-only protein, where caspase-8/10 truncate BID to tBID to activate BAX and BAK proteins to induce MOMP resulting in apoptotic cell death.

In contrast, the intrinsic (mitochondrial) pathway is induced by various mitochondrial stress signals such as reactive oxygen species (ROS), endoplasmic reticulum (ER)-stress, calcium (Ca2+), DNA damage etc. The intrinsic apoptotic pathway is vastly regulated by BCL-2 family proteins and control BH-3 only proteins, which stimulate BAX and BAK pro-apoptotic effector potiens. Activated BAX and BAK disrupts mitochondrial outer membrane potential (MOMP) to release cytochrome-c (Cyt-c), inducing factor (AIF), or second mitochondria-derived activator of caspases (SMAC) in the cytoplasm. The release of Cyt-c in cytoplasm, activates executioner caspase-3/7 to form apoptosome formation comprising of Cyt-c/Apaf-1/caspase-9. The release of SMAC in cytoplasm inhibits apoptosis inhibitor, X-linked inhibitor of apoptosis protein (XIAP) and

promote caspase-3/7 activation to execute apoptosis. Executioner caspase-3/7 and BH3-interacting domain death agonist (BID) BH3-only protein connects extrinsic and intrinsic apoptotic pathways via initiator caspase-8/10 mediated truncation of BID to tBID and activation of BAX and BAK effector pro-apoptotic proteins to disrupt MOMP (134).

Upon NDV infection in human tumour cells, TRAIL and TNF-α were secreted to fight the infection activating caspase-8 to trigger the extrinsic apoptotic pathway. However, in all human cancer cell lines used in the study, NDV-induced cytotoxicity was found to be independent of caspase-8 activation. Consequential cell demise was triggered because of caspase-9 activation in response to the loss of mitochondrial membrane potential, highlighting the instigation of the intrinsic apoptotic pathway leading to the oncolysis. Activation of apoptotic pathways was independent of type-I IFN-α induction, as apoptotic cell death upon NDV infection was also confirmed in IFN-α-defective cancer cells (132). The NDV MTH-68/H strain was reported to induce apoptotic cell death in infected PC12, rat pheochromocytoma cells in a dose-dependent manner independent of mitogen-activated protein kinases (MAPK) pathway participation (129). Fábián et al. (2007) reported activation of caspase-3 and -12 in MTH-68/H infected PC12 cells and independent of caspase-8 and -9. In the same study, infection of MTH-68/H in rat PC12 and human HeLa cells have confirmed the activation of virus-induced endoplasmic stress (ER) pathway, where activated caspase 3 and 12 increased the phosphorylation of eukaryotic Initiation Factor 2 (eIF2) located on ER through PKR-like endoplasmic reticulum kinase (PERK). The increased phosphorylation inactivated eIF2 and inhibited protein synthesis and led to cell death (135).

Bian et al. (2011) reported that mesogenic(moderately pathogenic) strain Beaudette C (BC) and velogenic (highly pathogenic) strain FMW induced more apoptotic cell death in A549 cells than lentogenic LaSota strain (136). However, all three strains activated the MAPK in all three associated pathways; ERKs (extracellular-signal-regulated kinases), JNKs (Jun amino-terminal kinases), and p38/SAPKs (stress-activated protein kinases) and downregulation of PI3K-Akt pathway in A549 cells. This study revealed that NDV induced apoptosis in A549 cells was caspase 8/9 and p38 MAPK dependent (136). Nevertheless, the exact mechanism of oncolysis has remained unclear. In this same study, Bian et al. could not reproduce phosphorylation of eIF2a and activation of caspase 12 in FMW strain of NDV infection in PC12 cells (136).

In several human cancer cells such as MCF-7, HeLa, and U373, lentogenic (non-pathogenic) NDV strain MTH-68/H infection triggered p53-independent apoptotic cell

death by activating the ER stress-mediated mechanism (135). There are discrepancies in the mechanisms described in NDV-induced apoptosis in different studies. For example, PC12 cells showed induction of apoptosis independent of the stress-inducible JNK pathway and the p38 pathway when infected with MTH-68/H (129, 137). However, in A549 cells LaSota, BC, and FMW strains of NDV induced apoptosis by activating caspases 8/9 and p38 pathway.

Recently the role of RNA viruses such as hepatitis C virus (HCV), influenza A virus (IAV), and retroviruses HIV-1 and human T-cell lymphotropic virus 1 (HTLV-1) was studied by Ryan et al. (2016) in the activation of DNA damage response (DDR) pathways (138). It is reported that RNA viruses irrespective of their diverse tropism and replication site in the infected cells induced DDR stimulated apoptosis, instigation of inflammatory responses, and promotion of genetic instability leading to the increased risk of tumorigenesis (138). For example, the core protein or nonstructural protein 3 (NS3) of HCV have been shown to activate the inducible nitrous oxide synthase (iNOS) and augmented release of ROS (138, 139). Accumulation of iNOS and ROS are known to induce double-stranded breaks (DSBs) in the infected cell DNA and activation of genetic abnormalities due to non-homologous end joining (NHEJ) repair involvement, said to be associated with HCV-driven oncogenesis in HCV-infected cells (138). Whereas 14 kDa viral protein R (Vpr) of HIV-1 is known to induce DNA damage by arresting cell cycle in G2 phase, and the activation of the ataxia telangiectasia mutated (ATM)-CHK2 pathway induce apoptotic cell death upon infection (138). Saeed et al. have reported ultramicroscopic observation of infected human glioblastoma multiforme (GBM) cells with AF2240, a Malaysian velogenic strain of NDV (140). In this study, Saeed et al. analysed the cellular DNA content in infected cells and reported the loss of DNA in treated cells in G1, S and G2/M phases of the cell cycle. Disruption of the cell cycle was reported to induce apoptotic cell death as indicated by typical features such as morphological changes of apoptosis, including shrinkage and blebbing of the membrane (140). The study of velogenic NDV AF2240 strain infected GBM cells has suggested the role of DDR in NDV-induced oncolysis.

Inconsistencies in these findings are explained by the differences between the cell lines, NDV strains (summarised in **Table 1.4**) and experimental designs. It can be postulated that NDV induces oncolysis in different transformed cells of various origins/sites and mammalian species differently in a completely *de novo* manner which is yet to be explored.

Table 1.4: Summary of NDV-induced cell death in different cell lines

Sr. No.	Cell line	Description	Type of NDV-induced cell death	References
1	PC-12	Rat pheochromocytoma cells	MTH-68/H (lentogenic/non-pathogenic strain) is reported to induce apoptosis independent of mitogen-activated protein kinases (MAPK) pathway.	(129)
2	A549	Human lung adenocarcinoma cells	Beaudette C (mesogenic/moderately pathogenic strain) is reported to induce apoptosis dependent of caspase 8/9 and p38 MAPK dependent.	(136)
3	Vero	Kidney epithelial cells from African green monkey	Vero cell-adpted NDV is reported to induce apoptosis through extrinsic and intrinsic apoptotic pathways.	(131)
4	U251	Human glioblastoma astrocytoma cells	Beaudette C (mesogenic/moderately pathogenic) is reported to induce autophagic cell death.	(141)
5	GL261	Murine glioma cells	Hitchner B1 (lentogenic/non-pathogenic strain) is reported to induce immunogenic cell death (ICD) independent of caspase signalling.	(142)
6	HeLa	Human cervical adenocarcinoma cells	MTH-68/H (lentogenic/non-pathogenic strain) is reported to induce p53-independent endoplasmic reticulum stress-mediated apoptosis.	(135)
7	MCF-7	Human mammary tumor MCF-7 cell line	AF2240 (velogenic/highly pathogenic strain) is reported to induce apoptosis.	(143)
8	DT6606PDA	Murine pancreatic adenocarcinoma cell lines	NDV R75/98 strain isolated from field is reported to activate NK cells mediated the CD4+ T cell infiltration, and CD8+ T-cell mediated cytotoxicity.	(144)
9	Panc02			

1.11.2. Indirect mechanism of NDV-induced oncolysis

Apart from straightforward NDV-induced cell death as a result of virus replication, NDV induces oncolysis by activating the innate and adaptive immune system at the site of infection and virus spread. In various studies, different non-pathogenic NDV strains activated murine macrophages by secreting adenosine deaminase (ADA), iNOS, acid phosphatases, and lysozymes leading to the upregulation of nitrous oxide (NO) and TNF-α causing cytotoxicity in both *in vitro* and *in vivo* models of study (145-148). NDV Ulster strain activated human monocytes by triggering TRAIL expression in the macrophages regardless of viral replication. NDV-activated macrophages induced TRAIL-mediated cytotoxicity in human cancer cells (149). NDV-HN protein alone was

capable of activating TRAIL and IFN-α in human peripheral blood mononuclear cells (PBMCs) highlighting that viral replication is not necessary to instigate the innate immune system (121). Ni et al. have also shown that NDV-HN plasmid DNA-based vaccination alone stimulated anti-tumour activity in a prophylactic mammary carcinoma DA3 tumour mouse model by inducing IFN-α, diminishing the tumour growth (150). Anti-tumour events resulted in increased NK cell infiltration and decreased infiltration of myeloid-derived suppressor cells (MDSC) inside tumour microenvironment after vaccination with HN plasmid DNA (150).

Ulster and MTH-68/H NDV lentogenic (non-pathogenic) strains have shown increased expression of natural cytotoxicity receptors NKp44 and NKp46, and not NKp30 upon infection in melanoma and other carcinoma cells (151). NDV-HN proteins were associated with NK cell activation leading to the secretion of IFN-γ and TNF-α, which contributed to NDV antineoplastic properties (151). NDV-HN protein is also known to modify cell adherence strength and lymphocyte interactions with T-cell co-stimulation along with antigenic peptide presentation to CTL (122-124).

NDV replication in human tumour cells have been shown to induce IFN-β and chemokines such as RANTES (regulated on activation, normal T cell expressed and secreted, which is also known as CCL5) and IFN-γ-inducible protein-10 (IP-10). Besides these chemokines, NDV is also known to upregulate adhesion molecule ICAM-I (CD54) and LFA-3 (CD58) in MCF-7 breast carcinoma cells, and to trigger cell death by apoptosis (152).

NDV infection in cancer cells triggers cell death not only by apoptotic pathways but also by inducing immunogenic cell death (ICD). NDV Hitchner B1 strain induced ICD in an orthotopic, allograft murine glioblastoma cell line GL261 model. NDV infection resulted in translocation of danger signals such as calreticulin to the plasma membrane and release of HMGB1 along with increased premelanosome protein 17 (PMEL17) cancer antigen protein expression prompting necroptotic and autophagic cell death. In an animal study, increased infiltration of IFN-γ+ T-cells was reported at the site of oncolysis (153). NDV-induced oncolysis releases various danger signals (dsRNA, IFN-α, viral glycoprotein HN, HSPs, calreticulin, HMGB1 etc.) these DAMPs and PAMPs that stimulate not only the innate immune system as discussed above, but also play a crucial role in activating the adaptive immune response. NDV-mediated cell death activates NK cells, DC, and secreted chemokines (IP-10, RANTES, IL), attracts APCs and also presents otherwise hindered TAAs-activated DC cells, CD4+, and CD8+ T-cells (154). Schwaiger et al. have shown that NDV-mediated rejection of pancreatic tumour cells

(DT6606PDA and Panc02) in a syngeneic orthotopic tumour model by activated NK cells. Activated NK cells mediated the CD4+ T cell infiltration, and CD8+ T-cell mediated cytotoxicity to avoid tumour recurrence (144). NDV Ulster strain-infected autologous primary melanoma cell lysates have shown that T-cell penetration was costimulatory receptor CD28 dependent and independent of the co-inhibitory receptor CTLA-4 and pathways involving shared ligands CD80 (B7-1) and CD86 (B7-2) (155).

Zamarin et al. reported the localised NDV intratumoural therapy in a B16 melanoma murine model to confirm the infiltration of tumour-specific CD4+ and CD8+ T lymphocytes and NDV-induced cytokine stimulation at a distant untreated tumour site without any sign of virus replication at the remote location (156).

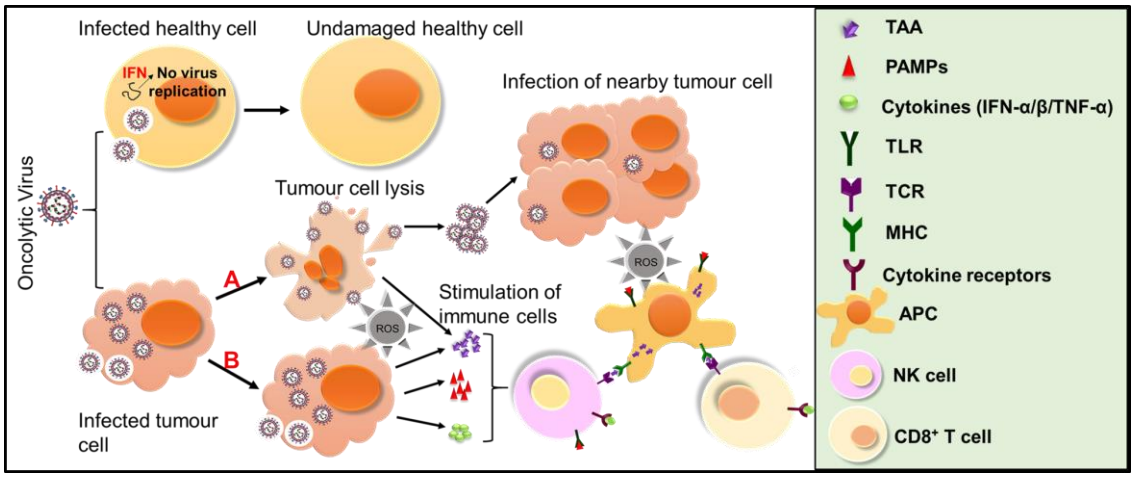

Figure 1.7. **An illustration of the oncolytic mechanisms of action of NDV, adapted from Howells et al. (2017) (157).** Cytotoxic activity of NDV in cancer cells channelled via direct (A) and indirect (B) mechanisms. The mechanisms involved in the NDV infection and replication resulting in the formation of multinucleated syncytia, activation of the extrinsic as well as an intrinsic apoptotic pathway, activation of ER stress pathway, and participation of MAPK pathways. The indirect mechanisms include secretion of proinflammatory cytokines and chemokines, which employ mediators of both innate and adaptive immune system such as NK cells, macrophages, and lymphocytes. Anti-tumour immune responses are further improved by the enhanced adhesion of leukocytes, through binding to the viral glycoproteins HN and F expressed on the surface of infected cells, by upregulation of MHC and cell adhesion molecules, which serve to activate tumour-specific T lymphocytes, and by activation of macrophages.
(Note: ROS-reactive oxygen species, TAA-tumour associated antigens, PAMPs-Pathogen associated molecular patterns, TLR-toll like receptors, TCR-T-cell receptors, MHC-major histocompatibility complex, and APC- Antigen presenting cells)

Different strains of NDV (both lentogenic/non-pathogenic and velogenic/pathogenic type) have been shown to induce virus-mediated indirect oncolysis through apoptosis, necroptosis, autophagic and immunogenic cell death in various mammal tumour cells activating type-I IFN pathways, as well as T-cell-mediated cytotoxic pathways by

releasing PAMPs and DAMPs recognised by PRR to activate NK cells, DC cells, macrophages, CD4+, and CD8+ T-cell activation (154).

1.12. Genetically modified NDV strains used in oncovirotherapy

The advent of reverse genetic engineering approaches for negative-strand RNA viruses has opened up new avenues to modify NDV genetically and allowed to underpin the efficacy of oncolytic potential of modified oncolytic modified NDV strains by inserting foreign genes (158, 159).

Hitchner B1 strain of NDV was genetically engineered by modifying the cleavage site of the F protein with polybasic F with a green fluorescent protein (GFP) to get NDV (F3aa)-GFP to improve its oncolytic potential. The oncolytic potential was tested *in vivo* in a peritoneal carcinomatosis gastric tumour mouse model bearing MKN-74 human gastric cancer cells, and cancer cells were administered with NDV intraperitoneally (IP). Insertion of the GFP made monitoring of virus replication easy. The genetically modified NDV showed oncolysis in gastric tumour cells without any sign of toxicity (160). The genetically modified NDV vector rNDV/F3aa(L289A), containing the L289A mutation within the F gene shown better fusion activity and enhanced cytotoxicity in an *in vitro* model of hepatocellular carcinoma (HCC) cells compared to the NDV (F3aa)-GFP virus (161).

Another genetically modified Hitchner B1 strain of NDV expressing pathogenic F protein showed better anti-tumour efficacy than unmodified NDV when injected intratumorally and increased survival when injected intravenously in CT26 bearing mouse model (162). Similarly, recombinant NDVs (rNDVs) generated for expressing GM-CSF, IFN-γ, IL-2, or TNF-α tested in colon carcinoma tumour models have also shown improved rNDV-mediated oncolysis (163). rNDV with IL-2 notably revealed the striking outcome of 60% improved long-term survival rate compared of 20% induced by the parental virus. Higher levels of activation of IFN-γ and presentation of CD4+ and CD8+ T-cells near the site of virus infection and lymph nodes adjacent the tumour microenvironment (163). Zamarin et al. confirmed the significant improvement in immunomodulation of malignant melanoma in a syngeneic mouse model by NDV(F3aa)-IL-2 virus leading to clearance of tumour cells in 87% (7/8) of the animals used in the study (164, 165).

A potential threat of using genetically modified NDV with the pathogenic F protein expression comes from the biosafety to the poultry and wild birds. Pathogenic strains can cause an economic burden on the poultry industry. Recombinant fusogenic NDV of Hitchner B1 strain (NDV/F3aa) had been tested in the chicken and not found pathogenic

with strong innate immune response. However, the mean death time (MDT) in embryonated hen eggs have confirmed the mesogenic profile. A detailed study recombinant fusogenic NDV in chickens essential to be considered to reduce the risks to birds in the wild before considering the potential oncovirotherapy (166).

Elankumaran et al. modified the mesogenic strain of NDV BC with a mutation in the P gene resulting in defective V protein expression (rBC-edit virus). The variation in V attenuates the pathogenic BC strain into the non-pathogenic strain. This mutated virus was reported to show restricted replication in healthy cells specifying the tumour-selective replication whereas in a human fibrosarcoma-bearing nude mouse model regressed the tumour more effectively and stimulated IFN-α via IRF-7 pathway (167).

Influenza NS1 protein is a multifunctional protein having IFN inhibitory and anti-apoptotic properties through binding to the dsRNA, an inhibition of RIG-I and PKR as well as TLR3-mediated type-I IFN induction. An rNDV expressing influenza NS1 showed enhanced oncolysis in a syngeneic murine melanoma model. rNDV activated type-I IFN by inhibiting the RIG-I helicase activity and triggering the CTLs (168).

NDV modified with a VP3, an apoptin protein from chicken infectious anaemia virus (CIAV) to rNDV-rFMW/AP was tested *in vitro* and *in vivo,* human tumour models revealed increased oncolysis by apoptosis better than unmodified virus when infected at high MOI of 10. The apparent shortcoming *in vivo* model was early apoptotic cell death resulting in the monocyclic virus replication and limiting the virus spread before achieving the desired effect (169).

MTH68 is a mesogenic strain of NDV modified by Puhler et al. by inserting two transgenes, heavy (50 kDa) and light chain (25 kDa) of IgG antibody against a tumour-specific vascular marker antigen extradomain B (ED-B) of fibronectin, in the genome without compromising the virus stability. Functional antibody expression successfully was shown in fibrosarcoma xenograft as well as *in vitro* models. This modification opens new roads to develop cancer vaccines targeting tumours with the delivery of specific therapeutic agents (170).

TAA and IL-2 expressing NDV showed increase in tumour-specific T-cell infiltration after intratumoral administration of NDV in mice bearing CT26 tumour (162). rNDV expressing lacZ gene encoding model TAA peptide epitope TPHPARIGL presented to MHC class I molecules led to complete tumour regression in 60% of animals used in the study compared to the 20% of animals treated with unmodified control viruses. When

treatment included IL-2 rNDV along with TAA, the results were improved by 90% (162). rNDV expressing codon-optimised HIV-gag protein, activated gag-specific CD8+ T-cells in mice. The oncolytic property was further enhanced by the addition of a single-chain variable fragment (Fv) (scFv) antibody explicit to the DC-restricted antigen uptake receptor DEC205 encoded by F protein. This approach improved CD4+ and CD8+ T-cell responses and protected tumours upon recombinant vaccinia virus expressing HIV-1 Gag (Vac-gag) infection (171). Nevertheless, the strategy of expressing TAA was limited by the complexity of tumours, vast numbers of families of TAA, continuously hyper mutating cancer DNA, and mostly weaker immunostimulation by TAA.

Bian et al. have developed a novel approach to engineering NDV using enhanced green fluorescent (EGFP) protein and bispecific F protein connected with IL-2 and HN proteins (NDFL-EGFP/aHN-IL-2) especially targeting IL-2 receptor-expressing human leukaemia MT-2 tumour cells. Further assessment of NDFL-EGFP/aHN-IL-2 has revealed that biodistribution NDV in liver, spleen, kidney, lung and thymus was reduced to 35-100%, whereas 98% of the transgene was delivered to IL-2R+ tumours, significantly reducing the off-target effect and resulting in better safety (172-174).

Haas et al. further modified the strategy of bispecific scFv (bsscFv) antibody, which specifically bind to HN proteins and to either CD3 or CD28 on human T lymphocytes, bsHN-CD3 and bsHN-CD28 antibody respectively. Human T-cell activation was achieved by using autologous tumor vaccine-NDV (ATV-NDV) modified with bsHN-CD3 or bsHN-CD28 bsscFv antibody. ATV-NDV vaccine is prepared by isolating tumour cells from surgically operated tumour. Isolated tumour cells are infected with Ulster strain of NDV for 1h. NDV-infected tumour cells inactivated by 200 Gy-irradiation to inhibit tumour cell proliferation without affecting NDV replication. ATV-NDV then mosified by adding soluble bsHN-CD3 or bsHN-CD28 bsscFv antibody. A strong and durable antitumour activity was demonstrated in human lymphocytes using bsHN-CD3 or bsHN-CD28 bsscFv antibody modified ATV-NDV (175). Similarly, bispecific scFv bsHN-IL2 or bsHN-CD28 antibody modified ATV-NDV vaccine co-culturing with PBMCs or T-cells demonstrated stimulation of naive T-cells through CD3 and IL-2 mediated signalling cascade with upregulation of PLC-γ1, Grb-2, Vav-1 and PDE-4A. Further on validation, this approach was even more effective when aHN-IL-2 fusion protein used for T-cell stimulation instead of bsHN-CD28 protein (176).

So far, the development of genetically engineered NDV expressing modified F proteins, cytokines such as IL-2/IFN-γ/GM-CSF/TNF-α, TAA, antigen-specific antibodies alone or

as in bispecific approaches in cellular as well as in animal models, have demonstrated the great potential and a strategic place of NDV in future as an effective oncovirotherapy to treat various cancers. Many of these candidates have already been in different phases of clinical trials to generate more field data to improve NDV-mediated oncolysis.

1.13. Clinical NDV trials

First study was published by Goto et al. in 1959, where the oncolytic possibility of NDV strains Sato and Miyadera were tested in the Yoshida sarcoma rat model (177).

Numerous preclinical studies have now established the substantial anti-cancer activity of naturally occurring and recombinant NDV in pre-clinical models. Encouraging results were documented in preclinical models of leukaemia, lymphoma, melanoma, neuroblastoma, fibrosarcoma, rat pheochromocytoma, colon carcinoma, lung carcinoma, prostate carcinoma, breast carcinoma, gastric carcinoma, mesothelioma, and head and neck carcinoma (164).

Wheelock and Dingle (1964) demonstrated for the first time oncolytic potential of intravenously injected NDV in a acute human leukaemia patient showed up to 75% reduction in peripheral myeloblasts within 18 h of the first injection. The mild fever recorded within 3 h of the first injection, was passed after 3 h (178). Soon after this, Cassel and Garret (1965) evaluated the oncolytic properties of 73T NDV strain in a woman with inoperable cervix carcinoma without previous treatment. Just with a single intratumoral injection, a significant tumour regression of lymph node (LN) was observed with subjective improvement in the patient for a short time (94). Cassel et al. employed NDV 73T strain in 83 patients with stage II malignant melanoma were inoculated with autologous or allogeneic NDV oncolysates. A long-term follow-up of these patients confirmed over 60% for 10-year survival without any recurrence of the disease (179). A 15-year survival phase-II study included AJCC stage III malignant melanoma patients and was conducted in two groups, group I (32 patients) and group II (51 patients). Patients were treated with subcutaneous injection of NDV 73T oncolysates post-operatively. Independent analysis of both groups demonstrated survival of 59% (18/30) in group I and 53% (23/44) in group II with overall 55% survival in 15-years (180).

Schirrmacher and colleagues employed a different strategy where irradiated entire autologous tumour cells were infected with vaccine strain Ulster of NDV and developed autologous tumour vaccine with NDV (ATV-NDV), which was administered with cytokines. The first successful prevention of the metastatic spread of tumour in ATV-NDV treated post-operated tumour model (181). The efficacy of ATV-NDV was

established first in Esb lymphoma, B16 melanoma, and 3LL Lewis lung carcinoma preclinical animal models with improved immune responses (182-184). Several clinical studies in phase I and II were carried out based on ATV-NDV tumour vaccines in colorectal cancer cells, which has shown augmented immunogenicity by activating innate and adaptive immune responses with improved long term survival in various phase II clinical trials (185). Patients with advanced colorectal carcinoma were vaccinated with ATV-NDV vaccine after potential curative tumour resection, where delayed-type hypersensitivity (DTH) was measured in all vaccinated patients. NDV vaccination was reported to be well-tolerated amongst all patients, 75% (12/16) of patients have shown NDV sensitisation confirmed by the histological examination and helper T-cell infiltration (186). A group of 23 colorectal cancer patients were treated with ATV-NDV in phase II after post-operative resection of liver metastases. In adjuvant vaccination settings, 61% of patients have shown recurrence of cancer compared to the 87% control group (187).

Liang et al. conducted the most extensive study of treatment of digestive tract tumours with an autologous NDV-modified tumour cell vaccine using non-lytic NDV strain LaSota (188). In this phase III study, NDV virotherapy with resection and immunotherapy was used in 310 patients in stage I-IV colorectal cancer and compared to 257 patients treated with resection alone. There was not enough information on randomisation or allocation, as there was a lack of mention of sampling and additional chemotherapy. In this study, a statistically significant median of overall survival was reported of 7 years in the vaccine group compared to 4.46 years in the resection alone group was recorded (188). Additionally, a one-year survival rate was 96% for 25 patients treated with NDV immunotherapy with unresectable colorectal, stomach, liver, pancreatic, and gallbladder cancers who were all treated with ATV-NDV vaccines. Although this study has presented some clinical benefits with encouraging short term survival further rigorous randomised clinical trials would be necessary to reach more decisive conclusion (188).

In a pilot study, 23 patients of glioblastoma were postoperatively vaccinated with ATV-NDV and compared with 87 non-vaccinated control patients. Vaccination resulted in statistically significant median progression-free survival of 40 weeks in treated patients (vs 26 weeks in controls), and the median overall survival of vaccinated patients was 100 weeks (vs 49 weeks in controls), where 91% treated patients survived for one year, 39% survived for two years, and 4% were long-term survivors (189).

Later, NDV MTH/68 and HUJ strain-based phase I clinical studies were conducted in GBM brain tumour patients. MTH/68 intravenous injection in 4 high-grade glioma

patients showed 5 to 9 years of long term survival and the HUJ based vaccination achieved a complete response in 9% (1/11) of the patients, only rest showed recurrence of progressive disease (190, 191).

In a PV701 based phase I trial, 79 patients were treated through intravenous injections to determine the MTD for the single-dose and multiple-dose schedules. Flu-like symptoms were the most common adverse effects, consistent with cytokine induction. Most symptoms were associated with the first dose followed with subsequent doses. Subsequent doses were bwtter tolerated due to reduced induction of proinflammatory cytokines, which occurred before the development of antibodies against PV701 in all patients (115).

Primarily, direct administration of NDV to patients have revealed minimal toxicity with the recommendation of clinical benefits in some patients, necessitating further assessment. A summary of NDV clinical trials listed in **Table 1.5**.

Table 1.5: Summary of NDV clinical trials

NDV Strain	Mode of administration	Material, dose, and duration used for administration	Cancer	Clinical study design	Clinical outcome	Year	Reference
NDV-73 T Mesogenic	Subcutaneous Injection	Allogenic or autologous human melanoma cells infected with NDV, weekly injections	Melanoma (stage II)	Phase 2 (n=83)	Patients confirmed over 60% survival for 10-year without any recurrence and overall survival 55% for NDV-treated melanoma patients in 15 years	1992	(179, 180)
NDV-MTH-68 Mesogenic	Inhalation	4 $\times 10^3$ PFU (biweekly for six months)	Advanced cancers	Phase 2 (n=33)	1-year survival for 22 out of 33 versus 4 out of 26 in the control group; 2-year survival for 7 out of 33 versus 9 out of 26 in the control group	1993	(192)
NDV-PV701 Mesogenic	Intravenous	Dose intensified up to 1.20×10^{11} PFU/m^2	Advanced cancers	Phase 1 (n = 79)	Objective responses occurred at higher dose levels. Four out of 79 responses: two major, two minor, progression-free survival ranged from 4 to 31 months	2002	(115)
NDV Ulster lentogenic	Intradermal injections	Allogenic or autologous tumour cells infected with NDV, biweekly injections, 5 totals plus Per vaccine, 1×10^7 tumour cells were incubated for 1 h with 64 HA units of the NDV	Glioblastoma Multiforme	Phase 1/2 (n = 23)	1 patient was long term survivor versus none in a control group of 87 patients	2004	(189)
NDV-MTH-68 Mesogenic	Intravenous and inhalation	2×10^7 to 2.5×10^8 PFU (dosage step + maintenance dose) daily with alternate route delivery	Glioblastoma Multiforme	Case series (n = 14)	7 out of 14 responses; four major, 5 to 9 year survival or more	2004	(190)
NDV-HUJ lentogenic	Intravenous	Dose escalation up to 55×10^9 EID50	Glioblastoma Multiforme	Phase 1 (n = 11)	1 patient out of 11 achieved a complete response, and all others had progressive disease	2006	(191)
NDV-PV701 Mesogenic	Intravenous	Dose escalation up to 1.20×10^{11} PFU	Advanced cancers	Phase 1 (n = 16)	1 patient experienced the near-complete response with at least 1-year survival, four others from the treatment group had disease stabilisation	2006	(193)
NDV-PV701 Mesogenic	Intravenous	1.20×10^{11} PFU	Advanced cancers	Phase 1 (n = 18)	6 out of 18 responses: one complete, three partial, and two minor; six patients surviving rate of least 2 years	2007	(117, 194)

1.14. Potential for oncolytic NDV to break resistance to therapy

From the last five decades of study of NDV as an oncolytic virus, NDV disrupted tolerance or immune suppression by activating host immune mechanisms and destroying tumour cells by ICD. NDV has been demonstrated to be effective for break therapy resistance, as discussed below with the examples.

Breaking resistance to conventional treatments: Conventional chemotherapy (CT) and radiotherapy (RT) target the proliferating cells to kill the tumour, but non-proliferating tumour cells such as dormant tumour cells or cancer stem cells remain unaffected by it. However, NDV replicates in cell cytoplasm regardless of the host cell DNA replication and gives the advantage of replicating in non-proliferating cells. NDV is known to replicate in γ-irradiated cells (to develop ATV-NDV vaccines) (123). Meng et al. have demonstrated that NDV triggers caspase-9-mediated apoptosis in cisplatin-resistant A549 lung cancer cells demonstrating its potential to overcome drug resistance (195). In another study, NDV FMW strain modulated autophagic cell death in drug-resistant A549 cells (196). Bai et al. have shown the enhancement of proapoptotic properties of temozolomide (TMZ) in combination with LaSota in GBM cells *in vitro* as well as in *in vivo* models by down-regulating the AKT–mTOR signalling pathway but also by activating AMPK (197).

Breaking resistance to apoptosis: Oncolytic NDV has been shown to break apoptosis resistance in Bcl-xL antiapoptotic protein overexpressing A549 cells. Apoptosis-resistant cells favoured better viral replication and paradoxically induced apoptosis-resistant cells by activating the type-I IFN pathway (98). In another study, melanoma cells overexpressing Livin antiapoptotic protein NDV-HUJ strain broke apoptosis resistance by caspase-mediated cleavage of Livin (99). Both studies confirmed better viral replication in apoptosis-resistant cells, proving potential of NDV to break therapy resistance properties of NDV.

Breaking resistance to hypoxia: Solid tumour microenvironments comprise of dominant hypoxic areas with activated hypoxia-inducible factor-alpha (HIF-α) a transcription factor. It impacts gene expression and contributes to the resistance of tumours to CT and RT. Wei-Choong Ch'ng et al. have investigated the oncolytic efficacy of velogenic NDV strains with or without of HIF-2α expression in renal cell carcinoma (RCC) cell lines with defective or reconstituted wild type (wt) von Hippel-Lindau (VHL) activity. NDV stimulated IFN-β. Stimulation IFN-β was associated with increased STAT-

1 phosphorylation in RCC cells. Hypoxia augmented NDV-induced oncolysis irrespective of the HIF-2α status in the cells (198).

Breaking resistance to antiviral immunity: Antiviral immunity was measured as a significant obstacle for the productive therapeutic activity of oncolytic viruses. In a recent study from Ricca et al., it was reported that pre-existing immunity to oncolytic NDV LaSota enhances rather than constrains its immunotherapeutic efficacy, suggesting at least NDV LaSota has potential to break resistance to anti-viral immunity in a tumour model (66).

Breaking resistance to immune checkpoint blockade: Zamarin et al. (2014) demonstrated that oncolytic NDV broke down the resistance developed against CTLA-4 checkpoint blockade immunotherapy at the distant untreated tumour site when injected intratumorally in localised B16 mouse melanoma tumour model (156). The promising therapeutic effect was associated with infiltration with activated CD8+ and CD4+ effector cells but not with regulatory T-cells at distant tumour site. The result was dependent on CD8+ T-cells, NK cells, and type-I IFN (156). Later, the same group studied the immunogenic potential of NDV in bladder cancer, where the application of immune checkpoint inhibitory antibodies revealed only suboptimal response rates (199). NDV infection in human and mouse bladder cancer cells have induced ICD. Induction of ICD was found to be associated with upregulation of MHC and PD-L1 regardless of sensitivity to NDV-induced oncolysis. It has been reported that NDV-mediated localised activation of checkpoint PD-1 or CTLA-4 blockade therapy in both treated and distant tumours and even when administered in lysis-resistant tumour cells, in a bilateral flank test animal model (a mouse model where tumour cell transplantation is introduced at two opposite sides) (199).

1.15. Projections for NDV as oncolytic viruses

Since NDV was first recognised as an oncolytic virus, the understanding of NDV biology, oncotropism, and cancer cell biology has come a long way.

Numerous studies demonstrated tumour-specific NDV replication and immunomodulation of tumour microenvironment. NDV demonstrated various advantages over other OV candidates, such as lack pre-existing immunity in humans because NDV is an avian pathogen. Serological data suggests almost 96% of the human population is seronegative for NDV (200, 201). NDV is non-pathogenic to humans, and adverse effects like mild conjunctivitis, laryngitis, and mild flu-like symptoms are

observed only in high-risk personnel such as farmers and immunosuppressed or immunocompromised patients (118). NDV has demonstrated to have immunostimulatory properties by inducing type-I IFNs, activating NK cells, macrophages, dendritic cells, CD4+, and CD8+ T-cells. Anti-tumour immune responses were found to remain longer in vaccinated tumours to clear remaining virus replication and governs the safety profile. The large size of the NDV genome has allowed successful engineering to insert foreign genes without (any associated toxicity) hampering virus replication. As NDV is a negative-strand RNA virus that replicates in the cytoplasm there is no genetic integration with host cell genome (202). Considering all the discussed advantages of NDV as OV, there is scope to improve its potential. It can be achieved with some of the following approaches.

1.15.1. Improving tumour-specific targeting and systemic delivery

Conventional NDV vaccines are mass-produced using embryonated hen's eggs. However, to enhance tumour specificity of NDV vaccines requires modification of HN, and processing of NDV with modified HN poses constraints for production in eggs. Hence the development of a tissue culture-based system is required for NDV rescue, viral growth and production. Nonetheless, bispecific adapter F protein was successfully used for targeting tumours by Schirrmacher and colleagues, and similar approaches have been used for retargeting adenovirus (203). Alternatively, modification of the F protein cleavage site with tumour-specific proteases can be used in NDV to improve virus replication of non-lytic strains, already demonstrated for measles, Sendai, and retroviruses (204, 205).

RNA viruses are naturally limited from exploiting tissue-specific promoters, which is used with HSV-1 and adenoviruses to restrict their replication in tumour cells (206). Utilising RNA destabilising elements like AU-rich elements (ARE) encoded by viral proteins enhance the tumour-specific replication. Oncogenic pathways lead to activation of ARE-binding proteins like tristetraprolin (TTP) and human antigen R (HuR), which then stabilise mRNA of multiple tumour-promoting genes such as cytokines, chemokines, growth factors, and transcription factors. Viral mRNA destruction strategy by application of ARE in healthy cells will promote tumour-specific virus replication and overexpression of chemokines and cytokines in tumour microenvironment can be achieved (207).

In preclinical and clinical NDV trials, administration of NDV vaccine vectors via intravenous and intratumoural routes presented promising results by activating type-I

IFN responses upon NDV sensitisation, although the intravenous route of administration demonstrated better than intratumoural doses (154). Inefficient dose administration of viral vector vaccines, poor systemic delivery to the target, rapid clearance of virus, and off-target effects have resulted in reduced oncolysis (208). Overcoming this challenge requires attempting different approaches such as using mesenchymal stem cells (MSC) as carriers for measles virotherapy. Different types of cells such as MSCs and neural stem cells (NSC), immune cells, and cancer cells have demonstrated to have tumour-homing characteristics, which was used in measles virotherapy and shown to protect the virus from neutralising antibodies and to efficiently transfer the virus to tumours in an orthotopic xenograft ovarian cancer model (209, 210). Consideration of similar methods for delivery of NDV to target tissues will undoubtedly be essential and useful further development as a systemic agent.

One such strategy of combining ATV-NDV with DCs used to improve the *de novo* synthesis of TAA-specific cells from naïve T-cells. The Immunological and Oncological Center (IOZK) in Cologne (Germany) have developed a protocol for the generation of viral oncolysate-pulsed DCs (VOL-DCs), which has received an official permit for an individual application of this product to cancer patients in 2015 (202). Combination therapy of local hyperthermia (LHT) with ATV-NDV in VOL-DC induced a long-lasting antitumor memory T-cell response and achieved complete remission of prostate cancer with widespread bone metastases in a patient who had failed standard therapy (211). IOZK is running multimodal two-stem immunotherapy *in situ* vaccination first followed by second active-specific vaccination (154). Cancer patients were intravenously injected with NDV MTH-68 in combination with several ICD inducers such as moderate local electrohyperthermia (mEHT), ionising radiations, hydrostatic pressures etc. to trigger the immune system and to induce ICD in tumour cells; this is referred as *in situ* vaccination stage; the process is repeated 5 times in 5 days. In the second step of active vaccination, cancer patients were treated with VOL-DCs in combination with *in situ* vaccination intradermally. The dendritic cells were isolated from cancer patients to prepare VOL-DCs preparation. This multimodal two-step study is ongoing. So far, a significant increase in CD8+ T-cells infiltration with long-lasting memory T cells response has observed in various trials in GBM patients (154).

1.15.2. Enhancement of NDV-mediated immunomodulation and bypassing NDV neutralising immune responses

With recent advancement in the understanding of cancer biology, a lot is known about the T-cell co-stimulatory, and co-inhibitory receptors molecules, which have provided valid new targets for immune therapies for improvement in the stimulation of anti-tumour immune responses and to inverse the immunosuppressive mechanisms to the widespread tumour resistance to immune destruction. Substantial anti-tumour activity has been demonstrated using stimulatory antibodies to 4–1BB, OX40, and GITR, as well as inhibitory antibodies to PD-1 and CTLA-4. Identification of these immune checkpoint inhibitors opened new avenues for combinational therapies targeting cancer with even more precision (212). In phase III clinical trial of advanced melanoma patients, a significant improvement in median overall survival was demonstrated by treating patients with CTLA-4 antibody Ipilimumab, which led to the FDA approval for cancer treatment (213, 214). Simultaneously a therapeutic autologous antigen-presenting cell vaccine (Sipuleucel-T) got FDA approval for prostate cancer treatment after demonstrating the prolonged overall survival in compared to a placebo control group (215).

The potential synergy between oncovirotherapy and immunotherapy was studied in a preclinical and clinical trial, including NDV, HSV-1, adenoviruses, and other OVs. Recombinant oncolytic viruses demonstrated superior anti-tumour properties. Oseledchyk et al. have shown that a combination of intratumoral NDV with systemic PD-1 or CTLA-4 blockade led to improved local and abscopal tumour control and overall survival in a human and murine bladder model. These findings have encouraged upcoming clinical trials to combine intratumoral NDV therapy with systemic immunomodulatory agents (199). Likewise Vijayakumar et al. have also demonstrated benefits of six different recombinant NDV (rNDV-anti-CD28-mIL12, rNDV-anti-PD-1-mIL12 and rNDV-anti-PD-L-1-mIL12) targeting immune checkpoint blockades showed a survival benefit both in a highly aggressive unilateral and bilateral B16-F10 murine melanoma models (216).

As NDV is known for immunostimulatory properties, it elicits strong neutralising antibody responses. A premature anti-NDV antibody response would restrict oncolysis even after repeated administrations of multiple doses of NDV. In the face of the limited clinical data representation of sustained benefits in patients treated with multiple prescriptions, the problem of virus deactivation and clearance will be expected to limit its therapeutic effectiveness in majority of the patients. Impending solutions to this problem would

depend on the utilisation of different NDV strains, the use of viral carriers such as MSCs or NSCs, and modification of different viral surface proteins using reverse genetic engineering. Surprisingly, the oncolytic LaSota strain of NDV demonstrated to be unaffected by pre-existing antiviral immunity when injected intratumorally; in contrast, it potentiated the immunotherapeutic efficacy both *in vivo* and *in vitro* models (66).

Abrogation of secondary response to adenovirus vector from pre-existing immunity has been studied in immunised bilirubin-UDP-glucuronosyltransferase (BUGT)-deficient jaundiced Gunn rats upon infection with recombinant adenovirus (5×10^9 PFU/rat). This recombinant adenovirus expressed a human UDP-glucuronosyltransferase (BUGT1) gene (Ad-hBUGT). This study has demonstrated that well-tolerated doses for repeated adenovirus-directed gene transfer despite the presence of a residual antibody titre from previous adenoviral exposure (65). A similar strategy could be developed to overcome secondary responses against NDV antibodies to achieve effective virotherapy results.

1.16. Aims and objectives of the thesis

The mechanisms of NDV-induced oncolysis using lentogenic/avirulent non-reporter and reporter strains of NDV such as Hitchner B1, B1-GFP, LaSota, and LaSota-GFP are not clearly understood; therefore, the aims and objectives of the thesis are as follows:

Aim 1: Establish a model system to study oncolysis

Objective 1: Identify an NDV-sensitive cell line/s for lentogenic strains of NDV

Objective 2: Identify an effective lentogenic strain of NDV used for oncolysis in susceptible cells

Objective 3: Isolate persistently infected cells from the most susceptible cells upon NDV infection

Objective 4: Investigate the impact of persistent NDV infection in isolated cells in comparison with parental cells with or without NDV infection

Aim 2: Explore the differences between persistent and acute NDV infection in susceptible cells

Objective 1: RNA-seq analysis of persistently and acutely infected cells in comparison with uninfected cells

Objective 2: Analysis of differentially expressed genes (DEGs) in pair-wise comparisons of persistently and acutely infected cells in comparison with uninfected cells

Objective 3: Comparative analysis of RNA seq-analysis from this project with similar already published data

Aim 3: Investigate the mechanism of NDV-mediated induction of mitophagy in susceptible cells

Objective 1: Investigate the role of NDV in susceptible cells for the induction of mitophagy and the degradation of p62/SQSTM1 adapter protein

Chapter 2

2 Materials and Methods

2.1. Materials

2.1.1. Cells

Different human cancer and non-cancer cell lines along with chicken embryo fibroblast cells used in this PhD project, are listed in **Table 2.1**.

Table 2.1: List of cells/cell lines used in this study

Sr. No.	Cell	Description	Cell type	Biosafety level	Source	Cell line Authentication
1	DF-1	Chicken fibroblast cell line	Fibroblast, Adherent	1	Pirbright Institute cell services unit	NA
2	A549	Human lung adenocarcinoma cells	Epithelial, Adherent cells	1		ECACC
3	Hep G2	Human hepatocellular carcinoma cells	Epithelial, Adherent cells	1		NA
4	PC3	Human prostate adenocarcinoma cells derived from metastatic site: bone	Epithelial, Adherent cells	1		ECACC
5	HeLa	Human cervical adenocarcinoma cells	Epithelial, Adherent cells	2		NA
6	Caco-2	Human colorectal adenocarcinoma cells	Epithelial, Adherent cells	1		ECACC
7	Ox Caco-2	Human colorectal adenocarcinoma cells	Epithelial, Adherent cells	1	Oxford University	NA
8	VR (Virus-Resistant) Caco-2 cells	Cells were isolated from NDV-infected Caco-2 cells	Epithelial, Adherent cells	2	Isolated in this PhD	ECACC
9	MRC5	Human lung fibroblast cells	Fibroblast, Adherent	1	Pirbright Institute cell services unit	ECACC
10	HEK-293	Human embryonic kidney cells	Epithelial, Adherent cells	2		NA

Note: A549, PC3, MRC5, Caco-2 and VR Caco-2 cells (VR Caco-2 cells are discussed in chapter 3 section 3.2.3) were authenticated using short tandem repeat (STR) profiling from ECACC.

2.1.2. Viruses

Different avirulent strains of NDV, AIV (avian influenza virus), and VSV (vesicular stomatitis virus) used in this PhD project, are listed in **Table 2.2**.

Table 2.2: List of viruses used for infection studies

Sr. No.	Virus Strain	Family	Virus	Pathotype	NDV Genotype	Source
1	Ulster 2C	Paramyxoviridae	Newcastle disease virus (NDV)	Lentogenic	II	Pirbright Institute
2	LaSota	Paramyxoviridae	NDV	Lentogenic	II	Rescued by Manoja Rasamanikkam at The Pirbright Institute
3	LaSota-GFP	Paramyxoviridae	NDV	Lentogenic	II	
4	Hitchner B1	Paramyxoviridae	NDV	Lentogenic	II	Zoetis
5	B1-GFP	Paramyxoviridae	NDV	Lentogenic	II	Peter Palese, Department of Microbiology, Mount Sinai School of Medicine, New York
6	VSV-GFP	Rhabdoviridae	Vesicular stomatitis virus	Non-pathogenic	NA	The Pirbright Institute
7	H9N2-GFP	Orthomyxoviridae	Avian influenza virus	Low-pathogenic	NA	Munir Iqbal, Avian Influenza Virus, The Pirbright Institute

2.1.3. Primers

2.1.3.1. Amplification primers

Table 2.3: p62/SQSTM1 primer used to study CRISPR/Cas9 Knockout (KO)

Sr. No.	Primer Name	Forward Primer 5 prime to 3 prime	Reverse Primer 5 prime to 3 prime	Amplicon Length (in bp)
1	SQSTM1 (KO)	TCTAGATGAGGACGGGGACT	ACAAGTCGTAGTCTGGGCAG	1055

2.1.3.2. Cloning primers

Table 2.4: List of cloning primers used in this study

Sr. No	Gene	Forward Primer 5 prime to 3 prime	Reverse Primer 5 prime to 3 prime	Restriction enzymes	Vector used for cloning
1	NP (1.47 kb)	AAGAATTCATGTCTTC CGTATTTGATGAG	TTACTAGTTCAATAC CCCCAGTCGGTG	F- Eco RI, R-SpeI	pEFplink.2-V5 (provided by Steve Goodbourn's Lab, St. George's, University of London)
2	P (1.187 kb)	AAGAATTCATGGCCAC CTTTACAGATGCAG	TTACTAGTTTAGCCA TTTAGAGCAAGGCGC	F- Eco RI, R-SpeI	
3	M (1.09 kb)	AACCATGGCAATGGAC TCATCTAGGACAAT	GGACTAGTTTATTTC TTAAAAGGATTGTA	F-NcoI, R-SpeI	
4	F (1.662 kb)	AACCATGGCAATGGG CTCCAGACCTTCTAC	GGACTAGTTCACATT TTTGTAGTGGCTCTC	F-NcoI, R-SpeI	
5	HN (1.73 kb)	AGCCATGGCAATGGA CCGCGCCGTTAGCCA AG	ATTTCTAGACTAGCC AGACCTGGCTTCT	F-NcoI, R-XbaI	
6	HN (1.73 kb)	GATCAAGCTTATGGAC CGCGCCGTTAGCCA	GGATCCGCCAAGCC AGACCTGGCTTCTC	F-HindII, R-BamHI	pcDNA3.1 (+) EGFP (6.119 kb) (AVO Group, The Pirbright Institute)
7	pEFplink.2 (4.809 kb)	CAGGTGTCGTGAAGA ATTAG	AGCCACCACTTTCTG ATAGG	Sequencing primers	

2.1.3.3. NDV cDNA synthesis, amplification, and sequencing primers

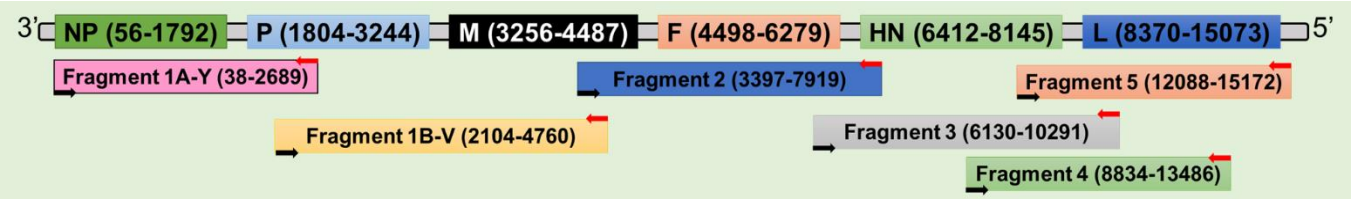

Figure 2.1. The schematic representation of the NDV genome fragmentation for Sanger sequencing. The strategy of Sanger sequencing by fragmenting 15,192 nucleotides long NDV whole genome in six different overlapping fragments

Table 2.5: List of primers used for NDV cDNA synthesis and PCR amplification

Sr. No.	NDV Fragment (Sanger sequencing)	Forward Primer 5 prime to 3 prime	Reverse Primer 5 prime to 3 prime	Amplicon Length (in bp)
1	Fragment 1A-Y (38-2689 bp)	AGGAGCAATTGAAGTC GCAC (38 to 57 bp)	GGCTTCCATGACTGCAAC AA (2689 to 2708 bp)	2651
2	Fragment 1B-V (2104 to 4760 bp)	ACAAACAACCATCCACA CCC (2104 to 2123 bp)	TATCCTTGGGCAGATTCG GG (4741 to 4760 bp)	2656
3	Fragment 2 (3397 to 7919 bp)	AATCGCCCCGCAATATA GGA (3397 to 3416 bp)	GACGCAGGGTTAAGTCTT GC (7900 to 7919 bp)	4522
4	Fragment 3 (6130 to 10291 bp)	AAAGGCGCAACAAAAG ACCT (6130 to 6149 bp)	GAAGGTTGCAACTCTCCG AC (10272 to 10291 bp)	4161
5	Fragment 4 (8834 to 13486 bp)	GAGGAGTTCAGCAGCA TTCG (8834 to 8853 bp)	AGGTTGTCGGGTGAATGG AT (13467 to 13486 bp)	4652
6	Fragment 5 (12088 to 15172 bp)	GACTGCTGCTCTCACGA TTG (12088 to 12107 bp)	TGGTGAATGACGAGACTA CACT (15151 to 15172 bp)	3084

Table 2.6: List of sequencing primers used to sequence NDV fragment

Fragments	Sequencing primers	5 prime to 3 prime Orientation
Fragment 1 A-Y: 38 to 2689 bp	AGGAGCAATTGAAGTCGCAC (38 to 57 bp)	Forward
	ATTGGCCGTGCTTGAGATTG (415 to 434 bp)	
	CTCAAGTACGGAATCAACACCA (932 to 953 bp)	
	CCTACAAGGCGGATCGAATAG (1399 to 1419 bp)	
	ACAAACAACCATCCACACCC (2104 to 2123 bp)	

	GGCTTCCATGACTGCAACAA (2689 to 2708 bp)	
Fragment 1 B-V: 2104 to 4741 bp	ACAAACAACCATCCACACCC (2104 to 2123 bp)	Forward
	CAACCAGTGCCACATCCATC (2871 to 2890 bp)	
	AGCAACCTGTTAGCATTTCCG (3341 to 3361 bp)	
	ACAAGATCCCAGCTGCAGTA (3849 to 3868 bp)	
	TTACCTGTCCATCAAGTTAG (4471 bp to 4490 bp)	
	TATCCTTGGGCAGATTCGGG (4741 to 4760 bp)	
Fragment 2= 4523 bp (3397 to 7919 bp)	AATCGCCCCGCAATATAGGA (3397 to 3416 bp)	Forward
	GAAAGCGCCAGAGAAGATCC (3760 to 3779 bp)	
	CCAAAAGCTTAGTCCGTGCA (4141 bp to 4160 bp)	Reverse
	CCAAGCAGGTACCCAACG (4276 to 4293 bp)	Forward
	CCCGAATCTGCCCAAGGATA (4741 to 4760 bp)	
	TCTAGCTGGTGGGAATATGGA (5263 to 5283 bp)	
	GCAATGTTTTATCCTTAGGCGG (5814 to 5835 bp)	
	GTGGCCCTTGAGTCTCCATT (6673 to 6692 bp)	
	CCACGGAGACAGAGGAAGAA (7172 to 7191 bp)	
	GACGCAGGGTTAAGTCTTGC (7900 to 7919 bp)	Reverse
Fragment 3= 4162 bp (6130 to 10291 bp)	AAAGGCGCAACAAAAGACCT (6130 to 6149 bp)	Forward
	CTTGGTGTGCTCCGGACAT (7033 to 7051 bp)	
	AGTAGGCGCCGGGATAAAAT (6893 bp to 6912 bp)	Reverse
	TTGGTGGGAAACGCATACAG (7502 to 7521 bp)	Forward
	ACCTCATTCTCAGCCGACAA (8523 to 8542 bp)	
	GGAGGGCAGAGATATGGTCA (9103 to 9122 bp)	
	AAATGTGCGCACCGAAAATG (9510 to 9529 bp)	
	GAAGGTTGCAACTCTCCGAC (10272 to 10291 bp)	Reverse
Fragment 4= 4653 bp (8834 to 13486 bp)	GAGGAGTTCAGCAGCATTCG (8834 to 8853 bp)	Forward
	TCTGCACTTGAATTTGAGCCA (9722 to 9742 bp)	
	GCCACACACCTGCATTCTTC (9598 to 9617 bp)	Reverse
	GTATCTTCAAACCGCAATCATGA (10232 to 10254 bp)	Forward
	CCGTAATGTCCTGTGCCAAC (10905 to 10924 bp)	
	GGCAGAAGAGAAGGCATTGG (11431 to 11450 bp)	
	ACCAGCAAGAATCCTCCGAT (11924 to 11943 bp)	
	TTTGAATATGCAGCACTTGAAGT (12770 to 12792 bp)	
	CCCCGATCAAGTGAGCTCTA (13276 to 13295 bp)	
	AGGTTGTCGGGTGAATGGAT (13467 to 13486 bp)	Reverse
Fragment 5= 3100 bp (12088 to 15172 bp)	GACTGCTGCTCTCACGATTG (12088 to 12107 bp)	Forward
	TCAAGGTTACATGCAGTGGG (12938 to 12957 bp)	
	TGGTAAGAACGGTGGAGGAG (12794 bp to 12813 bp)	Reverse
	GGTGCTCGAGTGAAAGATCC (13451 to 13470 bp)	Forward
	GTTATTCACCTCACAGCGGC (14374 to 14393 bp)	
	TGGTGAATGACGAGACTACACT (15151 to 15172 bp)	Reverse

2.1.3.4. SYBR Green qRT-PCR primers

Table 2.7: List of SYBR-Green qRT-PCR primers used in this study

Sr. No.	Primer Name	Forward Primer 5 prime to 3 prime	Reverse Primer 5 prime to 3 prime	Amplicon length (in bp)
1	GAPDH	CTCTGCTCCTCCTGTTCGAC	GTTAAAAGCAGCCCTGGTGA	237
2	IFN-B	AGGACAGGATGAACTTTGAC	TGATAGACATTAGCCAGGAG	181
3	ISG-15	TGGCGGGCAACGAATT	GGGTGATCTGCGCCTTCA	72
4	APMV1 M+4100	AGTGATGTGCTCGGACCTTC	CCTGAGGAGAGGCATTTGCTA	120

2.1.3.5. TaqMan qRT-PCR primers and probes

Table 2.8: TaqMan primers and probes used in this study

Sr. No.	Primer Name	Probes and primers	Source
1	hsa-miR-155	UUAAUGCUAAUCGUGAUAGGGG	Thermo Scientific™: TM000479, Catalogue number: 4427975
2	hsa-miR-223-3p Mimic	UGUCAGUUUGUCAAAUACCCCA	Thermo Scientific™: MC12301, Catalogue number: 4464066

2.1.4. Antibodies

2.1.4.1. Primary antibodies

Table 2.9: List of primary antibodies used in this study

Sr. No.	Antibody	Type	Source and catalogue number	Use
1	Anti-SQSTM1	Rabbit monoclonal	Abcam, ab109012	Indirect immunofluorescence (IF) and western blotting (WB) assays
2	Anti-GAPDH	Mouse monoclonal	Invitrogen™, AM4300	
3	Anti-α-Tubulin	Mouse monoclonal	Invitrogen™, 13-800	
4	Anti-V5-Tag	Mouse monoclonal	Sigma, V8012	
5	Anti-NDV	Chicken polyclonal	Abcam, ab 34402	IF, WB, and plaque assay

2.1.4.2. Secondary antibodies

Table 2.10: List of secondary antibodies used in this study

Sr. No.	Antibody	Host	Reactivity	Source	Use
1	Goat anti-Rabbit IgG (H+L), Alexa Fluor Plus 488	Goat	Rabbit	Invitrogen™, A32731	Indirect immunofluorescence (IF) assays
2	Goat anti-Rabbit IgG (H+L), Alexa Fluor 568	Goat	Rabbit	Invitrogen™, A-11011	
3	Goat anti-Mouse IgG (H+L), Alexa Fluor Plus 488	Goat	Mouse	Invitrogen™, A32723	
4	Goat anti-Mouse IgG (H+L), Alexa Fluor 568	Goat	Mouse	Invitrogen™, A-11031	
5	Goat anti-Chicken IgY (H+L), Alexa Fluor Plus 488	Goat	Chicken	Invitrogen™, A32931	
6	Goat anti-Chicken IgY (H+L), Alexa Fluor 568	Goat	Chicken	Invitrogen™, A-11041	
7	IRDye® 800CW anti-Chicken IgG (H+L)	Donkey	Chicken	LI-COR, 926-68071	Odyssey® Western blot detection
8	IRDye® 800CW Goat anti-Rabbit IgG (H + L)	Goat	Rabbit	LI-COR, 926-32211	
9	IRDye® 680RD Goat anti-Mouse IgG (H + L)	Goat	Mouse	LI-COR, 926-68070	

2.1.5. Media and Buffers

2.1.5.1. Media and solutions

Table 2.11: List of media and solutions used in this study

Sr. No.	Media	Supplements added to prepare complete growth media or selective media preparation	Use
1	MEM-Minimum essential medium eagle with Earle's salts and sodium bicarbonate without L-Glutamine (Sigma-Aldrich, D5796)	1% Penicillin-Streptomycin (10,000 U/ml) (Gibco™-15140122), 1x NEAA (Gibco™-11140050), 4 mM L-Glutamine (Gibco™-25030081), 1 µg/ml Amphotericin B (Gibco™-15290026), 20% foetal bovine serum (FBS) (Gibco™-10099141)	Caco-2, Ox Caco-2, and VR Caco-2 cells culturing
2	MEM-Minimum essential medium eagle with Earle's salts and sodium bicarbonate without L-Glutamine (Sigma-Aldrich, D5796)	1% Penicillin-Streptomycin (10,000 U/ml) (Gibco™-15140122), 4 mM L-Glutamine (Gibco™-25030081), 1 µg/ml Amphotericin B (Gibco™-15290026), 10% FBS (Gibco™-10099141)	HepG2 and MRC5 cells culturing
3	DMEM-Dulbecco's modified eagle's medium (with high glucose 4.5 µg/ml), L-Glutamine and sodium bicarbonate without sodium pyruvate (Sigma-Aldrich, D5796)	1% Penicillin-Streptomycin (10,000 U/ml) (Gibco™™-15140122), 1 mM Sodium Pyruvate (Gibco™-11360070), 1 µg/ml Amphotericin B (Gibco™-15290026), 10% FBS (Gibco™-10099141)	DF-1, HEK-293, and A549 cells culturing
4	RPMI (Roswell Park Memorial Institute), -1640 medium with L-Glutamine and sodium bicarbonate (Sigma-Aldrich, R8758)	1% Penicillin-Streptomycin (10,000 U/ml) (Gibco™-15140122),1 µg/ml Amphotericin B (Gibco™-15290026), 10% FBS (Gibco™-10099141)	HeLa cells culturing
5	Ham's F-12K (Kaighn's) Medium (Gibco™, 21127022)	1% Penicillin-Streptomycin (10,000 U/ml) (Gibco™-15140122),1 µg/ml Amphotericin B (Gibco™-15290026), 10% FBS (Gibco™-10099141)	PC3 cells culturing

6	2.5 % Trypsin, no phenol red, (Gibco™, 15090046)	NA	Used in Versene-Trypsin solution preparation
7	VERSENE, (0.53 mM) aqueous solution of the tetrasodium salt of ethylenediaminetetraacetic acid Na_4EDTA (prepared in house)	0.25% Trypsin and 0.53 mM Versene mixed in 1:1 ratio	Cell trypsinisation
8	Opti-MEM™ I Reduced Serum Medium (Gibco™-31985070)	NA	Cell transfection
9	DMEM-Dulbecco's modified EAGLE'S medium-high glucose with 4.5 µg/ml glucose, L-Glutamine and sodium bicarbonate without sodium pyruvate (Sigma-Aldrich, R8758)	5% FBS (Gibco™-10099141)	Cell transfection
10	Luria Broth (LB) (Gibco™™, 10855021)	100 µg/ml Ampicillin (Sigma-Aldrich-A5354) or 50 µg/ml (Sigma-Aldrich-K0254)	Bacterial growth
11	LB Agar plate (Pirbright Institute cell services unit)	100 µg/ml Ampicillin (Sigma-Aldrich-A5354) or 50 µg/ml (Sigma-Aldrich-K0254)	Bacterial transformation
12	S.O.C. Medium (Invitrogen™™, 15544034)	NA	Bacterial transformation
13	Plaque assay 0.8% Methyl cellulose overlay media	1x DMEM (Sigma-Aldrich, R8758), pre-sterile 0.8% Methyl cellulose (Sigma-Aldrich, M0512), 2% FBS (Gibco™-10099141),10% freshly collected from 10 days old SPF chicken embryonic eggs (Valo Biomedia GmbH), 1% Penicillin-Streptomycin (10,000 U/ml) (Gibco™-15140122), 1 µg/ml Amphotericin B (Gibco™-15290026)	Virus plaque assay
Note: Foetal bovine serum (FBS) (Gibco™-10099141) heat-inactivated at $56^{O}C$ in a water bath for 30 minutes before adding to the cell culture media.			

2.1.5.2. Buffers

Table 2.12: List of buffers used in this study

Sr. No.	Buffer	Composition	Use
1	PBSa	Ca^{+2}- Mg^{+2} free phosphate-buffered saline (PBS), pH 7.4 (Pirbright Institute cell services unit)	Cell wash
2	4% PFA	4% Paraformaldehyde (PFA) solution in PBS (Chem Cruz SC-281692)	Cells and virus-infected cells fixation
3	Indirect immunofluorescence (IF) blocking buffer	0.5% Bovine serum albumin (BSA) (Sigma-Aldrich, 810533) in PBSa solution	Blocking of cells before IF staining and antibody dilution
4	Cell lysis buffer	RIPA (Radio-Immuno precipitation assay) cell lysis buffer (Thermo Scientific™, 89900)	Cell lysate preparation
5	PBST	0.01% v/v Tween 20 (Sigma, P2287) in PBSa	Western blot washing
6	WB blocking buffer	10% Skim Milk Powder (Millipore, 70166) in PBST	Blocking of western blot before staining
7	WB blocking buffer	5% Skim Milk Powder (Millipore, 70166) in PBST	Antibody dilution for western blotting
8	1x SDS-PAGE running buffer	20x TruPAGE™ TEA-Tricine SDS Running Buffer (Sigma-Aldrich, PCG3001)-1:5 dilution in deionised water	SDS-PAGE protein gel running
9	Protein loading buffer	0.1% v/v NuPAGE™ Sample Reducing Agent (10X) (Invitrogen™, NP0004) in NuPAGE™ LDS Sample Buffer (4X) (Invitrogen™, NP0008)	Protein samples (cell lysates) loading on 4-20% TruPAGE™ Precast Gels (Sigma-Aldrich, PCG2004)
10	1x Agarose gel preparation and running buffer	UltraPure™ TBE Buffer, 10X (Invitrogen™, 15581044)-1:10 dilution in deionised water	DNA Agarose (Invitrogen™™, 16500500) gel electrophoresis
10	Cell permeation buffer	0.01% v/v Triton™ X-100 (Sigma-Aldrich, X100) in PBSa	Cells treatment in IF assay and plaque assay
11	Blocking buffer (plaque assay)	5 mg/ml BSA (Sigma-Aldrich, 810533), and 0.01% v/v Tween 20 (Sigma-Aldrich, P2287) in PBSa	IF plaque assay-blocking of cells before immunostaining and antibody dilution

2.5.1.3. Commonly used reagents

Table 2.13: List of common reagents used in this study

Sr. No.	Reagent Name	Use
1	No SDS Gel Loading Dye, Purple (6X), (NEB, B7025S)	1x PCR Samples prepared in a loading dye (Agarose gel electrophoresis)
2	GelRed™ Nucleic Acid Gel Stain, 10,000X in Water, (Biotium, BT41003)	Nucleic acid visualisation on agarose gel using Bio-Rad Gel Doc™ EZ System
3	1 kb Plus DNA Ladder (NEB, N3200)	DNA marker for western blotting
4	Precision Plus Protein™ All Blue Prestained Protein Standards (Bio-Rad, #1610373)	Protein marker for western blotting
5	NuPAGE™ LDS Sample Buffer (4X) (Invitrogen™, NP0008)	Loading buffer of protein samples
6	NuPAGE™ Sample Reducing Agent (10X) (Invitrogen™, NP0004)	Dithiothreitol (DTT) used to reduce the disulphide bonds of proteins and peptides

2.2. Methods

2.2.1. Cell culture techniques

2.2.1.1. Culturing, passaging, and storage of adherent cells

Cell lines listed in table 2.1 **(section 2.1.1.)** were revived from the frozen state by flash thawing in 37^{O}C water bath and resuspended in a cell line-specific complete growth media listed in Table 2.11 **(section 2.1.5.1.)** and centrifuged at 325 x g. The supernatant was discarded, and the cell pellet resuspended in complete growth media. The cells were cultured in 25 cm^3 tissue culture flasks, incubated at 37^{O}C inside 5% CO_2 incubator until 80 to 90% confluence attained. Once cells were 80 to 90% confluent, cells were washed with sterile PBSa **(Table 2.12)** solution and covered with 0.25% (w/v) Trypsin - 0.53 mM Versene solution **(Table 2.11)** until cells were detached from the flask surface (detachment of cells was confirmed under a bright-field microscope). The trypsinisation was stopped by inactivation of Trypsin-Versene solution with the addition of FBS-containing growth media and centrifuged at 325 x g before passaging into new culture flasks. All cells used in the

study were frequently tested before cell freezing and after frozen cell revival for mycoplasma contamination using MycoAlert™ Mycoplasma Detection Kit (Lonza, LT07-118) according to the manufacturer's instructions.

Every after ten passages, cells were stored in liquid nitrogen tanks. Cells were cultured to attain 80 to 90% confluence, trypsinised, and pelleted in sterile 50 ml Falcon tubes. The cell pellet was resuspended in freezing media consisting of 90% FBS and 10% dimethyl sulfoxide (DMSO) (Sigma-Aldrich, DM8418). The cell suspension containing 1 to 3 × 10^6 cells/ml aliquoted in cryovials and stored overnight at -80^{O}C in isopropanol filled Mr Frosty™ Freezing container (Thermo Scientific™, 5100-0001). Next day, frozen cryovials were transferred to the liquid nitrogen tank until further use.

2.2.1.2. Cell counting and cell seeding in culture vessels

The number of viable cells was counted using a Neubauer Hemocytometer based on dye exclusion principle utilising 0.4% trypan blue solution (Gibco™-15250061). Cells were diluted ten fold using 0.4% trypan blue solution (10 µl cell suspension with 90 µl 0.4% trypan blue solution) before loading 10 µl on the grid of the haemocytometer. Trypan blue dye is absorbed only by dying cells due to permeable cell membranes and stains the cell cytoplasm blue which differentiate viable cells from dead cells. Viable cells per ml of the suspension were counted using the following formula.

$$\text{Cells per ml} = \frac{\text{Average no. cells X Dilution factor (10) X Neubauer chamber volume } (10^4)}{\text{Number of Neubauer chambers (4 Big squares)}}$$

Viable cell count was used for seeding the cells in various types of culture vessels (plates and flasks) for 24 h based on the experimental requirement.

2.2.1.3. Transfection

Viable cells were seeded in 24- or 12-well plates 24 h before the transfection of plasmid DNA to attain 60 to 75% confluence. Plasmid DNA was transfected in cells using Opti-MEM I reduced serum media **(Table 2.11)** and Lipofectamine® 2000 transfection reagent (Invitrogen™, 11668019). Plasmid DNA and Lipofectamine® 2000 dilutions were prepared using Opti-MEM I media according to the manufacturer's instructions. Transfection mixture (plasmid DNA+ Lipofectamine + Opti-MEM I) was incubated for 30 minutes at room temperature to facilitate DNA uptake and condensation inside the micelle (Lipofectamine).

Cells to be transfected were washed with sterile PBS and replenished with 5% FBS containing antibiotic-free transfection media **(Table 2.11)**, the transfection mixture was added onto cells drop by drop covering the culture plate surface area. Cells were incubated at 37^{O}C inside 5% CO_2 incubator. The media replaced with complete growth media **(Table 2.11)** 6 to 8 hpi. The list of plasmids used in this PhD project are presented in **Table 2.14**.

Table 2.14: List of plasmids used in this study

Sr. No.	Plasmid Name	Gene expression
1	pEFplink.2-V5 Empty (Steve Goodbourn's Lab)	Empty
2	pEFplink.2-V5/NP (Cloned in this PhD)	NDV-NP
3	pEFplink.2-V5/P (Cloned in this PhD)	NDV-P
4	pEFplink.2-V5/M (Cloned in this PhD)	NDV-M
5	pEFplink.2-V5/V (Cloned by Manoja Rasamanikkam, PhD, Pirbright Institute)	NDV-V
6	pEFplink.2-V5/F (Cloned in this PhD)	NDV-F
7	pEFplink.2-V5/HN (Cloned in this PhD)	NDV-HN
8	pcDNA3.1(+) EGFP (AVO Group, Pirbright Institute)	EGFP only
9	pcDNA3.1(+) EGFP/HN (Cloned in this PhD)	NDV-HN and EGFP
10	pAT016 (mito-mRFP-EGFP) (provided by PD Dr Andreas Till, University of Bonn, Germany)	In frame expression of RFP and EGFP
11	pBABEpuro-HA-p62 (Addgene, 71305)	p62/SQSTM1
12	pLV01 (All in one lentiviral vector from Sigma-Aldrich), three plasmids expressing different gRNA targeting p62/SQSTM1 pLV01-p62-18, pLV01-p62-19, and pLV01-p62-20	Guide RNA (gRNA) targeting SQSTM1, Puromycin N-acetyltransferase (PAC), Cas9, and GFP)
13	pGEM-T SV40 Renilla PolyA MfeI (AVO Group, Pirbright Institute)	Renilla luciferase from sea pansy (*Renilla reniformis*)
14	pNiFty-Luc (Dalan Bailey lab, Pirbright Institute)	ELAM proximal promoter, five NF-κB repeated transcription factor binding sites (TFBS) and a Luc reporter gene. (Firefly luciferase from beetles *Photinus pyralis*)
15	SQSTM1 1 nanomole siRNA (siRNA ID s16962, Ambion) Sense strand: 5'CUUCCGAAUCUACAUUAAAtt 3' (21) Antisense: 3'UUUAAUGUAGAUUCGGAAat 5' (21)	siRNA transfection to knockdown p62/SQSTM1 in Caco-2 cells
16	Silencer™ Negative Control No. 1 siRNA (Invitrogen™, AM4611)	Negative control for siRNA silencing

2.2.1.4. Cell viability and cell toxicity assay

For both the cell viability and cell cytotoxicity assays, 1 x 10^5 cells were plated per well of a 96-well plate for all the treatments 24 h before the virus infection studies. Promega GloMax® Explorer multimode microplate reader was used to read the plate.

A) Cell Viability Assay

Viability of NDV-infected cells was measured using CellTiter-Blue® Cell Viability Assay (Promega, G8080) comparative to the mock-infected control cells. The cell viability assay was performed according to the manufacturer's instructions. The principle of the assay was based on the metabolic conversion of resazurin in fluorescent resorufin by viable cells **(Figure 2.2)**. The fluorescence was measured at 590 nm. The fluorescence was directly proportional to the number of viable cells.

Human cancer cells (Table 2.1) were plated at 1x 10^5 cells per well in 96-well plates and cultured at 37^{O}C inside 5% CO_2 incubator. Once cells were 90% confluent they were infected with ten-fold dilutions of NDV strains mentioned **(Table 2.2)** and incubated until different time points (0 to 6 dpi and 9 dpi) post-infection. Cell viabilities were measured by adding 20 µl of CellTiter-Blue® reagent to 100 µl growth medium in each well of a 96-well plate. The plates were incubated 4 to 6 h at 37^{O}C inside 5% CO_2 incubator, before measuring the fluorescence in the plate reader.

Measured cell viabilities were converted in viability fraction; the viability fraction was calculated using the following formula.

$$\text{Viability Fraction} = \frac{\text{Normalised fluorescence reading of infected cells at } (560_{Ex}/590_{Em})}{\text{Normalised fluorescence reading of uninfected cells at } (560_{Ex}/590_{Em})}$$

Note: fluorescence readings were normalised with blank reagent controls.

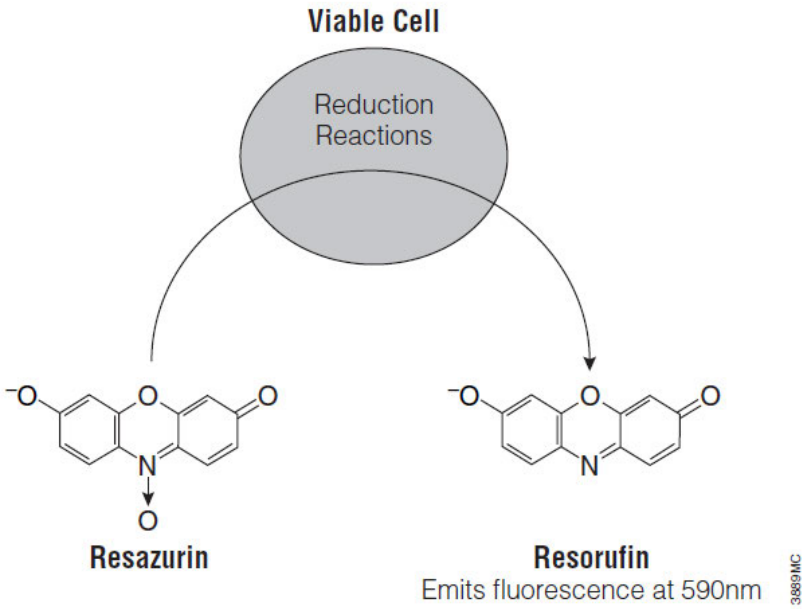

Figure 2.2. Viable cells metabolically convert resazurin to resorufin (Taken from Promega protocol). Metabolically active cells reduce resazurin substrate into a fluorescent product resorufin in up to 4 to 6 h incubation at 37^{O}C inside 5% CO_2 incubator. The fluorescent resorufin measured at 590 nm using Promega GloMax® Explorer Multimode Microplate Reader. The fluorescence produced is proportional to the number of viable cells.

B) Cell death assay

Cell death induced by NDV infection was measured using CellTox™ Green Cytotoxicity Assay (Promega, G8741). The principle involved in cytotoxicity assay was based on the changes in the membrane integrity of dying cells. A proprietary asymmetric CellTox™ Green DNA binding cyanine dye was taken up by dead cells, excluding the living cells as a result of a disruption in membrane integrity. The dye binding to the dead cell DNA resulted in the enhanced and robust fluorescent signal, which was measured at 520–530 nm. The fluorescent signal produced by the dye-bound dead-cell DNA was directly proportional to cytotoxicity in the cells. Caco-2 and VR Caco-2 cells were infected with NDV strains **(Table 2.2)** at 0.1 MOI for 4 days. End-point cytotoxicity assay was performed using the manufacturer's instructions in NDV-infected cells. The fold change in cytotoxicity was calculated using the following formula.

$$\text{Fold change cytotoxicity} = \frac{\text{Cytotoxicity of NDV-infected cells normalised with blank reagent}}{\text{Cytotoxicity of mock-infected cells normalised with blank reagent}}$$

2.2.1.5. Caspase-3/7 activity assay

The NDV-induced apoptotic activity was measured in NDV-infected Caco-2 and VR Caco-2 cells by using Caspase-Glo® 3/7 assay (Promega, G8090). Both cells were plated at 1 x 10^5 cells per well in a 96-well plate for 48 h before infection to ensure 90% confluence. Cells were infected with NDV strains **(Table 2.2)** at MOI **(discussed in section 2.2.2.6)** of 1 for 24 h. Both cells were treated with 10 µM Staurosporine (Sigma-Aldrich, S5921) as a positive control for 8 h before the addition of Caspase-Glo® 3/7 reagent. The assay was performed as per manufacturer's instructions; plates were incubated for 30 minutes in the dark before reading the luminescence (in relative light units (RLU)) on Promega GloMax® Explorer multimode microplate reader.

The luminescence produced was directly proportional to the caspase 3 and 7 activity in the cells.

2.2.1.6. Luciferase assay

The pNiFty-Luc is an NF-KB-inducible luciferase reporter plasmid, which expresses transcription factor binding sites (TFBS) regulated by NF-kB-specific endothelial cell-leukocyte adhesion molecule (ELAM-1) promoter. Nuclear factor NF-kB gets activated by various PRRs stimulated by PAMPs. The NF-kB transcription factor is composed of p65 and p60 subunits, which bind to TFBS and induce firefly luciferase activity. The luciferase activity is directly proportional to induction of NF-kB in the cells. Renilla luciferase was used as a control for firefly luciferase mediated NF-kB induction.

The NF-kB activity was measured in the uninfected Caco-2 cells, NDV-infected Caco-2 and VR Caco-2 cells using Dual-Glo® Luciferase assay system (Promega, E2940). All cells were transiently co-transfected with pGEM-T SV40 Renilla and pNiFty-Luc plasmids **(Table 2.14)** in 1:2 ratio using Lipofectamine® 2000 transfection reagent **(section 2.2.1.2.)** for 48 h. Caco-2 cells were infected with B1-GFP NDV strain at MOI of 5 for 18 h. All the cells were lysed using Dual-Glo® Luciferase reagents, and the dual-luciferase assay was performed according to the manufacturer's instructions. The luminescence of firefly and renilla luciferases sequentially measured (in RLU) using the Promega GloMax® Explorer, multimode microplate reader.

The NF-kB activity was calculated using the following formula.

$$\text{Firefly luciferase / Renilla luciferase (in RLU)} = \frac{\text{Firefly luciferase of sample - Firefly luciferase of blank}}{\text{Renilla luciferase of sample – (Firefly + Renilla) luciferase of blank}}$$

2.2.1.7. Cell proliferation assay

Cell proliferation assay in Caco-2 and VR Caco-2 cells was measured based on CFSE dye dilution principle in dividing cells using the CellTrace™ CFSE cell proliferation Kit, (Invitrogen™, C34570) and flow cytometry analysis of CFSE labelled cells at 488 nm.

Both cell lines were cultured in T-25 tissue culture flasks, incubated at 37^{O}C inside 5% CO_2 incubator until 80 to 90% confluence attained. Cells were trypsinised and centrifuged at 325 x g, and cell pellets were washed with serum-free MEM media. Cell pellets were resuspended in serum-free MEM media. Suspended cells were mixed with 5 µM CFSE buffer (5 µl of 10 mM CFSE stock in 10 ml of serum-free MEM media) to maintain 1 x 10^6 cells/ml in 2.5 µM CFSE buffer. Cells in CFSE buffer were in incubated in 37^{O}C water bath for 15 minutes to label DNA. CFSE labelled cells were washed with serum-free MEM media and resuspended in complete growth media **(Table 2.11)** at 37^{O}C water bath for 1 h. Cells were washed again and resuspended in complete media. Cells were plated in 24 well plates at 5 x 10^5 cells/well and incubated at 37^{O}C inside 5% CO_2 incubator. Cells were collected at five different time points 0, 12, 24, 48, and 72 h of post CFSE labelling. The fluorescence of CFSE cells was measured at each time point using MACSQuant Analyzer (Miltenyi Biotec).

Cell proliferation of Caco-2 and VR Caco-2 cells was also monitored using the IncuCyte Live-cell Analysis system (Sartorius) in real-time. Both types of cells were seeded in 96-well plates at different seeding densities (5k/well, 10k/well, and 15k/well) and cell proliferation was observed by taking an account of cell confluence at different time points.

2.2.1.8. Indirect immunofluorescence (IF) assay

Indirect immunofluorescence staining approach was used to detect the expressions of NDV proteins (NP, P, M, V, F, and HN) and endogenous expression of p62/SQSTM1 protein in Caco-2 and VR Caco- 2 cells. Cells were either transiently transfected with p62/SQSTM1 expressing plasmidsor were infected with NDV.

For IF staining, cells were cultured on coverslips (13 mm diameter) in a 24-well plate to attain 50 to 60% confluence before transfection or infection. Cells with or without virus infection and with or without plasmid transfection were fixed using cold 4% PFA **(Table 2.12)** for 1 h at room temperature. Fixed cells were permeabilised by treating cells with 0.1% Triton X100 PBSa buffer **(Table 2.12)** for 15 minutes. Cells were blocked with 0.5% BSA blocking buffer **(Table 2.12)** for 1 h at room temperature and stained with respective primary antibody (1:1000) listed in **Table 2.9** for 1 h at room temperature on a rocking

platform. Primary antibody-treated cells were washed three times with PBSa and then treated with respective Alexa Flour 488/568 secondary antibodies (1:500) **(Table 2.10)** for 45 minutes at room temperature on a rocking platform in the dark and finally washed again with PBSa three times. Coverslips were then mounted carefully on grease-free glass slides using VECTASHIELD® (Vectorlabs, H-1200), the mounting medium containing nucleic acid stain DAPI. Treated cells were imaged using the confocal microscope with a Leica application suite (LAS) software for imaging (Leica, UK).

2.2.1.9. siRNA mediated to knockdown

The RNA interference (RNAi) approach was used in silencing sqstm1 mRNA transcript, which encodes p62/SQSTM1 adapter protein involved in the selective mitophagy and tumorigenesis.

Caco-2 cells were plated at 5 x 10^5 cells in a 24-well plate, 24 to 36 h before transfection to ensure 60 to 70% cell confluence. A 21-nucleotide long small interfering RNA (siRNA) targeting sqstm1 mRNA and negative control siRNA were transfected in Caco-2 cells using Lipofectamine® 2000 transfection reagent **(Table 2.14)**. Three different concentrations 25 nM, 50 nM, and 100 nM prepared from 20 µM siRNA stocks in Opti-MEM I media; 0.5 % Lipofectamine® 2000 transfection reagent prepared in used Opti-MEM I media as mentioned in **Table 2.15**. The mixture of siRNA, Lipofectamine® 2000, and Opti-MEM I media incubated at room temperature for 30 minutes. Cells were washed with PBSa and replenished with 200 µl of antibiotic-free 5% FBS supplemented DMEM media. The transfection mixture was added drop by drop on the top cells and incubated at 37^{O}C inside 5% CO_2 incubator. The media replaced with complete growth media **(Table 2.11)** 6 to 8 hpi and incubated for 24 to 48 h at 37^{O}C.

Table 2.15: siRNA transfection mixture preparation

Sr. No.	Reagent	Mixture A in µl per well	Mixture B in µl per well	Final siRNA concentration for 300 µl (100 µl transfection mixture + 200 µl antibiotic-free 5% FBS transfection media)
1	Opti-MEM	50	50	
2	Lipofectamine 2000	-	1.5 (0.5% of total media volume)	
3	20 µM siRNA	1.5	-	100 nM
		0.75	-	50 nM
		0.375	-	25 nM
4	Incubate mixture A and B at room temperature for 5 minutes			

5	Mixture B was added to the mixture A (siRNA + Lipofectamine® 2000 + Opti-MEM I media), incubate the mixture at room temperature for 30 minutes.

2.2.1.10. CRISPR/Cas9 KO

CRISPR/Cas9 uses RNA guided target-specific editing of the gene of interest through Cas9 (DNA endonuclease) enzyme upstream to PAM (protospacer adjacent motif) associated with the target DNA sequence.

CRISPR/Cas9 based KO of *sqstm1* gene encoding p62/SQSTM1 protein in human cells was accomplished by using an all-in-one lentiviral vector pLV01 (Sigma-Aldrich). The pLV01 encoded guide RNA (gRNA) targeting *sqstm1*under mammalian U6 promoter and puromycin N-acetyltransferase (PAC), Cas9, and GFP under EF1a promoter (vector map shown in **Figure 2.4B**). Three pLV01 vectors expressing different gRNAs were ordered to KO the *sqstm1* gene (list of gRNAs ordered shown in **Figure 2.4A**) in HEK-293 and Caco-2 cells. All three *sqstm1* targeting plasmids were transformed in high-efficiency NEB® stable, competent *E. coli* cells **(section 2.2.3.5.3.)** and then plasmids purified using QIAGEN plasmid purification kit **(section 2.2.3.6.)**.

Caco-2 and HEK-293 cells were plated at 1 x 10^6 cells/ml in a 6-well plate and incubated at 37^{O}C inside 5% CO_2 incubator. Cells were washed with PBSa after 70 to 80% confluence was attained and transfected with a lentiviral vector pLV01using Lipofectamine® 2000 transfection reagent and Opti-MEM I media **(section 2.2.1.3.)**. Transfected cells were incubated at 37^{O}C for 48 to 72 h before puromycin (Sigma-Aldrich, P8833) selection in Caco-2 and HEK-293 cells. Puromycin concentrations was optimised by kill curve in both the cell lines, 2.5 µg/ml and 5 µg/ml puromycin concentrations to select transfected HEK-293 and Caco-2 cells, respectively. Puromycin selection and GFP expression qualitatively confirmed the expression of gRNA and Cas9 genes in transfected cells. Puromycin selected GFP positive cells were serially diluted to get 1 cell/ml in complete growth media and plated in 24 well plate to grow single-cell clones of gRNA and Cas9 expression system. Single cells were incubated at 37^{O}C in 5% CO_2 incubator until cells were grown as colonies, which were then trypsinised and cultured in a new 24-well plate with fresh complete growth medium. Single-cell clones were tested for sqstm1 KO by IF staining and confocal imaging, western blotting and PCR amplification methods.

A

Target ID/Clone Name	Target Sequence:5'-3' (does not include with PAM)	PAM	RefseqId/Target mRNA Exon	Gene Symbol, Gene ID, Chromosome	Start Coordinate
HS0000134618	CGGTGGGCGGTGGTCCCGC	CGG	NM_003900/3 XM_017010010/3 NM_001142298/4 NM_001142299/4	SQSTM1 8878 5	179823871
HS0000134619	ATTGGGGTGCACCATGTTG	CGG	NM_003900/3 XM_017010010/3 NM_001142298/4 NM_001142299/4		179823910
HS0000134620	GCCATCGCAGATCACATTG	GGG	NM_003900/3 XM_017010010/3 NM_001142298/4 NM_001142299/4		179823925

B

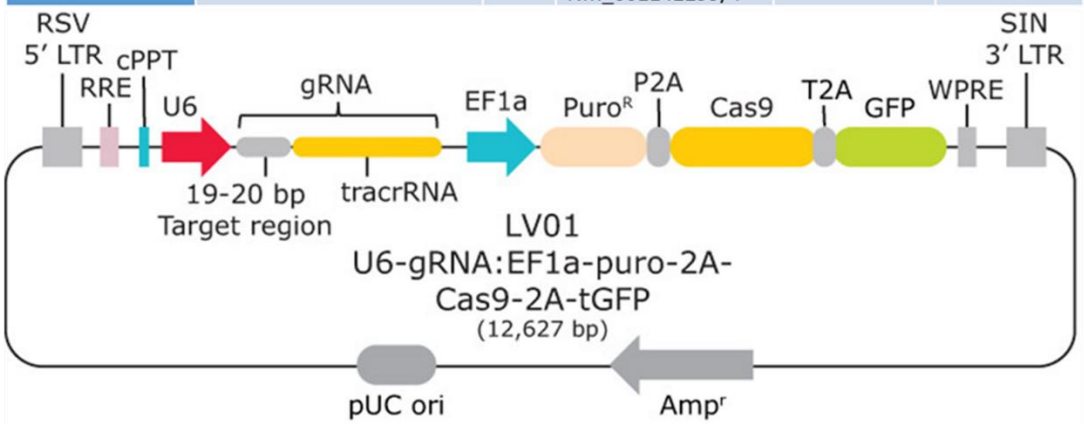

Figure 2.3. The strategy of lentiviral vector-based CRISPR/Cas9 KO of p62/SQSTM1. (A) Sequences of guide RNAs (gRNA) to knockout human p62/SQSTM1 transcripts. **(B)** Lentiviral pLV01 vector map showing all-in-one custom gRNA expression plasmid provided by Sigma-Merck expresses gRNA under mammalian U6 promoter and Cas9, GFP, and a puromycin N-acetyltransferase (PAC) under EF-1a promoter.

2.2.2. Virology techniques

2.2.2.1. Propagation of virus

A) NDV propagation

NDV strains listed in **Table 2.2**, were propagated in 10-day-old specific pathogen-free (SPF) embryonated eggs (Valo Biomedia GmbH). Eggs were candled to check the viability of the embryo and to mark the air sac before virus inoculation. Viable eggs were disinfected with 70% ethanol, and a hole was punctured on the top of the air sac. Then 100 µl of virus dilution (1:1000 virus dilution in sterile PBSa) inoculated in the allantoic cavity through 1 ml syringe using 22 G needle passing through the chorioallantoic membrane in 45^{O} angle. Inoculated eggs were incubated in 60% humidified incubator at 37^{O}C on the egg turner for 72 h. After incubation, eggs were euthanised by chilling in the refrigerator for at least for 4 h to overnight. The allantoic fluid and amniotic fluid was harvested and pooled together from the eggs. The combined virus was centrifuged at 3000 x g for 20 to 30 minutes at 4^{O}C; the cleared virus was aliquoted in 1ml volume into cryovials and stored in -80^{O}C.

B) Vesicular stomatitis virus (VSV) propagation

VSV tagged with EGFP was grown in the cell culture. Caco-2 cells were cultured in 75 cm^3 tissue culture flask and at 37^{O}C inside 5% CO_2 incubator to attain 90% confluence. Then cells were infected by adding 1 ml of virus dilution (1:1000 virus dilution in sterile PBSa) into culture flask, and infected cells were incubated at 37^{O}C inside 5% CO_2 incubator for 24 h. Cell supernatant was harvested and centrifuged at 3000 x g for 20-30 minutes at 4^{O}C; the cleared virus was aliquoted in 1ml volume into cryovials and stored at -80^{O}C.

2.2.2.2. Confirmation of virus by haemagglutination assay (HA)

Haemagglutination assay (HA assay) was used to confirm NDV propagation in the viable embryonated eggs. A two-fold serial dilution of the virus in PBSa was achieved in a V-bottom 96-well plate (Greiner Bio-One) using a multichannel pipette. In a V-bottom 96-well plate, each well contained 50 µl of each two-fold dilution of virus (from neat virus, 1:2, 1:4, up to 1:1024) in triplicates. Similarly, 50 µl of PBSa and allantoic fluid from PBS-inoculated eggs were used as controls for the assay. Then 50 µl of 1% chicken red blood cells (cRBCs) (from Pirbright animal facility) prepared in PBS was added to the V-bottom 96 well plate followed by 1 h incubation at 4^{O}C or on ice. Haemagglutination was observed as a result of NDV-HN protein binding to the sialic acid receptors on cRBCs in the form of the immobile lattice at the bottom of the plate, whereas in case of PBS and allantoic fluid cRBCs settled at the bottom were mobile. HA assay was also used to calculate HAU (haemagglutinating units) based on last virus dilution showing hemagglutination in the V-bottom 96-well plate.

2.2.2.3. Receptor binding avidity assay

Receptor binding avidity assay was used to determine the affinity of the NDV-HN protein to the host cell sialic acid receptors by using the α2-3,6,8 neuraminidase (NEB, P0720S) enzyme. The α2-3,6,8 neuraminidase enzyme isolated from *Clostridium perferingens* cleaves α2-3, α2-6 and α2-8 linked N-acetyl-neuraminic acid (sialic acid residues) from glycoproteins and oligosaccharides. cRBCs were treated using different enzyme units of α2-3,6,8 Neuraminidase. Initially, two-fold dilutions of α2-3,6,8 neuraminidase enzyme prepared, as shown in **Table 2.16**.

Table 2.16: Two-fold dilutions α2-3,6,8 neuraminidase enzyme in PBSa

Dilution	α2-3,6,8 neuraminidase (50,000 U/ml) in µl	PBS in µl	Final conc. of in U/ µl
1:2	2.5	2.5	25
1:4	2.5 of (1:2)	2.5	12.5
1:8	2.5 of (1:4)	2.5	6.25
1:16	2.5 of (1:8)	2.5	3.125
1:32	2.5 of (1:16)	2.5	1.5625
1:64	2.5 of (1:32)	2.5	0.78125
1:128	2.5 of (1:64)	2.5	0.390625

1 ml of 10% cRBCs were treated with different α2-3,6,8 Neuraminidase units, as shown in **Table 2.17**.

Table 2.17: α2-3,6,8 Neuraminidase enzyme in units used for cRBCs treatment

α2-3,6,8 neuraminidase (50,000 U/ml) stock added	Estimated final concentration of α2-3,6,8 neuraminidase (in U) in 1 ml of 10% cRBCs
10 µl (from stock)	500 U
5 µl (from stock)	250 U
2.5 µl (from stock)	125 U
2.5 µl (from 1:2)	62.5 U
2.5 µl (from 1:4)	31.25 U
2.5 µl (from 1:8)	15.6 U
2.5 µl (from 1:16)	8 U
2.5 µl (from 1:32)	4 U
2.5 µl (from 1:64)	2 U
2.5 µl (from 1:128)	1 U

α2-3,6,8 Neuraminidase treated 10% cRBCs were incubated in 37^{O}C water bath for 2 h with intermittent mixing every 15 minutes to ensure homogenous enzyme treatment of cRBCs. In the meantime, viruses to be tested for NDV-HN receptor binding avidity assay for sialic receptors expressed on cRBCs were titrated using HA assay **(section 2.2.2.2.)**, for each virus, HAU was maintained at 4 HAU per 50 µl volume. Two hours later, treated cRBCs were washed with PBSa and resuspended to 10 ml to get 1% cRBCs. All treated

cRBCs at α2-3,6,8 neuraminidase mentioned in **Table 2.17** were used for HA assay in triplicate using 4 HAU per 50 µl of the virus. The negative control with PBSa for each treated cRBCs was used. The highest α2-3,6,8 neuraminidase unit treated cRBCs showing haemagglutination was recorded as an indication of affinity to partially desialylated cRBCs.

2.2.2.4. Virus infection

Cells were plated in desired cell culture plates (96-well, 24-well, 12-well or 6-well plates) at a required seeding density of cells to attain >90% confluence on the day of infection. For cell infections, virus stock was diluted in cold serum-free media. Cells were washed with PBSa before infection, and then the volume of virus dilution was added to each well on top of the cells depending upon the culture vessel (0.05 ml for 96-well plate, 0.25 ml for 24-well plate, 0.5 ml for 12-well plate or 1 ml for 6-well plate) to cover the surface area and uniform distribution of virus throughout the plate. Infected cells were incubated at 37^{O}C inside 5% CO_2 incubator for 1 h. Cells were washed with PBSa after 1 h of incubation to remove the unattached virus particles and replaced with either 1 ml of complete growth media or plaque assay 0.8% methylcellulose overlay media **(Table 2.11)**.

Cells infected with the reporter viruses **(Table 2.2)** were imaged in real-time using the IncuCyte Live-cell Analysis system (Sartorius) to monitor the virus replication as indicated by the expression of the reporter protein (GFP).

2.2.2.5. Virus titration using plaque assay

Plaque assay methods for NDV and VSV in chicken DF-1 and human Caco-2 cells are discribed below. Plaque forming units per ml (PFU/ml) of both the viruses were calculated using the below formula.

PFU/ml = Average no. of plaques / (D x V)

D = Dilution factor of virus used to count the number of plaques

V = Volume of virus dilution used in the infection

A) NDV plaque assay

NDV plaque assays were carried in chicken DF-1 cells and human Caco-2 cells **(Table 2.1)** in a 24 well plate. Ten-fold virus dilutions were used in the infection, and cells were infected as described in **section 2.2.2.4**. For the plaque assay, 0.8% methylcellulose overlay media was used **(Table 2.11)**. Infected plates were incubated for 7 days at 37^{O}C inside 5% CO_2 incubator. The infected cells were fixed by adding 1 ml of cold 4% PFA **(Table 2.12)**

overnight and plates were kept at room temperature in a closed container inside the fume hood. The plaque assay overlay media with 4% PFA was discarded, and cells were washed with PBSa four times to remove contents of media and cell debris. Fixed cells were permeabilised with 0.1% Triton X100 PBSa solution **(Table 2.12)** for 15 minutes and then blocked with blocking buffer (5 mg/ml BSA and v/v 0.01% Tween 20 in PBSa, **Table 2.12**) for 1 h at room temperature. Cells were treated with the anti-NDV chicken sera **(Table 2.9)** (1:2000 dilution prepared in the blocking buffer) for 1 h at room temperature on the rocking plate. Cells probed with anti-NDV chicken sera, were washed for three times with PBSa five minutes each. Then cells were incubated with secondary fluorescent donkey IRDye® 800CW anti-Chicken antibody **(Table 2.10)** for 45 to 60 minutes in the dark on the rocking plate. Finally, cells were washed with PBSa three times for five minutes each in the dark. Stained plates were read using the Odyssey® CLx Imaging System (LI-COR) and analysed using Image Studio Lite software (LI-COR) for the detection of plaque-forming units.

B) VSV-GFP plaque assay

VSV-GFP plaque assays were carried in chicken DF-1 cells and human Caco-2 cells **(Table 2.1)** in a 12 well plate. Ten-fold virus dilutions were used to infect the cells **(section 2.2.2.4)**. For the plaque assay, 0.8% methylcellulose overlay media was used. Infected plates were incubated for 3 days at 37^{O}C inside 5% CO_2 incubator in an upright position. The cells in infected plates were fixed by adding 1 ml of cold 4% PFA **(Table 2.12)** for overnight and plates were kept at room temperature in a container inside the fume hood. The plaque assay overlay media with 4% PFA was discarded, and cells were washed with PBSa four times to remove contents of media and cell debris. Fixed cells were stained with 0.1% crystal violet (Sigma-Aldrich, C0775) solution prepared in 20% methanol for 1 to 2 h. Stained cells were washed under running tap water to visualise the plaques.

2.2.2.6. Multiplicity of infection (MOI) calculation

The multiplicity of infection (MOI) is a critical aspect to control and estimate the number of virus particles entering the host cell in virus-infection studies. The plaque-forming unit (PFU) is a measure of the number of an infectious virus particle, which used in the calculation of MOI.

MOI is a measure of the number of virus particles per cells, calculated by the following formula.

$$\text{Multiplicity of infection (MOI)} = \frac{\text{PFU/ml of virus used in the infection}}{\text{Number of cells to be infected}}$$

For virus-infection studies in this PhD project, the volume of virus dilution or stock was calculated to achieve infection at required MOI by using the following formula.

$$\text{Volume of virus dilution or stock} = \frac{\text{MOI to be achieved X Number of cells to be infected}}{\text{PFU/ml count of the virus}}$$

2.2.2.7. Use of flow cytometry to quantify virus infection

Caco-2 and VR Caco-2 cells were infected with different reporter viruses listed in **Table 2.2**. The cells were infected **(section 2.2.2.4.)** with NDV reporter viruses (B1-GFP and LaSota-GFP), avian influenza reporter virus (H9N2-GFP), and VSV-GFP at MOI of 0.1 (calculated as mentioned in **section 2.2.2.6.**). Cells were trypsinised after 48 hpi and fixed with 4% PFA for 1 h at room temperature. After fixation cells were washed and resuspended in cold PBSa to measure GFP intensity at 488 nm using MACSQuant Analyzer. The fluorescence intensity of GFP was directly proportional to the % of reporter virus replication in the cells.

2.2.3. Molecular techniques

2.2.3.1. DNA Extraction

DNA was extracted from sqstm1 KO HEK-293 cell clones and HEK-293 cells using DNeasy Blood & Tissue Kit (Qiagen, 69504) according to the manufacturer's protocol. Genomic DNA was eluted using 100 µl of AE buffer.

2.2.3.2. Polymerase chain reaction (PCR) amplification

Polymerase chain reactions were used to amplify genes of interest with gene-specific primers using Q5® High-Fidelity 2X Master Mix (NEB, M0492). Gene-specific forward and reverse primers **(section 2.1.3.)** 1.25 µl each, and 10-100 ng DNA was added to 12.5 µl of

2X master mix. The reaction volume was made up to 25 µl using nuclease-free water. Thermal cycling conditions were set according to the manufacturer's instructions, and annealing temperatures were calculated using the **NEB Tm calculator**. All PCR products were separated by agarose gel electrophoresis **(section 2.2.3.3.)**.

2.2.3.3. Agarose gel electrophoresis

Agarose gel electrophoresis was used to separate DNA; 0.5% to 2% agarose gels were prepared in 1x Tris/borate/EDTA (TBE) **(Table 2.12)** buffer depending upon the size of DNA fragments. DNA samples were prepared in 6x purple gel loading dye and 1 kb Plus DNA ladder **(Table 2.13)** was loaded on the gel with samples for identification of separated DNA fragments. A DNA binding dye GelRed™ was added in the gel for DNA visualisation. DNA gel was run at between 80-100V using 1x TBE buffer **(Table 2.12)**. A Gel Doc™ EZ Imager (Bio-Rad) was used for DNA gels using the 'GelRed' setting.

2.2.3.4. PCR product purification and Gel extraction

All PCR products used for sequencing and cloning preparations were cleaned up by using QIAquick PCR Purification Kit (Qiagen, 28104) and DNA fragments of interest were extracted from agarose gel by using QIAquick Gel Extraction Kit (Qiagen, 28704). Manufacturer's protocols were used for PCR product clean up, and DNA extraction from agarose gel, DNA was eluted in 25-50 µl volume using elution buffer. Eluted DNA samples were quantified using NanoDrop Lite Spectrophotometer (Thermo Scientific).

2.2.3.5. Gene cloning

NDV genes were cloned using conventional restriction digestion of insert DNA and vector DNA, followed by ligation of complementary ends of the insert with self-replicating vector DNA before transformation in competent *E. coli* cells. NDV genes (NP, P, M, F, and HN) were PCR amplified using cloning primers mentioned in **Table 2.4** as described earlier in **section 2.2.3.2**, and gel extracted and purified as specified in **2.2.3.4**.

2.2.3.5.1. Restriction digestion

All PCR amplified and gel purified NDV genes and expression vectors pEFplink2.V5 and pcDNA3.1(+) EGFP were used for restriction digestion. NDV genes NP, P, M, F, and HN

were cloned into pEFplink.2-V5 and NDV-HN gene was also cloned into pcDNA3.1(+) EGFP vector. Both the vectors were double digested with restriction enzymes based on the insert restriction sites, mentioned in **Table 2.4**. High-fidelity restriction enzymes (RE) were purchased from NEB. Double-digestion of 1 µg vector DNA and 500 ng of PCR products were performed overnight at 37^{O}C using manufacturer's protocol. RE digested vector DNAs were gel electrophoresed to confirm the complete digestion. All RE treated products were purified using either PCR clean-up kit (PCR products) or gel extraction purification kit (vector DNAs) as **(section 2.2.3.4.)**. Restriction digestion used here generated sticky-end products.

2.2.3.5.2. T4-DNA ligation

Respective NDV inserts and vector DNA pairs were ligated using T4 DNA ligase (NEB, M0202). DNA inserts and vector DNA were mixed in 3:1 molar ratio, calculated using **NEBioCalculator**. A 10 µl ligation reaction was set according to the manufacturer's instructions at 4^{O}C for overnight.

2.2.3.5.3. *E. coli* transformation

Ligated recombinant plasmids and plasmids used in this PhD project were propagated using bacterial transformation. Highly efficient chemically competent *E. coli* cells (NEB® Stable Competent *E. coli*, C3040) were used. Briefly, 50 µl of *E. coli* cells were thawed carefully on ice, and 1 to 5 µl of ligation mixture or 100 pg to 100 ng of plasmid DNA was added to the cells. Cells and plasmid DNA mix were incubated on ice for 30 minutes, and heat-shock treated at 42^{O}C for precisely 45 seconds and chilled on ice for 2 minutes. Transformed cells were incubated at 37^{O}C for 1 h on bacterial shaker after addition 250 µl pre-warmed of S.O.C. media. Pre-warmed selection L.B. agar plates **(Table 2.11)** were used for 50 µl bacterial culture spreading on the plates and incubated in 37^{O}C bacterial incubator overnight.

2.2.3.5.4. Plasmid DNA screening

Transformed plasmids were screened to detect DNA insert in the expression vector by using colony PCR, mini preparation of plasmid DNA, and RE digestion of isolated plasmid DNA.

A) Colony PCR

Randomly, 10 to 25 colonies were selected from bacterial transformation plates for colony PCR to amplify inserted DNA. Bacterial colonies were used as a source of plasmid DNA; colonies were transferred on the new pre-warmed L.B. agar selection plates using sterile 10 µl tip and with the same tip was used to transfer colony remnants in PCR tube to maintain the same source of plasmid DNA in the screening. Cloning primers mentioned in **Table 2.4** were used in colony PCR with GoTaq® Green Master Mix (Promega, M7122). Master mix and primers were added to the colony containing a PCR tube and amplified at temperature programme as per the manufacturer's instructions. Final PCR products were separated using agarose gel electrophoresis **(section 2.2.3.3)**.

B) Small-scale plasmid DNA preparation

Positive screens from colony PCR grown on the screening L.B. selection agar plate was selected for plasmid DNA isolation on a smaller scale using the QIAGEN Plasmid Mini Kit (Qiagen, 12123). Positive colonies were inoculated in 5 ml of selection L.B. media **(Table 2.11)**, and cultures were incubated overnight at 37^{O}C in a bacterial incubator. Plasmid DNA was isolated according to the manufacturer's instructions. Plasmid DNA was eluted in 30 µl volume of elution buffer.

C) Restriction digestion

Plasmid DNA isolated from the mini preparations were used to detect DNA insert in the vector DNA by restriction digestion. Plasmids were double-digested, as described in **section 2.2.3.5.1.** at 37^{O}C overnight and gel electrophoresed to identify the cut DNA insert and linear vector DNA compared to cut and uncut vector DNA.

2.2.3.6. Large-scale plasmid DNA preparation

Once cloned plasmids were confirmed for the DNA insertion in the vector DNA **(section 2.2.3.5.4.)**, then confirmed clones were inoculated in 250 ml antibiotic containing L.B. media **(Table 2.11)** and incubated at 37^{O}C on a bacterial shaker overnight for large scale isolation of the plasmid DNA. Plasmid DNA was isolated on a large scale by using the QIAGEN Plasmid Maxi Kit (Qiagen, 12162). The plasmid DNA was isolated as per the

manufacturer's instructions. The plasmid DNA pellet was dissolved in 0.5 ml nuclease-free water and quantified using NanoDrop Lite Spectrophotometer (Thermo Scientific).

2.2.3.7. Plasmid DNA and PCR product sequencing

Plasmids and PCR products of interest were sequenced using Sanger sequencing services provided by Eurofins Genomics (UK). The DNA and primers were prepared as per the company's requirement for sequencing.

NDV genes cloned in pEFplink.2-V5 vectors were sequenced using pEFplink.2-V5 vector primers (forward and reverse) **(Table 2.4)** and NDV-HN gene cloned in pcDNA3.1(+) EGFP vector sequenced using M13 primers (forward and reverse).

DNA chromatograms were visualised using Flinch TV 1.4.0 (Geospiza), and DNA sequences were analysed by using Vector NTI® Express Designer software (Thermo Scientific).

2.2.3.8. RNA Extraction

2.2.3.8.1. Total RNA Extraction

Total RNA was extracted from virus-infected and non-infected Caco-2 cells, Ox-Caco-2, A549 cells, and VR Caco-2 cells using the TRIzol™ reagent (Invitrogen™, 15596018). To extract RNA from cells, 0.25 ml of TRIzol™ reagent was added to each well of 12-well plate and collected in 1.5 ml microtube. The cells were lysed, pipetted up and down several times and incubated for 5 minutes to ensure dissociation of the nucleoprotein complexes. Then 0.05 ml of chloroform was added to the tube and vortexed vigorously for 10 seconds and incubated for 2-3 minutes. The tubes were centrifuged at 12,000 x g at 4^{O}C for 15 minutes. The mixture got separated into three layers: top aqueous phase (RNA), interphase, and bottom phenol-chloroform organic phase (DNA and proteins). The aqueous phase was carefully transferred to RNase-free 1.5 ml microtube and RNA was precipitated by the addition of 0.125 ml of isopropanol and incubation for 10 minutes at room temperature. Total RNA was pelleted down by centrifugation at 12,000 x g at 4^{O}C for 10 minutes. The supernatant was carefully discarded using a micropipette and the pellet was washed with 0.5 ml of 75% ethanol prepared in RNase-free water at 7500 x g at 4^{O}C for 5 minutes. Then the RNA pellet was air-dried after careful discarding of 0.75% ethanol. The air-dried RNA pellet was resuspended in 15 to 30 µl of RNase-free water, and RNA was quantified using

NanoDrop Lite Spectrophotometer (Thermo Scientific). A ratio of A260/280 of ~2 was considered pure enough for SYBR-Green qRT-PCR analysis.

2.2.3.8.2. MicroRNA extraction

MicroRNA was isolated from NDV-infected, uninfected Caco-2 cells and VR Caco-2 cells using miRNeasy Mini Kit (Qiagen, 217004) and QIAzol® Lysis Reagent (Qiagen, 79306). The total RNA, including small RNAs, were isolated from the cells according to the manufacturer's instructions. The elution volume 30 to 50 µl RNase free water was used to collect the RNA and quantified using NanoDrop Lite Spectrophotometer (Thermo Scientific). The total RNA with small RNAs from all three cell types were used to quantify miR-155 using TaqMan RT-PCR.

2.2.3.8.3. RNA Quantification

Isolated total RNA was selectively and accurately measured at the lower concentration for sensitive assays using the Qubit™ RNA HS Assay Kit (Invitrogen™, Q32852). RNA samples and RNA standards were diluted in Qubit® assay tubes (Invitrogen™, Q32856) using Qubit® working solution (Qubit® RNA HS Reagent diluted 1:200 using Qubit® RNA HS Buffer) according to the manufacturer's recommendations. All samples and standards were incubated for 2 minutes at room temperature. RNA standards were used to calibrate Qubit® Fluorometer (Thermo Scientific). RNA concentrations were calculated using the following formula.

RNA concentration = QF value × (200 / A) x DF

Where, QF value = the value given by the Qubit® 2.0 Fluorometer

A = the number of microliters of sample added to the assay tube

DF = dilution factor of RNA

2.2.3.8.4. DNase Treatment

Isolated total RNA from cells was treated with RNase-free DNase I recombinant enzyme (Roche, 04716728001). The reaction mixture was prepared by adding 2U of DNase I per 1 µg of RNA and 1 µl of 10x reaction buffer (supplied by the manufacturer), made up to 10 µl reaction volume with RNase-free water. The reaction mixture was incubated at room temperature for 30 minutes. DNase I was heat-inactivated at 75^{O}C for 5 minutes. DNase I treated samples were stored at -80^{O}C and used for qRT-PCR or cDNA synthesis.

2.2.3.8.5. cDNA synthesis

Total RNA was isolated from NDV-infected Caco-2 and VR Caco-2 cells **(section 2.2.3.8.1.)** and treated with DNase I **(section 2.2.3.8.4.)**. Total RNA was used for cDNA preparation, which was used for Sanger sequencing of the NDV genome strategy **(section 2.1.3.3.)**. Hence NDV fragments were reverse transcribed to generate cDNA from isolated total RNA using SuperScript™ III First-Strand Synthesis System (Invitrogen™, 18080051). NDV genome was divided into six overlapping fragments; all six fragments were reverse transcribed using fragment-specific primers **(Table 2.5)**. Manufacturer's instructions were followed to synthesise all cDNA fragments.

cDNA fragments were PCR amplified **(section 2.2.3.2.)** and purified using a gel extraction method **(section 2.2.3.4.).** Purified PCR fragments were sent for Sanger sequencing using sequencing primers listed in **Table 2.6** and sequences were analysed **(section 2.2.3.7.)**.

2.2.3.9. Quantitative real-time (qRT)-PCR

2.2.3.9.1. One-step SYBR Green qRT-PCR

One-step SYBR Green qRT-PCR analysis was used to quantify log2 fold changes in IFN-β, ISG-15 and NDV-M mRNAs in virus-infected Caco-2, Ox Caco-2, A549, and VR Caco-2 cells. All cells were infected with NDV strains (Hitchner B1 and B1-GFP) at MOI of 5 for 12 h, with VSV-GFP at MOI of 0.1. All cells were transfected with dsRNA mimic polyinosinic-polycytidylic acid [poly(I:C)] high molecular weight (HMW) (Invivogen, tlrl-pic) at 0.2 µg/ml concentration for 12 h in A549 cells and 24 h in Caco-2 cells. Total RNA was isolated from all cells using the TRIzol method **(section 2.2.3.8.1.)**, and total RNA was treated with DNase I enzyme **(section 2.2.3.8.4.)**. SuperScript™ III Platinum™ SYBR™ Green One-Step qRT-PCR Kit (Invitrogen™, 11736051) was used for GAPDH, IFN-β, ISG-15 and NDV-M mRNA quantification using the primers listed in **Table 2.7**. The reaction mixtures were prepared according to the manufacturer's protocol. The thermal cycling programme used for cDNA synthesis was 50^{O}C for 3 minutes, hold at 95^{O}C for 5 minutes, followed by 40 PCR cycles at 15 seconds at 95^{O}C, annealing and elongation at 58 ^{O}C and final hold at 40^{O}C for 1 minute. Melt curve programme was used to ensure primer-specific amplification. SYBR Green qRT-PCR data were acquired and analysed using ABI 7500 Fast RT-PCR software (Applied Biosystems™).

2.2.3.9.2. TaqMan qRT-PCR

The number of copies of miR-155 was quantified using TaqMan qRT-PCR in Caco-2 cells with or without NDV infection and VR Caco-2 cells. MicroRNA isolated from all cells **(section 2.2.3.8.2.)** was used in this assay. The microRNA mimic miR-223-3p was used to prepare the standard curve to quantify miR-155 copies. Where 2 µM of miR-223-3p was diluted to get 6 x 10^8 copies/µl. Micro RNAs from all samples along with 6 x 10^8 copies/µl stock of miR-223-3p MicroRNA mimic were reverse transcribed to synthesise cDNA as described in following **Table 2.18** using TaqMan™ MicroRNA Reverse Transcription Kit (Applied Biosystems™, 4366596). The cDNA synthesis was completed using a temperature programme of 16^{O}C for 30 minutes and 42^{O}C for 30 minutes and the reaction was stopped at 85^{O}C for 5 minutes. Once cDNA synthesis was finished, all cDNAs samples were diluted up to 150 µl (135 µl nuclease-free water added); dilution of miR-223-3p mimic diluted to give 1 x 10^8 copies/ µl which then serially diluted ten-times in nuclease-free water to prepare dilutions for standard curve 1 x 10^8 copies/µl up to 1 x 10^1 copies/µl. The reaction mixtures for PCR were prepared in 20 µl volume (for all samples including all the standard dilutions) by adding 5 µl cDNA from stocks, 10 µl of 2x PCR master mix, 0.5 µl of TaqMan probe specific to miR-155 and miR-223-3p mimic microRNAs **(Table 2.8)**, and 4.5 µl of nuclease-free water. The plate was centrifuged at 1000 x g for 2 minutes before loading plate into RT-PCR machine. Temperature programme was 50^{O}C for 2 minutes for uracil-N-glycosylase (UNG) activation (UNG was used for degrading many contaminating carryover amplicons), 95^{O}C for 10 minutes for enzyme activation and 40 cycles were set using 95^{O}C for 2 minutes (denaturation) and 60^{O}C for 1 minute (annealing and primer extension). TaqMan qRT-PCR data were acquired and analysed using ABI 7500 Fast RT-PCR software (Applied Biosystems™). The copies of miR-155 were calculated using the following formulae.

Y= Slope X + Constant (from standard curve)

X = (average Ct - Constant) / slope

Antilog(X) = Number of miR-155 copies

Table 2.18: MicroRNA-specific cDNA synthesis reaction mixture

cDNA synthesis Master Mix 1		
Components	Volume in µl	Centrifuged briefly to collect reaction at the bottom of the tube and kept on ice
100mM dNTPs (with dTTP)	0.15	
MultiScribe™ Reverse Transcriptase, 50 U/µl	1	
10x Reverse Transcription Buffer	1.5	
RNase Inhibitor, 20 U/µl	0.19	
Nuclease-free Water	4.16	
Total volume	7	
cDNA synthesis Master Mix 2		
Components	Volume in µl	Incubation
5x RT Primer	3	85°C for 5 minutes 65°C for 5 minutes
RNA template	2	
Nuclease-free Water	3	
Total volume	8	
Centrifuged briefly to collect reaction at the bottom of the tube		
Master mix 1 was added to master mix 2 (total 15 µl)		

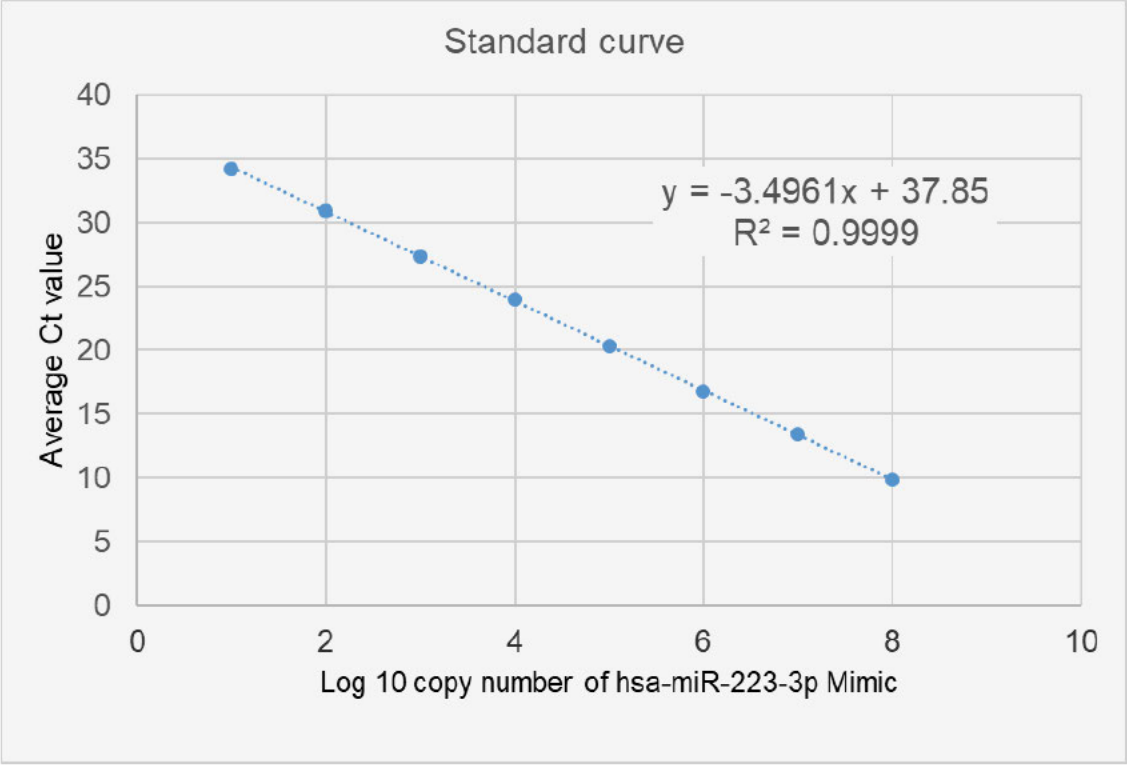

Figure 2.4. Standard curve of miR-223-3p mimic microRNA used for absolute quantification of miR-155 in all cells used in the assay.

2.2.3.10. Protein analysis

A) Cell lysis of protein sample preparation

Caco-2 cells were transfected with different plasmids **(section 2.2.1.2.)**, and Caco-2 cells were infected with NDV **(section 2.2.2.4.)**, before lysing the cells. Cells were washed with ice-cold PBSa and then lysed using 100-150 µl of radioimmunoprecipitation assay buffer (RIPA) buffer **(Table 2.12)** containing 1x Protease Inhibitor Cocktail (Promega, G6521). The cells were incubated with RIPA buffer on ice for 30 minutes. Lysed cells were collected in 1.5 ml microfuge tube and passed through 25 G needle probed in 1 ml syringe 5-6 times to break all the cell debris. To the cell lysates, protein loading buffer **(Table 2.13)** containing 1x reducing agent was added before protein reduction. The protein reduction was carried out by heating the samples at 98^{O}C for 5 to 10 minutes. Reduced protein samples were either stored at -20^{O}C or loaded on a protein gel.

B) Sodium dodecyl sulfate (SDS)- polyacrylamide gel electrophoresis (PAGE) and western blotting.

Denatured protein samples were loaded on 4 to 20% TruPAGE™ Precast Gels (Sigma-Aldrich, PCG2004) for protein separation along with precision plus all blue protein marker **(Table 2.13)**. The SDS-PAGE gel was run at 100 to 120V using 1x TruPAGE buffer **(Table 2.12)** for 1 to 2 h until the complete separation of protein markers in the 4% resolving gel. The SDS-PAGE gel was then used to transfer separated protein samples from gel to on PVDF membrane iBlot™ 2 Transfer Stacks (Invitrogen™, IB24002) using the iBlot 2 Gel Transfer Device (Invitrogen™) according to the manufacturer's instructions. Transferred western blot was moved in 10% skimmed milk blocking buffer without any delay **(Table 2.12)** for 1 h at room temperature on the rocking plate. Western blot was probed with a 1:1000 to 1:5000 dilution of primary antibody **(Table 2.9)** in 5% blocking buffer **(Table 2.12)** targeting separated proteins of interest for overnight at 4^{O}C on a rocking platform. Western blot was washed with PBST buffer **(Table 2.12.)** three times 10 minutes each before treating with secondary antibody. Either 1:15000 dilution of secondary IRDye® 680RD or IRDye 800CW antibodies **(Table 2.10)** in 5% blocking buffer was incubated at room temperature in the dark on the rocking plate. Finally, western blot was washed in the dark with PBST three times for 10 minutes and a last wash in PBS. The membrane was scanned using the Odyssey® CLx Imaging System (LI-COR) and analysed using Image Studio Lite software (LI-COR).

2.2.4. Sample preparation for RNA-seq analysis

Caco-2 cells were infected with B1-GFP strain at MOI of 0.1 for two-time points 18 h and 36 h in a 6-well plate **(section 2.2.2.4.)**. Total RNA was extracted from NDV-infected Caco-2 cells (18 h and 36 h), uninfected Caco-2 cells (3 technical replicates), and VR Caco-2 cells (3 technical replicates, late passage P-25) using TRIzol method **(section 2.2.3.8.1.)**. Total RNA was quantified using Qubit™ RNA HS Assay **(section 2.2.3.8.4.)**, and quality was checked using a Bioanalyser 2100 RNA Pico kit (Agilent, San Diego, CA). Amounts of RNA were normalised for approximately 200 ng input. Total RNA was enriched for mRNA using a polyA enrichment kit (NEB, Ipswich, MA) before sequencing library preparation using a NEBNext directional Ultra RNA-Seq kit (NEB, Ipswich, MA). Library QC was performed using the Bioanalyser 2100 DNA 1000 kit and Qubit, before pooling. For NDV inocula, the library pools were quantified using a NEBNEXT Illumina library quantitation kit (NEB) with APMV-1 universal primers for M gene M+4100 /M-4220, before being diluted and loaded onto a High output 150 cycle NextSeq reagent cartridge v2.5 and flow cell for (a) 2x75 paired-end sequencing run (b) 1x150 cycle sequencing run. The RNA-Seq samples preparation, quality checks, and runs were conducted by the High Throughput Sequencing Unit, The Pirbright Institute, UK.

2.2.5. Sample preparation for Mass spectrometry analysis

Caco-2 cells and VR Caco-2 (late passage P-25) were cultured (three technical replicates each) **(section 2.2.1.1.)** to get $1x10^7$ cells for both the cell types and for all the replicates. All cells were washed with PBSa and trypsinised using Versene-Trypsin buffer. The cell pellets were rewashed with PBSa and pelleted at 325 x g. All cell pellets were stored in -80^{O}C and submitted to Dr Stuart Armstrong's group, at The University of Liverpool for Mass spectrometry sample preparation and analysis. Dr Stuart Armstrong provided the protocol for Mass spectrometry sample preparation and analysis.

Caco-2 cell pellets (persistently infected and mock) were lysed in 100 mM TEAB buffer, 0.1% (w/v) Rapigest detergent (Waters), with complete mini EDTA free protease inhibitor (Roche) and Benzonase (25 U/ml, Merck) for 1 h on ice. Then was followed by 3 cycles of sonication on ice (Vibra-cell 130PB sonicator, 20Hz, with microprobe, 10 seconds sonication alternating with 30 seconds incubation on ice). The samples were centrifuged at 13,000 x g for 10 minutes at 4°C and supernatant was removed and retained. Protein concentrations of the samples were determined using a Bradford protein assay (Thermo Scientific). All samples were normalised to 100 µg total protein with 100 mM TEAB. Proteins were reduced with 4 mM DTT (Sigma) at 60°C for 10 miutes and cooled. Then alkylated

with 14 mM iodoacetamide (Sigma) at RT for 30 minutes in the dark. All steps were performed with intermittent vortex-mixing. Proteomic-grade trypsin (Sigma) was added at a protein to trypsin in a ratio of 50:1 and incubated at 37^{O}C overnight. A small aliquot (5 µl), was used to check that protein digestion was complete (by SDS PAGE). Rapigest was removed by adding TFA to a final concentration of 0.5% (v/v). Peptide samples were centrifuged at 13,000 x g for 30 minutes to remove precipitated Rapigest. Peptide samples were desalted using Pierce peptide desalting spin columns (ThermoFisher) and evaporated to dryness with a centrifugal evaporator (Eppendorf). Each sample was reconstituted in 100 µl 100 mM TEAB ready for TMT labelling.

Desalted peptides were labelled with TMT (10 plex) reagents according to the manufacturer's instructions (Thermo). Each 0.8 mg vial of TMT reagent was reconstituted in 41 µl of acetonitrile and added to the sample for 1 h at RT. The labelling reaction was quenched with 8 µl of 5% hydroxylamine for 15 minutes at RT. An aliquot (5 µl) of each sample was pooled for label QC checking. The remaining labelled samples were stored at -80°C until analysis.

The QC samples were acidified with TFA, desalted using Pierce peptide desalting spin columns (ThermoFisher), and dried down before reconstitution in 0.1% TFA, 3% methanol. The samples were run on the Q-Exactive mass spectrometer to check label incorporation. The analysis was performed using PEAKs platform as described below but using TMT10plex as a variable modification. TMT label incorporation was >98%.

Remaining samples were mixed in 1:1:1:1:1:1 ratio and dried down before reconstitution in bRPC buffer A (20mM ammonium hydroxide pH 10, 3% acetonitrile). The peptides were fractionated (10 fractions) using high pH reverse-phase liquid chromatography (RPLC) (column: Agilent Zorbax 80A extend C18, 3.5 µm, 3 x 150mm).

Table 2.19: Sample TMT Labels

Sample	Name	Tag
1	P51 R1	TMT10_126
2	P51 R2	TMT10_127N
3	P51 R3	TMT10_128C
4	P25 R1	TMT10_129N
5	P25 R2	TMT10_130C
6	P25 R3	TMT10_131

LC-MS/MS analysis

The peptides were analysed by on-line nanoflow LC using the Thermo EASY-nLC 1000 LC system (Thermo Fisher Scientific) coupled with Q-Exactive HF mass spectrometer (Thermo

Fisher Scientific). The samples were loaded on a trap column (Acclaim PepMap 100, 2 cm × 75 µm inner diameter, C18, 3 µm, 100 Å) at 5 µl per minute with an aqueous solution containing 0.1% (v/v) TFA and 2% (v/v) acetonitrile. After 3 minutes, the trap column was set in-line an analytical column (Easy-Spray PepMap® RSLC 50 cm × 75 µm inner diameter, C18, 2 µm, 100 Å) was fused to a silica nano-electrospray emitter (Dionex). The column was operated at a constant temperature of 30°C. The liquid chromatography was performed with a buffer system consisting of 0.1 % formic acid (buffer A) and 80 % acetonitrile in 0.1% formic acid (buffer B). The peptides were separated using a linear gradient of 3.8 to 50% buffer B over 90 minutes at 300 nl/minute flow rate. The Q-Exactive HF was operated in data-dependent mode with survey scans acquired at a resolution of 120,000 at m/z (mass to charge ratio). From the top 10 most abundant isotope patterns with charge states +2 to +5 of the survey scan were designated with an isolation window of 1.2Th and fragmented by higher-energy collisional dissociation with normalised collision energies of 32. MS2 resolution was set at 60,000. The maximum ion injection times for the survey scan and the MS/MS scans were 100 and 110 ms, respectively, and the ion target value was set to 3E6 for survey scans and 1E5 for the MS/MS scans. Repetitive sequencing of peptides was minimised through the dynamic exclusion of the sequenced peptides for 90 seconds.

Analysis of MS data

Spectral data were analysed using the PEAKS studio 10 software (Bioinformatics Solutions Inc., Waterloo, ON, Canada) and analysis was based on the method developed by Cox and Mann (2008) (217). Tandem MS data were searched against the predicted protein set of the human reference genome sequence (Uniprot, 2018), Newcastle disease virus (strain Chicken/United States/B1/48) (Uniprot, 2019) and an additional contaminants database (cRAP protein sequences, GPM, https://www.thegpm.org/crap/). Search parameters were as follows; precursor mass tolerance set to 10ppm and fragment mass tolerance set to 0.02 Da. Two missed tryptic cleavages were permitted. Carbamidomethylation (cysteine) and TMT10plex (Lys, Nterm) were set as fixed modifications and oxidation (methionine) set as a variable modification. The false discovery rate was set at 1%. Quantification was performed using PEAKS Q. Results were filtered to include only proteins with greater than 2 unique peptides and a fold change of greater than two-fold (compared to cells group). Significant differences were tested by the PEAKSQ method (like Significance B method, 1) with a 1% FDR filter (Benjamini–Hochberg adjusted p-value). Data was auto normalized.

2.2.6. RNA-seq data analysis

Dr Luca Ferretti from Big Data Institute (University of Oxford, UK) analysed the RNA-seq data. Briefly, RNA was sequenced from uninfected Caco-2 cells (3 technical replicates), NDV-infected Caco-2 cells (18 hpi and 36 hpi at MOI of 0.1), and persistently NDV-infected VR Caco-2 cells (3 technical replicates, late passage P-27). For each sample, sequenced reads were trimmed using TrimGalore version 0.5 (218) with default parameters to remove adapter sequences and low-quality bases before reading (219). Reads shorter than 50 bases were filtered out (if sequenced using a paired-end (PE) protocol) or 75 bases (if single-end (SE)). The remaining reads were then aligned to the concatenation of the human genome (GRCH38 release 25) and the NDV B1 genome (AF375823) using the RNA-seq pipeline implemented in GEM with default parameters (220). The counts for all transcripts in the human and NDV transcriptomes were extracted for each sample using the same pipeline with default filtering parameters. The resulting transcriptomic counts were analysed for differentially expressed genes (DEGs) using the R package DESeq2 (221) with standard parameters and ape-GLM shrinkage for the log2 fold changes (LFCs) (222). Genes covered by less than 20 reads across all conditions were excluded from the analysis. All other analyses were implemented in R (223). The same pipeline was applied to the analysis of the datasets already published from CEF and Caco-2 cells. Statistical over-representation and enrichment analyses for GO biological processes and Reactome pathways were performed using PantherDB (224) and IPA (QIAGEN Inc) (225).

2.2.7. Statistical analysis

Statistical analysis was performed using GraphPad Prism 8 software. Data obtained from NDV-infected Caco-2 and VR Caco-2 cells were analysed with Shapiro-Wilk normality test and Two-way ANOVA with Sidak's multiple comparison test. Paired t-test was used to compare receptor binding avidity assay in egg harvested B1-GFP and NDV released in VR Caco-2 cells supernatant. Data obtained from qRT-PCR assays were analysed using Two-way ANOVA with Tukey's multiple comparison test. The standard error bars were obtained from calculated means of three independent readings (mean ±SD), p-value <0.05 was considered statistically significant. The symbols represented levels of p-values significance: *$p<0.05$, **$p<0.01$, ***$p<0.001$ and ****$p<0.0001$ in the experimental comparisons.

Chapter 3

3 Establishment of a model system to study oncolytic properties of lentogenic strains of Newcastle disease virus (NDV)

3.1. Introduction

NDV is a well-known naturally occurring oncolytic virus; various lentogenic (non-pathogenic), mesogenic (moderately pathogenic) and velogenic (highly pathogenic) strains of NDV have been reported to be oncolytic in a diverse type of cancer cells (94, 132, 146, 202, 226). The haemagglutinin-neuraminidase (HN) and fusion (F) proteins are the glycoproteins embedded in the viral envelope, are responsible for virus attachment and fusion activity to facilitate entry into host cells (84). The HN glycoprotein of NDV tethers to sialyl glycoconjugate receptors on the host cell (80, 81). Human cancer cells are known to express sialylated glycoconjugates in an unregulated manner (227, 228). NDV interacts efficiently with α-2, 3 and α-2, 6 N-linked sialic acids (82, 83) consequently, cancer cells derived from various tissues can be targeted to study NDV-induced oncolysis.

NDV is an economically important poultry pathogen known worldwide. More than 250 species of birds, including poultry, are susceptible to NDV infection. The use of virulent strains as oncolytic virus poses some threat to domestic poultry and wild birds and risks the environment biosafety (68). Hence in this study, lentogenic (non-pathogenic) strains of NDV were used for model establishment.

In this chapter, *in vitro* model system was established using different lentogenic strains of NDV in the most susceptible cancer cell line selected from the panel representing neoplastic cells derived from diverse tissue origins. Firstly we focused on using the green fluorescent protein (GFP) expressing lentogenic strains of NDV: Hitchner B1-GFP (obtained from Peter Palese, Department of Microbiology, Mount Sinai School of Medicine, New York (103) and LaSota-GFP (rescued by Manoja Rasamanikkam, The Pirbright Institute, UK), which made monitoring of the viral infection and spread upon infection easy.

3.1.1. Chapter objectives

- Identify NDV susceptible human cancer cell line
- Assess NDV strain-specific oncolysis in susceptible cancer cells
- Isolate and characterise persistently NDV-infected VR Caco-2 cells
- Validate persistence of NDV-infection in VR Caco-2 cells
- Investigate VR Caco-2 cells response to virus infections in comparison with the parental Caco-2 cells
- Assess IFN-B and ISG15 mRNA induction in Caco-2 cells and VR Caco-2 cells

3.2. Results

3.2.1. Cell line screening for *in vitro* NDV-induced oncolysis study

To establish the NDV susceptible cancer cell system, reporter viruses were employed in a dose-dependent manner into five different human cancer cell lines derived from different tissues such as colon (Caco-2), prostate adenocarcinoma cells derived from metastatic site in bone (PC3), lung (A549), liver (Hep G2), cervix (HeLa), and a non-cancerous fibroblast continuous cell line derived from healthy human lung (MRC5). Initially, reporter lentogenic strains of NDV: Hitchner B1-GFP and LaSota-GFP were used, which assured easy monitoring of viral infection and spread. Neat virus and ten-fold dilutions of both the strains were used to infect all the cell lines **(section 2.2.2.4.)**. NDV-induced cell death was measured using CellTiter-Blue® Cell Viability Assay **(section 2.2.1.4.)** in comparison with mock infection to each day in nine day virus killing curve study. The study was carried out for three independent times for each virus and each cell line.

In this study, Caco-2 cells, a heterogeneous colorectal cancer cell line derived from the large intestine, was identified as a most susceptible to NDV infection, as presented in **Figure 3.1**. The decrease in the cell viabilities of B1-GFP (**Figure 3.1.A**) and LaSota-GFP (**Figure 3.1 B**) infected Caco-2 cells were demonstrated in a time- and dose-dependent manner. The B1-GFP virus infection reduced Caco-2 cell viability >90% within 48 h of neat virus infection and a gradual decrease in cell viability was observed in successive ten-fold dilutions of B1-GFP infected Caco-2 cells after 48 h of infection (hpi) (**Figure 3.1.A**).

However, LaSota-GFP infection in Caco-2 cells demonstrated a >90% reduction in cell viability in all viral doses 9 days post-infection (dpi) (**Figure 3.1 B**).

PC3 and A549 cells were found to be moderately susceptible to the B1-GFP infection only at higher viral doses (neat virus, 10^{-1}, and 10^{-2} dilutions for PC3 cells and Neat virus, and 10^{-1} dilution for A549 cells) (**Figure 3.1.A**) compared to the LaSota-GFP infection. Whereas, HeLa cells remained unaffected by B1-GFP and LaSota-GFP infection regardless of viral dose or duration of the infection. Liver cancer Hep G2 cells were susceptible only to the B1-GFP neat virus infection within 72 hpi (**Figure 3.1 A**) and Hep G2 cells were unaffected by the successive ten-fold virus dilutions and all the doses of LaSota-GFP irrespective of the duration of the infection (**Figure 3.1 B**).

A decrease in cell viability of non-cancerous human lung fibroblast MRC5 cells was observed upon B1-GFP and LaSota-GFP infection (neat virus and 1:10 dilution) within 48 h. However, increase in the cell viability of MRC5 cells was observed after 5 dpi with 1:10 dilution of B1-GFP (**Figure 3.1 A**). A similar trend was found in the LaSota-GFP neat virus and its 1:10 dilution infected MRC5 cells (**Figure 3.1 B**). Here the decrease in the cell viability of virus-infected MRC5 cells with the higher doses (neat virus and its 1:10 dilution) of B1-GFP and LaSota-GFP suggested that higher viral doses induced stress for 5 dpi (resulting in the decrease in the cell viability) and later cells recovered from viral stress, which led to increase in the cell viability measured at 9 dpi, as demonstrated by **Figure 3.1**.

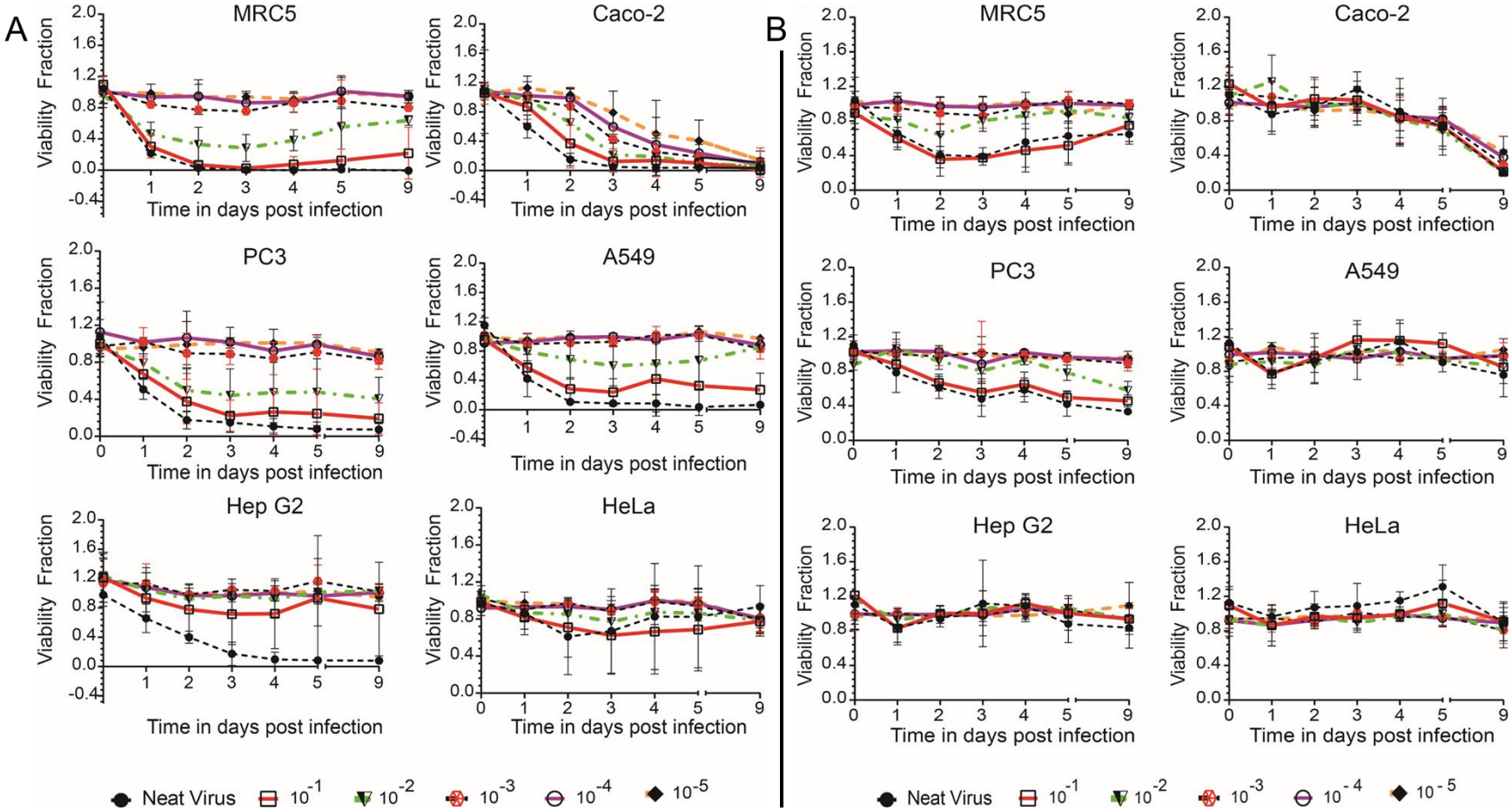

Figure 3.1. Time and NDV dose-dependent CellTiter-Blue® Cell Viability Assay in different human cancer cells. Cell lines derived from different cancerous tissues such as the colon (Caco-2), prostate adenocarcinoma cells derived from the metastatic site in bone (PC3), lung (A549), liver (Hep G2), cervix (HeLa) and non-cancerous human lung fibroblast cells (MRC5) were used for the study. These cell lines were infected with a neat virus, and its ten-fold dilutions of lentogenic reporter strains of NDV B1-GFP **(A)** and LaSota-GFP **(B)** and cell viability was measured throughout nine days of infection study. Data (mean ± SD) represented here is the combination of three repeats for each virus and each cell line. (Viability fraction is a ratio of normalised fluorescence reading of infected cells to uninfected cells at 560Ex/590Em. Fluorescence readings are normalised with blank reagent controls.)

3.2.2. Caco-2 cells response to different lentogenic strains of NDV

After establishing the predisposition of Caco-2 cells to B1-GFP and LaSota-GFP viruses, further study was focussed on the Caco-2 cells, reporter (B1-GFP and LaSota-GFP), and non-reporter (LaSota, and Ulster 2C) lentogenic strains of the NDV. Neat virus and ten-fold dilutions of each strain were used to infect Caco-2 cells for 5 days to examine the effect of different avirulent NDV strains. Cell death was measured in comparison with the mock infection each day for 5 days of infection study. The cell death measurements of virus-infected Caco-2 cells with all four strains of NDV (B1-GFP, LaSota-GFP, LaSota, and Ulster 2C) demonstrated the susceptibility of Caco-2 cells to all NDV strains in a dose-dependent manner (**Figure 3.2)**. However, the LaSota-GFP virus had delayed response in Caco-2 cells compared to LaSota strain, as shown in **Figure 3.2**. Differential response of LaSota and LaSota-GFP could be explained by the position of GFP in NDV genome. GFP gene is placed at 3 prime end of NP gene in the LaSota-GFP. Nonetheless, all lentogenic strains were oncolytic in Caco-2 cells showing different oncolysis trends. The reporter B1-GFP virus was chosen for further studies as it has shown effective oncolysis at all the employed doses in a dose-dependent manner and expression of GFP provides easy monitoring of the virus replication in infected Caco-2 cells.

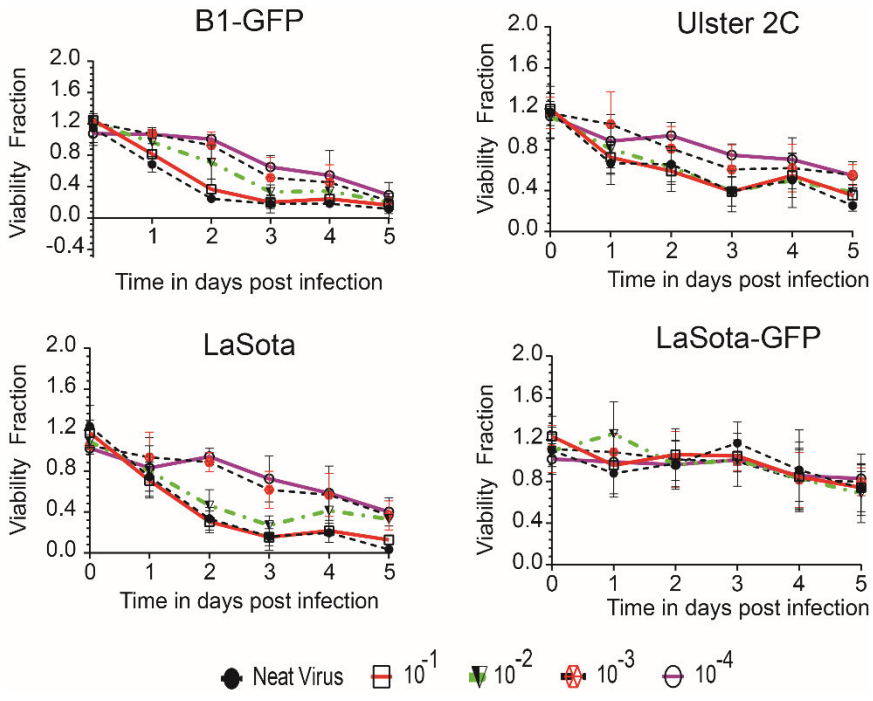

Figure 3.2. Time and NDV dose-dependent CellTiter-Blue® Cell Viability Assay in Caco-2 cells infected with different avirulent NDV strains. Caco-2 cells infected with a neat virus and its ten-fold dilutions of lentogenic reporter strains B1-GFP, LaSota-GFP and non-reporter strains LaSota, and Ulster 2C of NDV for five days. Cell death was measured for each virus each day separately. Data (mean ± SD) represented here is the combination of three independent repeats. (Viability fraction is a ratio of normalised fluorescence reading of infected cells to uninfected cells at 560Ex/590Em. Fluorescence readings are normalised with blank reagent controls.)

Tumour-selective replication of the NDV in Caco-2 cells was confirmed using a low multiplicity of infection (MOI) of 0.1 infection assay for four different strains of NDV: Hitchner B1, B1-GFP, LaSota, and LaSota-GFP. For this assay, MRC5, Caco-2, and A549 cells were infected with each strain at 0.1 MOI (calculated as discribed in **section 2.2.2.6.**), and cell death was measured using CellTiter-Blue® Cell Viability Assay **(section 2.2.1.3.)**. The comparison of NDV-infected MRC5 and Caco-2 cells at 5 dpi revealed that non-cancerous MRC5 remained unaffected by NDV infection **(Figure 3.3 A)**. The cell viability of MRC5 cells compared to the Caco-2 cells upon NDV infection has remained significantly higher for all NDV strains 5 dpi. NDV-infected MRC5 cells were found stressed under brightfield microscope showing poor cell health within 24 h of infection and also decrease in cell viability was observed in B1-GFP infected MRC5 cells in a time and dose-dependent study (as shown in **Figure 3.1 A)**. The stress of virus infection in healthy MRC5 cells was seen as a result of the antiviral response to NDV. Whereas, cancerous Caco-2 cells promoted a favourable condition for NDV replication and shown significant oncolysis as a result of virus replication indicated by significantly reduced cell viabilities (**Figure 3.3)**.

NDV-induced oncolysis was confirmed to be a cancer cell line-specific characteristic demonstrated comparative Caco-2 and A549 NDV infection for 6 days at MOI of 0.1 **(Figure 3.3 B)**. The relative cell viability assay of A549 and Caco-2 cells with all four NDV strain infections have shown significantly higher cell viabilities in the infected A549 cells (**** $p < 0.0001$, by two-way ANOVA with Sidak's multiple comparisons test) regardless of the strain**.**

The Caco-2 cells upon infection with all four NDV strains have confirmed significant oncolysis in comparison with A549 and MRC5 cells. These has validated cancer line-specific NDV replication is dependent on the type of cancer cell lines and virus strain used.

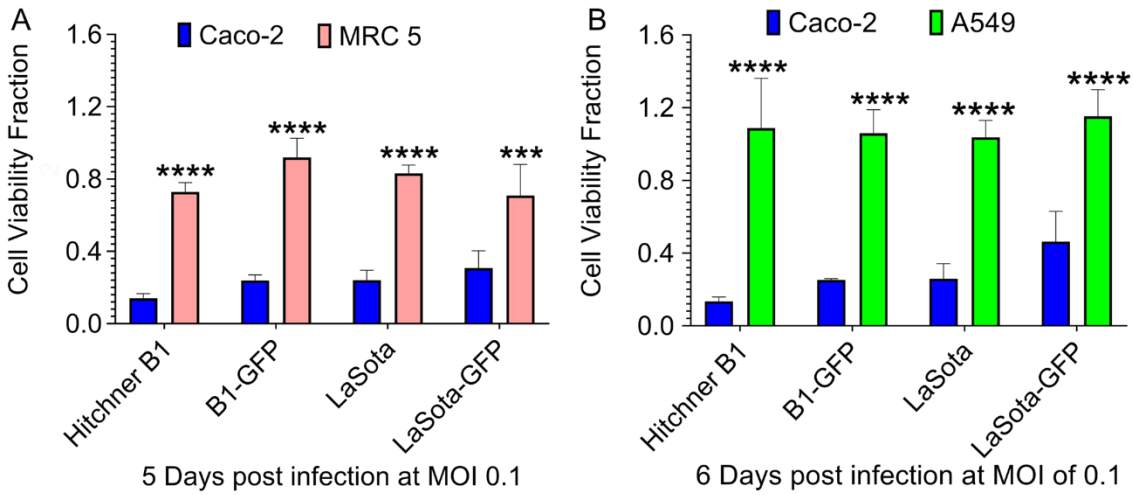

Figure 3.3. Tumour selective NDV replication in Caco-2 cells. Caco-2, MRC5, A549 cells infected with lentogenic non-reporter strains Hitchner B1, LaSota, and reporter strains B1-GFP, LaSota-GFP at MOI of 0.1. The comparative cell CellTiter-Blue® Cell Viability Assay between (**A)** Caco-2 and MRC5 5 dpi **(B)** Caco-2 and A549 6 dpi. Data (mean ± SD) represented here is the combination of three independent experiments for each virus-infected cells. Statistical analysis was performed using a Shapiro-Wilk normality test, and Two-way ANOVA with Sidak's multiple comparisons test (*** $p<0.001$ and **** $p< 0.0001$). (Viability fraction is a ratio of normalised fluorescence reading of infected cells to uninfected cells at 560Ex/590Em. Fluorescence readings are normalised with blank reagent controls.)

3.2.3. Isolation of NDV-resistant VR Caco-2 cells

In previous experiments, Caco-2 cells were shown to be susceptible to NDV infection regardless of the strains. Initial NDV virus killing curve assays were set up for12 days. When Caco-2 cells were infected with the B1-GFP virus at higher MOI (neat virus resulting in an estimated MOI of 100), the majority of cells were infected and consequently most died after 48 hpi. Despite the high levels of oncolysis in Caco-2 cells, a small population of surviving cells was identified at 12 dpi and named virus-resistant Caco-2 (VR Caco-2) cells for easy identification from the parental Caco-2 cells. Isolation of VR Caco-2 cells was accidental observation, it is an outcome, where few colonies of Caco-2 cells observed microscopically 12 dpi. The strategy of the isolation of VR Caco-2 cells from B1-GFP infected Caco-2 cells explained in **Figure 3.4**. All NDV strains were able to produce VR Caco-2 cells. The VR Caco-2 cells were isolated from Hitchner B1 infected Caco-2 cells, explained later in **Figure 3.7 C**, where supernatants from VR Caco-2 cells (isolated from both Hitchner B1 and B1-GFP) used for virus-titration by plaque assay. VR Caco-2 cells were cultured in complete growth media (**Table 2.11** and **section 2.1.5.1.**). VR Caco-2 cells isolated from B1-GFP infected Caco-2 cells were used in further studies unless mentioned otherwise.

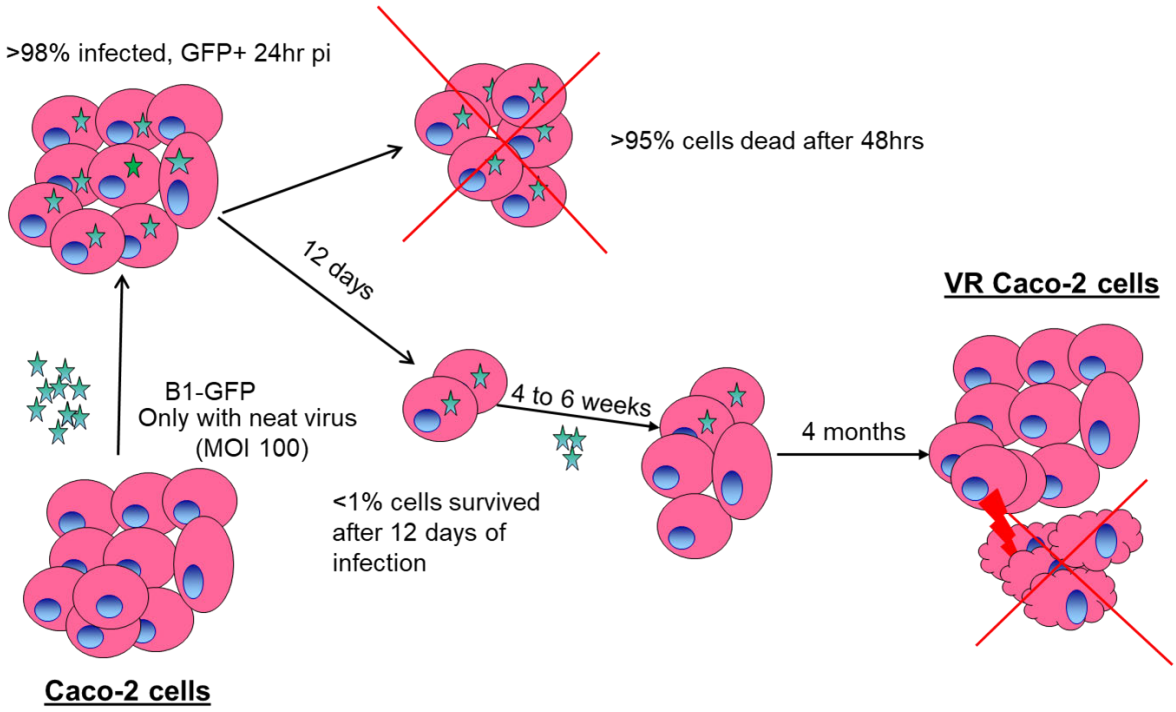

Figure 3.4. Schematic representation of Virus Resistant Caco-2 cells isolation from B1-GFP infected Caco-2 cells. Caco-2 cells were infected with B1-GFP (a neat virus). About >98% cells were infected within 24 h and >95% of infected cells were dead within 48 hpi. Few cells survived the infection 12 dpi. The surviving cells were cultured in a complete growth medium and isolated from B1-GFP superinfected Caco-2 cells. Isolated cells were named virus-resistant Caco-2 cells (VR Caco-2 cells).

Initially, surviving VR Caco-2 cells took almost 4 to 6 weeks to form colonies and about 4 months to attain 80 to 90% confluence. Microscopic observations confirmed a slower proliferation of VR Caco-2 cells than uninfected Caco-2 cells. The VR Caco-2 cells isolated from B1-GFP infected Caco-2 cells had shown GFP expression of lower intensity than acutely B1-GFP-infected Caco-2 cells under a fluorescence microscope in early passages (P). Flow cytometric analysis of early passages of VR Caco-2 cells (P1 and P4) along with acute B1-GFP-infected Caco-2 cells, and B1-GFP re-infected VR Caco-2 cells confirmed the complete reduction of GFP expression from P1 to P4 of VR Caco-2 cells **(Figure 3.5 A and B)**. Surprisingly, VR Caco-2 cells remained unaffected by GFP virus re-infection demonstrated in **Figure 3.5 A and B**. Further microscopic analysis was done in VR Caco-2 cells infected with B1-GFP virus at MOI 5 alongside the parental Caco-2 cells. No cytopathic effects (CPE) were observed in VR Caco-2 cells, whereas acutely infected Caco-2 cells have shown CPE within 24 h of infection as shown in **Figure 3.5 C**.

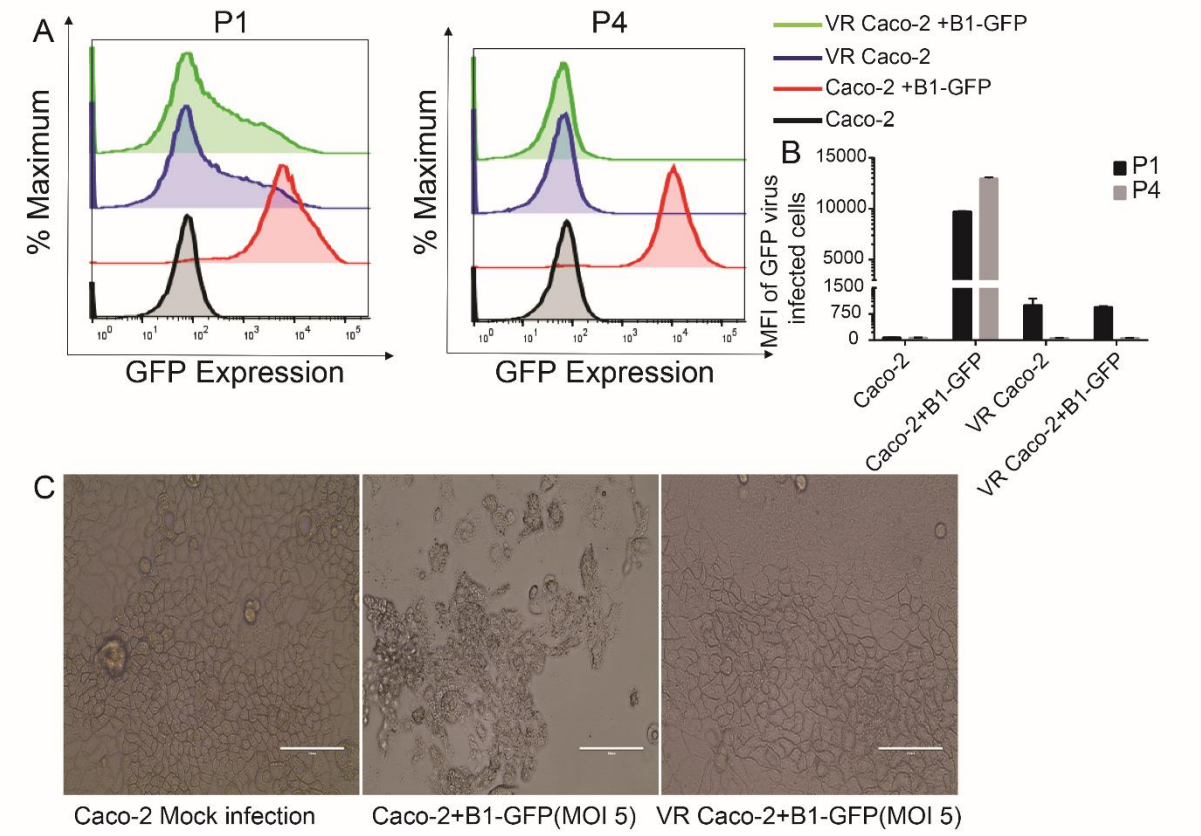

Figure 3.5. Loss of GFP expression in VR Caco-2 cells. (A) An overlay of histograms showing the GFP positive population of VR Caco-2 cells in passage 1 (P1) and passage 4 (P4) by fow cytometry analysis. In the histogram overlay % maximum represents the maximum count for events of GFP expressing cells. **(B)** A comparative GFP MFI (mean fluorescence intensity) of P1 and P4 in B1-GFP infected Caco-2 and VR Caco-2 cells. **(C)** Bright-field microscopic images of mock or B1-GFP (MOI 5, 24 hpi) infected Caco-2 and VR Caco-2 (100 µm scale bar).

3.2.4. Characterisation of VR Caco-2 cells

Previously, the GFP expression in earlier passages of VR Caco-2 cells radically reduced in subsequent passages **(Figure 3.5 A and B)**. In addition, CPE was not detected in B1-GFP (MOI=5) infected VR Caco-2 cells. With this unpredicted outcome, VR Caco-2 cells were characterised further. Indirect immunofluorescence (IF) staining assay was used to assess the presence of NDV proteins. Uninfected VR Caco-2 cells, mock or NDV infected Caco-2 cells were stained with anti-NDV chicken sera and Goat Alexa Fluor 568 anti-Chicken IgY (H+L) secondary antibody (discussed in **section 2.2.1.7.**). The IF assay in VR Caco-2 cells confirmed the expression of NDV proteins. The syncytium formation was not observed in LaSota infected Caco-2 cells 18 hpi, whereas VR Caco-2 cells showed the

syncytium formation represented in **Figure 3.6 A** as multinucleated bodies encapsulated by NDV proteins.

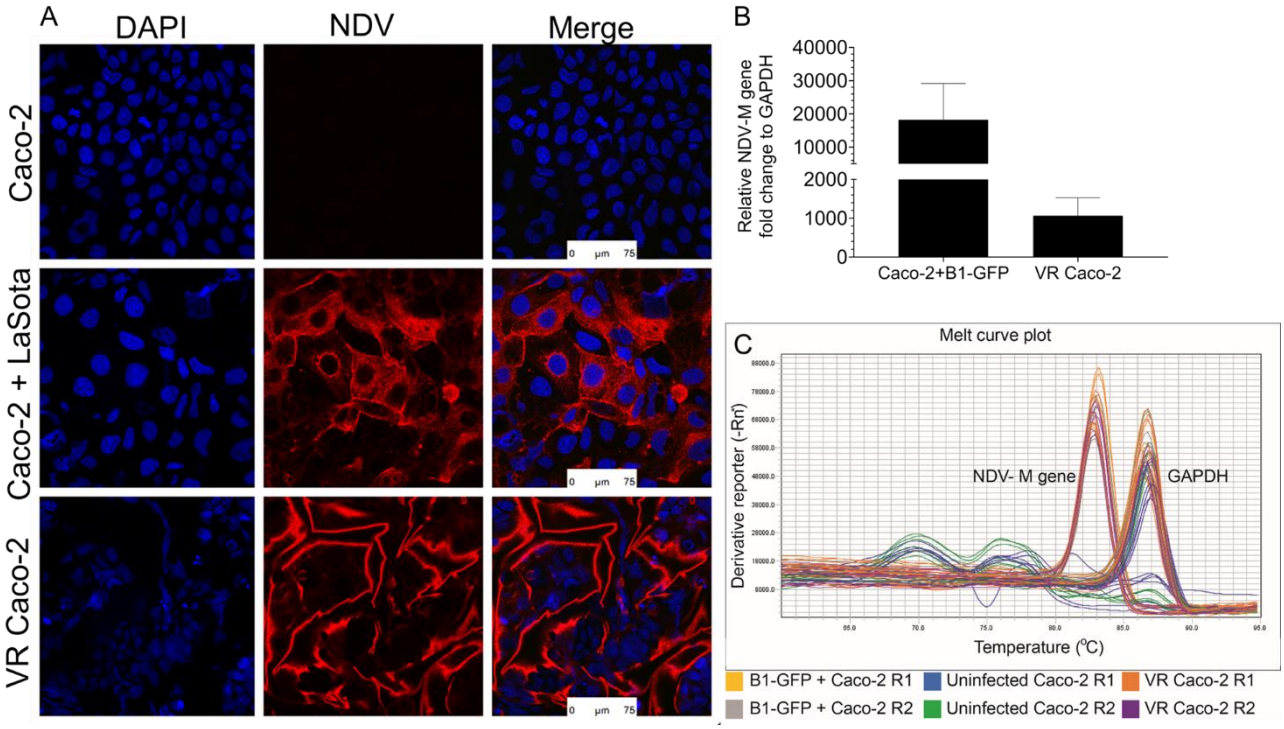

Figure 3.6. Confirmation of persistent NDV infection in VR Caco-2 cells using IF and qRT-PCR assays. (A) Immunofluorescence analysis of NDV proteins expression in uninfected, LaSota infected Caco-2 cells (MOI 1, 18 hpi) and VR Caco-2 cells. 4% PFA fixed cells were probed with NDV-specific chicken serum and incubated with Alexa Fluor® 568 goat anti-chicken antibody. Cell nuclei stained with DAPI (scalebar 75 µm). **(B)** NDV-M gene expression profile in NDV infected Caco-2 and VR Caco-2 cells using SYBR Green qRT-PCR analysis. Data (mean ± SD) represented here is a combination of three independent experiments. **(C)** The melting curve analysis confirmed primer specific amplification of NDV-M gene.

The percentage of NDV expressing population varied from passage to passage; not all the cells were positive for NDV in VR Caco-2 cells. To obtain further details of the virus-host interactions in these cells, we examined the expression of NDV-M gene. NDV-M is one of the abundantly expressed genes during NDV replication and also used as a universal marker to detect NDV replication. A markedly lower NDV-M gene copy number was detected in VR Caco-2 cells compared to the acutely infected Caco-2 cells (**Figure 3.6 B and C**). In conclusion, based on the NDV gene and protein expression, NDV established persistent infection in VR Caco-2 cells (**Figure 3.6**).

Once the persistent infection was established in VR Caco-2 cells, the infectivity of the virus was tested by plaque assay using immunofluorescence staining with anti-NDV chicken sera (discussed in **section 2.2.2.5.**). The supernatant from VR Caco-2 cells and virus stocks of Hitchner B1 and B1-GFP were used for the virus quantification. All the plaque assays were performed in Caco-2 cells. The methodology of virus titration briefly described in **Figure 3.7 A**.

The plaque assay of VR Caco-2 cells supernatant has demonstrated the production of infectious viral particles in VR Caco-2 cells **(Figure 3.7 C)**. The haemagglutination assay (HA) was used to titre NDV in VR Caco-2 cell supernatant (discussed in **section 2.2.2.2.**). Two-fold virus dilutions and 1% chicken red blood cells (cRBCs) were used to assess NDV. HA assays were the straightforward approach for the quick estimation of NDV titre in cell supernatant and virus stock. The cell supernatant from VR Caco-2 cells was checked regularly using HA titration and plaque assays. The HA titration confirmed a significantly lower viral load produced in VR Caco-2 cells as compared to the egg propagated NDV strains **(Figure 3.7 D)**.

VR Caco-2 cells produced low levels of virus and the titre fluctuated from passage to passage and never increased beyond 10^5 PFU/ml compared to the high titres of Hitchner B1 and B1-GFP in Caco-2 cells (**Figure 3.7 B** and **Table 3.1**). Virus quantification by plaque assay and HA titration revealed that virus titres were significantly lower in VR Caco-2 cells **(Figure 3.7 E)**.

Table 3.1: PFU/ml count in different passages of VR Caco-2 cell supernatant.

VR Caco-2 Passage number	PFU/ml
P-3	56000
P-5	2E+05
P-6	4E+05
P-25	6E+05
P-29	2E+05
P-30	1E+05
P-31	4E+05

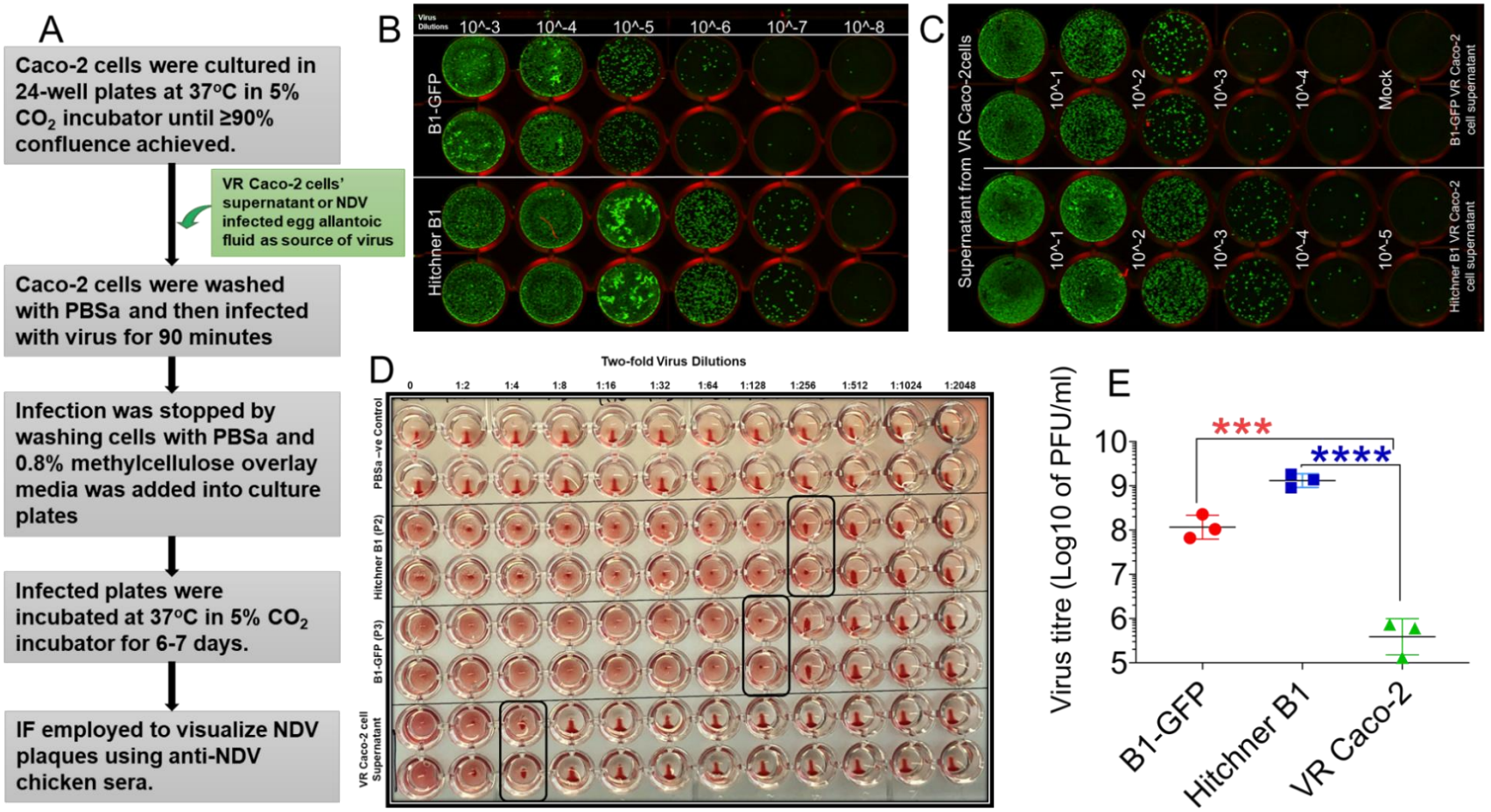

Figure 3.7. Confirmation of persistent NDV infection in VR Caco-2 cells using HA and plaque assays. (A) Flow chart explaining the methodology of plaque assay. **(B)** B1-GFP and Hitchner B1 IF plaque assay in Caco-2 cells. **(C)** VR Caco-2 cells (generated from B1-GFP and Hitchner B1 superinfected Caco-2 cells) supernatant used for infection in Caco-2 cells and IF plaque assay plate. **(D)** HA assay confirming the hemagglutination characteristic of NDV or supernatant of VR Caco-2 cells. **(E)** A graphical representation of significantly differential viral titres of NDV strains (Hitchner B1 and B1-GFP) to VR Caco-2 supernatant (late passage P-25, P-29, and P-31) in Caco-2 cells. Data (mean ± SD) shown here are from three independent experiments. Statistical analysis was performed using a Shapiro-Wilk normality test, and one-way ANOVA with Tukey's multiple comparisons test (*** $p < 0.001$, and **** $p < 0.0001$).

Results from the qRT-PCR assays have demonstrated the expression of viral NDV-M gene in VR Caco-2 cells at a markedly lower level than acute B1-GFP infected Caco-2 cells **(Figure 3.6)**. Virus titration of VR Caco-2 cell supernatant using HA assays and plaque assays have also demonstrated the production of infectious replication-competent NDV particles in VR Caco-2 cells at a significantly lower titre **(Figure 3.7)**. Therefore, confirmed that NDV established persistent infection in isolated VR Caco-2 cells **(Figure 3.4)** by maintaining virus replication at low titers. VR Caco-2 cells maintained continuous production of reproducible infectious virus at varying titres at every passage **(Table 3.1)** . The NDV produced in VR Caco-2 cells named VR NDV (VR NDV nomenclature is used further in this chapter).

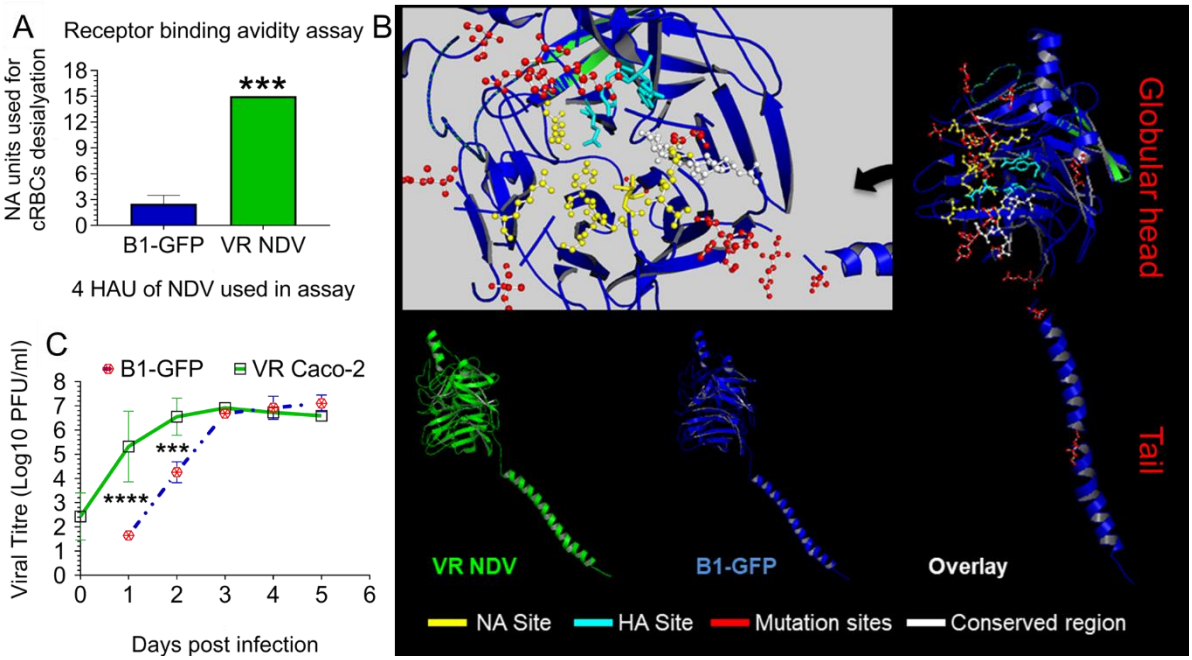

Figure 3.8. Analysis of NDV-HN protein. (A) Receptor avidity assay using 4 HAU of B1-GFP virus and NDV from VR Caco-2 supernatant demonstrated higher affinity of VR NDV to the desialylated chicken RBCs. Data (mean ± SD) shown here are from four independent experiments. Paired t-test was used to analyse data (***p<0.0001). **(B)** Mutation sites located in HN protein of VR NDV compared to the B1-GFP HN protein. Protein structures predicted using Phyre2 and aligned using PyMOL. **(C)** VR NDV from VR Caco-2 supernatant and B1-GFP virus used to study replication kinetics of NDV in Caco-2 cells. Data (mean ± SD) shown here are from three independent experiments and analysed using One-way ANOVA with Sidak's multiple comparisons test (*** p= 0.0009, and **** p< 0.0001).

Once the viral persistence was confirmed in VR Caco-2 cells, the NDV HN and F sequences were analysed. Thirteen different mutations in the HN protein of VR NDV were discovered. The receptor binding avidity assays were carried out to investigate the functional differences in VR NDV and B1-GFP virus **(section 2.2.2.3.)**. The receptor binding avidity assay measured the avidity of binding of HN protein to sialic acid depleted cRBCs. Partially sialic acid depleted cRBCs were obtained by α2-3,6,8 neuraminidase enzyme treatment. The optimised VR NDV and B1-GFP virus stocks (4 HAU) were tested with sialic acid depleted cRBCs to determine the virus avidity. This assay has demonstrated 6x higher avidity of VR NDV to partially depleted cRBCs than B1-GFP virus **(Figure 3.8 A)**. The increased receptor binding avidity of VR NDV to partially depleted cRBCs suggested mutations in HN protein, which were identified by HN protein sequence analysis.

The HN sequence analysis of VR NDV and B1-GFP viruses confirmed 13 amino acid mutations in VR NDV compared to the B1-GFP virus shown in **Figure 3.8 B**. None of the amino acid mutation sites was found in HA, NA and antigenic sites in globular head of HN protein of VR NDV. Out of 13 mutations, 10 mutations (G134E, Y203H, P226S, V254A, K259E, S324T, W363R, P464S, V495E, and T522I) were located in the globular head in closest proximity of shared antigenic site 23 (F193, S194, S200, H201, and H203) (229), receptor binding (R174, I175, E258, Y299, Y317, E401, R416, R498, Y526, and E547) (80), and NA (R174, I175, D198, K236, R416, Y526 and E547) (80) active sites. However, Y203H mutation is in the linear amino acid sequence of antigenic site 23. The other three mutation sites K98N, E118A, and S121R) are in the tail domain of HN protein. The tail domain is responsible for F-protein interaction, neuraminidase activity, and protein oligomerisation. The increased avidity to desialylated cRBCs could be the outcome of these mutations, to pinpoint the exact site needs further investigation.

The replication pattern of VR NDV in Caco-2 cells was compared with the B1-GFP strain of NDV. VR NDV has shown a similar trend of infectivity to that of B1-GFP virus in growth curve studies shown in **Figure 3.8 C**. The difference can be seen at earlier time points because of the differences in the inoculum at the time of infection. For this study, 100 PFU of B1-GFP infected Caco-2 cells compared with the unknown titres of VR Caco-2 supernatant-infected Caco-2 cells. Irrespective of the differences at initial time points of the replication study of VR NDV confirmed similarity in the infectivity.

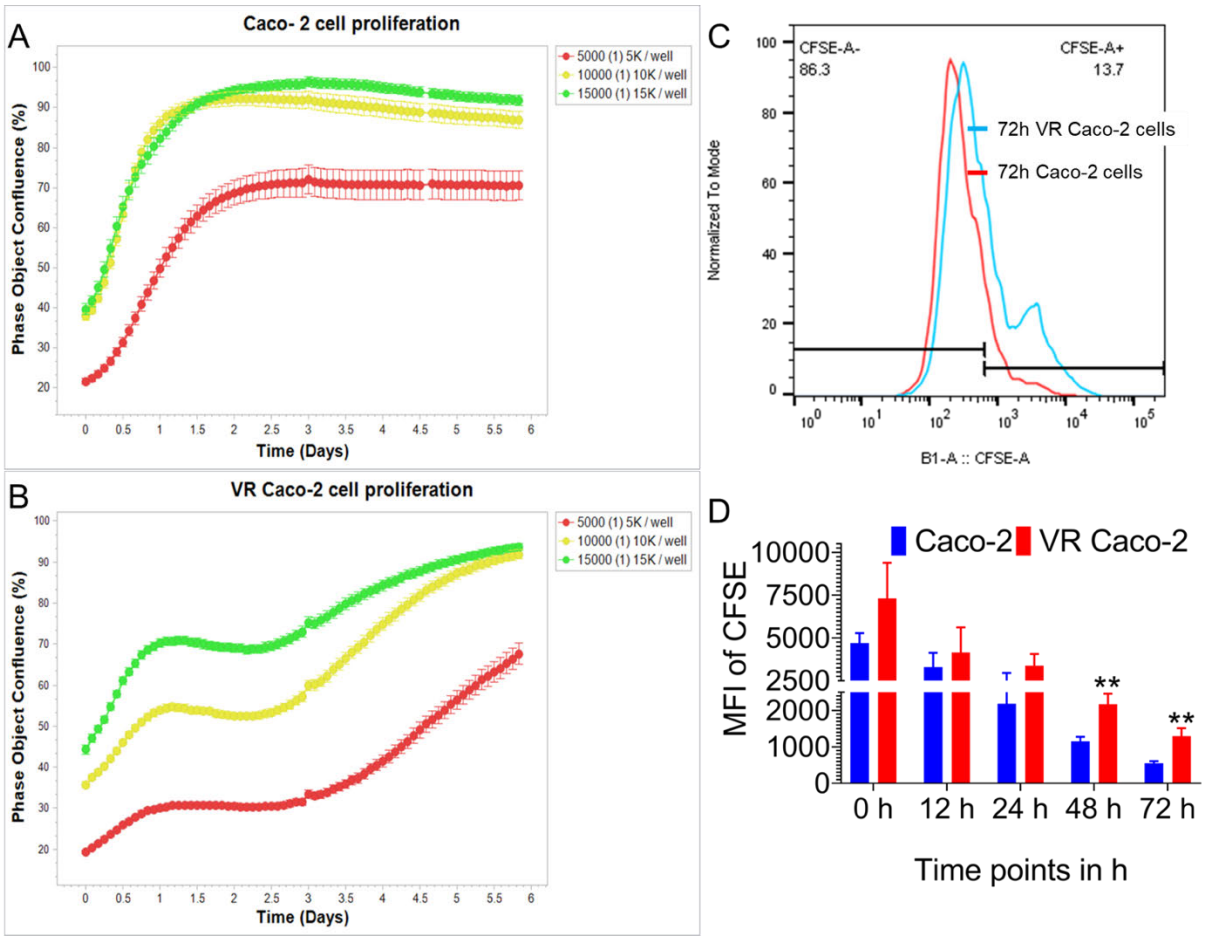

Figure 3.9. Cell proliferation assays. (A and B) Caco-2 and VR Caco-2 cell confluence monitored in real-time using the IncuCyte imaging system at different seeding densities, respectively. Phase object confluence (%) represents the surface area covered by cell monolayer in the culture plate. **(C)** Flow cytometry analysis showing the overlapped histograms of Caco-2 and VR Caco-2 cells 72 h post CFSE staining (CFSE is a fluorescent cell staining dye). CFSE dilution is significant at 72 h in Caco-2 cells indicating more number of cell divisions than VR Caco-2 cells. **(D)** MFI of CFSE stained Caco-2 and VR Caco-2 cells at different proliferation time points. Data (mean ± SD) shown here are from three independent experiments and analysed using multiple nonparametric t-tests (p = 0.005).

The real-time monitoring of cell confluence using IncuCyte Live-cell Analysis system at different cell seeding densities (5000 cells/well, 10000 cells/well, and 15000 cells/well) in a 96 well plate has revealed slower growth of VR Caco-2 cells than Caco-2 cells. Caco-2 cells spent less than 12 h in lag phase and entered in log phase to attain more than 90% confluence in 1.5 days after seeding at 10K and 15K cells/well and consequently went into a stationary phase. A similar trend was also observed in 5K cells/well 70% confluence and started stationary development **(Figure 3.9 A)**. On the other hand, VR Caco-2 cells spent around three days in the lag phase in all three

densities regardless of the confluence before entering the exponential phase **(Figure 3.9 B)**. VR Caco-2 cells certainly had different growth phase curve from the Caco-2 cells irrespective of cell density. VR Caco-2 cells at 10K and 15K cells/well seeding took 5.5 days to attain >90% cell confluence. The CFSE cell proliferation assay **(section 2.2.1.6.)** verified the 2x times slower cell proliferation of VR Caco-2 cells than Caco-2 cells at 48 and 72 h post CFSE staining **(Figure 3.9 C)**. The trend of decreasing CFSE intensity was demonstrated by measuring the mean fluorescent intensities (MFI) of CFSE labelled Caco-2 and VR Caco-2 cells at 0-72 h **Figure 3.9 D**. The microscopic observation has confirmed identical cellular morphology in Caco-2 and VR Caco-2 cells **(Figure 3.10)**.

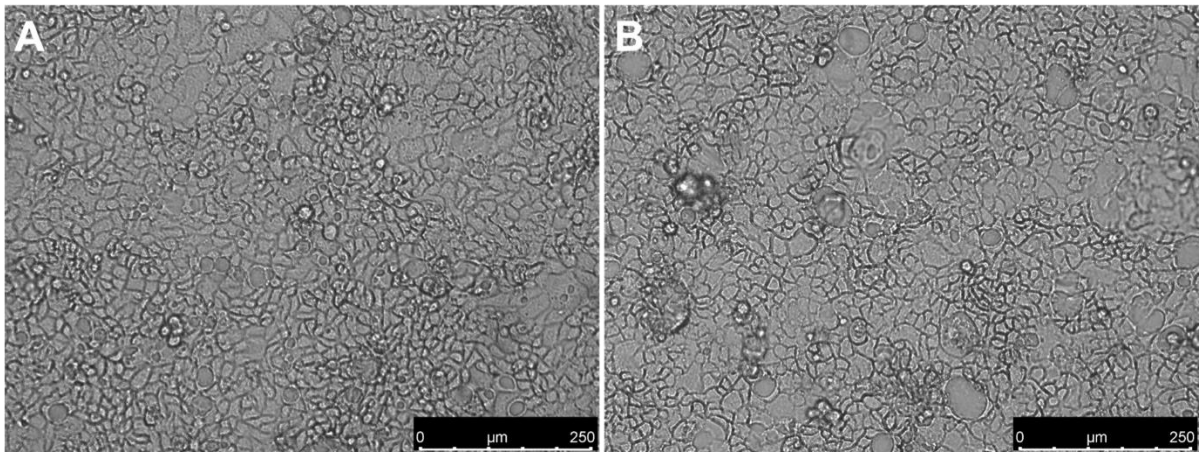

Figure 3.10. Microscopic observation of Caco-2 and VR Caco-2 cells. Bright-field microscopic images of Caco-2 cells **(A)** and VR Caco-2 cells **(B)** (scalebar 250 µm).

3.2.5. NDV re-infection study in VR Caco-2 cells

Caco-2 and VR Caco-2 cells were infected with a neat virus, and ten-fold dilutions of NDV strains (B1-GFP, LaSota, and Ulster 2C) and the cell viability was measured **(section 2.2.1.3.A)** each day up to 5 dpi. The assay has demonstrated a significant difference in the cell viabilities of infected Caco-2 and VR Caco-2 cells. VR Caco-2 cells were unaffected with all the NDV strains and virus doses at all the time points, whereas Caco-2 cells responded to all strains in a dose-dependent manner resulting in the decreased cell viability. No B1-GFP infection and replication were evident in VR Caco-2 cells as no GFP expression was seen compared to the B1-GFP infected Caco-2 cells **(Figure 3.12)**. No cytopathic effects were observed in the NDV infected VR Caco-2 cells regardless of the strain and the dose of infection. The cell cytotoxicity was measured **(2.2.1.3.B**) in reporter and non-reporter NDV strains-infected Caco-2 and VR Caco-2

cells at low MOI of 0.1; Caco-2 cells showed significantly higher cytotoxicity to the VR Caco-2 upon infection illustrated in **Figure 3.11 B**. Both assays validated the NDV resistance in VR Caco-2 cells. The resistance to NDV infection potentially can be explained either by receptor modification of VR Caco-2 cells or by the establishment of an antiviral state in VR Caco-2 cells; however, this needs further investigation. Virus killing curve assay demonstrated resistance to NDV-induced cell death in VR Caco-2 cells compared to the parental Caco-2 cells **(Figure 3.11 A)**.

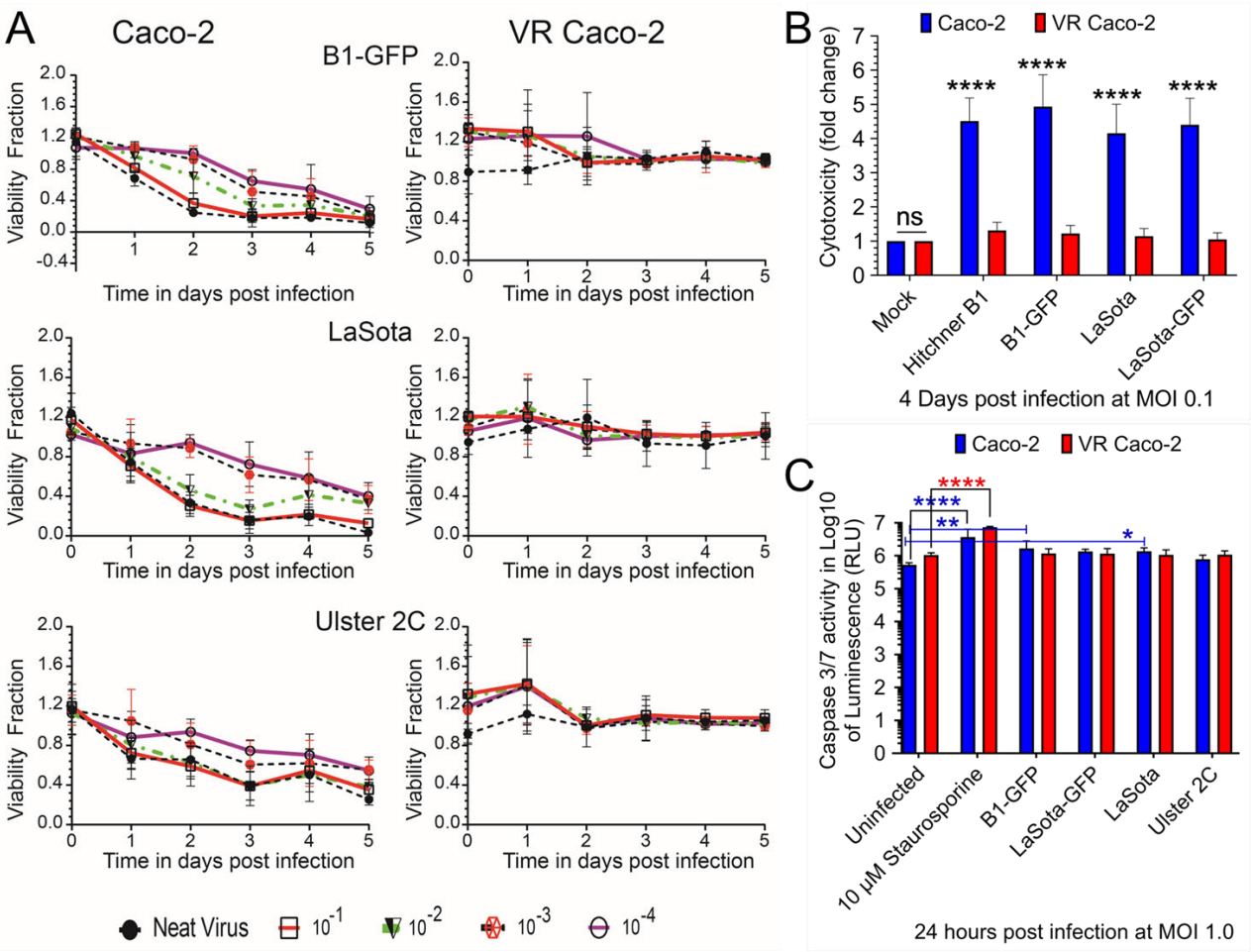

Figure 3.11. Resistance to NDV re-infection demonstrated in VR Caco-2 cells. (A) Cell viability measured in NDV (B1-GFP, LaSota, and Ulster 2C) neat virus and ten-fold virus dilutions infected Caco-2 and VR Caco-2 cells in 5 days virus killing curve assay. (Viability fraction is a ratio of normalised fluorescence reading of infected cells to uninfected cells at 560Ex/590Em. Fluorescence readings are normalised with blank reagent controls.) **(B)** Cell cytotoxicity assay of 0.1 MOI NDV (Hitchner B1, B1-GFP, LaSota, and LaSota-GFP) infected Caco-2 and VR Caco-2 cells 4 dpi demonstrated reduced cytotoxicity of VR Caco-2 cells. **(C)** Caspase3/7 activity measured to assess the apoptosis in NDV infected Caco-2 and VR Caco-2 cells at MOI of 1 24 hpi. Data (mean ± SD) shown are of three independent experiments. Statistical analysis was performed using a Shapiro-Wilk normality test, and one-way ANOVA with Tukey's multiple comparisons test (* $p<0.05$, ** $p<0.001$, *** $p< 0.001$, and **** $p< 0.0001$).

Type of cell death in NDV-infected Caco-2 and VR Caco-2 cells was investigated by infecting Caco-2 and VR Caco-2 cells with different strains of NDV at MOI of 1 for 24 h **(section 2.2.1.4.)**. Then executioner caspases 3 and 7 activity measured using Cas3/7 Glo Luciferase assay to confirm the ongoing apoptosis. There was no significant difference in Cas3/7 activity of VR Caco-2 cells with or without infection **(Figure 3.11 C)**. However, B1-GFP and LaSota infected Caco-2 cells were significantly positive, showing Caspase 3/7 activity at set parameters. These observations demonstrated that NDV-induced cell death by apoptosis occurs in a strain-specific manner only in Caco-2 cells but not in NDV re-infection-resistant VR Caco-2 cells.

3.2.6. Confirmation of NDV-specific resistance in VR Caco-2 cells

The question was whether the established resistance of VR Caco-2 cells was exclusive to the NDV or also extended to other viruses, once resistance to the NDV re-infection confirmed in VR Caco-2 cells. Therefore, VR Caco-2 cells were infected with reporter viruses of avian influenza A strain (AIV) H9N2-GFP and vesicular stomatitis virus (VSV-GFP) along with parental Caco-2 cells. The GFP-expressing viruses used to their advantage to confirm infection and spread of the virus in Caco-2 and VR Caco-2 cells observed under a fluorescence microscope.

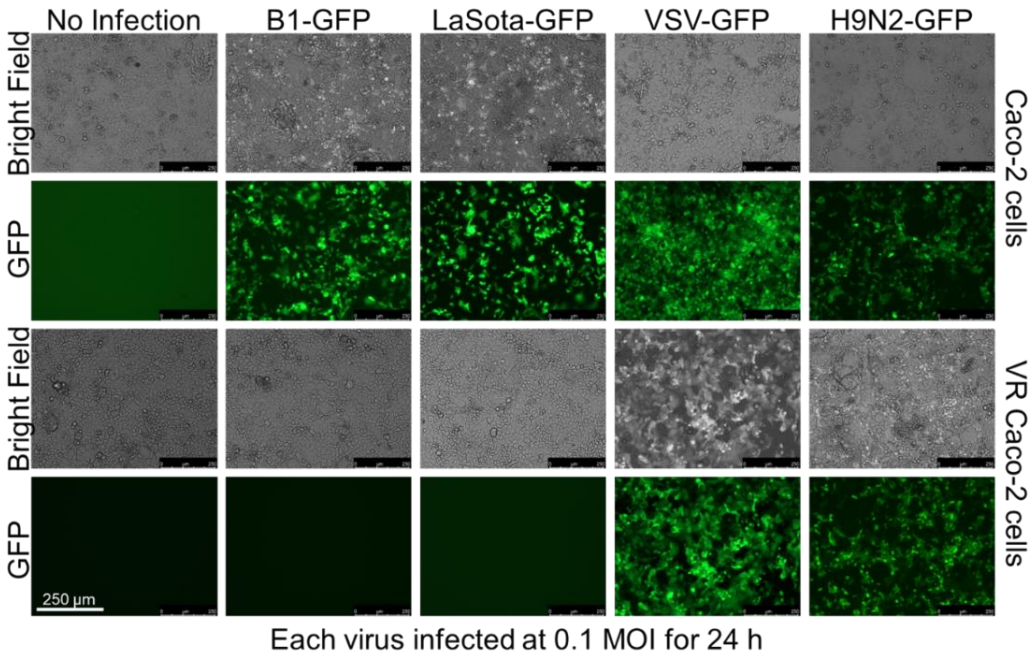

Figure 3.12. VR Caco-2 cells showed susceptibility to H9N2, and VSV infections only. Microscopic observation of NDV (B1-GFP and LaSota-GFP), avian influenza virus H9N2-GFP, and vesicular stomatitis virus (VSV-GFP) infected Caco-2 and VR Caco-2 cells at MOI of 0.1 for 24 h. The expression of GFP confirmed virus replication inside cells (scale bar 250 µm).

This study has confirmed the NDV-specific resistance of VR Caco-2 cells. Microscopic observations clearly showed H9N2-GFP and VSV-GFP replication in VR Caco-2 cells **(Figure 3.12)**. The flow cytometry analysis of NDV- reporter viruses (B1-GFP and LaSota-GFP), H9N2-GFP, and VSV-GFP virus also verified the permissibility of VR Caco-2 cells to H9N2-GFP and VSV-GFP viruses, but not to the NDV viruses shown in **Figure 3.13**. NDV and AIV use the sialic acid receptor to facilitate virus entry inside the cells. The permissibility of VR Caco-2 cells to AIV discuss the possibility of receptor modification in VR Caco-2 cells to explain NDV-specific resistance. The establishment of an antiviral state is also potentially questionable as VR Caco-2 cells were infected with both AIV and VSV.

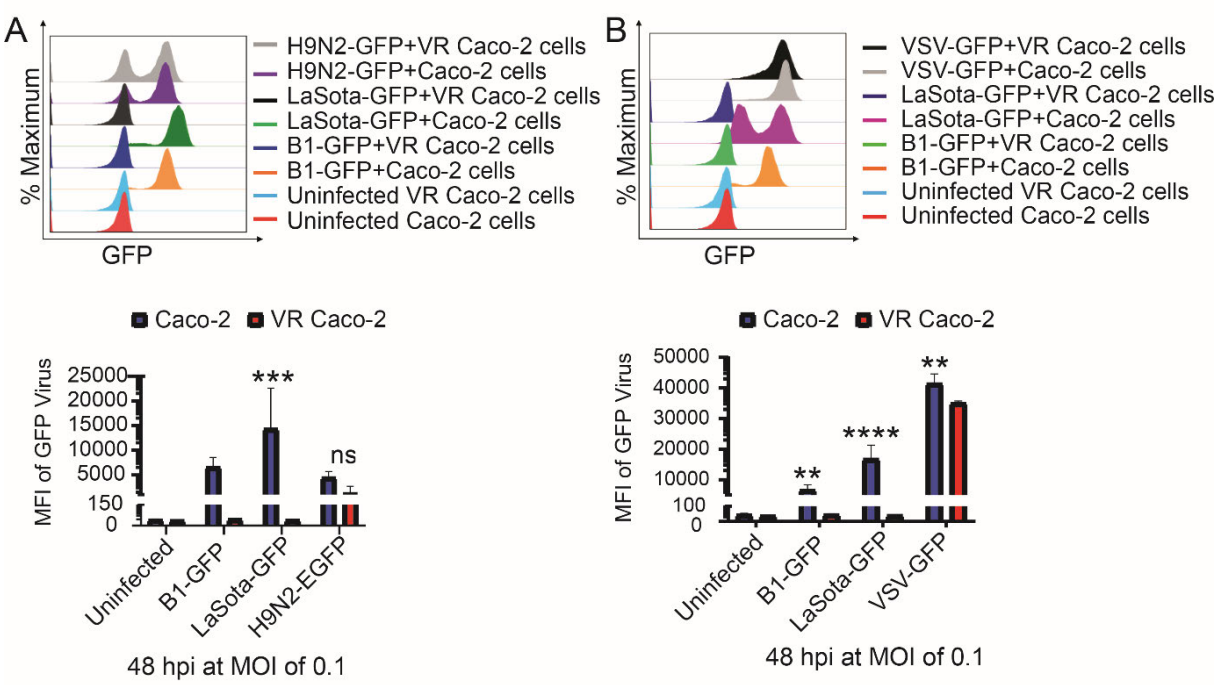

Figure 3.13. Validation of NDV-specific resistance in VR Caco-2 cells. Caco-2 and VR Caco-2 cells were infected with various reporter strains of NDV, Influenza A virus, and VSV at MOI of 0.1. Virus infection was determined at 48 hpi using flow cytometry. An overlay of histograms and MFI (mean fluorescence intensity) of GFP representing the virus replication in virus-infected cells demonstrated the susceptibility of Caco-2 and VR Caco-2 cells. A comparative account of NDV reporter viruses (B1-GFP and LaSota-GFP) alongside H9N2-GFP **(A)** and VSV-GFP **(B)** NDV-specific resistance of VR Caco-2 cells. In histogram overlays, % maximum represents the maximum count for events of GFP expressing cells. Data (mean ± SD) shown are the representation of three independent experiments and analysed using two-way ANOVA with Sidak's multiple comparison test (**p<0.005, *** p=0.0001, and **** p< 0.0001).

The infection and replication of VSV-GFP, LaSota-GFP, and B1-GFP was examined in Caco-2 and VR Caco-2 cells in real-time using the IncuCyte Live-cell Analysis system. The intensity of GFP-expressing infected cells was measured throughout the infection indicated the real virus infection and replication in real-time shown in **Figure 3.14 A**. VR Caco-2 cells confirmed VSV-GFP replication only. However, the GFP intensity of the VSV-GFP in VR Caco-2 cells significantly lower than in Caco-2 cells even though >99% population was infected with the VSV **(Figure 3.14 B)**. The possible explanation for it may be based on the fact that VR Caco-2 cells persistently producing NDV, and therefore the VSV-GFP, grow slower in VR Caco-2 cells, but the virus successfully induced cell death in both Caco-2 and VR Caco-2 cells, as depicted in **Figure 3.14 B**.

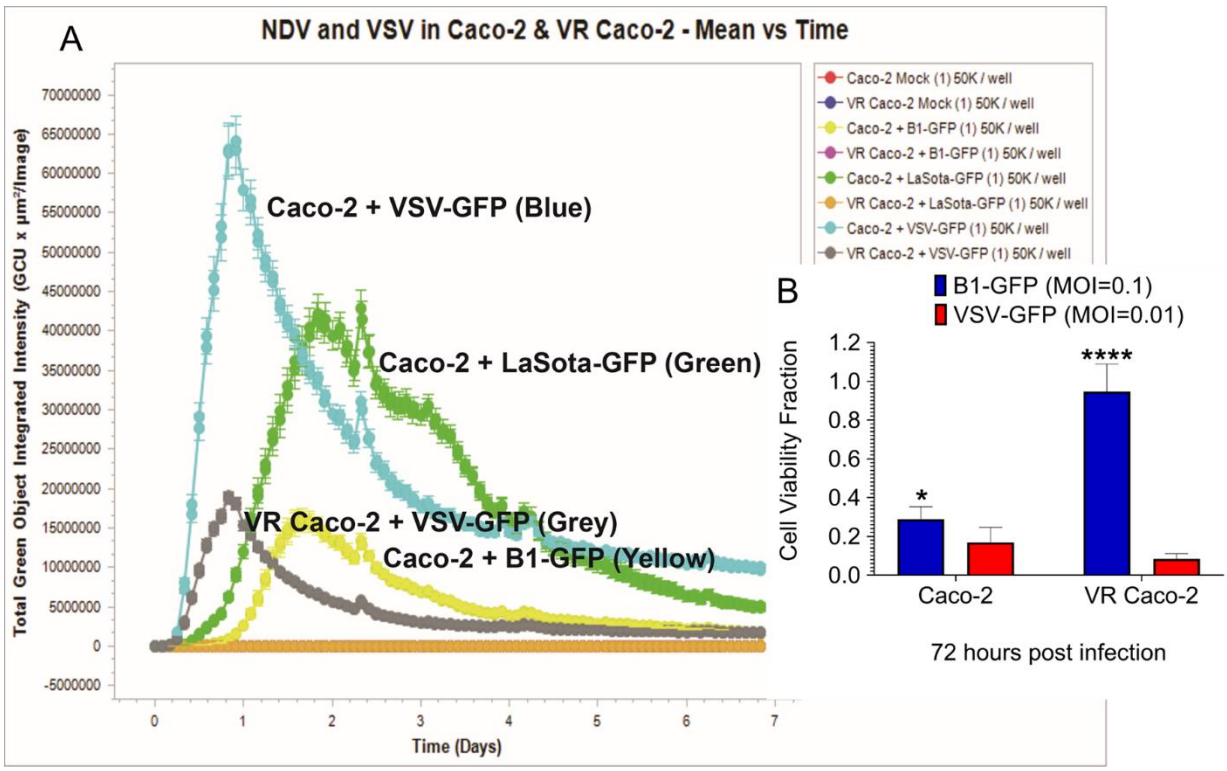

Figure 3.14. VSV replication and cell death assay in VR Caco-2 cells. (A) Caco-2 and VR Caco-2 cells were infected with reporter strains of NDV (B1-GFP and LaSota-GFP) at MOI of 1, and VSV-GFP at MOI of 0.1 respectively. Real-Time monitoring of GFP expression under 10x objective of IncuCyte live imaging system affirming the virus replication in Caco-2 and VR Caco-2 cells on a timely basis (n=3). Phase object confluence (%) represents the surface area covered by cell monolayer in the culture plate. **(B)** Caco-2 and VR Caco-2 cells infected with NDV (B1-GFP at MOI 0.1) and VSV-GFP (MOI 0.01) validated VSV-induced cell death in VR Caco-2 cells 72 hpi. the replication cycle is of VSV is 2-3 h whereas, NDV replication cycle is 8-12 h in Caco-2 cells. Hence, different MOI of infection used in the assay. Data (mean ± SD) shown are the representation of seven independent experiments and analysed using a Shapiro-Wilk normality test, and Two-way ANOVA with Sidak's multiple comparisons test (*p=0.04 and **** p< 0.0001).

3.2.7. IFN-β induction study in Caco-2 cells

A strong antiviral innate immune response is evoked by virus-infected cells as the first line of defence. Antiviral status of infected cells obtained by the induction of type-I interferons (IFNs) such as IFN-α and IFN-β which then binds to IFN-α/β receptors (IFNAR) activating the JAK/STAT pathways to express IFN stimulated genes (ISGs). Several antiviral ISGs have been identified to abort the viral replication cycle like ISG15, ISG20, Mx1/2, and OAS1/2/3 etc. Here we investigated the IFN-β and ISG15 mRNA induction in NDV infected cells to define the antiviral status.

In order to rule out any clonal bias of the Caco-2 cell populations, two independent sources of Caco-2 cells from The Pirbright Institute and Caco-2 cells from Oxford University (Ox Caco-2) were used in the study to understand the induction of IFN in response to different stimuli such as viruses (NDV-B1/B1-GFP and VSV-GFP) and long synthetic analogue of dsRNA poly(I:C) HMW. A549 cells are known to induce strong type-I IFN production hence used as a positive control in this study. A549, Caco-2, VR Caco-2 and Ox-Caco-2 cells were infected with VSV-GFP at MOI of 0.1 for 12 h, with B1 and B1-GFP viruses at MOI of 5 for 12 h. A549 cells were transfected with 0.2 µg/ml of Poly(I:C) for 12 h whereas Caco-2 and Ox-Caco-2 cells were transfected for 24 h **(section 2.2.3.9.1.)**. Caco-2 cells were found unresponsive to the poly(I:C) transfection, whereas Ox Caco-2 cells responded inconsistently **(Figure 3.15)**. As a result, no significant induction of IFN-β mRNA was detected, whereas B1-infected Caco-2 and Ox-Caco-2 cells showed slightly higher induction of *IFN-β* and *ISG15* mRNAs **(Figure 3.15)**. *IFN-β* and *ISG15* mRNA expression in poly(I:C) transfected Ox Caco-2 cells was considerably higher to the Caco-2 cells **(Figure 3.15)**. The VR Caco-2 cells showed no induction of IFN-β and a slight increase in *ISG15* in comparison with unstimulated Caco-2 cells **(Figure 3.15)**. A549 cells expressed high levels of *IFN-β* and *ISG15* mRNA in response to all the stimuli. (Simultaneously, infection in all cells was confirmed by measuring the NDV-M gene fold changes.)

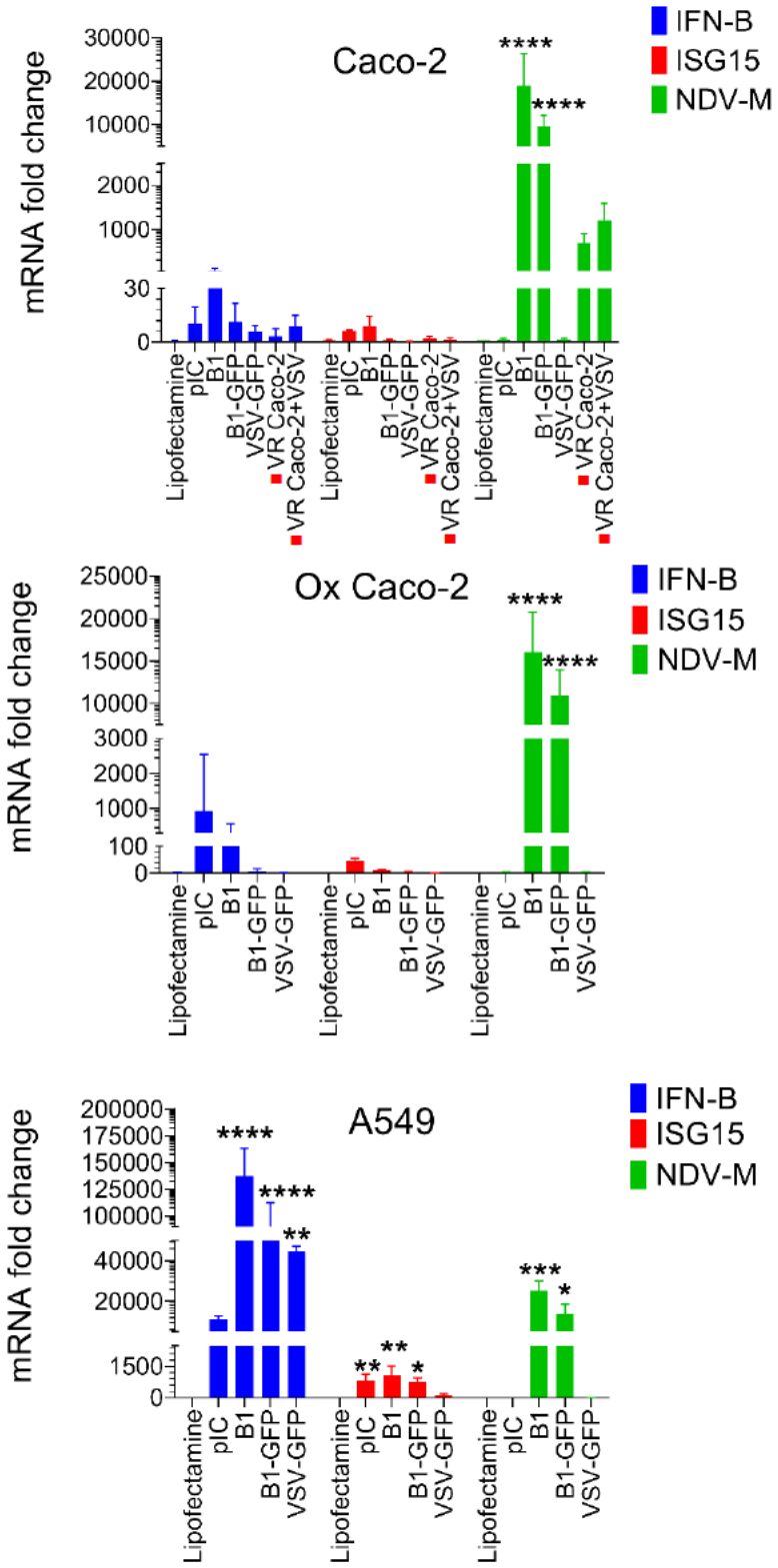

Figure 3.15. Inefficient IFN-β induction in Caco-2 cells and VR Caco-2 cells. Caco-2, VR Caco-2 (highlighted in top-most figure by red squares), Ox Caco-2 and A549 cells were stimulated with viruses Hitchner B1, B1-GFP (NDV at MOI of 5) and VSV-GFP at MOI of 0.1 for 12h and synthetic dsRNA analogue poly(I:C) HMW to study IFN-β, ISG15, and NDV-M mRNA expression profile. Fold change was calculated in comparison with house keeping gene GAPDH in all cells. Data (mean ± SD) shown are the representation of three independent experiments and analysed using a Shapiro-Wilk normality test, and

One-way ANOVA with Dunnett's multiple comparisons test (*p=0.01, **p<0.002, *** p< 0.001, and ****p< 0.0001).

3.2.8. Role of miR-155 in VR Caco-2 cells

MiR-155 is an 18 to 23 nucleotide short small noncoding multifunctional microRNA (miRNA), which is confirmed to be involved in post-transcriptional gene regulation by interacting with the 3′-untranslated region of target mRNA, leading to either mRNA degradation or protein synthesis suppression. MiR-155 regulation is known to affect various biological processes such as haematopoiesis, inflammation and immunity (230, 231). MiR-155 is also an oncomir, where it is thought to function by downregulating tumour suppressor genes leading to oncogenesis. MiR-155 is overexpressed in several cancers such as oral, breast, pancreatic cancers and also has a role cancer cell proliferation, invasion and migration (230). However, Liu et al. (2018) reported that miR-155 overexpression limited colorectal cancer progression by targeting collagen triple helix repeat containing 1 (CTHRC1) *in vitro* colon cultures (232).

Formerly, VR Caco-2 cells were confirmed for the persistent NDV-infection, NDV-specific resistance, dysfunctional IFN response, and slower growth, with no evidence of apoptosis. A significant (p< 0.0001) upregulation of miR-155 and two-fold increased (p< 0.001) NF-kB activity was observed in the VR Caco-2 cells (**Figure 3.16**). There is no direct correlation reported so far between miR-155 **(**discussed in **section 2.2.3.9.2.)** and NF-kB **(**discussed in **section 2.2.1.6.)** activity. However, overexpression of miR-155 in VR Caco-2 cells could be the indication of imbalance of homeostasis between the regulatory function of the immune system and oncogenesis. The increased NF-kB activity indicated a substantial increase in cell survival and anti-apoptosis activity in VR Caco-2 cells. There was no difference in caspase 3/7 activity with or without NDV infection **(Figure 3.11 C)**, and slower but prolific cell proliferation was observed in the growth curves of VR Caco-2 cells **(Figure 3.9 A and B)** indicating the pro-survival and anti-apoptotic activity in VR Caco-2 cells.

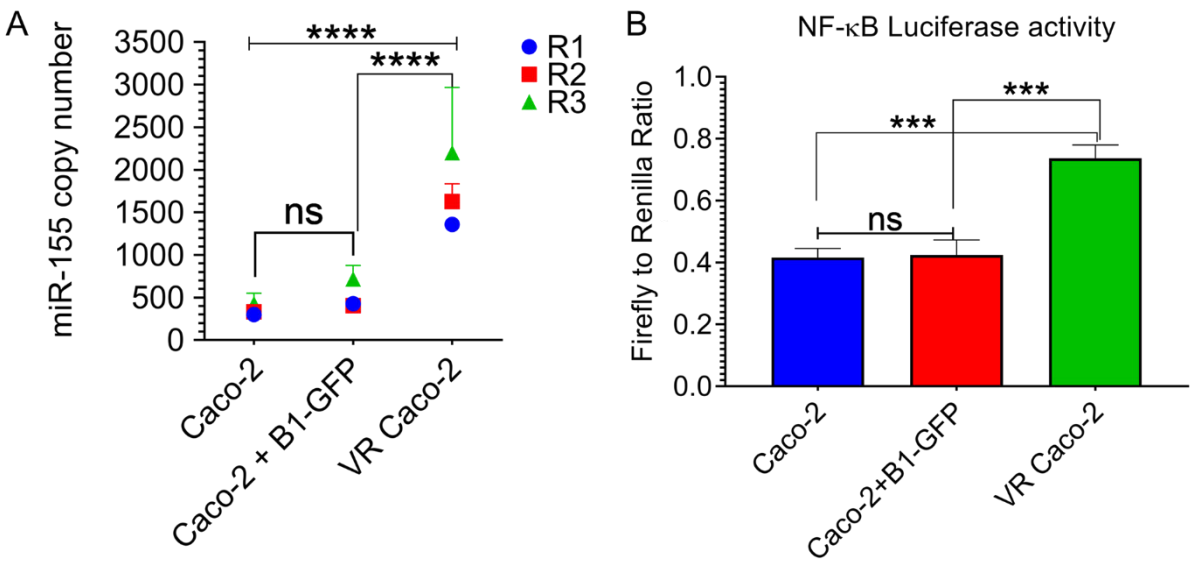

Figure 3.16. miR-155 expression and NF-kB activity in Caco-2 cells. (A) miR-155 copy number estimation by TaqMan qRT-PCR (n=3) **(B)** NF-kB luciferase activity was measured in Caco-2, acutely B1-GFP infected Caco-2 and VR Caco-2 cells (n=3). Data (mean ± SD) was analysed using a Shapiro-Wilk normality test, and two-way ANOVA with Sidak's multiple comparison test (*** $p< 0.001$ and **** $p<0.0001$).

3.3. Discussion

Cassel et al. reported the antineoplastic properties of NDV in human cancer cells for the very first time (94), and since then over the last fifty years, many advancements have been made with NDV as an oncolytic agent. The promising feature of NDV as an antineoplastic agent is because of the productive tumour-specific replication (96, 97) as cancer cells are defective of antiviral signalling pathways, defective of type-I IFN signalling pathways, defective of apoptotic pathways, activation of tumorigenic Ras signalling pathways, and expression Rac1 protein (111). In this chapter, the oncolytic potential of NDV avirulent strains was investigated in five different human cancer cell lines derived from different tissues. The study demonstrated that colorectal cancer Caco-2 cells are most vulnerable to NDV-induced cell death. This study validated the tumour-specific NDV replication and subsequent oncolysis in Caco-2 cells sparing the healthy normal cells.

Despite apparent susceptibility to NDV-induced cell death, NDV-persistent infection was confirmed in Caco-2 cells, and the isolated population was named VR Caco-2 cells. Persistent NDV infection is not a new phenomenon in its natural host, chicken organ cultures (233, 234) and non-human cell cultures (235, 236). Similar to other

paramyxoviruses such as Sendai and measles virus, persistent infection has been reported in the colorectal cancer cell line SW480 using velogenic NDV strain (237) and in an ovarian cancer cell line OVCAR3 with mesogenic NDV strain (238). In this study, it is demonstrated that VR Caco-2 cells acquired persistent NDV infection while maintaining the production of recoverable replicating virus at low titres with similar infectivity trend as of B1-GFP strain. Avian cells stably expressing NDV-HN (achieved by RCAS vector transfection) have shown resistance to the NDV re-infection potentially due to the receptor modification by constant HN expression with functional HA and NA activities (239). Persistently infected OVCAR3 cells confirmed the hyperfusogenic nature of NDV because of reported mutation in the cleavage site of NDV fusion protein at F_{117S} and altered receptor binding of HN protein due to mutation in the second sialic acid binding site at HN_{169R} (238). Protein sequences of both F and HN proteins investigated and did not find the reported mutations in either of the proteins. Evident syncytium formation was observed in VR Caco-2 cells compared to the acutely infected Caco-2 cells. Syncytium formation suggests fusogenic activity of NDV in VR Caco-2 cells and it probably helps spreading NDV infection in VR Caco-2 cells.

Nevertheless, there were ten mutation sites out of 13 found in the globular head of HN protein in the proximity of antigenic site 23, and the HA, and NA active sites. The other three mutation sites were located in the tail region of the HN protein. The tail domain of paramyxovirus HN protein is known to have specificity determinants for F-protein activation, which affects neuraminidase activity, and contributes significantly to the oligomerisation of the protein (240-242). These mutation sites collectively resulted in six-fold improved receptor binding avidity to the partially sialic acid depleted cRBCs in VR NDV compared to the B1-GFP strain. In future, these mutations could be validated by considering the rescue system to generate the mutant viruses to pin down exact mutations responsible for differential HA activity of VR NDV to the B1-GFP virus. The NA activity of VR NDV could be explored to conclude the role of HN protein acquiring persistent NDV infection in VR Caco-2 cells. As the trend of infectivity of VR NDV was reported similar to the B1-GFP strain at late time points while maintaining lower HA and PFU/ml titres; one can further investigate the production of defective interfering (DI) particles in VR Caco-2 cells as reported for Sendai (243) and measles (244) viruses.

The reduced cell cytotoxicity demonstrated upon NDV re-infection in VR Caco-2 cells in comparison with infected Caco-2 cells. A significant increase in miR-155 and two times increased NF-kB activity also have confirmed in VR Caco-2 cells. VR Caco-2 cells have shown two-times slower proliferation than of parental Caco-2 cells with higher NF-kB

activity with no sign of apoptosis so, pro-survival mechanism in VR Caco-2 cells could be confirmed further by investigating the NF-kB pathway.

An NDV-specific resistance and not to AIV (H9N2) and VSV was observed in VR Caco-2 cells. In other NDV persistent infection studies (237, 238), resistance to VSV has been reported as a result of the acquired antiviral status in persistently-infected cells. VR Caco-2 cells revealed a contrary behaviour showing susceptibility to VSV and AIV (H9N2) viruses. The H9N2 invasiveness in VR Caco-2 cells dismiss the possibility of receptor modification hypothesis to gain NDV-specific resistance. The limited resistance of VR Caco-2 cells to NDV could be expanded against paramyxoviruses other than NDV such as other avian paramyxoviruses (APMVs) or a bovine or human respiratory syncytial virus (RSV), measles virus, or Sendai virus. The infection of other paramyxoviruses in VR Caco-2 cells could explain whether the resistance is exclusive to the NDV or APMVs or other paramyxoviruses and could help to validate the mechanism of ongoing NDV infection in VR Caco-2 cells. VSV-induced cell death was also demonstrated in persistently infected VR Caco-2 cells. This finding opens up the possibility of the use of a combination of oncolytic viruses (OVs) to overcome persistent infection in human cancer cells. The combination of OVs could be a way forward to study the persistent infection in Caco-2 cells, and other cancer cell lines or recombinant NDV strains expressing immunostimulatory or oncolytic genes from other OVs could be employed to make NDV as a better and safer vaccine to treat cancer.

Human tumour cells infected with lentogenic (non-pathogenic) NDV strain Ulster 2C infected demonstrated the induction of *IFN-β*, *RANTES*, and *IP-10* mRNAs with activation of MHC as well as cell adhesion proteins ICAM-1 and LFA-3 (152, 245). Expressions of IFN-β and ISG15 mRNA was examined in Caco-2 and VR Caco-2 cells. No evident mRNA induction was found in Caco-2 and VR Caco-2 cells irrespective of the stimuli. This confirmed the inefficient antiviral status due to defective type-I IFN pathways in Caco-2 cells. Inefficient antiviral response in Caco-2 cells confirms better NDV infection and spread, resulting in active NDV-induced cell death in Caco-2 cells. In contrast, strong antiviral response in A549 cells regardless of similar NDV replication and supported ineffective NDV-induced oncolysis in A549 cells. This result was inconsistent with the reported NDV-induced apoptosis in A549 cells (242). However, the NDV-M gene copies at MOI 5 for 12 hpi demonstrated substantial monocyclic NDV replication in Hitchner B1, and B1-GFP infected A549 cells similar to infected Caco-2 cells, so intact type-I IFN pathways recovered the ongoing NDV infection in A549 cells. Persistent infection of NDV in A549 cells was not achieved, which is likely due to the

active type-I IFN pathways. The ineffective IFN system possibly could be the reason for NDV persistent infection in Caco-2 cells with all the non-pathogenic strains used in the study.

In summary, Caco-2 cells were most susceptible to NDV-induced oncolysis using avirulent NDV strains in a time and dose-dependent manner. Despite effective NDV-induced cell death in Caco-2 cells, NDV established persistent infection in Caco-2 cells, and was named VR Caco-2 cells. VR Caco-2 cells produced recoverable replicating virus and maintained virus at low viral titres in upto 34 passages. VR NDV (NDV produced in VR Caco-2 cells) showed six-fold higher receptor binding avidity compared to the B1-GFP virus. Sequence analysis of HN protein of VR NDV identified 13 mutation sites compared to the B1-GFP. Out of 13, 10 sites were found in the globular head in close proximity to antigenic site 23 and HA, and NA active sites and the other three were in the tail region. VR NDV has also shown similar replication trend in Caco-2 cells as B1-GFP virus. VR Caco-2 cells also have demonstrated two times slower cell proliferation than Caco-2 cells. However, VR Caco-2 cells have demonstrated NDV-specific resistance and remained susceptible to AIV and VSV infections and also have shown VSV-induced cell death. Ineffective *IFN-β* and *ISG15* mRNAs induction was reported in Caco-2 cells, which resulted in productive NDV-induced cell death in Caco-2 cells but also persistent NDV infection in Caco-2 cells.

Chapter 4

4 An integrated analysis of persistently NDV-infected VR Caco-2 cells using transcriptomic and proteomic approaches

4.1. Introduction

NDV established persistent infection in Caco-2 cells despite being the most susceptible cell line for NDV-induced oncolysis, as demonstrated in chapter 3. Persistently infected cells were named as VR (virus-resistant) Caco-2 cells, which developed different behaviour including two-times slower proliferation than uninfected Caco-2 cells, continuous production of recoverable replicating NDV viral particles with lower virus titres, and NDV-specific resistance upon re-infection in VR Caco-2 cells while permitting infections with AIV (avian influenza virus) and VSV (vesicular stomatitis virus). Given all the above differences in Caco-2 and VR Caco-2 cells, an integrated approach based on comparative methods such as RNA-seq and proteomic analysis was employed to understand the implications of persistent NDV infection in Caco-2 cells compared to the acute NDV infection and no infection in Caco-2 cells by analysing differential gene expression.

The use of RNA-seq approaches enabled an analysis of the transcriptomes of Caco-2 cells and NDV in parallel with easy monitoring of gene expressions of both host and pathogen while maintaining a high level of accuracy (provided that the read depth is sufficiently high), and amenable to computational analysis with or without prior knowledge of reference DNA sequences (246, 247). The use of proteomics study using mass spectrometry (MS) with a tandem mass tag (TMT) labelling assured precise identification of proteins, explaining the variable-dependent translation of abundant RNA transcripts into stable proteins in cells.

4.1.1. Chapter objectives

- RNA-seq data analysis to identify differentially expressed genes (DEGs)
- Comparative pairwise analysis between persistently NDV-infected VR Caco-2, acutely NDV-infected, and uninfected Caco-2 cells analysis
- Clustering of DEGs and GO/pathway enrichment analysis for identification of relevant functions/pathways and their behaviour across the infection
- Correlation of transcriptomic and proteomic data of VR Caco-2 cells compared with uninfected Caco-2 cells
- Comparative data analysis using publicly available RNA-seq datasets:

A) Comparison with Coxsackievirus B infected Caco-2 cells and with Caco-2 cells grown in 2D/3D cultures.

B) Comparison with NDV-infected chicken embryo fibroblast (CEF) cells

4.2. Results

4.2.1. RNA-seq datasets

A report summary statistics for the RNA-seq data generated in this PhD project, as well as data already published from NDV-infected CEF cells (248) and Coxsackievirus B (CVB) infected Caco-2 cells (249) used for the analysis. The RNA-seq data, protocol, and yield are summarised in **Table 4.1** and **4.2**. Caco-2 cells were infected with B1-GFP strain at MOI of 0.1 for two-time points 18 h and 36 h in a 6-well plate. Total RNA was extracted from NDV-infected Caco-2 cells (18 h and 36 h), uninfected Caco-2 cells (3 technical replicates), and VR Caco-2 cells (3 technical replicates, late passage P-25) using TRIzol method (RNA sample preparation discussed in detail in **section 2.2.4.**).

Table 4.1: Number of reads from Caco-2 cells (with or without NDV) and VR Caco-2 cells RNA-seq data

Sr. No.	Sample	Protocol and read length	Total reads	Cellular reads	Viral (NDV) reads
1	Caco-2 R1	PE 2x75bp	163101744	136165956	4
2	Caco-2 R2	PE 2x75bp	249099676	207143604	16
3	Caco-2 R3	PE 2x75bp	208334180	173535348	98
4	NDV 18 h Caco-2	SE 150bp	60305847	50759072	878722
5	NDV 36 h Caco-2	SE 150bp	60687628	43367516	5058895
6	VR Caco-2 R1	PE 2x75bp	169865200	136396814	422344
7	VR Caco-2 R2	PE 2x75bp	199240224	160157292	590062
8	VR Caco-2 R3	PE 2x75bp	192634102	157201210	545246

Table 4.2: Number of reads of RNA-seq samples from two different projects

Sr. No.	Samples	Protocol and read length	Total reads	Cellular reads	Viral (NDV) reads	Ref
1	CEF R1	PE 2x150bp	110981726	105289705	19193	(248)
2	CEF R2	PE 2x150bp	86062988	107316782	19202	
3	CEF R3	PE 2x150bp	93479188	82980071	18838	
4	NDV CEF R1	PE 2x150bp	83743856	86110590	4303890	
5	NDV CEF R2	PE 2x150bp	87401712	76973251	4107844	
6	NDV CEF R3	PE 2x150bp	83496140	80178138	4261925	
7	Caco-2 2D	SE 50bp	39585015	33144584	0	(249)
8	Caco-2 3D	SE 50bp	40354710	32575376	0	
9	Caco-2 2D	SE 50bp	41278742	35442092	0	
10	Caco-2 3D	SE 50bp	48849251	40545351	0	
11	Coxsackievirus Caco-2 2D	SE 50bp	47191310	25329368	0	
12	Coxsackievirus Caco-2 3D	SE 50bp	47655567	36606567	0	

Note for Table 4.1 and Table 4.1: Sr. No.- serial number, PE-paired end, and SE-single end (PE/SE are sequencing protocols).

4.2.2. Transcriptomics Data Analysis

Differential transcription profiles were investigated for human and viral genes in response to NDV acute and persistent infection in Caco-2 cells by comparing RNA-seq datasets of uninfected, acutely NDV-infected Caco-2 cells and persistently NDV-infected VR Caco-2 cells. Differential expression was estimated using the R package DESeq2. The mRNA expression values were estimated as normalised RPKM (Reads Per Kilobase of transcript per Million reads) as illustrated in **Figure 4.1**, with differentially expressed human and NDV genes (false-discovery rate [FDR] < 0.01 with multiple-testing correction using the Benjamini-Hochberg method) shown in red dots and genes

without significant differences shown in black dots in scatter plots across all the comparisons. In acutely NDV-infected Caco-2 cells, 7160 genes were differentially expressed in comparison with uninfected Caco-2 cells, versus 11012 genes in persistently infected VR Caco-2 cells **(Table 4.3)**. Hence, both acute and persistent NDV infection in Caco-2 cells resulted in extensive changes in the transcription level of thousands of genes compared to uninfected Caco-2 cells. A total of 10039 genes were also differentially expressed in VR Caco-2 cells compared to the acute NDV infection **(Table 4.3)**. All NDV genes were expressed in both acutely NDV-infected Caco-2 and persistently infected VR Caco-2 cells.

Table 4.3: Number of DEGs across all conditions in Caco-2 cells

Sr. No.	Pair-wise comparison between Caco-2 cells conditions	Number of DEGs
1	Acute NDV-infection in Caco-2 Vs No infection in Caco-2 cells	7160
2	Persistent NDV-infection in VR Caco-2 Vs No infection in Caco-2 cells	11012
3	Persistent NDV-infection in VR Caco-2 Vs Acute NDV-infection in Caco-2	10039

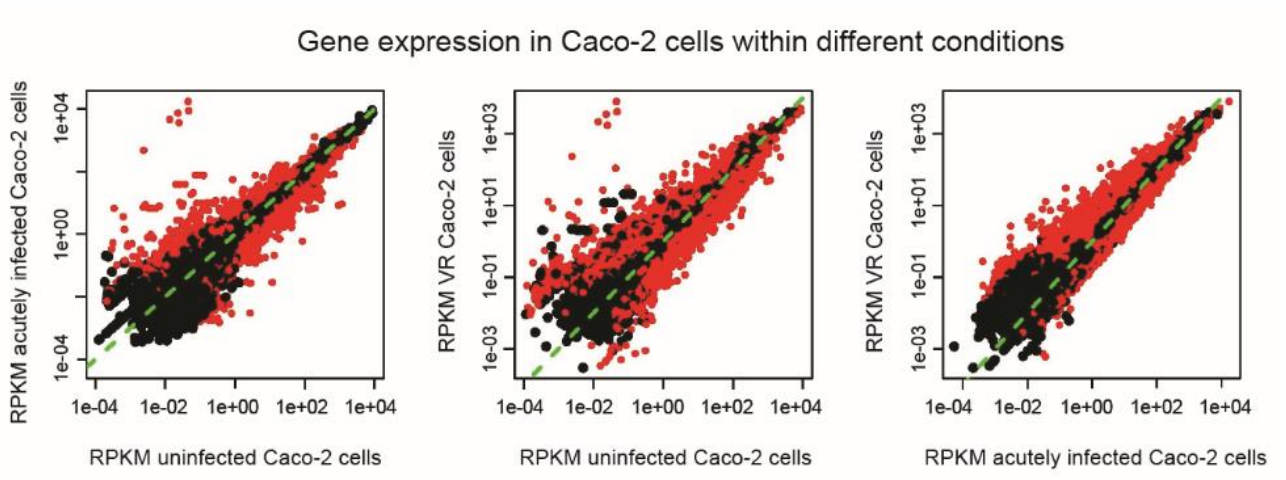

Figure 4.1. Scatter plots representing the gene expression profile in Caco-2 cells across different conditions. A comparison made between RPKM values representing gene expressions for human and NDV genes in uninfected, acutely NDV-infected Caco-2 cells, and persistently infected VR Caco-2 cells. Differentially expressed genes (FDR <0.01) shown in red dots and genes without significant differences shown in black dots.

The pattern of differential gene regulation was examined across all the conditions in Caco-2 and VR Caco-2 cells by quantifying log2 fold changes (LFCs) and adjusted p-values using the DESeq2 tool to determine the number of DEGs in all the conditions. LFCs and DEGs between acute and persistent NDV infection and uninfected Caco-2 cells were compared in three different pairwise comparisons: (1) relative LFCs and DEGs in acutely NDV infected Caco-2 cells and persistently infected VR Caco-2 cells compared with the uninfected Caco-2 cells ("Acute infection Vs No infection" compared to "VR Caco-2 Vs No infection"). (2) relative LFCs and DEGs in acutely NDV infected Caco-2 cells to uninfected Caco-2 cells compared with persistent NDV infection compared to the acute NDV infection ("Acute infection Vs no infection" compared to "Persistent infection of VR Caco-2 Vs acute NDV infection"). (3) relative LFCs and DEGs in persistent NDV infection in relation to the acute NDV infection compared with persistent NDV infection relative to the uninfected Caco-2 cells ("VR Caco-2 Vs acute NDV infection" compared to "VR Caco-2 Vs no infection"). A schematic representation of all the comparisons is shown in **Figure 4.2**, where DEGs expressed in both conditions are shown in red, whereas DEGs expressed in only one condition are shown in orange colour and genes without significant differences are shown in black. In all three pairwise comparisons, thousands of genes were differentially expressed, where DEGs are specific to one condition (orange genes) as well as DEGs showed in both the conditions (red genes). Genes under or overexpressed in all three pairwise comparisons are listed in **Table 4.4**, **Table 4.5**, and **Table 4.6**.

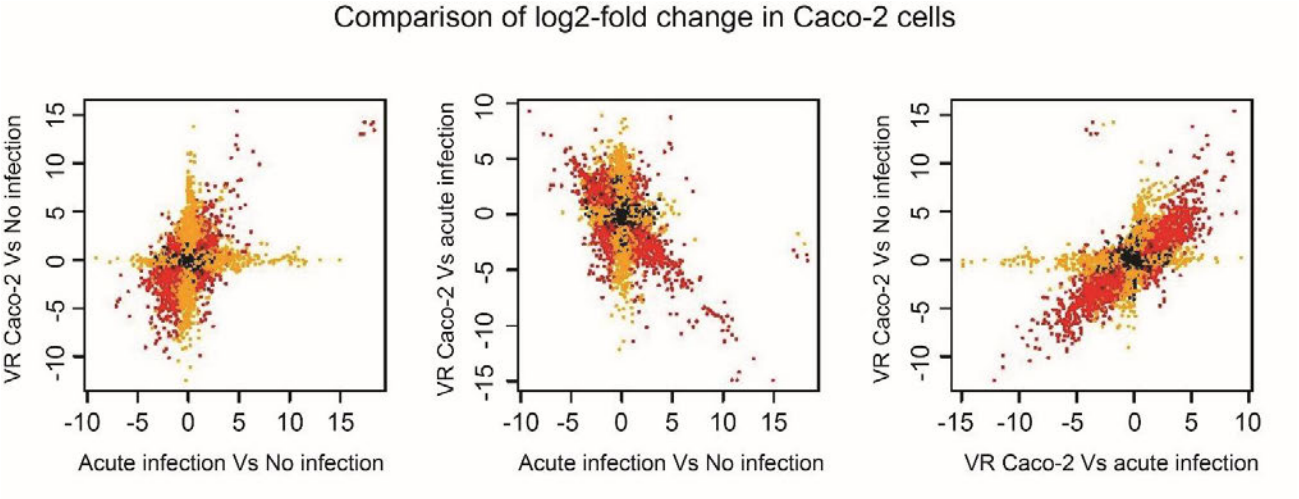

Figure 4.2. Relative account of differential genes expression in pairwise comparisons across all conditions in Caco-2 cells (acute or persistent NDV infection and no infection). Scatter plots demonstrating apeGLM-shrinked log2-fold changes in Caco-2 cells across multiple conditions. Genes are shown in red if they were expressed in both comparisons and genes shown in orange if they were expressed in only one comparison.

The patterns of significantly upregulated and downregulated genes are illustrated through the Venn diagrams **(Figure 4.3)**. Total number of DEGs overlapped across all pairwise comparisons explained by Venn diagram are shown in **Figure 4.3 A**, where all three comparisons share 1755 DEGs. VR Caco-2 cells showed expression of a significantly higher number of DEG in comparison with no infection (2698) and acute infection (1266) confirming the broader impact of persistent NDV-infection in VR Caco-2 cells **(Figure 4.3 A)**.

Table 4.4: Genes under or overexpressed in acutely NDV-infected Caco-2 cells in comparison with uninfected Caco-2 cells

Sr. No.	Gene ID	Gene Name	LFCs	padj	Function
1	NP	NP	18.33680872	4.93E-44	The NDV-Nucleocapsid protein binds to viral RNA and forms RNP complex
2	F	F	18.25506865	2.37E-81	NDV-Fusion protein involved in viral entry and egress
3	P	P	18.0208011	9.24E-32	NDV-Phosphoprotein, forms RNP complex
4	L	L	17.36765684	6.41E-33	NDV-Large RNA polymerase, viral RNA synthesis
5	M	M	17.34340765	3.78E-56	NDV-Matrix protein responsible for viral assembly
6	HN	HN	16.9842281	5.21E-49	NDV-HN protein possess haemagglutinin (HA) and neuraminidase (NA) activities and receptor binding
7	ENSG00000228736.9	RGL2	14.92565371	1.24E-26	Ral Guanine Nucleotide Dissociation Stimulator Like 2 protein is probable guanine nucleotide exchange factor and putative effector of Ras and/or Rap. Associates with the GTP-bound form of Rap 1A and H-Ras *in vitro*
8	ENSG00000204435.13	CSNK2B	13.01124313	9.90E-20	Casein Kinase 2 Beta protein, a ubiquitous protein kinase which regulates metabolic pathways, signal transduction, transcription, translation, and replication
9	ENSG00000204220.10	PFDN6	11.5807309	1.25E-20	Prefoldin Subunit 6 protein binds specifically to cytosolic chaperonin (c-CPN) and transfers target proteins to it. Binds to nascent polypeptide chain and promotes folding in an environment in which there are many competing pathways for non-native proteins
10	ENSG00000237441.9	RGL2	11.40088636	5.02E-26	Ral Guanine Nucleotide Dissociation Stimulator Like 2 protein is probable guanine nucleotide exchange factor and putative effector of Ras and/or Rap. Associates with the GTP-bound form of Rap 1A and H-Ras *in vitro*
11	ENSG00000206406.9	CSNK2B	-5.594047023	0.000361263	Casein Kinase 2 Beta protein, a ubiquitous protein kinase which regulates metabolic pathways, signal transduction, transcription, translation, and replication
12	ENSG00000241146.1	RPL7P41	-5.840970274	0.000304711	Ribosomal Protein L7 Pseudogene 41
13	ENSG00000122877.14	EGR2	-5.952234653	1.11E-85	Early Growth Response 2 protein, Sequence-specific DNA-binding transcription factor. Binds to two specific DNA sites located in the promoter region of HOXA4.
14	ENSG00000232992.2	AHCYP4	-6.625595612	6.94E-05	Adenosylhomocysteinase Pseudogene 4
15	ENSG00000120738.7	EGR1	-6.745860281	1.64E-230	Early Growth Response-1 protein binds double-stranded target DNA, irrespective of the cytosine methylation status and Plays a role in the regulation of cell survival, proliferation and cell death. Activates

					expression of p53/TP53 and TGFB1, and thereby helps prevent tumour formation.
16	ENSG00000170345.9	FOS	-6.947062206	1.33E-254	FOS Proto-Oncogene encodes leucine zipper proteins that can dimerise with proteins of the JUN family, thereby forming the transcription factor complex AP-1. As such, the FOS proteins have been implicated as regulators of cell proliferation, differentiation, and transformation.
17	ENSG00000280175.1	AL354828.2	-7.001060767	1.30E-05	lnc-MKRN2-42:1 targets AL354828.2
18	ENSG00000125740.13	FOSB	-7.11886449	7.25E-153	FOSB Proto-Oncogene encodes leucine zipper proteins that can dimerise with proteins of the JUN family, thereby forming the transcription factor complex AP-1. As such, the FOS proteins have been implicated as regulators of cell proliferation, differentiation, and transformation.
19	ENSG00000210127.1	MT-TA	-7.717135085	2.36E-06	Mitochondrially encoded tRNA-Ala (GCN)
20	ENSG00000266340.1	RP11-848P1.4	-9.130395133	1.88E-08	Antisense RNF135 (Ring Finger Protein 135 -involved in protein-protein and protein-DNA interactions)

Table 4.5: Genes under or overexpressed in persistently NDV-infected VR Caco-2 cells in comparison with uninfected Caco-2 cells

Sr. No.	Gene ID	Gene name	LFCs	padj	Function
1	ENSG00000134321.11	RSAD2	15.42625176	2.84E-30	Interferon-inducible iron-sulphur (4FE-4S) cluster-binding antiviral protein which plays a major role in the cell antiviral state induced by type-I and type-II interferon.
2	F	F	14.27000281	6.24E-60	NDV-Fusion protein involved in viral entry and egress
3	L	L	14.24826748	9.87E-28	NDV-Large RNA polymerase, viral RNA synthesis
4	P	P	14.00538752	1.42E-24	NDV-Phosphoprotein, forms RNP complex
5	ENSG00000137965.10	IFI44	13.79872114	7.35E-10	This protein aggregates to form microtubular structures, participate in immune response
6	NP	NP	13.41890592	3.12E-30	The NDV-Nucleocapsid protein binds to viral RNA and forms RNP complex
7	HN	HN	13.05284591	1.71E-36	NDV-HN protein, possess haemagglutinin (HA) and neuraminidase (NA) activities and receptor binding
8	M	M	13.01888602	8.34E-40	NDV-Matrix protein responsible for viral assembly
9	ENSG00000134326.11	CMPK2	12.88674322	5.99E-21	Cytidine/Uridine Monophosphate Kinase 2, catalyses the phosphorylation of uridine and cytidine

10	ENSG00000169248.12	CXCL11	11.89230585	9.38E-20	Chemotactic for interleukin-activated T-cells but not unstimulated T-cells, neutrophils or monocytes
11	ENSG00000249346.6	LINC01016	-9.068806052	6.21E-10	Long Intergenic Non-Protein Coding RNA 1016, associated with Breast cancer
12	ENSG00000109610.5	SOD3	-9.1358896	5.03E-10	Protect the extracellular space from the toxic effect of reactive oxygen intermediates by converting superoxide radicals into hydrogen peroxide and oxygen
13	ENSG00000113492.13	AGXT2	-9.206935161	2.05E-10	Alanine-Glyoxylate Aminotransferase 2, metabolize asymmetric dimethylarginine (ADMA)-a potent inhibitor of nitric-oxide (NO) synthase
14	ENSG00000224652.1	LINC00885	-9.231189025	1.47E-10	Long Intergenic Non-Protein Coding RNA 885, affiliated with the lncRNA class
15	ENSG00000186910.3	SERPINA11	-9.430285938	6.19E-11	Serine-type endopeptidase inhibitor
16	ENSG00000188803.14	SHISA6	-9.937239463	1.82E-12	Involved in maintenance of high-frequency synaptic transmission at hippocampal CA3-CA1 synapses
17	ENSG00000225756.1	DBH-AS1	-10.14549397	1.38E-12	DBH (Dopamine Beta-Hydroxylase) Antisense RNA 1
18	ENSG00000263961.6	C1orf186	-10.46125752	9.73E-14	Acts as a signalling transduction factor of the EPO-EPOR signalling pathway promoting erythroid cell differentiation
19	ENSG00000146477.5	SLC22A3	-11.15651349	1.50E-15	Solute Carrier Family 22 Member 3 protein mediates potential-dependent transport of a variety of organic cations
20	ENSG00000167755.13	KLK6	-12.44877645	2.93E-19	S1 family of serine proteases are implicated in carcinogenesis, and some have potential as novel cancer and other disease biomarkers

Table 4.6: Genes under or overexpressed in persistently NDV-infected VR Caco-2 cells in comparison with acutely NDV-infected Caco-2 cells

Sr. No.	Gene ID	Gene Name	LFCs	padj	Function
1	ENSG00000266340.1	RP11-848P1.4	9.306312353	3.01E-09	Antisense RNF135 (Ring Finger Protein 135 -involved in protein-protein and protein-DNA interactions)
2	ENSG00000127954.12	STEAP4	8.88137341	2.43E-08	Six transmembrane epithelial antigens of prostate express on Golgi apparatus and functions as a metalloreductase that has the ability to reduce both Fe (3+) to Fe (2+) and Cu (2+) to Cu (1+), using NAD (+) as acceptor.
3	ENSG00000134321.11	RSAD2	8.733407549	2.24E-29	Interferon-inducible iron-sulphur (4FE-4S) cluster-binding antiviral protein which plays a major role in the cell antiviral state induced by type-I and type-II interferon.
4	ENSG00000163565.18	IFI16	8.612546879	3.07E-12	Interferon Gamma Inducible Protein 16, interacts with p53 and retinoblastoma-1, modulation of p53 function inhibits cell growth in the Ras/Raf signalling pathway

5	ENSG00000137959.15	IFI44L	8.571449464	9.80E-10	Interferon Induced Protein 44 Like, exhibits a low antiviral activity against hepatitis C virus.
6	ENSG00000148346.11	LCN2	8.259449423	3.27E-07	Lipocalin family protein involved in the transport of small hydrophobic molecules such as lipids, steroid hormones and retinoids
7	ENSG00000128422.15	KRT17	7.874557344	1.45E-72	Keratin 17, regulates protein synthesis and epithelial cell growth through binding to the adapter protein SFN and by stimulating Akt/mTOR pathway
8	ENSG00000198774.4	RASSF9	7.699679129	1.27E-19	Ras Association Domain Family Member 9 perinuclear endosomal protein, may play a role in regulating vesicular trafficking in cells
9	ENSG00000177409.11	SAMD9L	7.640052869	3.52E-21	A cytoplasmic protein that acts as a tumour suppressor but also plays a key role in cell proliferation and the innate immune response to viral infection
10	ENSG00000163739.4	CXCL1	7.334585611	2.38E-21	C-X-C Motif Chemokine Ligand 1 plays a role in inflammation and as a chemoattractant for neutrophils. Aberrant expression of this protein is associated with the growth and progression of certain tumours
11	ENSG00000237825.9	RGL2	-11.33073939	1.96E-26	Probable guanine nucleotide exchange factor. Putative effector of Ras and/or Rap. Associates with the GTP-bound form of Rap 1A and H-Ras *in vitro*
12	ENSG00000188803.14	SHISA6	-11.4072178	1.51E-15	Involved in maintenance of high-frequency synaptic transmission at hippocampal CA3-CA1 synapses
13	ENSG00000146477.5	SLC22A3	-11.4087811	9.05E-16	Solute Carrier Family 22 Member 3 protein mediates potential-dependent transport of a variety of organic cations
14	ENSG00000235692.8	PFDN6	-11.50504825	5.42E-21	Prefoldin Subunit 6 protein binds specifically to cytosolic chaperonin (c-CPN) and transfers target proteins to it. Binds to nascent polypeptide chain and promotes folding in an environment in which there are many competing pathways for non-native proteins
15	ENSG00000167755.13	KLK6	-12.14103661	5.77E-18	S1 family of serine proteases are implicated in carcinogenesis, and some have potential as novel cancer and other disease biomarkers
16	ENSG00000204435.13	CSNK2B	-12.95881742	4.21E-20	Casein Kinase 2 Beta protein, a ubiquitous protein kinase which regulates metabolic pathways, signal transduction, transcription, translation, and replication
17	ENSG00000204220.10	PFDN6	-14.14317051	1.87E-24	Chaperone-mediated protein complex assembly
18	ENSG00000224841.9	RGL2	-14.87774209	5.30E-27	Ral Guanine Nucleotide Dissociation Stimulator Like 2 protein is probable guanine nucleotide exchange factor and putative effector of Ras and Rap. Associates with the GTP-bound form of Rap 1A and H-Ras *in vitro*
19	ENSG00000237441.9	RGL2	-14.87922383	5.64E-27	
20	ENSG00000228736.9	RGL2	-14.88458331	5.38E-27	

Numerous genes overlapped in upregulation and downregulation and while most DEGs were specific to two comparisons, some were restricted to one pairwise comparison, and a few hundred were identified across all three pairwise comparisons as well **(Figure 4.3 B)**. In total, 203 genes were upregulated, and 477 genes were downregulated across all three comparisons. Persistent NDV infection in VR Caco-2 cells compared to acute NDV infection in Caco-2 cells induced exclusive upregulation of 529 genes and downregulation of 737 genes. However, 471 genes are exclusively overexpressed and 369 genes underexpressed in acutely NDV-infected Caco-2 cells compared to uninfected Caco-2 cells. Whereas 1635 genes are exclusively overexpressed and 1063 genes underexpressed in persistently infected VR Caco-2 cells in contrast with uninfected Caco-2 cells. NDV infection regardless of the acute or persistent status has resulted in the regulation of numerous genes in Caco-2 cells and VR Caco-2 cells. There is clear evidence of a trend of broader changes in regulation in persistently infected cells, compared to acutely infected ones.

Interestingly, sets of 1774 genes are downregulated and 1813 genes upregulated in acutely infected Caco-2 cells, but these genes are inversely regulated respectively in the persistently infected VR Caco-2 cells compared to the acute infection. These DEGs are most likely a response to the high amount of virus during acute infection. There are 1005 genes upregulated and 1323 genes downregulated in both acute and persistent infection phases in a similar trend. The substantial similarity and dissimilarity of gene regulation observed in acute and persistent NDV infection in Caco-2, and VR Caco-2 cells in comparison with uninfected Caco-2 cells could explain changed behaviour of VR Caco-2 cells from parental uninfected Caco-2 cells.

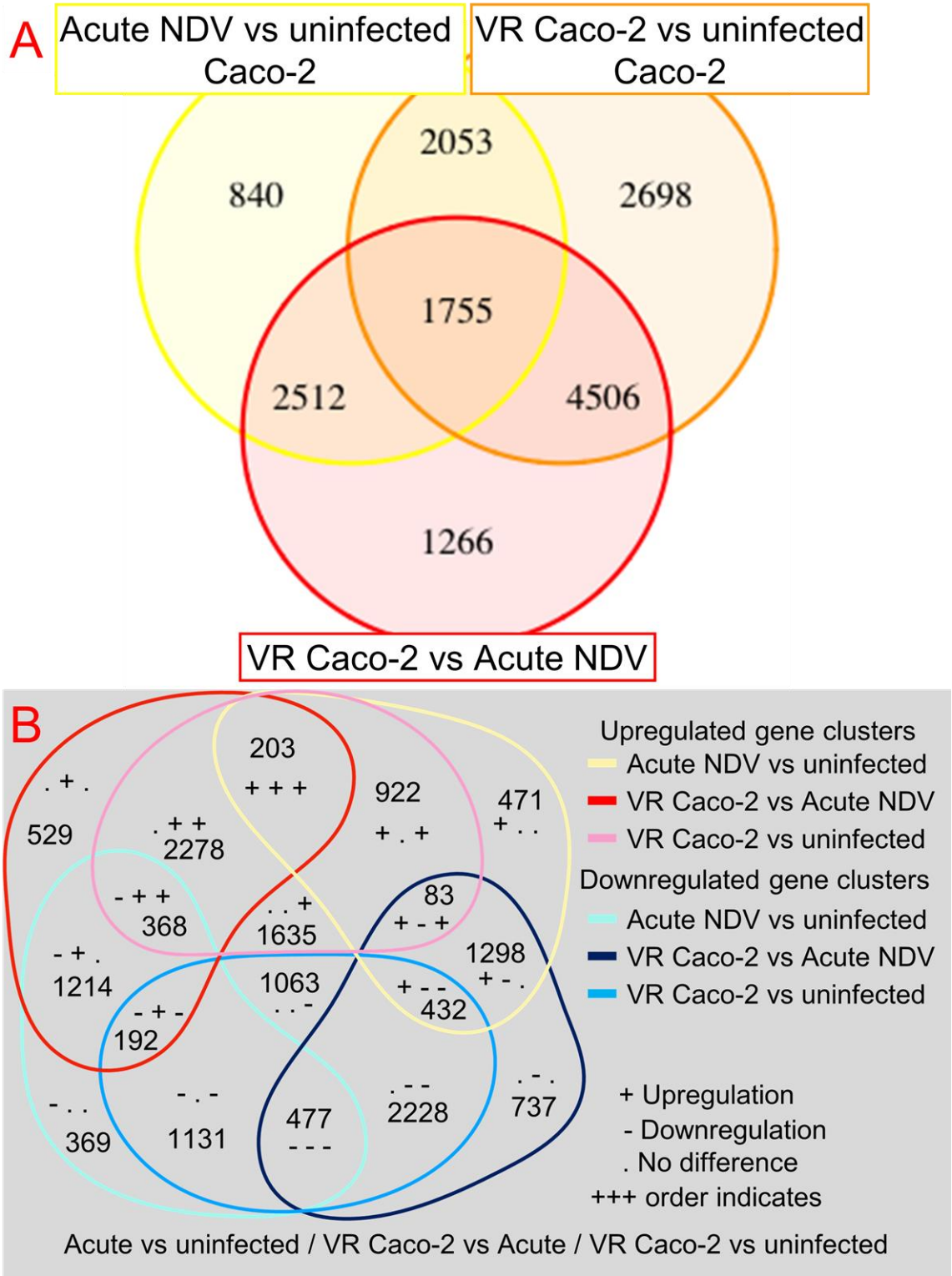

Figure 4.3. Venn diagram summarising distribution pattern of differentially expressed genes (DEGs) (FDR<0.01) in three pairwise comparisons (Pairwise comparisons are made between acutely NDV-infected Caco-2 cells, persistently infected VR Caco-2 cells, and uninfected Caco-2 cells). **(A)** Total number of DEGs overlapped across all pairs of conditions **(B)** Gene clusters showing significant upregulation or downregulation across all pairwise comparisons

The relationship of all three pairwise comparisons of LFC quantiles appeared to be correlated or anticorrelated. The mutual comparison of LFC of acute and persistent infection compared to the no infection fall in a weak positive monotonic relationship within both conditions indicated by r_s=0.309 (Spearman's correlation coefficient). A strong positive monotonic relationship with r_s=0.63315 was found in the mutual comparisons between LFCs of persistently infected VR Caco-2 compared with uninfected Caco-2 cells and acutely NDV-infected Caco-2 cells, demonstrating regulation of genes following similar trend in correlation within VR Caco-2 cells compared to the acutely NDV-infected Caco-2 cells shown in **Figure 4.4**. In both the comparisons, a strong association is found among hundreds of mostly upregulated and downregulated genes, as shown in dark colour (**Figure 4.4**).

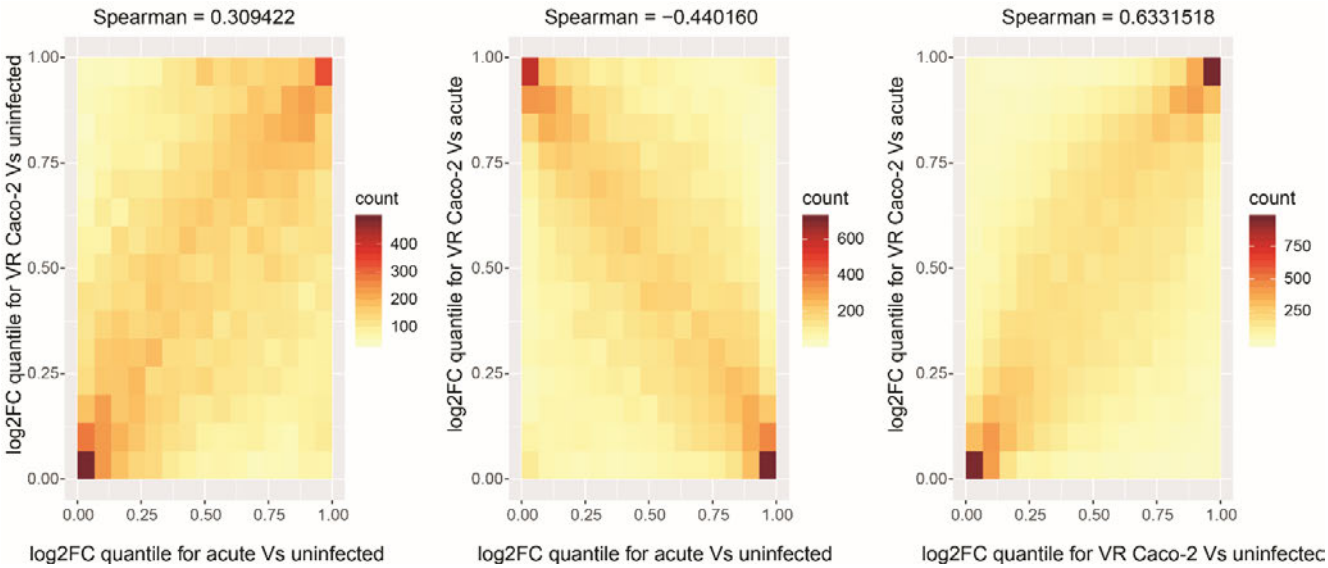

Figure 4.4. Quantile-quantile distribution of log2-fold changes across different pairwise conditions. The pattern of most upregulated and downregulated genes between different conditions indicated by apeGLM-shrinked log2-fold changes (FDR<0.01 with multiple-testing correction using the Benjamini-Hochberg method).

After identifying statistically significant DEGs based on DESeq2 LFCs and adjusted p-values in at least one of the three pairwise comparison among Caco-2 cells (FDR<0.05 and LFC>4), a hierarchical clustering approach based on log10 RPKM expression values was used to determine the expression profiles in time, comparing uninfected Caco-2 cells to acutely infected Caco-2 cells at 18 h and 36 h post-NDV infection and persistently NDV-infected VR Caco-2 cells. All 913 DEGs clustered according to the similar gene expression profile into nine different clusters, as shown in **Figure 4.5**. Upregulated expression of NDV viral genes with a clear difference between acute infection time points (18 h and 36 h) and VR Caco-2 cells are demonstrated in cluster 8. The gene expression profile of cluster 1

showed abrupt downregulation of 185 genes in VR Caco-2 cells, whereas these genes remained unaffected in the uninfected and acutely NDV-infected Caco-2 cells. However, in cluster 2, 170 genes were (continuously) downregulated in both acute infection and persistent NDV infection compared to the uninfected Caco-2 cells. In clusters 3 (164 genes) and 4 (163 genes), expression profiles demonstrated upregulation of genes in the VR Caco-2 cells with the opposite behaviour compared to clusters 1 and 2, respectively. In all clusters from 1 to 4 downregulation and upregulation of genes was not correlated to the amount of viral gene expression in acutely and persistently infected VR Caco-2 cells.

Surprisingly, VR Caco-2 cells established the regulation of some of the intestinal markers, which are primarily known to play a role in intestinal cell differentiation. Drummond et al. (2016) reported the expression of several genes associated with intestinal epithelial differentiation in Caco-2 cells when comparing transition from 2-Dimensional (2D) model to 3-Dimensional (3D) models, which attained a more complex structure from the 2D heterogeneous model in 21 days of culturing. These included downregulation of *PDGFRA* (platelet-derived growth factor receptor alpha), protease-activated transporter *SLC10A1* (Solute Carrier Family 10 Member 1) and upregulation of the transmembrane mucins abundantly expressing in the intestine like *MUC1*, *MUC13*, and *MUC17*. A downregulation of *Orm2* (Orosomucoid 1), *SLC38A4* (Solute Carrier Family 38 Member 4), and *ALB* (Albumin) genes in an early stage of culturing as well as downregulation of PDGFRA in a later stage of culturing (249). In VR Caco-2 cells, overexpression of *MUC17* and underexpression of *SLC10A1*, *MS4A10* (Membrane Spanning 4-Domains A10), *Orm2*, SLC38A4, and ALB genes have been observed in RNA-seq analysis. The similar trend of notified differentiation markers in VR Caco-2 suggested an increase in complexity of VR Caco-2 cells related to the one observed in the 3D model of Caco-2 cells. Reactive oxygen species (ROS) produced by NADPH oxidases (NOX)- *NOX2* and *NOX4* genes are found to be downregulated (Cluster 1) in VR Caco-2 cells. Several genes responsible for antiviral cellular responses were found to be overexpressed in VR Caco-2 cells but not in acutely NDV infected Caco-2 cells like *IL-15, OASL, IFIT1, C3, CASP1, DDX60* etc. (cluster 3 and 4) were upregulated significantly in comparison with acute NDV-infection and no infection in Caco-2 cells. There were plenty of genes that are highly overexpressed (clusters 5 and 8) or underexpressed (clusters 6 and 9) only in an acute NDV infection and not in uninfected Caco-2 and VR Caco-2 cells, in direct relation to highly expressed NDV genes.

Overall, 913 significantly differentially expressed genes in acute and persistent NDV infected Caco-2 cells resulted in profound changes in VR Caco-2 cells, which hinder the capacity to pinpoint specific mechanisms acquired to define NDV-specific resistance.

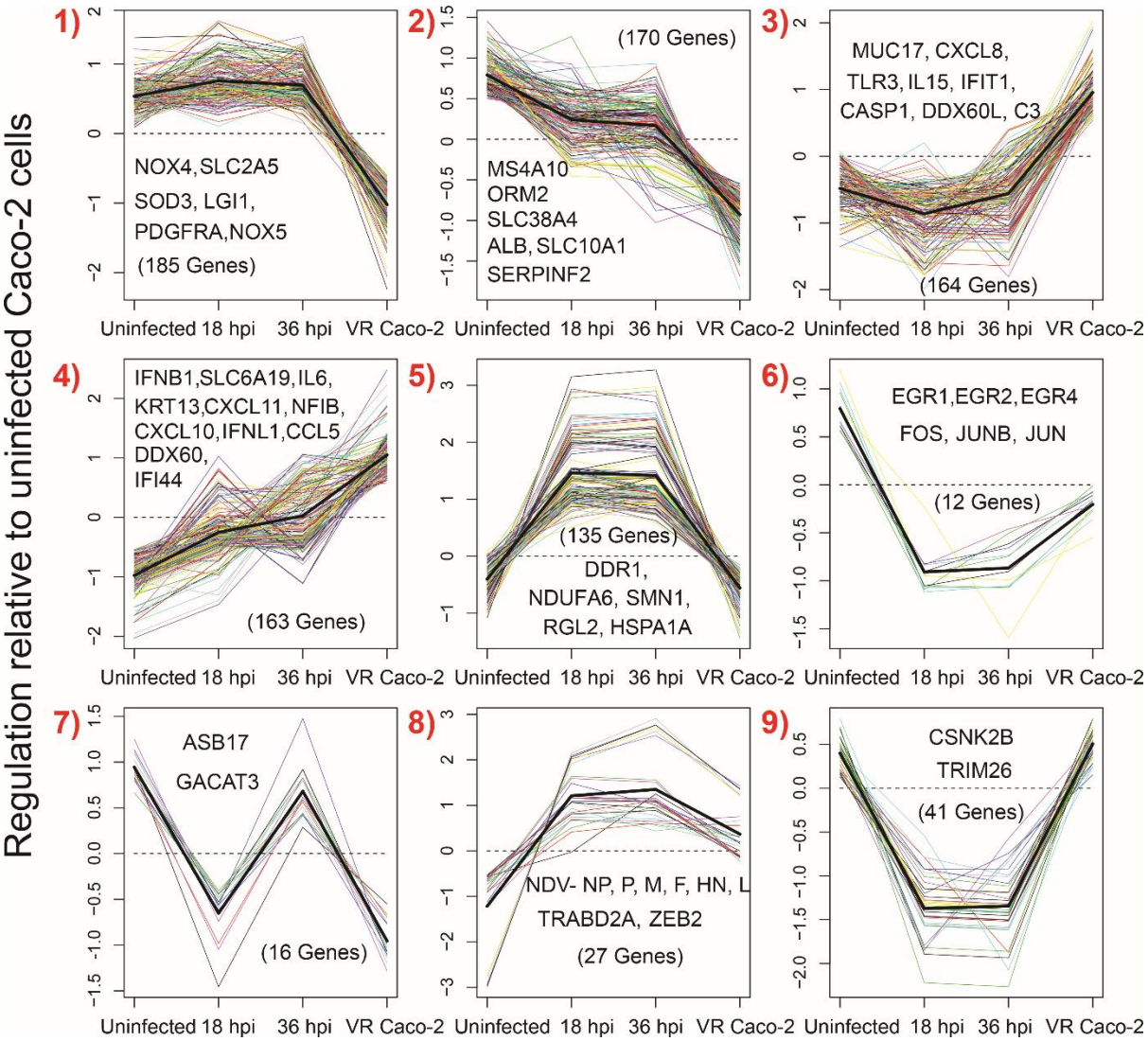

Figure 4.5. Cluster analysis of gene expression profiles. Gene expression (log10 RPKM) profiles are shown for uninfected, acutely infected (18 hpi and 36 hpi, NDV MOI=0.01), and persistently infected VR Caco-2 cells and for all genes with significant differential expression (FDR<0.05 and LFC>4) between any pair of conditions, rescaled and grouped in hierarchical 9 clusters. In each cluster, a few representative genes are outlined. The thick black line represents the average gene expression, while a dotted line indicates the basal level.

Gene Ontology and pathway overrepresentation analysis were performed using significant DEGs from all Caco-2 cells conditions to understand which GO (Gene Ontology) biological processes and Reactome pathways would play a role. However, only a few significant signals could be found after multiple test corrections, due to the reduced numbers of genes and the complexity of the infection. For this reason, we used a different approach, combining enrichment analysis and time profile reconstruction. First, we obtained adjusted p-values for all GOs and pathways using PantherDB; then, we inferred the trend in time from the significance of the p-values, and we grouped these trends in 9 clusters, each

representing different functional roles of genes in the infection process. **Figure 4.6** illustrated this dynamic classification of the regulation of processes and pathways relative to uninfected Caco-2 cells, representing an overall of 707 differentially expressed processes/pathways grouped in 9 clusters with representative examples. In cluster 1 **(Figure 4.6)** almost 134 processes are significantly downregulated in VR Caco-2 cells only while remained unchanged in uninfected Caco-2 cells and in acutely NDV-infected Caco-2 cells, where metabolic processes involved downregulation of glucose metabolism, pyruvate and citric acid (TCA) cycle, and respiratory electron transport chain mechanism amongst other processes. In cluster 5 (54 processes) and 8 (6 processes) **(Figure 4.6)** showed significant upregulation of processes involving IFN-mediated antiviral pathways and gradual increase in cytokine-mediated responses in response to persistent NDV infection in VR Caco-2 cells only whereas in acutely NDV-infected and uninfected Caco-2 cells remained unaffected.

In summary, pathways and processes underexpressed (in cluster 1) and overexpressed (in cluster 5 and 8) are regulated independently of viral load in Caco-2 cells similar to gene expression profiles (from **Figure 4.5** clusters 1, 2, 3, and 4). In clusters 2, 6, 7, and 9 all predicted pathway/processes were correlated to the viral load as significant upregulation (clusters 2, 7, and 9) and downregulation (cluster 6) was seen only in acutely NDV-infected Caco-2 cells and basal levels maintained in the uninfected Caco-2 and VR Caco-2 cells. All the upregulated and downregulated processes are expected in acutely NDV-infected Caco-2 cells as a result of active viral replication; upregulated processes involved the processing of 3 prime RNA synthesis, increased regulation of cell cycle phases and checkpoints, RNA transcription and transport, as well as ribonucleoprotein biosynthesis etc. However, cell division is downregulated in VR Caco-2 cells, and ribonucleoprotein biosynthesis is upregulated compared to no infection in Caco-2 cells. Whereas, downregulated processes included extracellular signal-regulated kinases (ERKs)-ERK1/ERK2 mediated cell survival mechanism, cellular differentiation and developmental process. Few pathways and metabolic processes are downregulated (cluster 3: 83 processes; like lipid metabolism, lipoprotein assembly in the plasma membrane, and regulated exocytosis etc.) and upregulated (cluster 4: 23 processes, including defence response to virus and generic transcription pathways) equally in both acute and persistent NDV infection of Caco-2 cells irrespective of the amount of active viral replication.

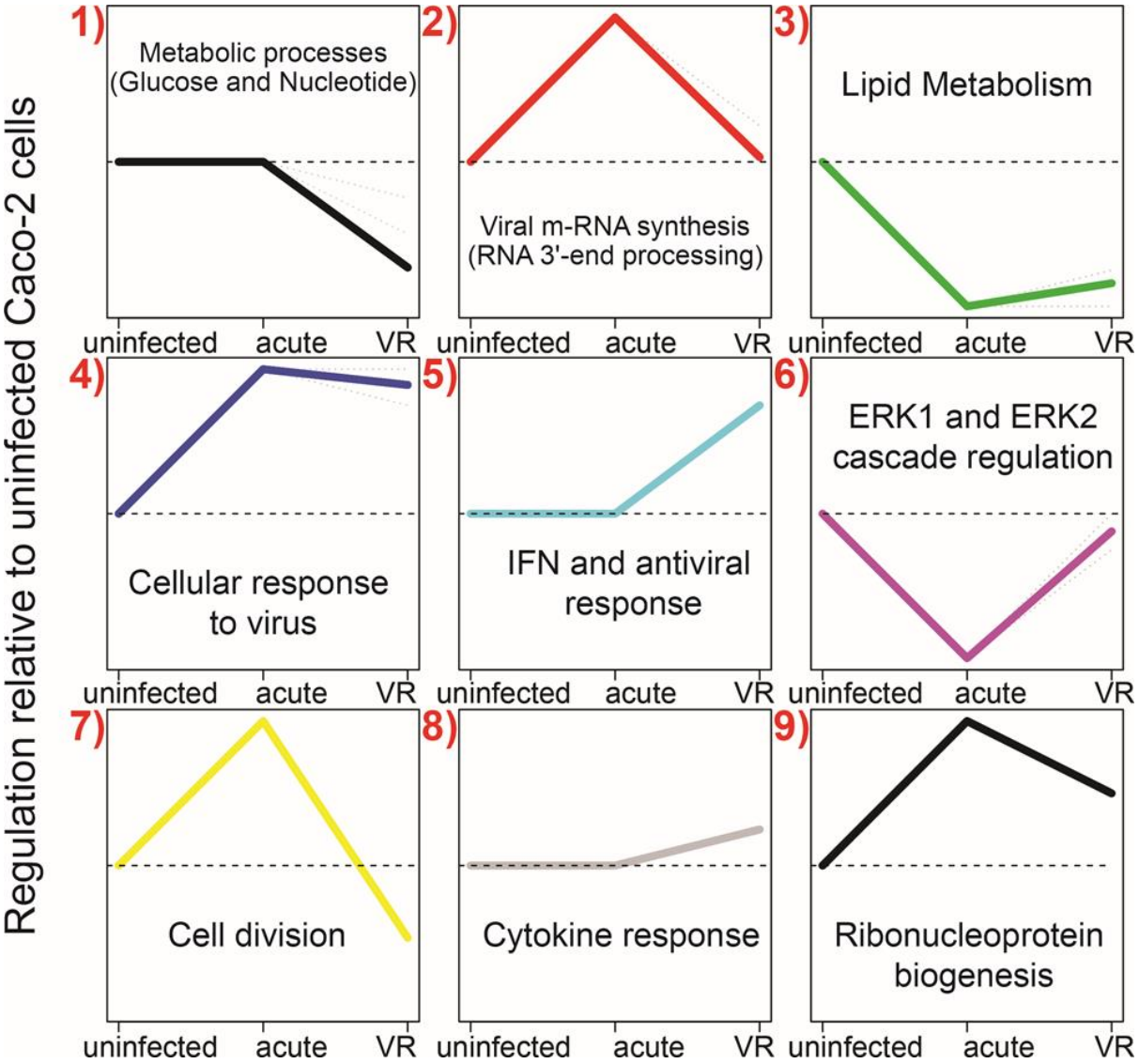

Figure 4.6. Dynamic classification of the functional profile of GOs (gene ontologies) and pathways in differentially regulated pathways in uninfected, acutely, and persistently NDV-infected Caco-2 cells. An example of metabolic process for each cluster written in the respective cluster, where dotted line indicated the basal level of expression of collective processes in uninfected Caco-2 cells.

Likewise, Ingenuity Pathway Analysis (IPA) pathway was used for overrepresentation analysis using significant DEGs from all Caco-2 cells conditions. IPA analysis showed a total of 99 canonical pathways differentially regulated across the conditions in Caco-2 cells grouped in 9 clusters, as illustrated in **Figure 4.7**. In cluster 1, 17 different pathways are downregulated in NDV-infected Caco-2 cells irrespective of the viral load, pathways include Dermatan Sulfate Biosynthesis (Dermatan sulfate (DS) is a glycosaminoglycan present in the extracellular matrix of the skin as well as i)n numerous other tissues), Liver X receptors (LXR)/ Retinoid X receptors (RXRs) pathway activation, and Cell division control protein 42 homolog (CDC42) signalling pathway. Whereas in cluster 2, a total of 9 canonical

processes are upregulated in NDV-infected Caco-2 and VR Caco-2 cells irrespective of the viral load, pathways include the role of PRRs in recognition of pathogens (Bacteria and Viruses), Activation of IRF (IFN-regulated factors) by cytosolic PRRs, and LPS (lipopolysaccharide) / IL-1 mediated inhibition of RXR function. However, as a result of active virus replication in acutely NDV-infected Caco-2 cells resulted in the downregulation of pathways in clusters 4 (6 pathways; example eNOS signalling pathway), 5 (9 pathways; example Acute phase response and TNFR2 signalling pathways), and 7 (3 pathways; example Endothelin-1 signalling pathway). VR Caco-2 cells showed significant upregulation and downregulation of pathways compared to the acute NDV-infection, and no change in uninfected Caco-2 cells in clusters 3 and 8 (upregulation) and clusters 6 and 9 (downregulation). In cluster 3 (22 pathways with the significant increase in VR Caco-2 cells) include IFN signalling, VEGF signalling, Death receptor signalling, cell cycle G2/M DNA Damage Checkpoint Regulation and PI3K/AKT signalling pathways. In cluster 8 (8 pathways with a slight increase in VR Caco-2 cells) processes include the role of CHK (checkpoint serine/threonine kinase) proteins in cell cycle checkpoint control, IL-17A signalling in Gastric Cells, and NRF2 (Nuclear factor erythroid-2-related factor 2)-mediated oxidative stress response pathways. Similarly, the downregulated pathways in cluster 6 (21 pathways) and 9 (3 pathways) include Sumoylation and cAMP-mediated signalling pathways respectively. IPA analysis also has confirmed significant regulation on the broader scale of VR Caco-2 cells compared to acute NDV-infection in Caco-2 cells.

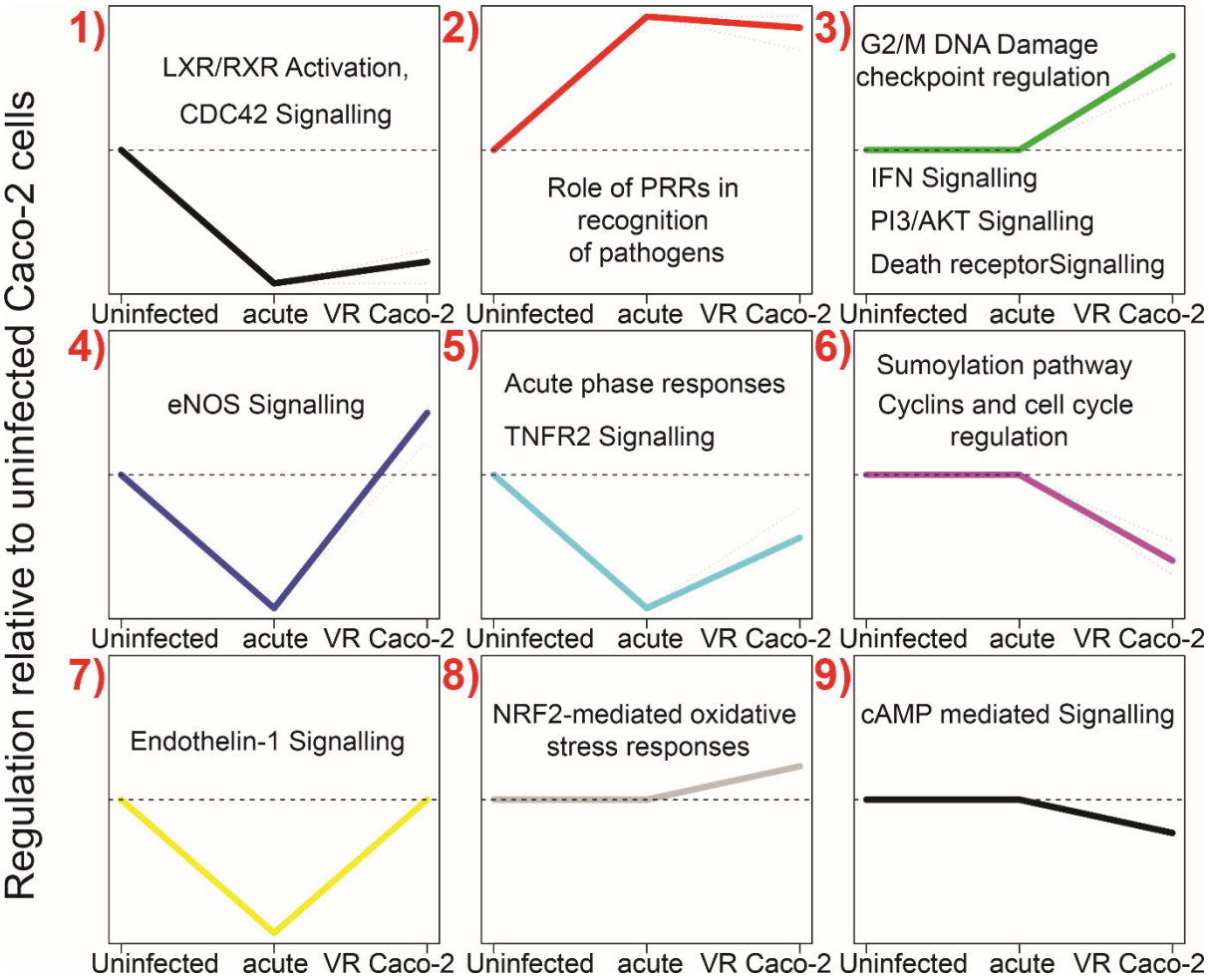

Figure 4.7. Clustering of the time profile of pathways from the Ingenuity Pathway Analysis (IPA). IPA analysis showed regulation of pathways in uninfected, acutely, and persistently NDV-infected Caco-2 cells. An example of metabolic processes for each cluster written in the respective cluster, where dotted line indicated the basal level of expression of collective processes in uninfected Caco-2 cells.

4.2.3. Comparative transcriptomics and proteomics data analysis

An integrated approach of transcriptomic and proteomic data analysis was used to detect relevant pathways and functions further. First, we examine the correlation between regulation of transcription and translation of host and viral genes in response to the persistent NDV infection in VR Caco-2 cells with the uninfected Caco-2 cells. After comparing LFCs quantile of most significantly differentially expressed genes and proteins with highly significant p values with FDR $p<10^{-12}$, the 359 candidates have shown a moderate correlation between transcription and translation processes in response to the persistent NDV infection in VR Caco-2 cells normalised with respect to the uninfected Caco-2 cells, as confirmed by Pearson correlation coefficient, $R^2=0.4658$ and illustrated by

distribution plot as shown in **Figure 4.8**. The expected reason behind moderate relationship in expressed proteins and genes could be explained by multiple factors controlling translation regardless of the mRNA abundance. NDV F and P proteins along with ISG15, L1CAM, KRT17, SP100 and RGCC proteins were significantly upregulated and proteins like ORM1, EPN3, APOA1, and PAGE4 downregulated with the strongest correlation with the mRNA transcripts.

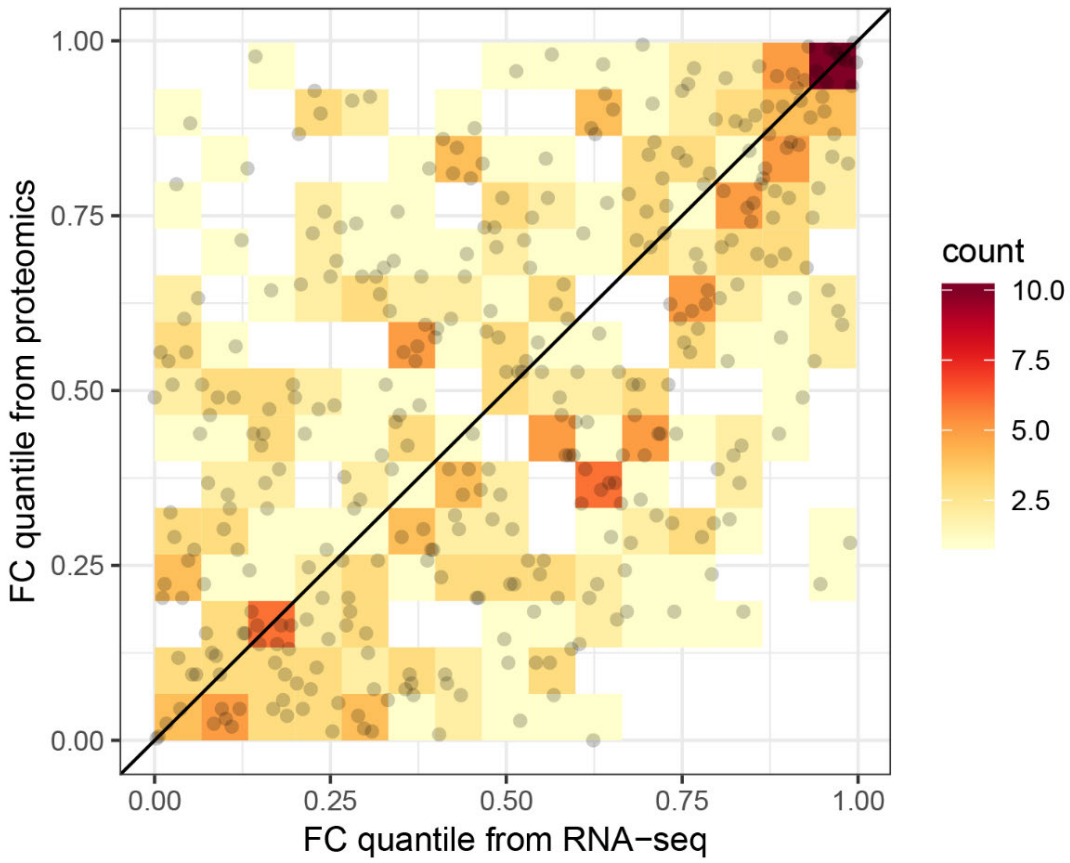

Figure 4.8. Quantile-quantile distribution of fold changes in mRNA abundance (RNA-seq) and protein abundance between VRCaco-2 and uninfected Caco-2 cells. Correlation analysis between the most significant differentially expressed genes and proteins in persistent NDV-infected VR Caco-2 cells relative to uninfected Caco-2 cells using only strongly differentially expressed genes (FDR (false discovery rate)<10^{-12}). (FC-fold change)

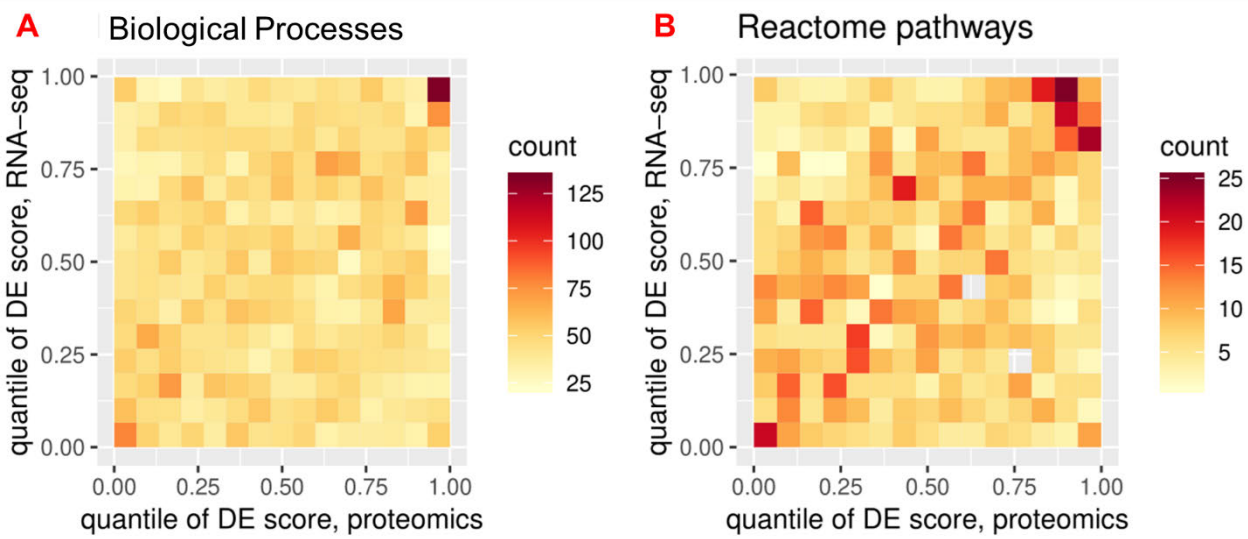

Figure 4.9. Comparison of pathways/GOs detected by proteomics and RNA-seq in persistently NDV-infection VR Caco-2 cells compared to the uninfected Caco-2 cells. Quantile-quantile distribution of differential expression (DE) scores for VRCaco-2 cells. DE scores are defined by -log10 (p-value) of Panther statistical enrichment analysis between VR Caco-2 and uninfected Caco-2 cells, multiplied by the sign of the difference the activation. Spearman correlations are 0.085 and 0.25, respectively.

The comparative analysis of significant DEGs and proteins expressed in VR Caco-2 compared to uninfected Caco-2 cells summarised in terms of GO biological processes and Reactome pathways demonstrated the weak relationship between proteomics and transcriptomics data, as illustrated in **Figure 4.9**. Analysis of Biological processes showed a strong correlation only in highly overexpressed pathways; otherwise, it is weak (r_s=0.085) in overall comparison, biological processes are summarised in **Table 4.7**. A total of 204 and 155 biological processes were highly upregulated and downregulated, respectively. The upregulated processes include antiviral responses such as responses to the virus, TNF-mediated signalling pathway, negative regulation of the virus life cycle, whereas downregulated processes included negative regulation of autophagy and acute inflammatory responses. However, Reactome analysis demonstrated slightly better correlations (r_s=0.25) in proteomics and RNA-seq data compared to the biological processes. Highly upregulated (139) and downregulated (32) Reactome pathways are summarised in **Table 4.8**; upregulated pathways include p53 independent DNA damage responses, p53 dependent G1/S DNA damage responses, regulation of apoptosis etc. and downregulated pathways include regulation of TLRs by endogenous ligands and Rho GTPase cycles.

Both GO biological processes, and Reactome pathways analysis demonstrated the regulation of functions/pathways in response to NDV to maintain virus replication below a

threshold and cell health by regulating pathways/functions controlling cell cycle and virus-induced damage in VR Caco-2 cells.

Table 4.7: Summary of Biological processes regulated in VR Caco-2 cells compared to Caco-2 cells from a relative to proteomics and transcriptomics data

Relative account of proteomics and transcriptomics data for Biological process in VR Caco-2 cells in comparison with Caco-2 cells	Numbers of process	Expression status	Examples of Biological process
	204	Highly upregulated	mRNA 3'-end processing (GO:0031124)
			Response to a virus (GO:0009615)
			Viral process (GO:0016032)
			IL-1-mediated signalling pathway (GO:0070498)
			Negative regulation of viral genome replication (GO:0045071)
			TNF-mediated signalling pathway (GO:0033209)
			Negative regulation of the viral life cycle (GO:1903901)
			Viral latency (GO:0019042)
			Mitochondrial transport (GO:0006839)
			Mitotic cell cycle phase (GO:0098763)
	155	Highly downregulated	An acute inflammatory response (GO:0002526)
			Negative regulation of autophagy (GO:0010507)
			Canonical Wnt signalling pathway (GO:0060070)
			Plasma membrane organization (GO:0007009)
			Regulation of Ras protein signal transduction (GO:0046578)
			Regulation of small GTPase mediated signal transduction (GO:0051056)
			Cell morphogenesis involved in differentiation (GO:0000904)
			regulation of cell communication (GO:0010646)

Table 4.8: Reactome pathway analysis of VR Caco-2 cells compared to Caco-2 cells from a relative to proteomics and transcriptomics data

Relative account of proteomics and transcriptomics data for Reactome pathways in VR Caco-2 cells in comparison with uninfected Caco-2 cells	Number of pathways	Expression status	Examples of Reactome pathways
	139	Highly upregulated	Mitotic Metaphase and Anaphase (R-HSA-2555396)
			Cell Cycle Checkpoints (R-HSA-69620)
			p53-Independent G1/S DNA damage checkpoint (R-HSA-69613)
			p53-Independent DNA Damage Response (R-HSA-69610)
			Infectious disease (R-HSA-5663205)
			p53-Dependent G1/S DNA damage checkpoint (R-HSA-69580)
			p53-Dependent G1 DNA Damage Response (R-HSA-69563)
			Regulation of Apoptosis (R-HSA-169911)
			NIK-->noncanonical NF-kB signalling (R-HSA-5676590)
			ER-Phagosome pathway (R-HSA-1236974)
			Influenza Infection (R-HSA-168254)

			Gene Silencing by RNA (R-HSA-211000)
			TNFR2 non-canonical NF-kB pathway (R-HSA-5668541)
			Glycolysis (R-HSA-70171)
			The citric acid (TCA) cycle and respiratory electron transport (R-HSA-1428517)
	32	Highly downregulated	Regulation of TLR by endogenous ligand (R-HSA-5686938)
			Rho GTPase cycle (R-HSA-194840)
			Plasma lipoprotein assembly (R-HSA-8963898)
			p130C as linkage to MAPK signalling for integrins (R-HSA-372708)
			GRB2: SOS provides linkage to MAPK signalling for Integrins (R-HSA-354194)

4.2.4. Comparative data analysis

4.2.4.1. NDV and Coxsackievirus infection in Caco-2 cells

The general effect of virus infection in Caco-2 cells was studied by comparing RNA-seq data from NDV infected, and Coxsackievirus B (CVB) infected Caco-2 cells.

Here RNA-seq data from Caco-2 cells grown in 2D or 3D cultures with or without CVB infection were used for two main reasons: First, CVB is a well-known oncolytic virus which has been studied by Drummond et al. (2016), where they established 3D Caco-2 cell model to replicate and study CVB infection efficiency due to lack of *in vivo* models to study enteroviruses such as CVB. Second, Caco-2 cells are heterogeneous when grown in 2D and 3D culture models using rotating wall vessel it mimicked properties of the intestinal epithelium, with apical-basolateral polarity, brush borders, the formation of well-developed tight junctions and multicellular complexity (249). The generated RNA-seq data demonstrated not only the CVB infection efficiency in the 3D model but also the impact of its oncolytic properties in Caco-2 cells. It also has demonstrated the complexity achieved by heterogenous Caco-2 cells. The comparison of Caco-2 in 2D/3D models with or without CVB infection with the Caco-2 cells with acute or persistent NDV infections have potentials to demonstrate similarities and dissimilarities not only in two different clonal populations of Caco-2 cells cultured differently but also the impact of two different oncolytic RNA viruses.

A) Comparison of NDV and CVB infection in Caco-2 cells

The RNA-seq data from Drummond et al. were analysed and compared with RNA-seq data from acutely NDV-infected Caco-2 cells and persistently infected VR Caco-2 cells. The LFCs quantile comparative analysis between CVB and NDV in Caco-2 cells demonstrated weak positive correlation (rs=0.28) between standard sets of genes upregulated,

downregulated, and unchanged in both virus infections in the Caco-2 cells, as shown in darker colours at the top-right and bottom-left in **Figure 4.10 A.** However, there are sets of genes explicitly regulated in response to each virus primarily. The mutual regulation of the cellular mechanism in response to virus demonstrated generic antiviral responses irrespective of its differential mechanisms of infection in Caco-2 cells. In contrast, LFCs are weakly correlated between VR Caco-2 cells and CVB-infected Caco-2 cells **(Figure 4.10 B)**. Notably, highly upregulated or downregulated genes are less consistently shared between persistent NDV-infection and acute CVB-infection in Caco-2 cells, and there is a large number of genes that are upregulated in one infection and downregulated in the other **(Figure 4.10 B).**

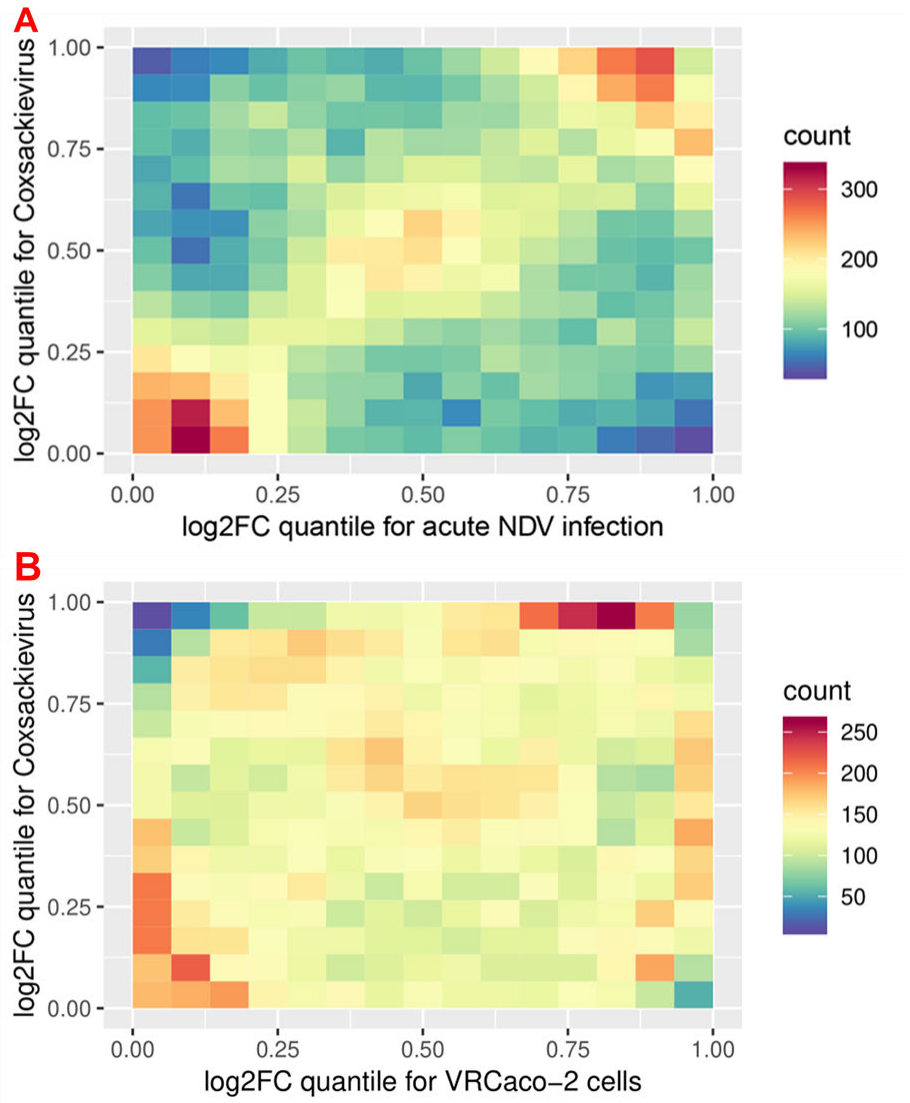

Figure 4.10. Quantile-quantile distribution of log2-fold changes between infected and uninfected Caco-2 cells. (A) Comparison between acute infections of NDV and Coxsackie virus in Caco-2 cells. **(B)** Comparison between acute Coxsackie virus in Caco-2 cells with persistent NDV-infection in VR Caco-2 cells

B) VR Caco-2 cells compared with Caco-2 cells grown in 2D and 3D culture models

Heatmap analysis of significant DEGs across all conditions of Caco-2 cells in **Figure 4.11 B** demonstrated that NDV acute and persistent infection and no infection in Caco-2 cells differ primarily from the CVB-infected and uninfected Caco-2 cells in 2D and 3D cultures. The drastic changes confirmed in NDV-infected Caco-2 and VR Caco-2 cells in a large number of gene clusters covering approximately ten thousand genes irrespective of acute and persistent infection with a significant difference than uninfected Caco-2 cells. However, CVB infection in 2D and 3D Caco-2 cell cultures showed comparatively fewer changes in gene cluster regulation **(Figure 4.11 B)**.

The similarity of Caco-2 cells grown in 2D and 3D cultures with or without CVB infection compared with the NDV-infected Caco-2, VR Caco-2, and uninfected Caco-2 cells was investigated by comparing log10RPKM values of gene expressions differing by a factor of more than 10 across all conditions. Correlation coefficients revealed a very weak but positive correlation of the expression of VR Caco-2 cells with the Caco-2 cells cultured in 3D **(Figure 4.11 A)**, whereas NDV-infected and uninfected Caco-2 cells resembled more the Caco-2 cells grown in 2D culture. The weaker correlation between 3D Caco-2 cells with VR Caco-2 cells also confirmed with the comparison analysis using LFCs and DEGs across both the conditions relative to the Caco-2 3D cells and uninfected Caco-2 cells respectively, as illustrated in **Figure 4.11 C**. The primary difference between Caco-2 cells in 2D and 3D cultures is intestinal cell differentiation with apical-basolateral polarity, brush borders, the formation of well-developed tight junctions and multicellular complexity. The weaker relationship can be explained by the expression of intestinal differentiation markers like *MUC 17, SLC10A1, MS4A10, Orm2, SLC38A4*, and *ALB* as shown in **Figure 4.5**.

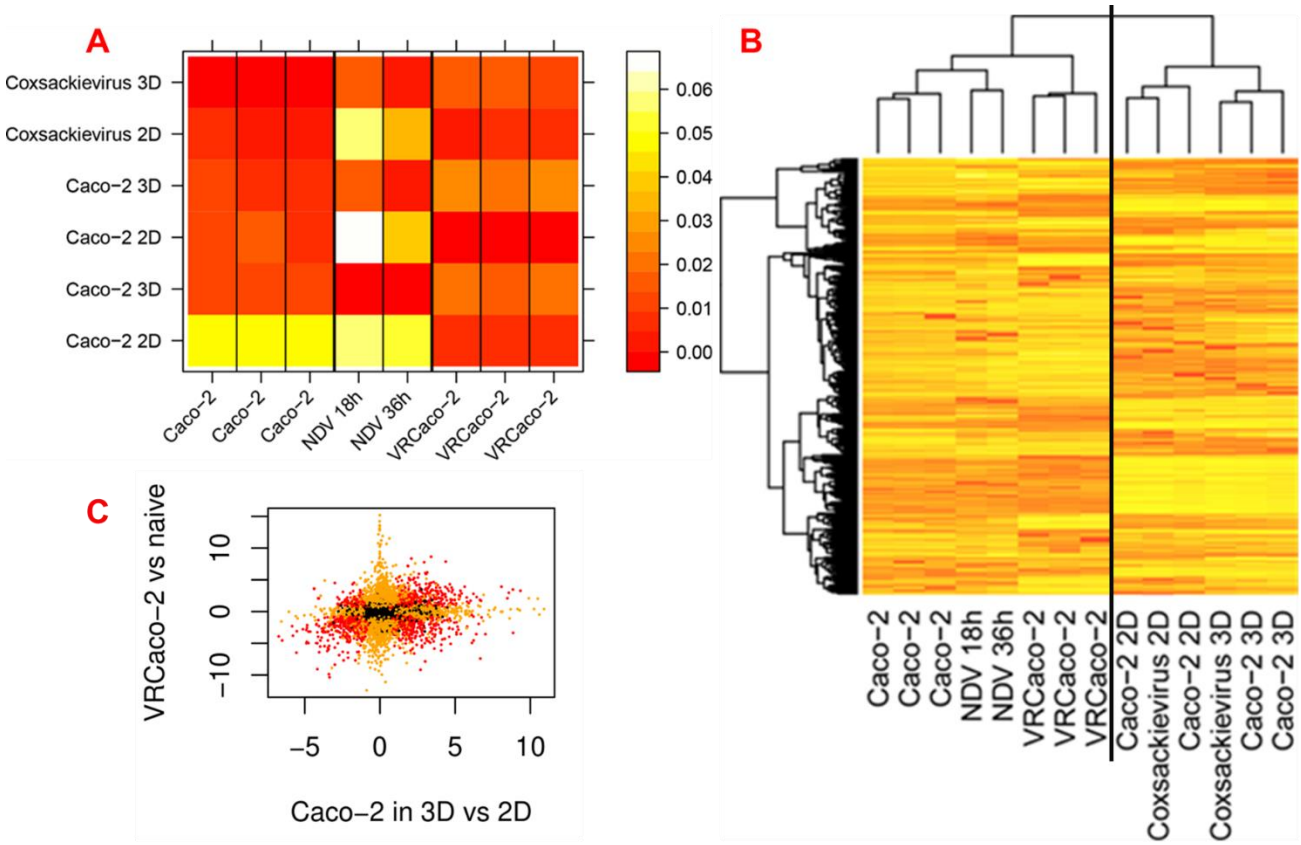

Figure 4.11. Comparative analysis of RNA-seq data from NDV-infected, persistently NDV-infected VR Caco-2 and uninfected Caco-2 cells with CVB-infected or uninfected Caco-2 cells grown in 2D and 3D cultures (Here genes only with values of RPKM variable more than a factor of 10 across conditions considered and values rescaled by the lowest correlation for each of uninfected and NDV-infected Caco-2 cells)**. (A)** Differential correlation analysis revealed a weaker relationship of VR Caco-2 cell culture with only Caco-2 cells grown in 3D culture confirmed by Pearson correlation between expression of normalised log10 (RPKM) values in individual samples of both datasets. **(B)** Heatmap of DEGs in log10 (RPKM) values across all the conditions of the Caco-2 cells culturing method with and without virus infection. **(C)** Scatter plot representing a comparison of apeGLM-shrinked log2-fold changes in Caco-2 cells in 2D/3D setup and persistent NDV-infection of VR Caco-2 cells compared to uninfected Caco-2 cells. Genes are shown in red (if differentially expressed in both comparisons, FDR<0.01) or orange (if differentially expressed in only one comparison).

4.2.4.2. NDV infection in Caco-2 and CEF cells

The impact of NDV infection in human cancer cells and also in chicken cells (chicken embryo fibroblast cells) was compared to understand how the NDV host-virus relationship depends on its host. RNA-seq data from Caco-2 cells acutely infected with NDV at MOI 0.1 for 18 and 36 h along with the persistently NDV-infected VR Caco-2 cells were compared with RNA-seq data from NDV-infected CEF cells at MOI 1 for 12 h studied by Liu et al. (2018) (248). A comparative analysis of the fraction of reads aligned to the NDV genome

relative to all host and viral reads demonstrated that 2% and 10% of reads are from NDV genes in 18 h and 36 h NDV-infected Caco-2 cells respectively, whereas in VR Caco-2 cells just 0.2% are viral reads, i.e. the number of viral transcripts in VR Caco-2 cells is 10-times and 50-times lower than in acutely NDV-infected Caco-2 cells at 18 h and 36 h, respectively. If we neglect potential differences in regulation of viral expression between cell types, the amount of viral transcript should be correlated with the number of infected cells. The NDV reads from infected CEF cells at MOI of 1 for 12 h are > 6%. Hence, it is confirmed that persistent NDV-infection in VR Caco-2 cells maintained at significantly lower levels of viral mRNA compared to the acutely NDV infected Caco-2 and CEF cells, as illustrated in **Figure 4.12 A**.

The distribution of LFCs of DEGs was analysed by DESeq2 using RNA-seq data in acutely NDV-infected Caco-2 cells was compared with NDV-infected CEF cells (chicken cells), persistently NDV-infected VR Caco-2 cells, CVB-infected Caco-2 cells by plotting violin plots **(Figure 4.12 B)**. Interestingly the distribution of all LFCs and DEGs in VR Caco-2 cells to other acutely infected cells corresponds to the broadest distribution across all comparisons, i.e. to the most significant expression LFCs, irrespective of 50-times lower viral reads to acute NDV infection. The comparison of the distribution of LFCs of DEGs in acutely NDV infected Caco-2 and CEF cells demonstrated that similar drastic changes are not achieved in CEF cells. Similarly, the width of the distribution is shrunk in CVB-infected Caco-2 cells, concluding that NDV infections have an enormous effect on the regulation of Caco-2 cells irrespective of the amount of virus found in acute and persistence state of NDV in Caco-2 and VR Caco-2 cells.

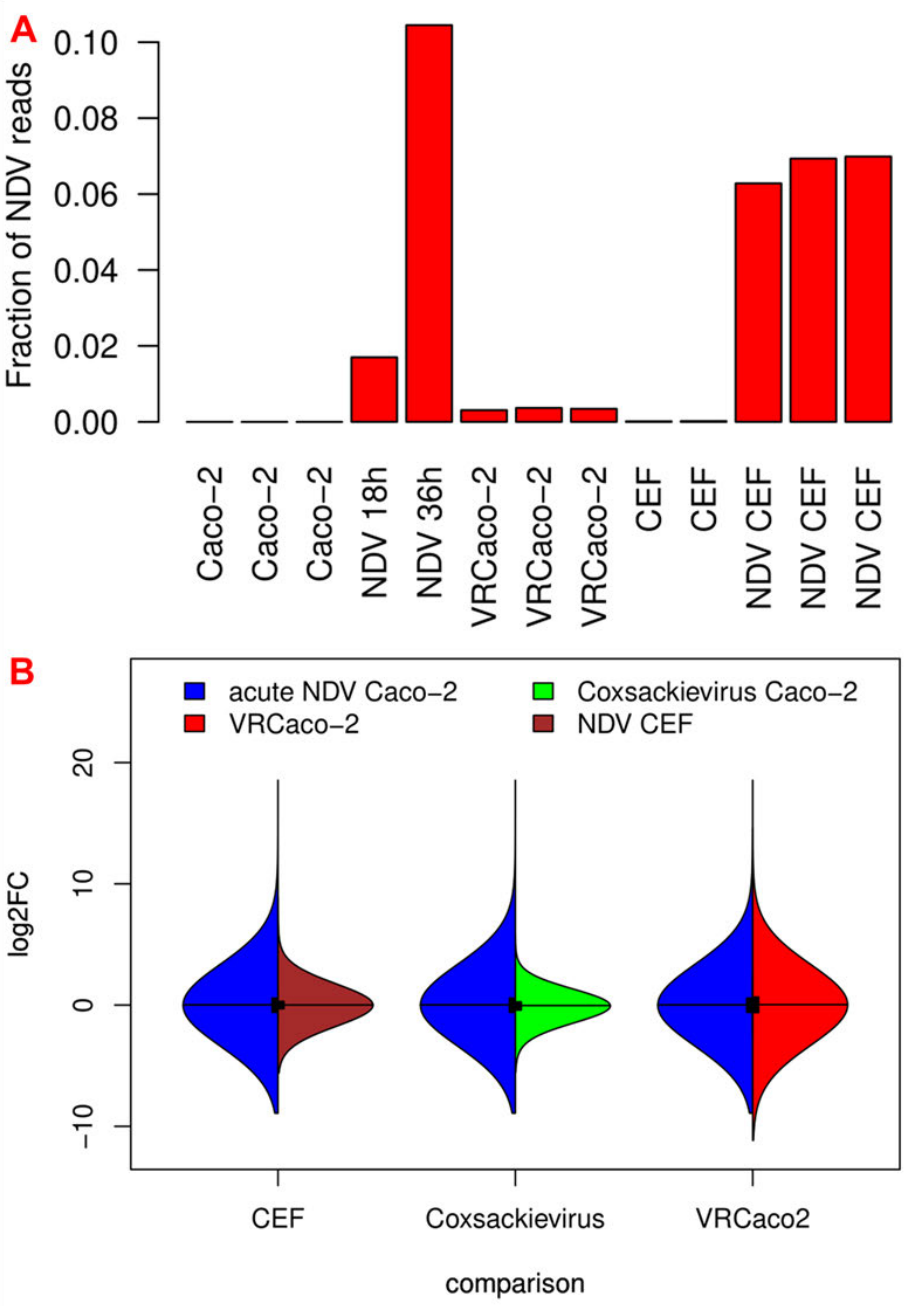

Figure 4.12. Comparative analysis of the effects of NDV infection in Caco-2, VR Caco-2, and CEF cells. (A) The relative amount of NDV reads in all NDV-infected cells where the fraction of NDV reads totalled to all aligned reads of each sample. **(B)** Violin plots demonstrating the full distributions of log2-fold changes of genes expression amongst virus-infected compared with respective uninfected cells. Fold changes were estimated from RNA-seq data using DESeq2. Acutely NDV-infected cells (Blue) comparison with NDV-infected CEF cells (Brown), CVB-infected Caco-2 cells (Green) and persistently NDV-infected VR Caco-2 cells (Red).

As a further confirmation of the significant differences in NDV-infected Caco-2 cells compared to NDV-infected CEF cells, we examined the trend of transcription of NDV genes using normalised log10 RPKM values of all viral genes in the Caco-2 cells in comparison with natural host cells **(Figure 4.13 A)**. A significant difference in the pattern of transcription

of NDV genes is observed in Caco-2 cells and CEF cells from 3 prime leader to 5 prime trailer genome orientation, whereas the trend of transcription of all viral genes is relatively similar in Caco-2 and VR Caco-2 cells irrespective of the number of transcripts. The amount of NP transcripts was most abundant as required for initiation of transcription process (as well as replication process), whereas P, M, F, and HN at transcripts were maintained relatively low abundance across all conditions in Caco-2 cells. The M and HN transcripts were slightly more abundant than NP, F, and L transcripts in the natural host (CEF cells) of NDV, with lower abundance of P transcripts. Surprisingly, the last gene at 5 prime end i.e. the large RNA polymerase L transcript, was kept at a significantly lower relative abundance in infected Caco-2 and VR Caco-2 cells compared to its higher abundance in chicken cells. The lower abundance of P transcripts to the NP and M transcripts could be partially explained by viral RNA polymerase mediated P mRNA editing to synthesise V (+G) and W (+GG) transcripts by adding non-template G residue/s at 484th nucleotide position of P transcript from 3' end, although the impact of co-transcriptional editing on mRNA level is unclear.

The proportion of P transcripts as well as the edited V and W transcripts were quantified in infected Caco-2, VR Caco-2 cells, and infected CEF cells, which demonstrated unusual proportion ratios in across conditions in all cells **(Figure 4.13 B)**. The P transcripts were significantly more abundant in CEF cells (**** $p < 0.0001$) than Caco-2 and VR Caco-2 cells, whereas V and especially W transcripts were significantly more abundant (**** $p < 0.0001$) in NDV-infected Caco-2 and VR Caco-2 cells than in CEF cells **(Figure 4.13 B)**. NDV-infected CEF cells showed a negligible level of W transcripts as well as a lower abundance of V transcripts. The W/V ratio is significantly lower in CEF cells compared to the NDV-infected Caco-2 and VR Caco-2 cells **(Figure 4.13 C)**. Accessory V protein plays an essential role in evasion of IFN system in chicken, and the function of W protein is unknown, but the higher abundance of V in IFN-defective Caco-2 cancer cells both in persistent and acute NDV infection is fascinating and possibly could have a role in oncolysis rather than infection in CEF cells.

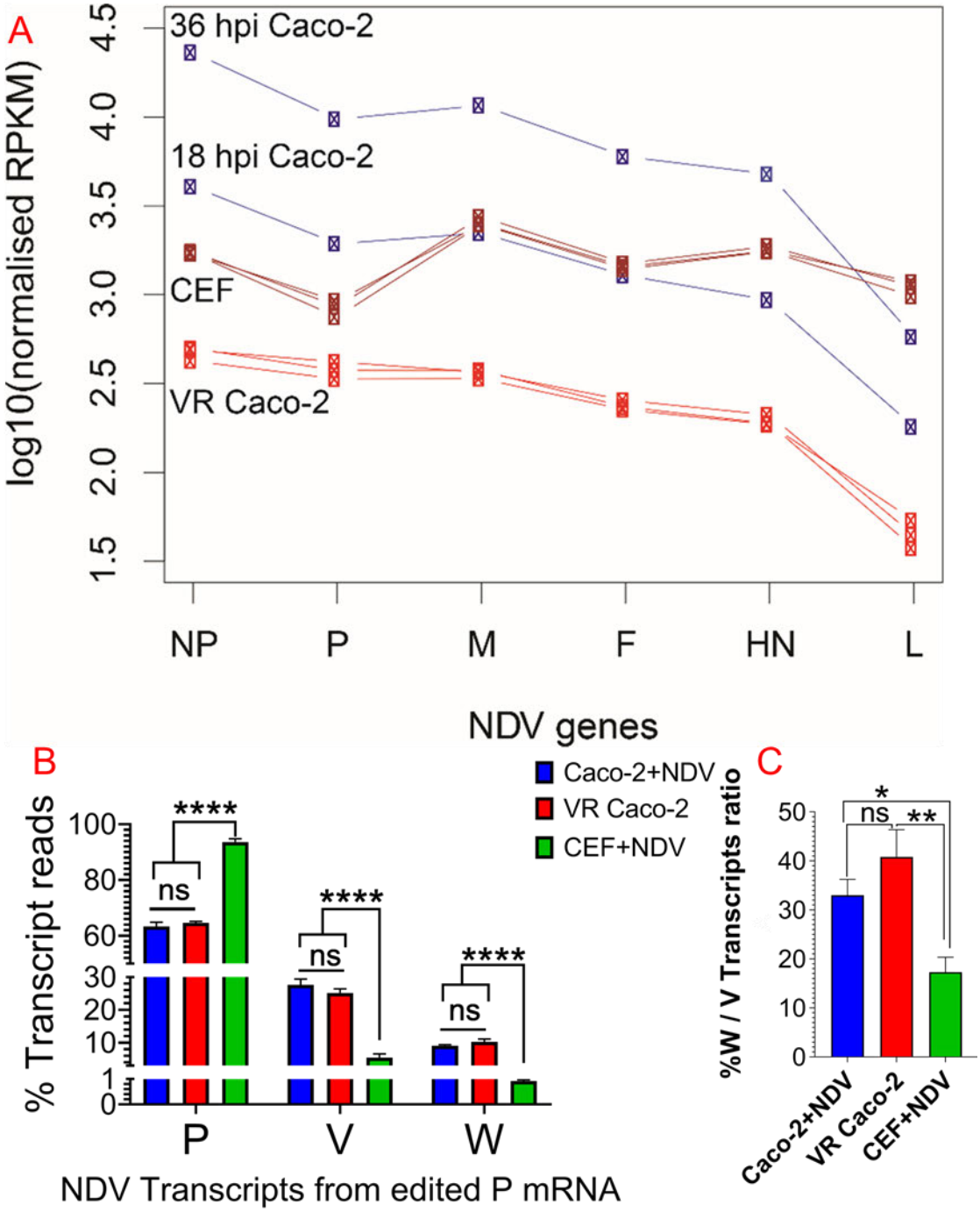

Figure 4.13. Expression analysis of NDV genes and P mRNA editing in infected Caco-2, VR Caco-2, and CEF cells. (A) The account of transcription trend of NDV genes in infected cells demonstrated by reading depth along the NDV genome, considered only reads/bases with mapping/base quality >30. **(B)** A comparative account of all transcripts from edited P mRNA in % transcripts reads, showing a significant difference in P/V/W mRNAs in CEF and Caco-2 cells. Data (mean ± SD) represented is analysed by Two-way ANOVA and Tukey's multiple comparisons test (**** p< 0.0001). **(C)** The % W/V ratio is significantly different between Caco-2, VR Caco-2 and CEF cells. Data (mean ± SD) represented is analysed by One-way ANOVA and Tukey's multiple comparisons test (*p< 0.023 and **p<0.0023).

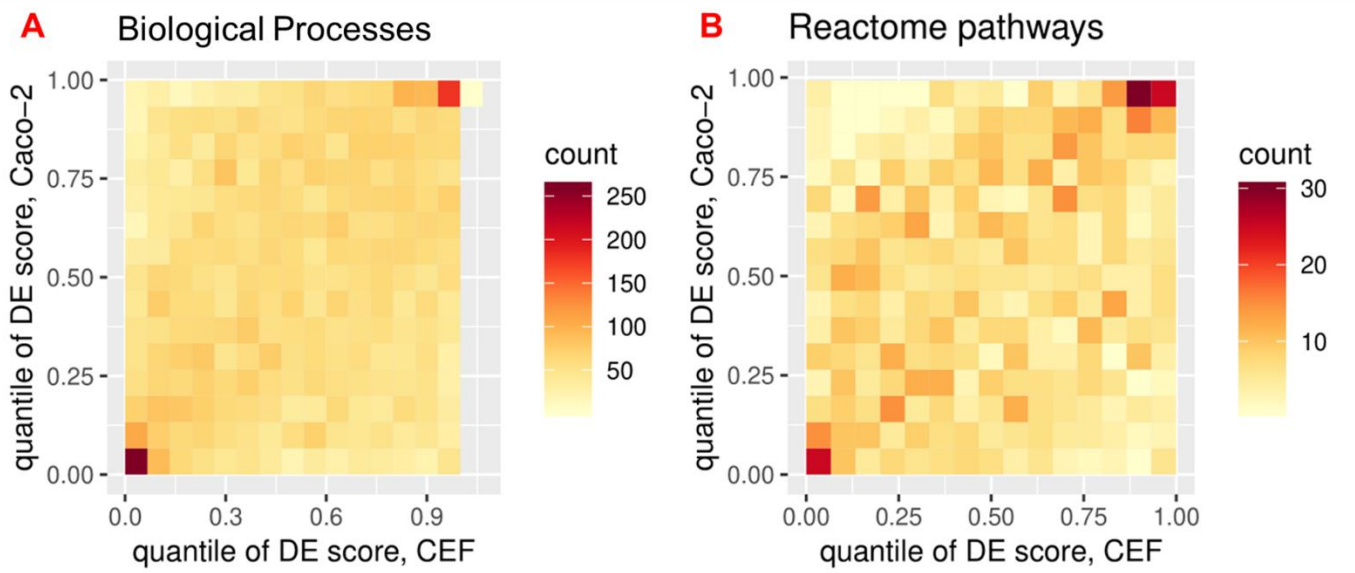

Figure 4.14. Assessment of acute NDV infection in Caco-2 and CEF cells. Quantile-quantile distribution of Differential Expression scores for Caco-2 compared with CEF cells. DE scores defined by -log10 (p-value) of PantherDB statistical enrichment analysis between acutely NDV infected and uninfected cells, multiplied by the sign of the difference of activation. Spearman correlations are (rs) 0.23 and 0.32, respectively.

The comparative analysis of significant DEGs expressed in NDV-infected Caco-2 and CEF cells summarised in terms of GO Biological processes, and Reactome pathways demonstrated that approximately the 5-10% more differentially over/under-expressed functions/ pathways tend to be shared across host species, but overall correlations are weak r_s=0.23 and r_s=0.32 respectively, as shown in **Figure 4.14**. All shared highly over/under-expressed Biological processes and Reactome pathways summarised in **Table 4.9** and **Table 4.10**. A comparison of total of highly upregulated (271) and downregulated (399) biological processes shared between infected CEF and Caco-2 cells. The upregulated biological processes include DNA repair process, DSBs repair via a nonhomologous end-joining mechanism, and dsRNA processing etc., whereas highly downregulated processes include regulation of the apoptotic process, regulation of cell population proliferation, and regulation of ERK1 and ERK2 cascades etc. We also considered a total of highly 50 upregulated and 44 downregulated Reactome pathways shared by infected CEF and Caco-2 cells. Highly upregulated pathways include p53-Dependent G1/S DNA damage checkpoints and cell cycle checkpoints, whereas downregulated pathways include regulation of TLR by endogenous ligand and Initial triggering of complement cascades.

Shared processes and pathways confirmed that some responses of CEF and Caco-2 cells are universal irrespective of the host species, such as activation of DNA repair pathways, responses against dsRNA, p53 dependent G1/S DNA damage checkpoint and deactivation of TLR regulation by endogenous ligands, complement responses, regulation of MAPK pathways indicating the involvement of universal machinery to combat the NDV infection.

Table 4.9: Biological processes commonly shared by NDV-infected Caco-2 and CEF cells

Relative account of shared Biological process in NDV-infected Caco-2 and CEF cells	Number of processes	Expression Status	Examples of Biological processes
	271	Highly upregulated	DNA repair (GO:0006281)
			DNA metabolic process (GO:0006259)
			Cell cycle G2/M phase transition (GO:0044839)
			Mitotic cell cycle checkpoint (GO:0007093
			Double-strand break repair via nonhomologous end-joining (GO:0006303)
			Viral process (GO:0016032)
			dsRNA processing (GO:0031050)
			Interleukin-2 secretion (GO:0070970)
			Interleukin-8 secretion (GO:0072606)
	399	Highly downregulated	Regulation of programmed cell death (GO:0043067)
			Negative regulation of interleukin-1 production (GO:0032692)
			Regulation of apoptotic process (GO:0042981)
			Regulation of cell population proliferation (GO:0042127)
			Positive regulation of MAPK cascade (GO:0043410)
			Regulation of ERK1 and ERK2 cascade (GO:0070372)
			Canonical Wnt signalling pathway (GO:0060070)

Table 4.10: Reactome pathways commonly shared by NDV-infected Caco-2 and CEF cells

A relative account of shared Reactome pathways in NDV-infected Caco-2 and CEF cells	Number of pathways	Expression Status	Examples of Reactome pathways
	50	Highly upregulated	Cell Cycle Checkpoints (R-HSA-69620)
			p53-Dependent G1/S DNA damage checkpoint (R-HSA-69580)
			p53-Dependent G1 DNA Damage Response (R-HSA-69563)
			Regulation of RAS by GAPs (R-HSA-5658442)
			Nucleotide Excision Repair (R-HSA-5696398)
			Rho GTPases Activate Formins (R-HSA-5663220)
	44	Highly downregulated	Complement cascade (R-HSA-166658)
			EGFR interacts with phospholipase C-gamma (R-HSA-212718)
			Regulation of TLR by endogenous ligand (R-HSA-5686938)
			Initial triggering of complement (R-HSA-166663)

4.3. Discussion

The objective of this chapter was to analyse the effects of acute NDV infection and persistent NDV-infection on gene expression profiles in Caco-2 and VR Caco-2 cells, respectively. Caco-2 cells are confirmed a useful model system to study oncolytic properties of NDV, where avirulent strains induced significant oncolysis in a dose-dependent manner. Despite high levels of oncolysis caused by NDV in Caco-2 cells, NDV managed to establish persistent infection in Caco-2 cells. Earlier shown that persistent NDV-infection of VR Caco-2 cells resulted in dramatic changes where VR Caco-2 cells acquired slower cell proliferation, produced replicating virus, NDV-specific resistance to NDV re-infection while maintaining susceptibility to avian influenza and VSV virus. The analysis of gene expression profile has identified the number of changes and potential pathways/functions affected by acute and persistent NDV infection in Caco-2 and VR Caco-2 cells.

Very little information is available on genome-wide gene expression profile in NDV-infected cells, and most of them were conducted using cDNA microarray. Munir et al. (2006) have studied gene expression profile using a 2950 element of chicken cDNA microarray chip in a velogenic Texas GB strain of NDV infected CEF cells and found 22 genes upregulated and 33 genes downregulated (250). Krishnamurthy et al. (2006) have studied genome-wide cDNA microarray in NDV-infected HT-1080 human fibrosarcoma cells and CCD-1122Sk normal human skin fibroblasts, where 399 genes were differentially regulated (104). Balogh et al. (2104) have studied genome-wide transcriptome in more detail in MTH-68/H-infected rat PC12 pheochromocytoma cells using the Affymetrix exon chip and found 729 genes upregulated and 612 genes downregulated in PC12 cells (251). However, Liu et al. (2018) utilised RNA-seq based approach in highly virulent NDV Herts/33 strain and the avirulent LaSota strain infected CEF cells and found 7603 (Herts/33) and 4105 (LaSota) transcripts differentially expressed in response to NDV infection out of which 3259 (Herts/33) and 1890 (LaSota) transcripts were related to interferon-stimulated genes (ISGs) (248).

B1 avirulent strain of NDV upon acute infection in Caco-2 cells demonstrated that 7160 genes differentially expressed and persistent infection in VR Caco-2 cells expressed 11012 genes compared to the uninfected Caco-2 cells whereas 10039 genes were differentially expressed in persistently infected VR Caco-2 cells compared to the acutely NDV-infected Caco-2 cells. The persistent NDV-infection in VR Caco-2 cells induced enormous changes while maintaining lower viral reads compared to the acute infection. VR Caco-2 cells were found to have a weaker positive correlation with Caco-2 cells grown in 3D culture by Drummond et al. (248), where key difference between Caco-2 cells in 2D and 3D cultures

was an intestinal cell differentiation to the intestinal epithelium, with apical-basolateral polarity, brush borders, the formation of well-developed tight junctions and multicellular complexity. VR Caco-2 cells have shown overexpression of *MUC 17* and underexpression of *SLC10A1*, *MS4A10*, *Orm2*, *SLC38A4*, and *ALB* intestinal markers in RNA-seq analysis similar to the Caco-2 cells grown in 3D culture (248). The weaker correlation of VR Caco-2 cells with 3D Caco-2 cells has demonstrated that NDV persistent NDV infection-induced changes resulted in higher complexity of heterogenous Caco-2 cells. A hierarchical clustering approach of DEGs, Gene Ontology and pathway overrepresentation analysis, and Ingenuity Pathway Analysis have confirmed the upregulation of antiviral responses associated with ISGs in VR Caco-2 cells compared to uninfected and acutely NDV-infected Caco-2cells: involved DEGs such as *IL15, OASL, IFIT1, C3, CASP1, DDX60* etc., and pathways included IFN-signalling, cytokine regulation and TLR activation by endogenous ligands.

Ryan et al. (2016) have reported that RNA viruses such as Hepatitis C virus (HCV), Influenza A virus (IAV), and retroviruses HIV-1 activate DNA damage response (DDR) pathways by inducible nitrous oxide synthase (iNOS) and augmented release of ROS (138). The build-up of iNOS and ROS are known to induce double-stranded breaks (DSBs) in the infected cell DNA and activation of genetic abnormalities due to non-homologous end joining (NHEJ) repair involvement and trigger apoptosis, instigation of inflammatory responses, and promotion of genomic instability leading to the increased risk of tumourigenesis (138). Similar effects have been confirmed by Saeed et al. (2019), where they have analysed cellular DNA content in highly pathogenic NDV AF2240 strain infected GBM cells and reported the loss in DNA in treated cells in G1, S and G2/M phases of the cell cycle (140). The disruption of the cell cycle was reported to induce apoptotic cell death as indicated by typical features such as morphologic changes of apoptosis, including shrinkage and blebbing of the membrane (140). Here the integrated analysis of VR Caco-2 cells in comparison with the uninfected Caco-2 cells using proteomics and RNA-seq data have shown activation of p53-Independent G1/S DNA damage checkpoint, p53-Dependent G1 DNA damage response, and regulation of apoptosis. A similar trend has been observed from the analysis of RNA-seq data in acutely NDV-infected Caco-2 and CEF cells indicating that NDV does activate DDR pathways irrespective of the host cell upon infection. Ultra-microscopic observations in NDV infected Caco-2 and VR Caco-2 cells would validate the role of NDV in DNA damage alongwith identifying the triggers for NDV-induced cell death.

Interestingly NDV has shown significantly different transcription trend of all genes in the Caco-2 and CEF cells, and the P mRNA editing also found significantly different in both the cells. The amount of V and especially W transcripts compared to the P transcripts were

found substantially higher in Caco-2 and VR Caco-2 cells compared to the CEF cells. Mebatsion et al. (2001) reported that 68% P-encoding mRNA, 29% V-encoding mRNA, and 2% W-encoding mRNAs were produced from the P gene in NDV-infected chicken cells (91). In contrast to that approximately 65% P, 25% V, and 10% W transcripts were found in NDV-infected Caco-2 and VR Caco-2 cells, whereas 94% P, 6% V, and 1% W transcripts in NDV-infected CEF cells. The NDV P protein plays a vital role in viral RNA synthesis by forming the RNP complex where P protein binds to NP and L proteins (81). The edited V and W mRNA encode accessory proteins, V protein has IFN antagonistic properties, and W protein expression and its function is unclear in NDV (81). Recently, Karsunke et al. (2019) have reported the expression of W protein in QM9 cells (quail muscle cells clone 9) transfected plasmids coding for NDV Cl30 W (252). Karsunke et al. also reported a nuclear accumulation of W protein nuclear localisation sequence (NLS) within its unique C-terminal end revealed by confocal microscopic analyses of infected cells (252). In this study, proteomic data analysis showed approximately 4-times log2 fold change in W protein expression in VR Caco-2 cells compared with uninfected Caco-2 cells (demonstrated in appendix). So, in future nuclear accumulation and localisation of W protein in VR Caco-2 and infected Caco-2 cells can be studied. The persistent infections caused by paramyxoviruses is common *in vitro* and *in vivo* cultures; however, the molecular mechanism is unknown. Recently Young et al. (2019) have reported the single mutation in one of the phosphorylation sites of P protein drive the switch between lytic to persistent infection of parainfluenza virus type 5 (PIV5) in A549 cells (253). Qui X et al. (2016) have identified the phosphorylation sites in NDV-P protein which are T44, S48, T271, S373 and T111 (254). The sequence analysis of NDV P mRNA transcripts from acutely NDV-infected and persistently NDV-infected VR Caco-2 cells have not reported any mutations/amino acid changes in the reported phosphorylation site; however, there are few other mutations in the P protein which can be investigated further to find out its role in the NDV replication as well as the P mRNA editing.

Defective viral genomes (DVGs) of several RNA viruses such as RSV, human metapneumovirus, Zika, chikungunya, and Ebola are known to persist infections *in vitro* and *in vivo* cultures (255). Timm et al. (2014) have identified and characterised the DVGs produced by vesicular stomatitis virus (VSV) cultured in BHK host cells by deep sequencing and validated by quantitative reverse transcription-PCR (256). Murra et al. (2017) have characterised DVGs produced by recombinant measles virus in infected human cells and found that non-encapsidated 5 prime copy-back DVGs (DVGs template where RNA template and polymerase attachment site is closer to 5 prime end (257)) were recognised by TLRs such as RIG-I and LGP2 which play a role in antiviral responses (244). Not much

is known about the DVGs produced by NDV unlike other paramyxoviruses such as Sendai virus, measles virus etc. DVGs have shown to play a role in antiviral responses as well as persistent infections in host cells (255). Using deep sequencing approaches, DVGs produced by NDV in human cancer cells, and CEF cells could be identified and characterised in the future to find out the role of DVGs in the elevated antiviral status of persistently infected VR Caco-2 cells by NDV infection.

Overall, A total of 10039 genes were significantly differentially expressed in persistently NDV-infected VR Caco-2 cells compared to acute NDV-infection in Caco-2 cells resulted in profound changes in VR Caco-2 cells, which suggest a complex process of transformation from Caco-2 to VR Caco-2 cells and that hindered our ability to pinpoint specific mechanisms acquired to define NDV-specific resistance. The heterogeneous nature of Caco-2 cells also must have a potential role in the establishment of persistent infection. Recently, Russell et al. (2019) have shown that single-cell sequencing approach in influenza-infected A549 cells to understand the impact of genetic variation of the virus population on antiviral responses (258). Single-cell sequencing and epigenomics could be applied in future to assess the effects of heterogeneity of Caco-2 cells and virus population of NDV in acutely infected and persistently infected VR Caco-2 cells.

Chapter 5

5 Newcastle disease virus (NDV)-mediated p62/SQSTM1 degradation

5.1. Introduction

Autophagy is a highly regulated self-destruction process mediated through lysosomal clearance of cellular organelles and cytoplasmic components to maintain the homeostasis by recycling mechanism inside the cell (259). Autophagy in cells can be induced by multiple factors including metabolic stress like growth factors or nutrient deprivation, hypoxia, reactive oxygen species (ROS), DNA damage, misfolded protein aggregates, damaged organelles, and pathogen invasion. The autophagic process initiates with membrane isolation by *de novo* synthesis known as phagophore formation. Phagophore sequesters damaged cellular components by invagination to form the double-membraned vesicle known as an autophagosome. The autophagosome then fuses with multivesicular endosomes to create an acidified mature autophagosome by the activation of endosomal proton pumps. Later, as the lysosome gets docked and merged with the matured autophagosome to become an autophagolysosome, where damaged organelles are degraded by lysosomal enzymes (260). The general scheme of the autophagic process is illustrated in **Figure 5.1**.

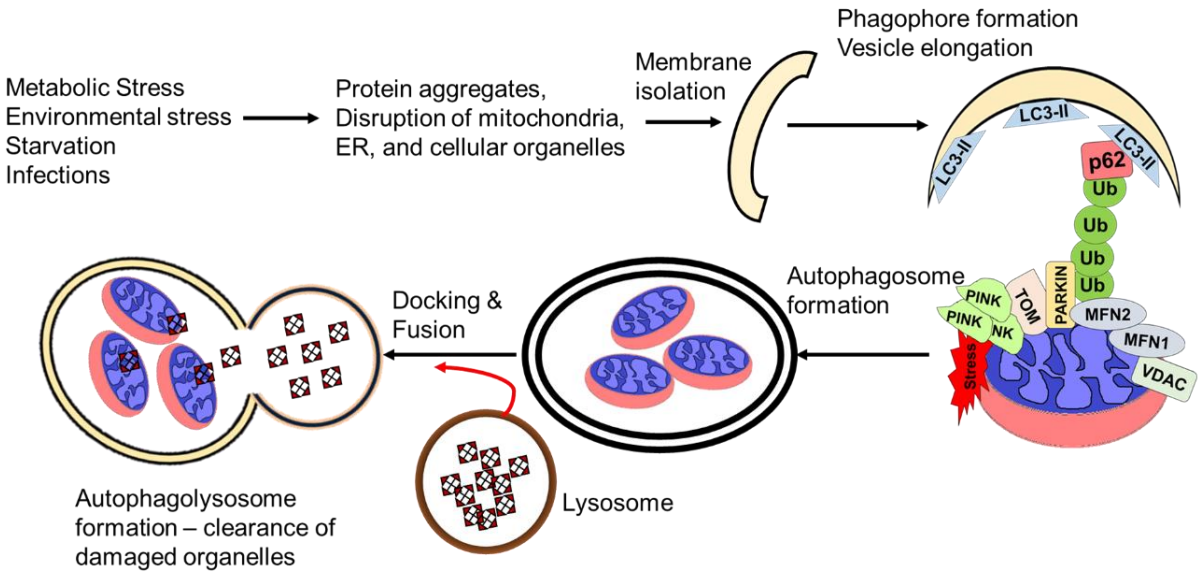

Figure 5.1. Schematic representation of the autophagic process, adapted from White et al., 2015 (261). Various types of stress induce the autophagic process within cell initiated by membrane isolation for phagophore formation, invagination to sequester damaged protein aggregates and cellular organelles by vesicle elongation to form autophagosome. Lysosome fuses with autophagosome to clear cargo by autophagolysosome formation.

Autophagy is an evolutionarily conserved cardinal process for normal cellular homeostasis where non-selective bulk degradation of damaged cytoplasmic components occurs, but selective elimination of undesirable elements such as dysfunctional organelles, abnormal proteins and lipid aggregates as well as invading pathogens is achieved by selective autophagy (262). Several types of selectve autophagy are known based on selective removal of damaged cellular organelle such as mitophagy (mitochondria), ER-phagy (endoplasmic reticulum), pexophagy (peroxisomes), and aggrephagy where protein aggregates are removed mediadted by ribosomes (263). Mitochondria are important organelles in the cell where that function in a variety of bioenergetic, metabolic, and developmental processes, so cells trigger numerous quality control mechanisms to maintain the functional integrity of mitochondria. Hence, clearance of damaged mitochondria through mitophagy is cardinal process in stressed cells to maintain cellular homeostasis.

Autophagic adaptors like p62/ SQSTM1 (sequestosome 1) and NBR1 (neighbour of Brca1 gene) are key regulators involved in the binding of ubiquitinated substrates (damaged cytoplasmic components) to microtubule-associated protein 1 light chain 3 (LC3) and gamma-aminobutyrate receptor-associated protein (GABARAP) receptors leading to degradation in selective autophagy (264).

Meng et al. reported mesogenic strain Beaudette C of NDV at MOI 10 triggered autophagy in human glioma U251 cells to enhance virus replication (141). Cheng et al. (2016), demonstrated NDV NP and P proteins induced autophagy in A549 human lung cancer cells mediated through endoplasmic reticulum (ER) stress-related unfolded protein response (UPR) pathways. Degradation of p62/SQSTM1 was confirmed in NDV NP, and P protein transfected A549 cells (265). Kang et al. also reported the degradation of p62/SQSTM1 and conversion of LC3-I to LC3-II in NDV-infected chicken embryo fibroblast (CEF) cells. They also demonstrated that inhibition of apoptosis resulted in enhanced autophagy, increased cell survival, and viral replication (266).

Human p62/ SQSTM1 is a multidomain and multifunctional protein encoded by the *sqstm1* gene located on chromosome 5 comprising eight exons including 16 kb long DNA sequence. The p62/SQSTM1 has five structural domains (PB1, ZZ, TB, LIR, and UBA) utilised in interactions with molecules involved in autophagy and signalling pathways **(Figure 5.2A)**. The PB1 is an oligomerisation domain at N-terminal end made up of Phox and Bpem1 (PB1) elements responsible for the homodimerisation of p62 or heterodimerisation with NBR1, atypical protein kinase C (aPKC), and extracellular signal-

regulated kinase (ERK). Next two are signalling domains consists of ZZ-type zinc finger (ZZ), and tumour necrosis-associated factor 6 (TRAF6)-binding site (TBS) domains responsible for the interactions with receptor-interacting serine/threonine-protein kinase 1 (RIP1), TRAF6, and interaction with mTOR raptor which plays an essential role in nutrient sensing for mTORC1 pathway (267). Autophagy domain consists of LC3 interacting region (LIR) and ubiquitin-associated (UBA) proteasomal activity domain at C-terminal end (268). The mechanism of SQSTM1-mediated balance between cell survival and apoptotic cell death is explained in **Figure 5.2B**.

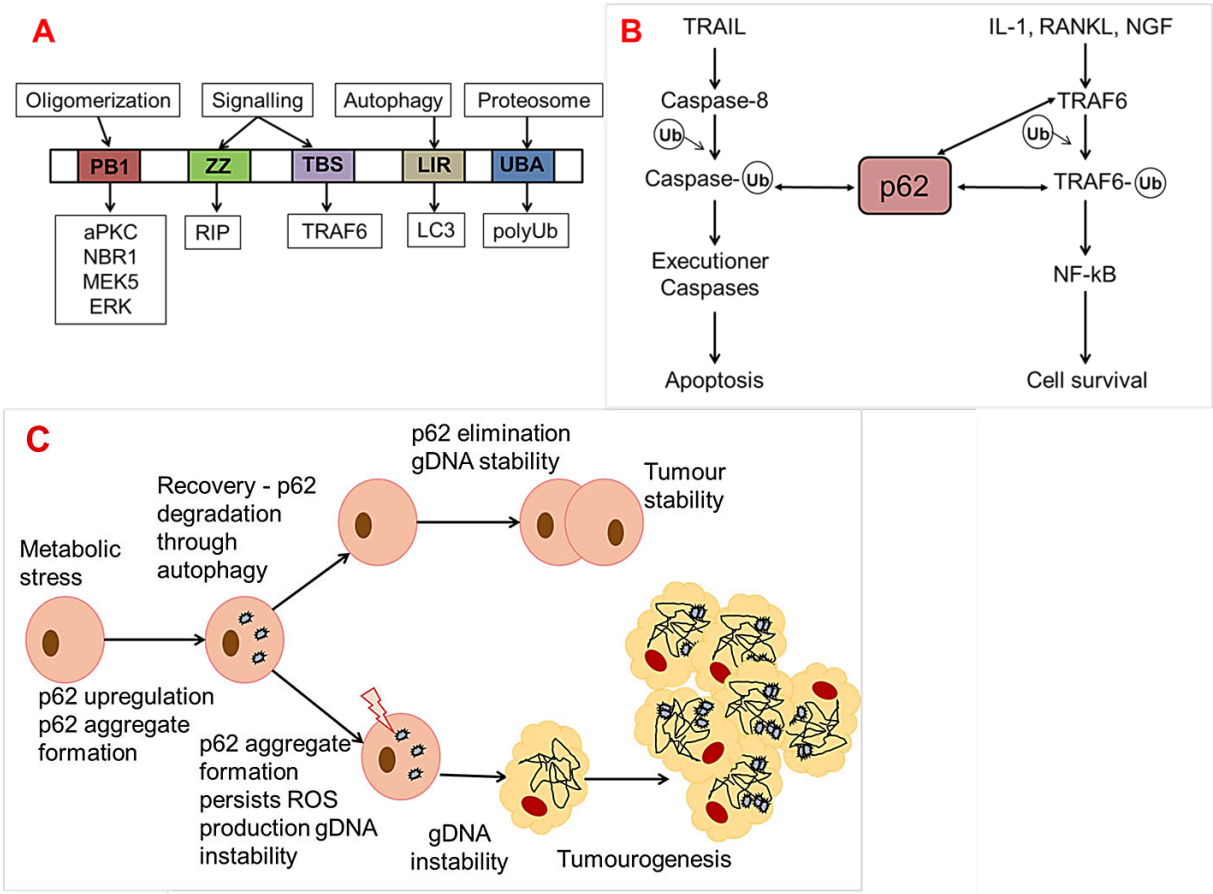

Figure 5.2. Cellular mechanisms of p62/SQSTM1 adapted from Moscat et al. 2009 (268).

(A) SQSTM1 structural domains and interacting partners. P62/SQSTM1 consists of five different interacting domains include; the oligomerisation domain at N-terminal Phox and Bpem1 (PB1) regulates self-oligomerisation of p62 as well as interacts with a p62 homologue protein NBR1, atypical PKC (aPKC) or ERK1. Next consists of two signalling domains ZZ-type zinc finger (ZZ) and TRAF6-binding site (TBS) domains bind with RIP1 and TRAF6 to regulate NF-KBpathway. Then followed by autophagy domain comprises LC3 interacting region (LIR) and last ubiquitin-associated (UBA) domain at C-terminal controlling proteasomal activity.

(B) Role of p62/SQSTM1 speckles in maintaining cellular homeostasis to balance cell survival and cell death. The particles of p62 promote oligomerisation of caspase-8 and TRAF6 regulating apoptotic cell death or NF-kB pathway-mediated cell survival.

(C) p62/SQSTM1 accumulation results in tumorigenesis. In autophagy-deficient cancer cells, metabolic stress triggers increased p62 aggregates, and damaged mitochondria activating reactive oxygen species (ROS) formation leading to the genomic DNA instability and tumorigenesis.

Cell stimulator downstream of transcription factor NF-kB such as interleukin-1 (IL-1), receptor activator of nuclear factor kappa-B ligand (RANKL), or nerve growth factor (NGF) promote interaction of the PB1 domain of p62 with aPKC. Self-oligomerised p62, p62-aPKC heterodimer, and ubiquitinated p62 bound protein aggregates bind with TRAF6 and caspase-8. TRAF6 is a lysine 63 (K63) E3 ubiquitin ligase that activates self-polyubiquitination, which activates the NF-kB pathway leading to the cell survival, whereas death receptors DR4 and DR5 activate TNF-related apoptosis-inducing ligand (TRAIL) promoting cullin-3 (E3) ubiquitin ligase mediated caspase-8 ubiquitination which interacts with the UBA domain of p62 and activates executioner caspases leading to apoptotic cell death **(Figure 5.2B)** (268).

Allelic exclusion of autophagy regulator beclin-1 results in autophagy deficiency in most cancer cells. Where, metabolic stress in autophagy-defective cancer cells promotes the accumulations of p62/SQSTM1 speckles, ROS, damaged organelles, and genomic DNA instability. Disruption in genomic DNA in autophagy-defective tumour cells leads to extensive tumorogenesis. Mathew et al. (269) demonstrated that p62 elimination resulted in the suppression of p62-mediated tumorigenesis, as illustrated in **Figure 5.2C**.

The role of p62 as a signalling pivot through its multidomain to control the balance of cell death and cell survival in cells and the accumulation of p62 speckles in autophagy-defective cancer cells leading to tumorigenesis, makes p62 as attractive candidate to study in virus-infected cancer cells to underpin the mechanisms involved in virus-induced cell death. Already, a group of researchers (141, 266) have confirmed NDV-mediated autophagy in various cells benefiting the virus replication by promoting cell survival. Here in this chapter, based on others findings, the status and role of p62/SQSTM1 were investigated primarily using indirect immunofluorescence (IF) and western blot analysis to confirm that NDV induces autophagic cell death in Caco-2 cells.

5.1.1. Chapter objectives

- Establish NDV-induced mitophagy in Caco-2 cells using a mito-mRFP-EGFP dual reporter plasmid
- Confirm NDV-induced p62/SQSTM1 degradation in Caco-2 cells
- Time-course study to detect p62/SQSTM1 degradation
- Investigate individual NDV protein role in p62/SQSTM1 degradation in Caco-2 cells
- CRISPR/Cas9-mediated p62/SQSTM1 knockout (KO) in Caco-2 cells to investigate the role of NDV-induced autophagy in Caco-2 cells.

5.2. Results

5.2.1. Confirmation of mitophagy in Caco-2 cells

A sensitive dual reporter vector mito-mRFP-EGFP expressed in-frame red fluorescent protein (RFP) and enhanced green fluorescent protein (EGFP) regulated by mitochondrial COX VIII promoter in transfected Caco-2 cells **(section 2.2.1.2)**. The principle of pH-based stability of fluorescent proteins is used to detect the induction of mitophagy in stressed Caco-2 cells. EGFP is a pH-sensitive fluorescent protein, which degrades in acidic pH, whereas RFP has better resistance in an acidic environment (270). When mito-mRFP-EGFP vector-transfected Caco-2 cells were stressed either with mitophagy inducer chemical CCCP (carbonyl cyanide m-chlorophenyl hydrazone) treated for 6 h or NDV Ulster 2C-infection for 18 h, demonstrated reduced numbers of EGFP puncta relative to the RFP puncta in stressed Caco-2 cells. **Figure 5.3** shown the detection of NDV-induced mitophagy in mito-mRFP-EGFP vector-transfected Caco-2 cells using the confocal microscope. Under no stress, transfected Caco-2 cells showed in-frame mitochondrial expression of RFP and EGFP proteins that created the bright yellow overlapping pattern of mitochondrial expression throughout the cell cytoplasm. However, NDV infection and CCCP treatment disrupted mitochondrial membrane potential and the induction of mitophagy, indicated by reduced EGFP puncta in stressed cells due to drop in pH because of fusion of lysosome with the autophagosome to form autophagolysosome. In the autophagolysosome, lysosomal enzymes degrade damaged mitochondria confirmed NDV-induced mitophagy in Caco-2 cells.

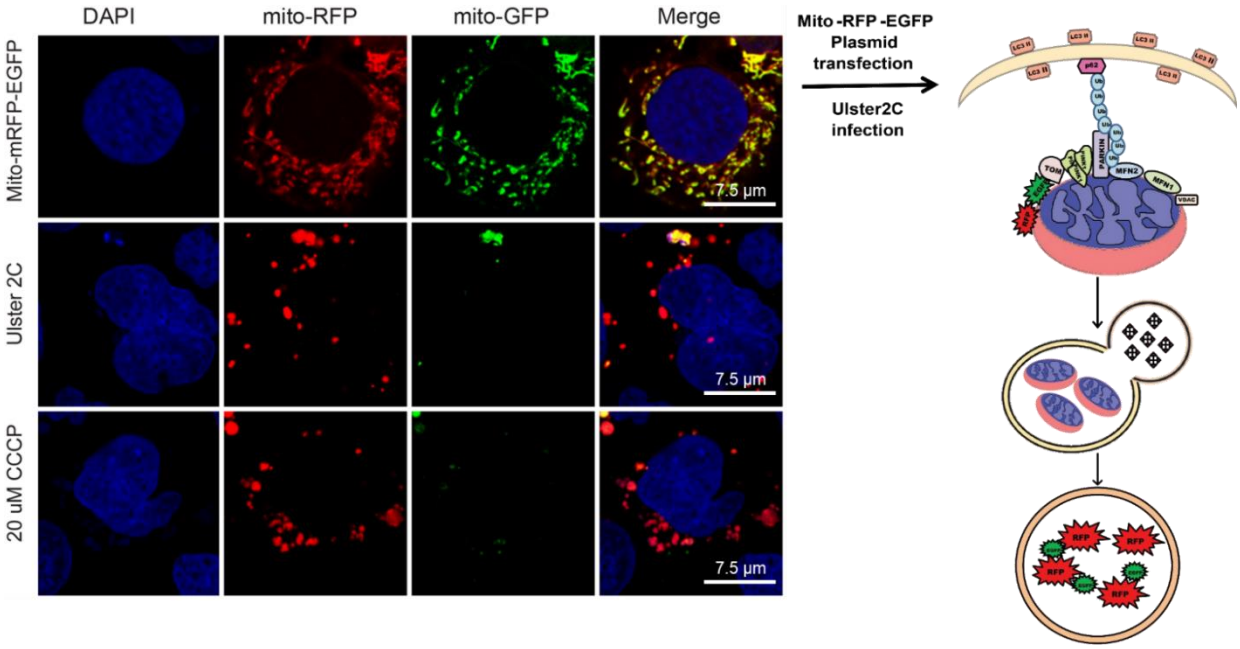

Figure 5.3. Confirmation of NDV-induced mitophagy in Caco-2 cells. A sensitive dual fluorescence reporter mito-mRFP-EGFP vector-transfected Caco-2 cells upon infection with Ulster 2C for 18 h and 20 µM CCCP treated for 6 h positive control demonstrated reduced green puncta formation as a result of reduced pH due to autophagolysosome formation. Mitochondrial COX VIII promoter drove expression of RFP (shown in red) and EGFP (shown in green), cell nuclei stained with DAPI (scalebar 7.5 µm, n=3).

5.2.2. p62/SQSTM1 degradation study using the IF assay

Once NDV-induced mitophagy was confirmed in Caco-2 cells, the status of p62/SQSTM1 protein with or without NDV infection was investigated in Caco-2 cells. It has been demonstrated that the cancer cells attain autophagy-deficient status due to allelic exclusion of autophagy regulator beclin 1, where metabolic stress in autophagy-deficient cancer cells activates accumulations of p62/SQSTM1 aggregates, ROS, and damaged mitochondria. Caco-2 cells with or without NDV-infection were fixed with 4% paraformaldehyde and probed for p62/SQSTM1 expression and reporter virus replication **(section 2.2.1.7)**, as shown in **Figure 5.4**. IF staining of p62/SQSTM1 (red) protein revealed an accumulation of endogenous p62/SQSTM1 protein in Caco-2 cells. NDV infection with reporter virus B1-GFP (green) at MOI 2 for 24 h resulted in a significant reduction of endogenous p62/SQSTM1 expression, as well as the accumulation of ectopically expressed p62/SQSTM1 in NDV-infected Caco-2 cells.

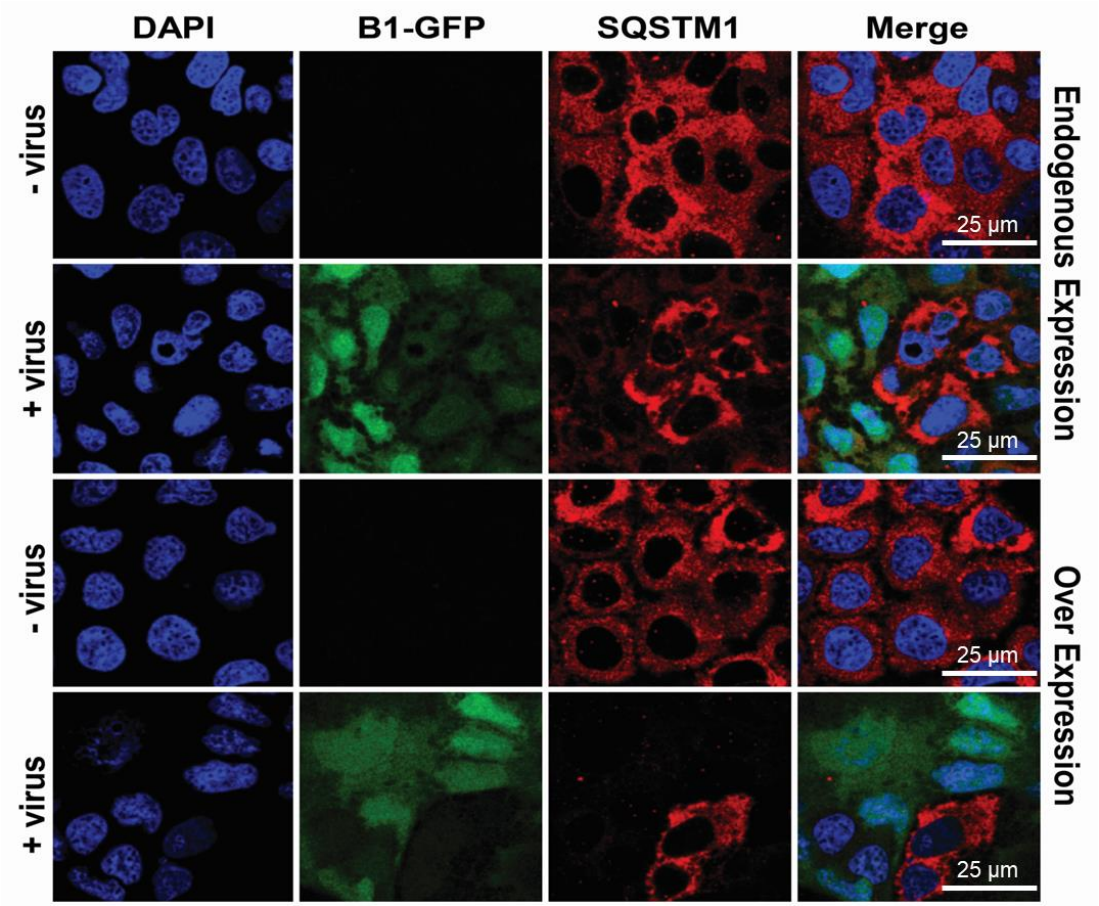

Figure 5.4. NDV-induced p62/SQSTM1 degradation in Caco-2 cells. NDV infection post 24 h demonstrated p62/SQSTM1 degradation at the endogenous as well as overexpressed level in Caco-2 cells. Fixed cells were probed with primary rabbit anti-SQSTM1 antibody and then incubated with Alexa Fluor® 568 goat anti-rabbit antibody (shown in red), NDV replication confirmed with GFP expressing reporter virus (shown in green), and cell nuclei stained with DAPI (shown in blue) (scalebar 25 µm, and n=3).

5.2.3. Time-course study of p62/SQSTM1 degradation in Caco-2 cells using IF and western blot assay

The time-course study was planned to detect the time of NDV-induced p62/SQSTM1 degradation in Caco-2 cells using IF **(section 2.2.1.8)**, and western blotting **(section 2.2.3.10)** approaches. Caco-2 cells with or without pBABEpuro-HA-p62 transfection and NDV-B1-GFP infection were fixed with 4% paraformaldehyde and stained for expression of p62/SQSTM1 (red), reporter virus replication indicated by GFP expression (green), and nucleic acid stain DAPI (blue) detected using a confocal microscope **(Figure 5.5)**. IF of p62/SQSTM1 (red) demonstrated evidence of p62 degradation at 24 hpi and 48 hpi in both endogenous and ectopic levels of p62/SQSTM1 in infected Caco-2 cells compared to uninfected Caco-2 cells.

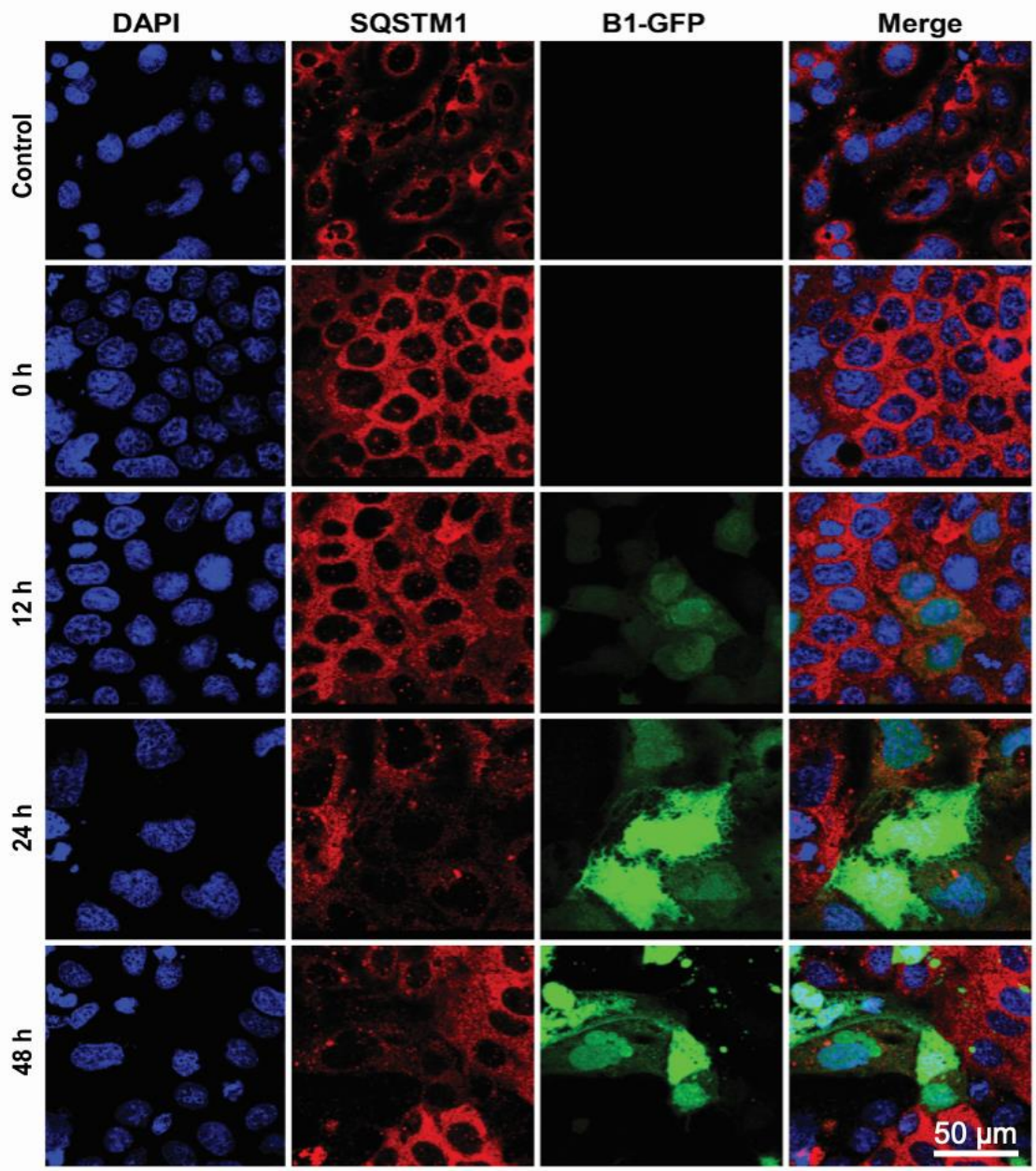

Figure 5.5. Time-course study for p62/SQSTM1 degradation in NDV-infected Caco-2 cells using indirect immunofluorescence (IF) assay. NDV infection demonstrated degradation of p62/SQSTM1 in Caco-2 cells 24 hpi and 48 hpi at MOI of 2. Fixed cells were probed with primary rabbit anti-SQSTM1 antibody and then incubated with Alexa Fluor® 568 goat anti-rabbit antibody (shown in red), NDV replication confirmed with GFP expressing reporter virus (shown in green), and cell nuclei stained with DAPI (shown in blue) (scalebar 50 µm, and n=2).

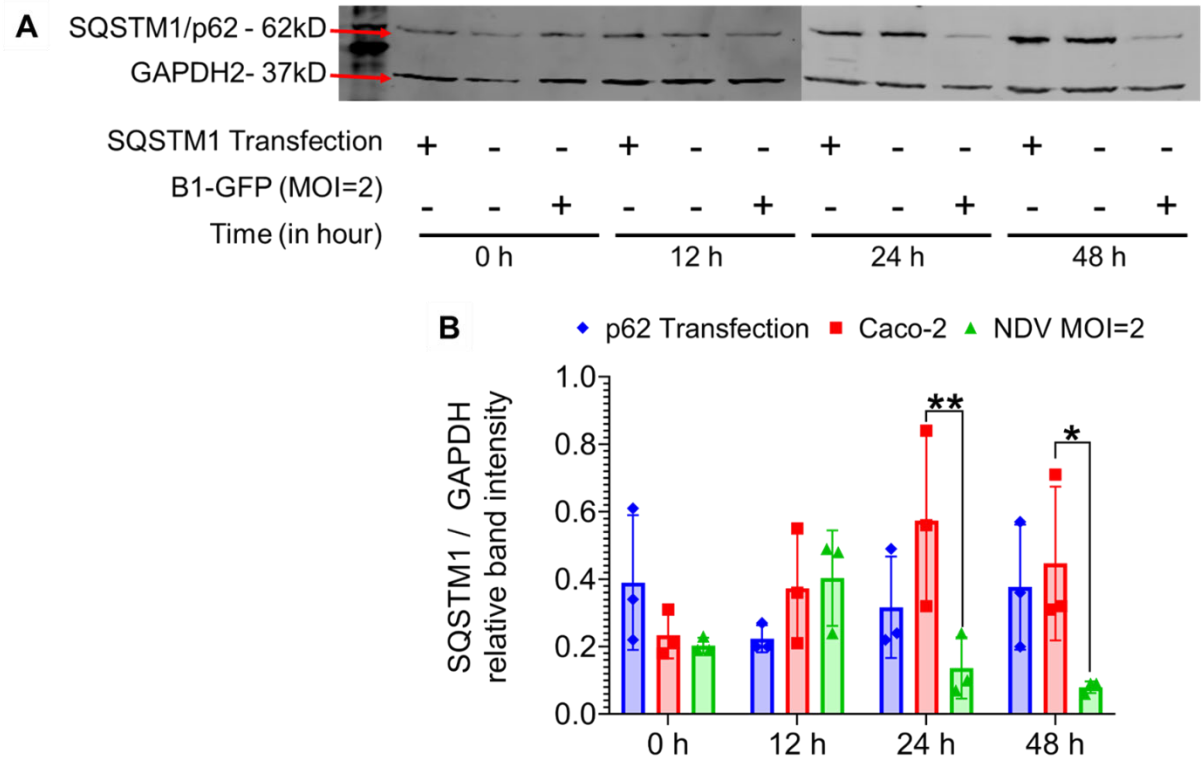

Figure 5.6. Time-course study for p62/SQSTM1 degradation in NDV-infected Caco-2 cells using western blotting. (A) Significant p62/SQSTM1 protein degradation on western blot was confirmed in Caco-2 cells 24 hpi and 48 hpi at MOI of 2. **(B)** Graph represents relative SQSTM1 band intensities in relation to the control GAPDH (n=3). Data (mean±SD) represented here were statistically analysed with Two-way ANOVA with Tukey's multiple comparison test (** $p < 0.05$ and * $p < 0.01$).

Cell lysates collected from untreated, B1-GFP (MOI of 2) infected, and pBABEpuro-HA-p62 vector-transfected Caco-2 cells at 0, 12, 24, and 48 h were used to estimate the degradation of 62 kD p62/SQSTM1 at each time point. Western blot analysis of cell lysates from all time points confirmed significant degradation of p62/SQSTM1 at 24 h (**$p<0.05$) and 48 h (* $p<0.01$) post-infection compared to uninfected Caco-2 cells illustrated in **Figure 5.6A and B**.

Both IF and western blot analysis revealed that ectopic expression levels of p62/SQSTM1, mediated by a pBABEpuro-HA-p62 vector, were not significantly different in Caco-2 cells. Whereas, p62/SQSTM1 degradation at 0 hpi and 12 hpi remained unchanged as a result of minimal NDV replication (indicated by negligible GFP expression in B1-GFP infected Caco-2 cells), as shown in **Figure 5.5**.

5.2.4. Investigation of role of each NDV protein in p62/SQSTM1 degradation

After establishing the NDV-induced p62/SQSTM1 degradation in Caco-2 cells, the role of each NDV protein in the p62/SQSTM1 degradation was investigated in cells transfected with plasmid constructs expressing individual NDV proteins. NDV genes (NP, P, M, F, and V) were cloned into V5-tagged pEFplink.2 plasmid, and NDV-HN gene was cloned in V5-tagged pEFplink.2 and pcDNA3.1(+) EGFP vectors. Caco-2 cells were transfected with plasmids encoding NDV genes for 48 h before cell lysate preparation **(section 2.2.3.10)**. The cell lysates from transfected cells with or without NDV infection were examined on western blot to confirm NDV and p62/SQSTM1 protein expression using mouse anti-V5-antibodies or NDV-specific chicken serum, and anti-p62/SQSTM1 antibodies, respectively. Western blot analysis revealed the expression of NP, P, and V proteins only **(Figure 5.7 A)**, and NDV M, F, and HN proteins were undetected by V5-antibodies or anti-NDV chicken sera. IF staining was used for the detection of NDV proteins in transfected Caco-2 cells. Only NDV NP, P, M, and V proteins (green) and nucleic acid stain DAPI (blue) were detected using a confocal microscope **(Figure 5.7 B)**.

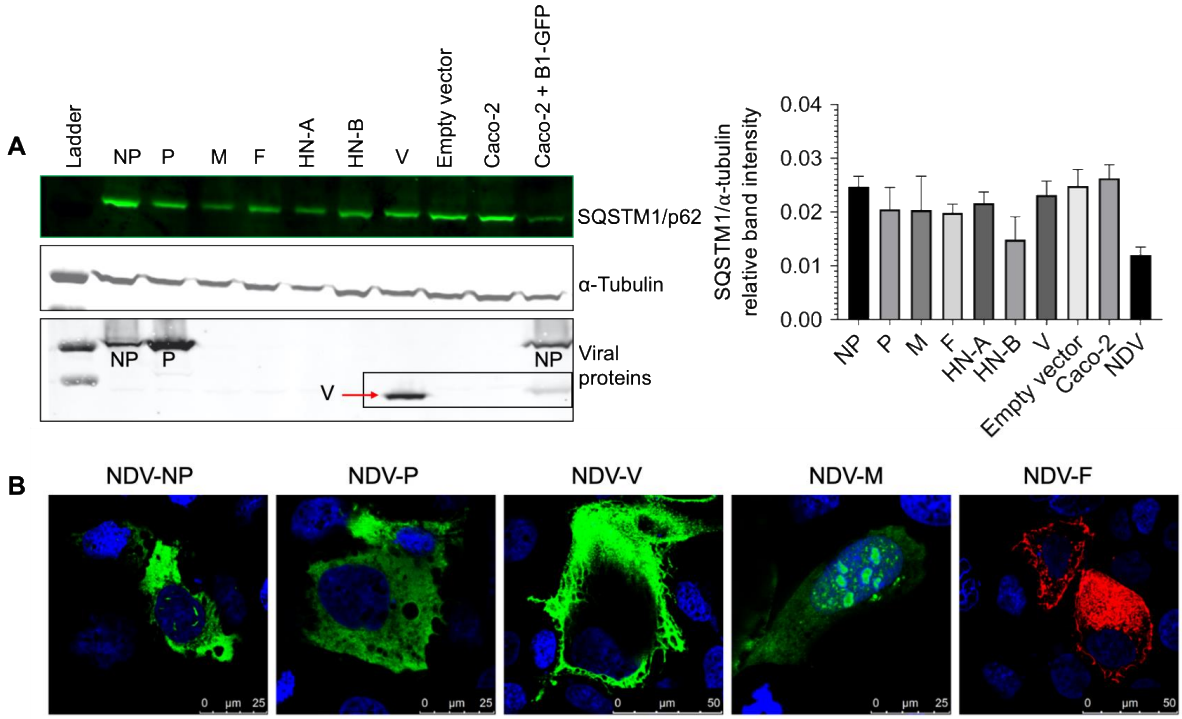

Figure 5.7. The investigation of the role of individual NDV protein in p62/SQSTM1 degradation. (A) Western blot analysis of each NDV protein participating in p62/SQSTM1 protein degradation 48 hpi in Caco-2 cells detected on the blot (n=2). Results showed that only NP, P, and V viral proteins were expressed and none of them induced p62/SQSTM1 degradation. (NDV clones expressing NDV proteins: HN-A→ HN cloned in V5-tagged pEFplink.2 vector, HN-B→ pcDNA3.1(+) EGFP vector, and NP/P/M/F/V cloned in V5-tagged pEFplink.2 vector) **(B)** IF assay detected expression of NDV proteins in transfected Caco-2 cells, where fixed cells probed with primary mouse anti-V5 antibody (V5 tagged

NDV NP, P, M, and V proteins) and anti-NDV chicken sera (NDV-F) then incubated with Alexa Fluor® 488 goat anti-mouse antibody (shown in green) and Alexa Fluor® 568 goat anti-chicken antibody (shown in red), and cell nuclei stained with DAPI (shown in blue) (scalebar NP, P, and M=25 µm; V and F=50 µm, and n=2).

However, the NDV F protein (red) **(Figure 5.7 B)** was detected only using anti-NDV chicken sera in IF assay under a confocal microscope. The anti-V5 antibody had not worked to detect NDV F protein expression, as V5-tag was at N-terminal of F plasmid construct. The V5-tag got cleaved with signal peptide during F protein transmembrane translocation as predicted using SignalP 4.0 **(Figure 5.8)**. The HN protein expression also had not been detected using anti-NDV chicken sera or V5-tag in Caco-2 cells. None of the individual NDV proteins that were detected in the transfected Caco-2 cells demonstrated degradation of p62/SQSTM1, suggesting that interaction of all NDV proteins or active viral replication are needed for SQSTM1 degradation in Caco-2 cells **(Figure 5.7A)**.

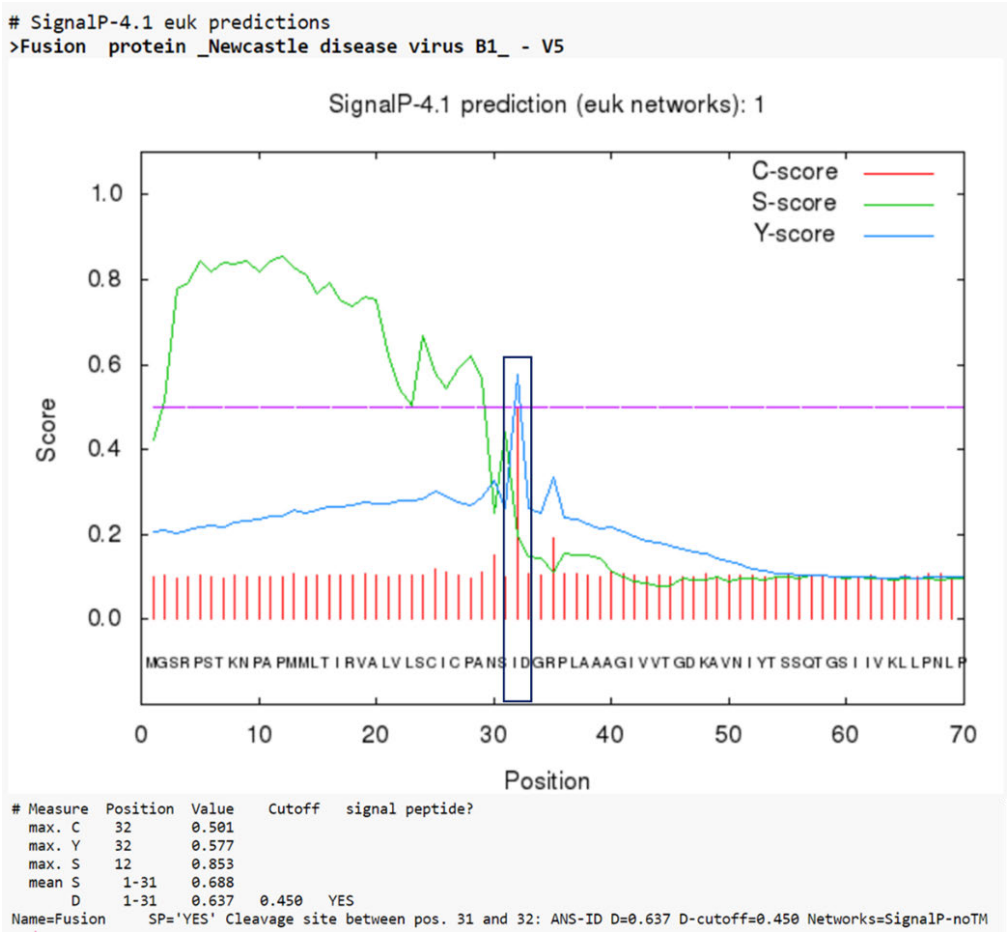

Figure 5.8. Prediction of signal peptide cleavge site in fusion protein sequence of NDV B1 strain. Signal peptide of fusion protein predicted using SignalP 4.0 confirmed cleavage site between 31 and 32 amino acids from N-terminal (highlighted as a rectangle). NDV F protein expressed by V5 tagged pEFplink.2 vector. F protein had V5 tag at N-terminal in close proximity of cleavage site of signal peptide.

5.2.5. CRISPR/Cas9 based p62/SQSTM1 Knockout approach in HEK-293 cells

To investigate the role of NDV and host protein interactions, p62/SQSTM1 knocked out Caco-2 cells would have a significant role in defining NDV-induced of p62 degradation in Caco-2 cells. The hypothesis was based on the interaction of NDV proteins with Caco-2 cell proteins with or without p62/SQSTM1 expression could shed light on the mechanisms of NDV-induced cell death in Caco-2 cells.

Initially, p62/SQSTM1 was knocked down using 21-nucleotide long siRNA that targeted SQSTM1 mRNA transcript for degradation in Caco-2 **(section 2.2.1.8)**. The concentration of anti-SQSTM1 siRNA was optimised in Caco-2 cells for efficient silencing of the SQSTM1, a 100 nM concentration was resulted in maximum knockdown of SQSTM1 transcripts **(Figure 5.9 B)**. IF staining of 100 nM anti-SQSTM1 siRNA-treated Caco-2 cells showed significant knockdown of SQSTM1 (red) compared to the negative control non-specific siRNA-treated and untreated Caco-2 cells together with B1-GFP virus replication (green) using a confocal microscope **(Figure 5.9 A)**. Cell lysates prepared from anti-SQSTM1 siRNA silenced Caco-2 cells with or without B1-GFP infection at MOI of 2 for 48 h were used to detect NDV proteins (NP, P, and V) expression using anti-NDV chicken sera on western blot **(Figure 5.9 C)**.

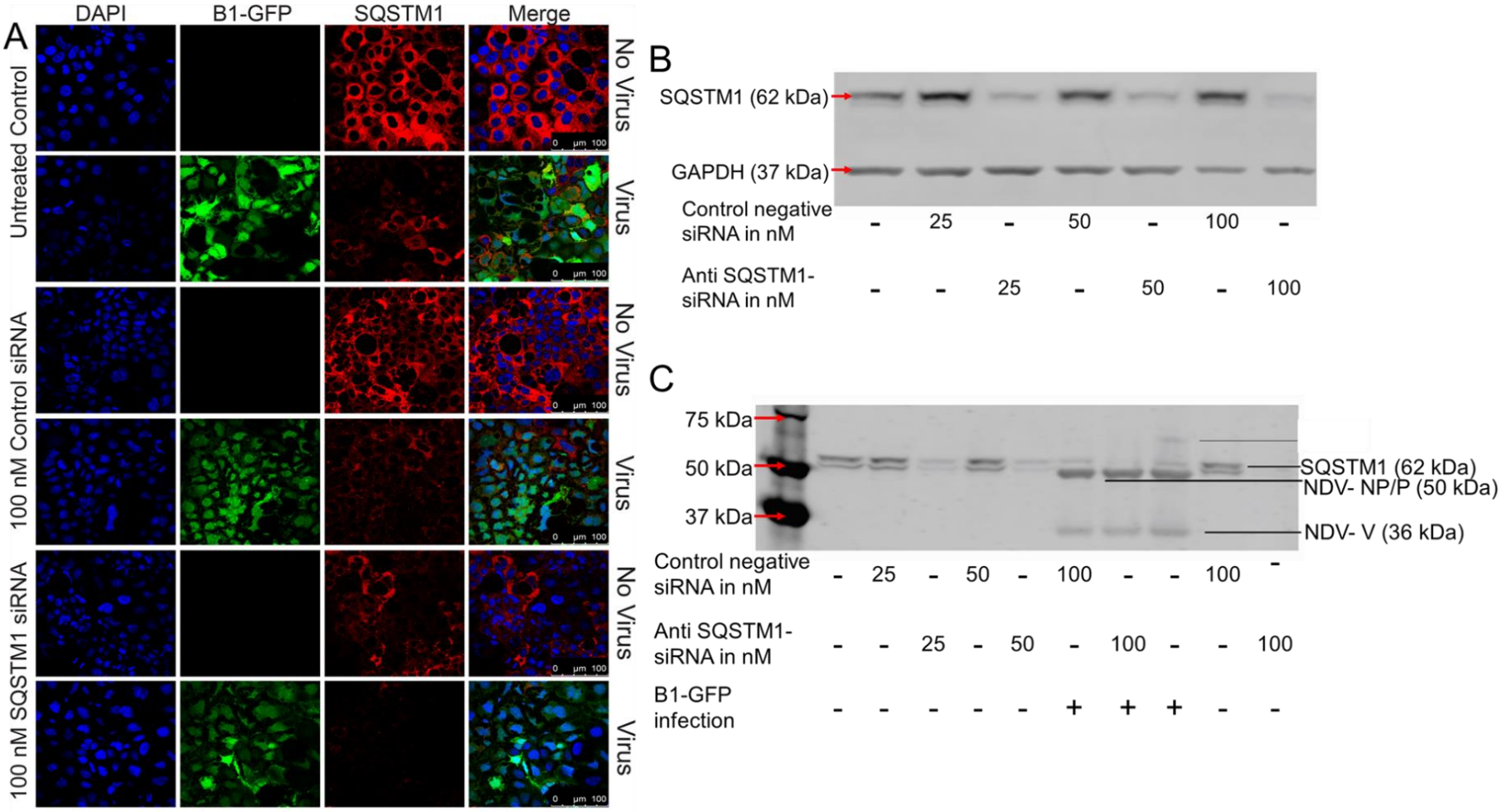

Figure 5.9. p62/SQSTM1 siRNA silencing in Caco-2 cells. (A) IF analysis demonstrated significant p62/SQSTM1 silencing in Caco-2 cells 24 hpi using the anti-SQSTM1 siRNA or negative control siRNA. NDV infection degraded SQSTM1 protein in Caco-2 cells. Fixed cells were probed with primary rabbit anti-SQSTM1 antibodies and then incubated with Alexa Fluor® 568 goat anti-rabbit antibodies (red), NDV replication confirmed with GFP expressing reporter virus (green), and cell nuclei stained with DAPI (blue) (scalebar 100 µm). **(B)** Western blot analysis confirmed the effective concentration of anti-SQSTM1 siRNA 24 h post-transfection in Caco-2 cells (n=3). **(C)** NDV replication remained unchanged irrespective of p62/SQSTM1 silencing 48 hpi at MOI of 2 in Caco-2 cells, NDV proteins detected on the blot (n=2).

Western blot analysis of anti-SQSTM1 siRNA silenced Caco-2 cells with or without NDV infection confirmed no change in NDV replication compared to untreated NDV-infected Caco-2 cells.

Efficient NDV replication in p62/SQSTM1 knocked down Caco-2 cells is encouraging to study the NDV interaction with Caco-2 cell proteins in the absence or presence of SQSTM1 protein. Hence, instead of transient siRNA-based knockdown of SQSTM1 in Caco-2 cells, a CRISPR/Cas9 based stable KO of SQSTM1 approach was planned.

CRISPR/Cas9 use RNA-guided DNA endonuclease Cas9 enzyme-mediated target gene editing by introducing double-strand breaks (DSBs) upstream to PAM (protospacer adjacent motif) associated with the target DNA sequence. The DSBs are repaired in a cell by two effective mechanisms: imprecise non-homologous end joining (NHEJ) and precise homology-directed repair (HDR). NHEJ pathway is error-prone where ends of DSBs processed by endogenous DNA repair machinery and re-joined resulting in insertions/deletions (indel) mutations at the site of the junction. The indel mutations in the coding region cause frameshifts, resulting in the KO of the gene by the creation of premature stop codons. In the HDR pathway, the repair template provided by sister chromatid allows precise editing and governs high fidelity.

Here, NHEJ based SQSTM1 CRISP/Cas9 KO was planned to use three guide RNAs (gRNAs) to target the sqstm1 gene in Caco-2 cells (enlisted in **Figure 5.9 A** table). 'All in one' custom synthesised lentiviral plasmid pLV01 (see vector map in **Figure 5.9 B**) provided by Sigma was used for SQSTM1 KO. The pLV01 plasmid is 12.627 kb in size consists of 3', and 5' LTR sequences useful in stable transfection of target cells. pLV01 vector expresses gRNA targeting sqstm1 under the mammalian U6 promoter and a puromycin N-acetyltransferase (PAC), Cas9, and GFP under EF-1a promoter. In-frame expression of PAC, Cas9 and GFP genes separated by 2A sequences which encode self-cleaving peptides, PAC and GFP expressions allow easy monitoring and selection of KO cells.

All three pLV01 vectors were named pLV01-p62-18, pLV01-p62-19 and pLV01-p62-20 based on Sigma target ID of gRNAs HS0000134618, HS0000134619, and HS0000134620 respectively. All three plasmids separately transfected in human embryonic kidney-293 (HEK-293) cells and Caco-2 cells **(section 2.2.1.9)**; HEK-293 cells were used as control cells because of its high transfection efficiency.

A

Target ID/Clone Name	Target Sequence:5'-3' (does not include with PAM)	PAM	RefseqId/Target mRNA Exon	Gene Symbol, Gene ID, Chromosome	Start Coordinate
HS0000134618	CGGTGGGCGGTGGTCCCGC	CGG	NM_003900/3 XM_017010010/3 NM_001142298/4 NM_001142299/4	SQSTM1 8878 5	179823871
HS0000134619	ATTGGGGTGCACCATGTTG	CGG	NM_003900/3 XM_017010010/3 NM_001142298/4 NM_001142299/4		179823910
HS0000134620	GCCATCGCAGATCACATTG	GGG	NM_003900/3 XM_017010010/3 NM_001142298/4 NM_001142299/4		179823925

B

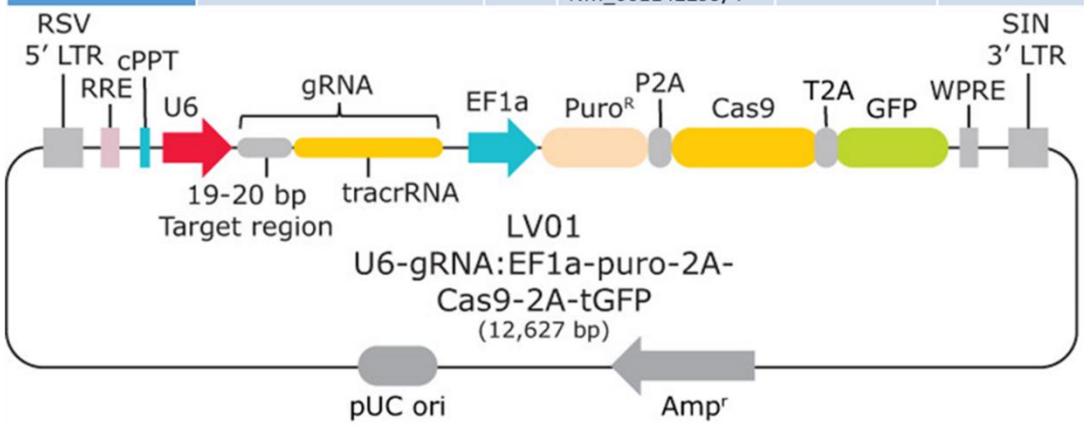

Figure 5.10. The strategy of lentiviral vector-based CRISPR/Cas9 KO of SQSTM1 in Caco-2 and HEK-293 cells. (A) Sequences of guide RNAs (gRNA) to KO human p62/SQSTM1 transcripts. **(B)** Lentiviral pLV01 vector map showing all-in-one custom gRNA expression plasmid provided by Sigma-Merck expresses gRNA under mammalian U6 promoter and Cas9, GFP, and a puromycin N-acetyltransferase (PAC) under EF-1a promoter.

Cell lysates were prepared from pLV01-p62-18, pLV01-p62-19 and pLV01-p62-20 plasmid-transfected Caco-2 cells, and HEK-293 cells and used for analysing the KO efficiency of plasmids in cells using western blot analysis to detect of 62 kDa p62/SQSTM1 on blot **(Figure 5.11)**. Western blot analysis demonstrated SQSTM1 remained undisrupted in Caco-2 cells, perhaps because of the poor transfection efficiency of 12.627 kb long pLV01 plasmids, whereas HEK-293 cells had higher transfection efficiency and SQSTM1 expression was undetected in all three-gRNA transfected HEK-293 cells indicating KO of the SQSTM1 gene only in HEK-293 cells.

Furthermore, pLV01-p62-20-transfected HEK-293 cells were cultured manually in single-cell clones **(section 2.2.1.9)** based on GFP expression to identify the SQSTM1 KO by PCR **(section 2.2.3.2)** and western blot **(section 2.2.3.10)** analysis. PCR analysis of genomic DNA isolated from single-cell clones confirmed partial KO of SQSTM1 on an agarose gel of pLV01-p62-20-transfected HEK-293 cells, where three different 700, 900, and 1055-nucleotide long KO products were detected confirming disruption of sqstm1 gene at several

sites in comparison with the wild type non-transfected HEK-293 cells, as shown in **Figure 5.12A**. Cell lysates prepared from isolated pLV01-p62-20-transfected HEK-293 single-cell clones used in western blot analysis to detect the expression of 62kD p62/SQSTM1 protein confirmed the KO of the gene in HEK-293 cells, as illustrated in **Figure 5.12B**.

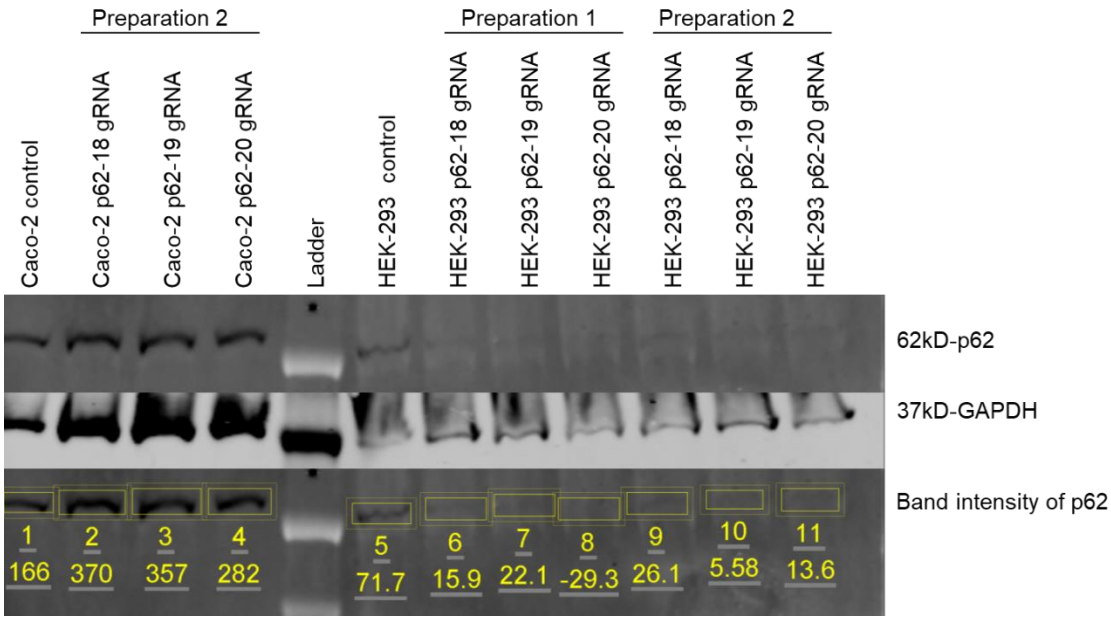

Figure 5.11. Identification of p62/SQSTM1 protein KO in Caco-2 and HEK-293 cells. Caco-2 and HEK-293 cells transfected with pLV01 plasmids expressing gRNA preparations confirmed SQSTM1 KO only in HEK-293 cells.

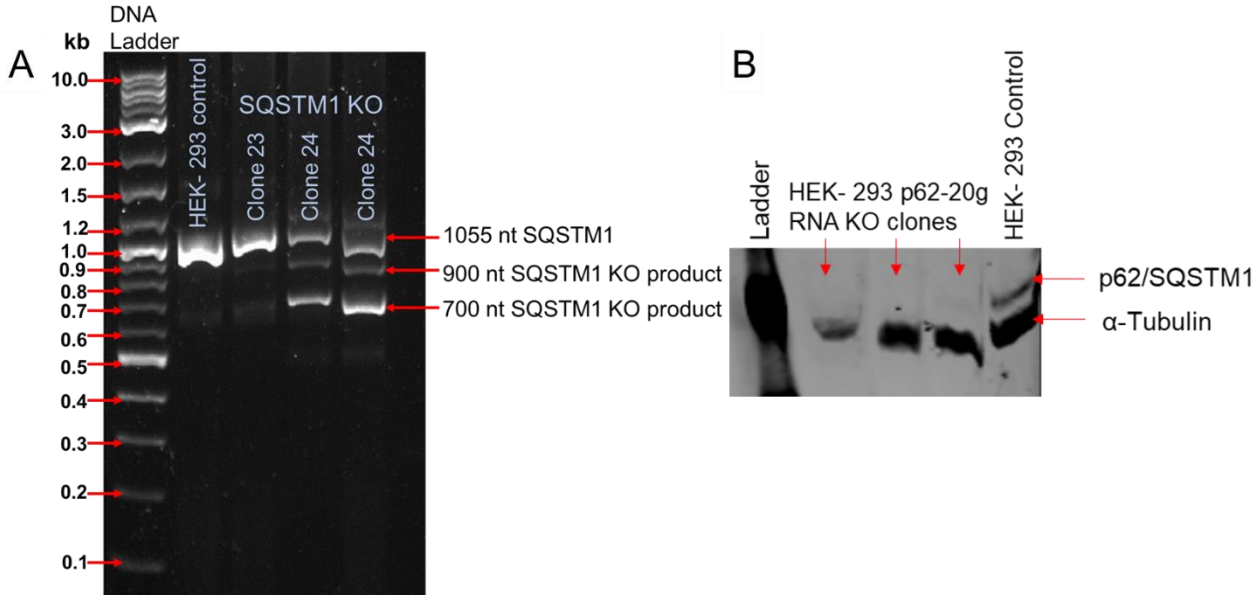

Figure 5.12. Confirmation of p62/SQSTM1 protein KO in HEK-293 cells. (A) Agarose gel electrophoresis of partial KO of p62/SQSTM1 in selected HEK-293 clones showing multiple KO products. **(B)** Western blot analysis of p62/SQSTM1 KO clones confirmed the complete deletion of SQSTM1 protein HEK-293 cells.

5.3. Discussion

Autophagy is the cardinal process to regulate cellular homeostasis by recycling mediated through lysosomal degradation of damaged cytoplasmic components and cytoplasmic organelles in the cell (259). Generally, autophagy non-selectively sequesters cellular organelles in bulk for nutrient recycling under metabolic stress. However, the clearance of unnecessary and undesired components such as misfolded proteins and lipid droplets, damaged DNA, defective organelles, and virus infections initiate selective autophagy of several types such as mitophagy (mitochondria), ER-phagy (endoplasmic reticulum), and pexophagy (peroxisomes) in stressed cells (271). In selective autophagy, p62/SQSTM1 plays a vital role as an adapter in tethering ubiquitinated cargo to the autophagy receptors such as LC3 leading to the elimination of damaged cargo (260, 268). SQSTM1 is a multifunctional, multidomain signalling hub that interacts with multiple partners to form either p62/SQSTM1 homodimers or heterodimers with proteins such as ERK, aPKC, and NBR1. Sanz et al. (2000) and Moscat et al., (2006) have demonstrated the active interaction of aPKC with PB1 domain stimulating NF-kB pathway by IL-1, RANKL, NGF cell stimulator activation downstream to the transcription factor NF-kB. TRAF6 self-ubiquitinises and interacts with the UBA domain of activated p62/SQSTM1 aggregates to activate NF-kB pathway leading to cell survival (272, 273). Likewise, Jin et al. (2009) have demonstrated p62/SQSTM1-mediated activation of extrinsic apoptotic pathways occur through the interaction with the ubiquitinated caspase-8. Cell surface death receptors such as DR4 and DR5 activate caspase-8 and TRAIL promote cullin-3-dependent caspase-8 ubiquitination leading to apoptotic cell death (274). Duran et al. (2011) have shown p62/SQSTM1-dependent regulation of nutrient-sensitive mTORC1 pathway, where the region between ZZ and TBS signalling domains of p62/SQSTM1 interacts with mTOR and raptor complex as well binds with Rag GTPases to form Rag dimer, and mTORC1 activation (267).

Similarly, Umemura et al. (2016) demonstrated the oncogenic transformation of non-tumour mice liver activated by overexpression of p62/SQSTM1. Ectopic expression of p62/SQSTM1 was reported, being required for instigation of NRF2 and mTORC1 in mice hepatocellular carcinoma (275). Both studies by Duran et al. and Umemura et al. have showed that upregulated p62/SQSTM1 aggregates in autophagy-deficient cells led to mTORC1 pathway mediated tumourigenesis. In contrast, Mathew et al. (2009) confirmed the suppression of tumorigenesis due to degradation of p62/SQSTM1 via autophagy (269). The role of p62/SQSTM1 in autophagy and other signalling pathways such as NF-kB and mTORC1 helps to strike a balance between cell death and survival depending on cell stimulators activation and type of stress in various cells. Nihira et al. (2014), have

demonstrated suppression of cell proliferation and induction of autophagic cell death in human adenocarcinoma and squamous cell carcinoma cell lines by inhibition of p62/SQSTM1 through siRNA-mediated silencing and chemical modulation of p62 (276).

Based on the importance of autophagy in cellular homeostasis under metabolic stresses like DNA damage, mitochondrial damage, and viral infection; several studies had been done to understand the significance of virus-induced selective autophagy. Meng et al. (2012) demonstrated that infection by the mesogenic strain of NDV Beaudette C at MOI of 10 in human glioma U251 cells resulted in the elevated conversion of LC3-I to LC3-II and degradation of p62/SQSTM1 with the involvement of class III phosphatidylinositol 3-kinase (PI3K)/Beclin-1 pathway (141). Jiang et al. (2014), demonstrated that NDV/FMV strain triggered autophagy in paclitaxel-resistant A549 cells by chemical modulation targeting the autophagy inhibiting the class-I PI3K/Akt/mTOR/p70S6K pathway. Chemotoxic autophagy modulators enhanced NDV-induced oncolysis in drug-resistant A549 cells (277). Cheng et al. (2016) have reported that NDV NP and P protein transfection alone were sufficient to induce autophagy in A549 cells through endoplasmic reticulum stress-related unfolded protein response (UPR) pathway (265). However, in this study, NP and P protein transfections were not sufficient to degrade p62/SQSTM1 protein in Caco-2 cells, as shown in **Figure 5.7 A**. Sun et al. (2014) reported the benefits of autophagy for NDV replication in chicken cells and tissues. Their study reported NDV-induced autophagy in DF-1 and CEF cells evident by the presence of double-membrane vesicle formation and LC3-I to LC3-II conversion. Inhibition of autophagy via RNA silencing and chemical modulators reduced virus replication, suggesting the importance of autophagy in NDV replication in chicken cells (278).

In all the above studies, NDV-induced autophagic fluctuation mediated by degradation in p62/SQSTM1 and LC3-II conversions were noticed. In this chapter, only the status of p62/SQSTM1 and impact of NDV replication on p62/SQSTM1 in NDV-infected Caco-2 cells was examined. The lentogenic NDV strain Hitchner B1 clearly induced p62/SQSTM1 degradation at MOI of 2, 24 hpi. However, experiments to examine the direct role of NDV proteins in p62/SQSTM1 degradation showed that at least NDV NP and P and V proteins expressed alone were not enough to cause degradation of p62/SQSTM1 in infected Caco-2 cells **(Figure 5.7 A)**. These findings suggested that interaction of some or all NDV proteins, and/or active viral replication, may perhaps be required. Additional detailed studies are required to understand the role of autophagy in Hitchner B1-induced oncolysis and pathways involved in Caco-2 cells.

The lack of working monoclonal antibodies (mAbs) targeting NDV F and HN proteins restricted the detection of their expression by western blot analysis. Further studies in the future using different cloning approaches and use of mAbs targeting NDV F and HN proteins, along with other NDV proteins, for a detailed examination of all interacting partners of p62/SQSTM1 are required to identify pathways involved in p62/SQSTM1 degradation and NDV replication in Caco-2 cells.

Poor transfection efficiency of Caco-2 cells posed limitations in establishing CRISPR/Cas9 based SQSTM1 KO in Caco-2 cells using stable transfection method. In future, by employing replication-defective lentiviral particles expressing pLV01 vector leading to perpetual expressions of gRNA targeting SQSTM1, Cas9, PAC, and GFP can be achieved using transduction approaches to produce SQSTM1 KO Caco-2 clones. Comparison of SQSTM1-deleted Caco-2 cells with wild type Caco-2 cells can be used to study NDV-host protein interaction as well as to understand the role of p62-dependent autophagic cell death in NDV-infected Caco-2 cells.

Chapter 6

6 Genomic diversity and evolution of quasi-species in Newcastle Disease Virus (NDV) infections

Note: This chapter is produced out of interest after gathering interesting results from the bioinformatic analysis of RNA-Seq data generated from acutely or persistently NDV-infected and uninfected Caco-2 cells in this PhD project. Prof Chan Ding (Shanghai Veterinary Research Institute, China) has kindly provided the RNA-seq data from LaSota or Herts/33 infected chicken embryonic fibroblasts (CEF) cells for the NDV quasi-species analysis. All evolutionary analyses were executed by Dr Luca Ferretti and Dr Lele Zhao (Big Data Institute, University of Oxford). I, the author of this thesis, have contributed in generating samples from B1-GFP infected Caco-2 cells (18 hpi and 36 hpi), VR Caco-2 cells, and uninfected Caco-2 cells (3 replicates of VR Caco-2 and Caco-2 cells) for RNA-seq analysis and I have contributed in writing the introduction and explaining the results of **Figure 6.1** and **Figure 6.2**. Dr Luca Ferretti has done most of the bioinformatics analysis of the RNA-seq data, interpretation of the results and writing of the rest of the chapter.

6.1. Introduction

RNA viruses often have high mutation rates due to the error-prone nature of RNA polymerases (279, 280). Inside a host, viral RNA polymerases induce roughly 10^{-4} mutations per nucleotide copied due to low fidelity, and this may result the formation of a viral swarm, i.e. a pool of similar genotypes differing only by a handful of mutations (279, 280). This is a distinctive pattern of intra-host genetic variability in organisms with high mutation rates. In viral infections, this is frequently related to quasi-species dynamics, with complex interactions between the viruses in the swarm (279, 280). Viral quasi-species is defined as an assortment of closely-related viral genomes subjected to a continuous process of genetic variation, competition between the generated variants, and selection of the fittest distributions in a specified environment (281).

NDV is thought to have a relatively low mutation rate per site per year among RNA viruses (282). However, recent phylogenetic estimates of the substitution rate are large enough to suggest the presence of within-host diversity (283). In fact, NDV infections are well known to harbour quasi-species, and a significant amount of research has been focused on the

different profiles of virulence determined by mutations in the fusion protein cleavage site. These mutations are sometimes polymorphic within NDV quasi-species and can transform avirulent lineages into highly pathogenic ones (284, 285) representing, therefore, a potential risk for animal health.

Despite this, very little is known or has been done about the characterisation of the genomic patterns of diversity and selection in NDV viral swarms. Mutational biases in NDV quasi-species have been recently described (286), but without any discussion of the patterns of variants across different strains, genes or hosts.

In this chapter, we have used the RNA-seq short-read data obtained for the transcriptomic analysis **(Table 6.1)** to extract information about the genomic patterns of variability and the signatures of selection within NDV swarms. The RNA-seq data include samples from acutely B1 strain infected Caco-2 cells (18 hpi and 36 hpi at 0.1 MOI), persistently NDV-infected VR Caco-2 cells, LaSota-infected CEF cells (12 hpi at 1 MOI) and Herts/33-infected CEF cells (12 hpi at 1 MOI). NDV strains B1 and LaSota are avirulent/vaccine strains that belong to genotype II, and Hers/33 is highly pathogenic/velogenic strain belonging to genotype IV. Here, comparisons made for both diversity patterns and selection pressure at the amino acid level (i.e. dN/dS) across different genes, strains (B1 and LaSota vs Herts/33) and host cells (Caco-2 vs CEF).

Table 6.1: Number of reads of different samples generated from two different deep sequencing projects

Sr. No.	Cell line	NDV Strain	Protocol and read length	Total reads	Cellular reads	Viral (NDV) reads	Ref
1	Caco-2 R1	NA	PE 2x75bp	163101744	136165956	4	Samples were generated in this PhD project
2	Caco-2 R2	NA	PE 2x75bp	249099676	207143604	16	
3	Caco-2 R3	NA	PE 2x75bp	208334180	173535348	98	
4	Caco-2 (18 hpi)	B1	SE 150bp	60305847	50759072	878722	
5	Caco-2 (36 hpi)	B1	SE 150bp	60687628	43367516	5058895	
6	VR Caco-2 R1	B1	PE 2x75bp	169865200	136396814	422344	
7	VR Caco-2 R2	B1	PE 2x75bp	199240224	160157292	590062	
8	VR Caco-2 R3	B1	PE 2x75bp	192634102	157201210	545246	
9	CEF R1	NA	PE 2x150bp	110981726	105289705	19193	Prof Chan Ding's lab provided RNA-seq data (248)
10	CEF R2	NA	PE 2x150bp	86062988	107316782	19202	
11	CEF R3	NA	PE 2x150bp	93479188	82980071	18838	
12	CEF R1 (12 hpi)	LaSota	PE 2x150bp	83743856	86110590	4303890	
13	CEF R2 (12 hpi)	LaSota	PE 2x150bp	87401712	76973251	4107844	
14	CEF R3 (12 hpi)	LaSota	PE 2x150bp	83496140	80178138	4261925	
15	CEF R1 (12 hpi)	Herts/33	PE 2x150bp	83496140	61949227	19375583	
16	CEF R2 (12 hpi)	Herts/33	PE 2x150bp	94400454	70699666	21306306	
17	CEF R3 (12 hpi)	Herts/33	PE 2x150bp	93150904	72638442	17886152	

6.1.1. Chapter objectives

1. Assess genetic diversity within different NDV strains and cell lines derived from different hosts (i.e. human Caco-2 cells and CEF cells).
2. Estimate the frequency spectrum of mutations of NDV cultured in Caco-2 and CEF cells to understand the genetic structure of the viral population.
3. Compare the diversity patterns and selection pressure at the amino acid level (i.e. dN/dS) across different genes, strains (B1 and LaSota vs Herts/33) and host cell lines (Caco-2 vs CEF).
4. Assess the differences between within-host and between-host selective pressures by comparing within-genotype divergence and within-sample polymorphisms.

6.2. Results

6.2.1. Genetic diversity

The RNA-seq reads were processed as for transcriptomic analysis **(Chapter 3, section 2.2.6.)**. All reads with mapping quality <30 and all bases with base quality <30 were discarded. SNPs (single nucleotide polymorphisms) and indels (insertions/deletions) were called on the resulting sequences using SiNPle (287) with parameter theta=0.01, retaining only variants with <5% posterior probability of being sequencing/amplification errors or artefacts.

All evolutionary analyses were implemented in R by Dr Luca Ferretti and Dr Lele Zhao (Big Data Institute, University of Oxford) using custom scripts and the APE package (288).

For most samples, the coverage varied widely along the NDV genome, with the lowest coverage in the sequence coding for the L protein **(Figure 6.1)**. The minimum of the typical coverage of L across samples was about 500. Read depth has a strong effect on estimates of genetic diversity (289). Hence, for the results to be comparable across genomic regions and samples, all sites with reading depth <400 were ignored. Similarly, all variants with frequency <0.005 (i.e. all variants in the regions with lowest read depth to be contained with at least two reads) were ignored. Where not specified otherwise, running averages across 250 bases are illustrated in all plots in this chapter.

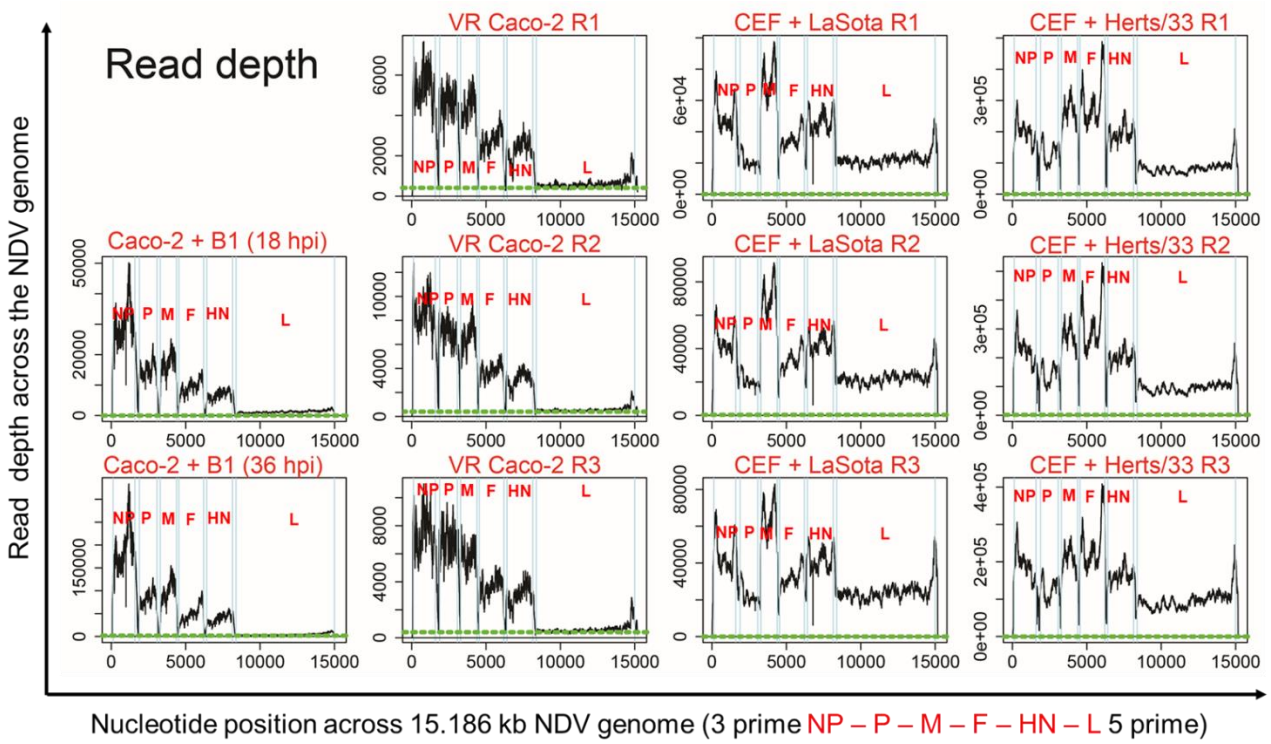

Figure 6.1. Read depth per position along the NDV genome. The green line represents the threshold for our analysis (read depth=400), which include most of the genome for all samples, where R1, R2, and R3 represents three different biological replicates of infected VR Caco-2 or CEF cells with different NDV strains.

Genetic variability amongst all samples was estimated by calculating three classical measures across all the SNP variants (289):

- The SNP density - i.e. the average fraction of polymorphic bases;
- The pairwise nucleotide diversity – i.e. the fraction of bases differing among two random sequences;
- The average entropy per base, which is another measure of diversity corresponding to Shannon's entropy applied to the distribution of variants in each base.

The averages per base of these different measures are illustrated in **Figure 6.2** in all compared NDV strains in Caco-2 and CEF cells. These measures of genetic variability show that genetic diversity increased in B1-infected (MOI=0.1) Caco-2 cells from 18 hpi to 36 hpi, as a result of the increased number of viral replication cycles and the consequent increase in the number and frequency of mutations. The genetic diversity was found to be even higher in persistently NDV-infected VR Caco-2 cells, which could be related to the selection pressure on the NDV population in VR Caco-2 cells during persistent NDV infection **(Figure 6.2)**. The genetic variability of avirulent B1 strain of NDV was higher in Caco-2 cells at 36 hpi and in VR Caco-2 cells compared to the highly pathogenic Herts/33

strain of NDV in chicken (CEF) cells **(Figure 6.2)**. In chicken cells, the more virulent strain (Herts/33) had higher diversity than the avirulent one (LaSota) as could be expected because of the larger viral population.

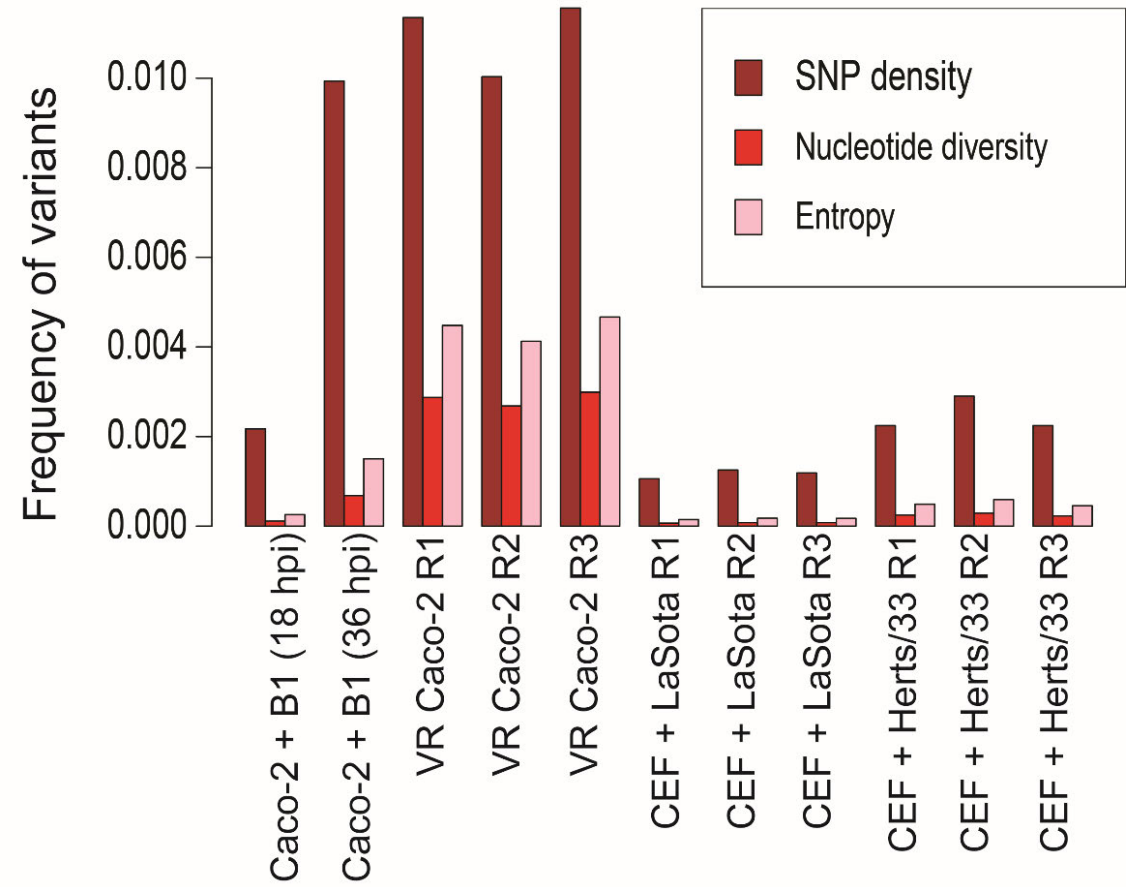

Figure 6.2. Diversity measurements per base across different samples. Higher genetic diversity was observed in Herts/33 compared with LaSota in infected CEF cells. An increase in viral diversity in time was observed in B1-infected Caco-2 cells from 18 hpi to 36 hpi and persistently NDV-infected VR Caco-2 cells. Here R1, R2, and R3 represent three different replicates of infected VR Caco-2 or CEF cells with different NDV strains (All samples have running averages of 250 bases, reading depth ≥400, and all variants with frequency ≥0.005).

Note:

- The SNP density is the average fraction of polymorphic bases;
- The pairwise nucleotide diversity is the fraction of bases differing among two random sequences;
- The average entropy per base, which is another measure of diversity corresponding to Shannon's entropy applied to the distribution of variants in each base

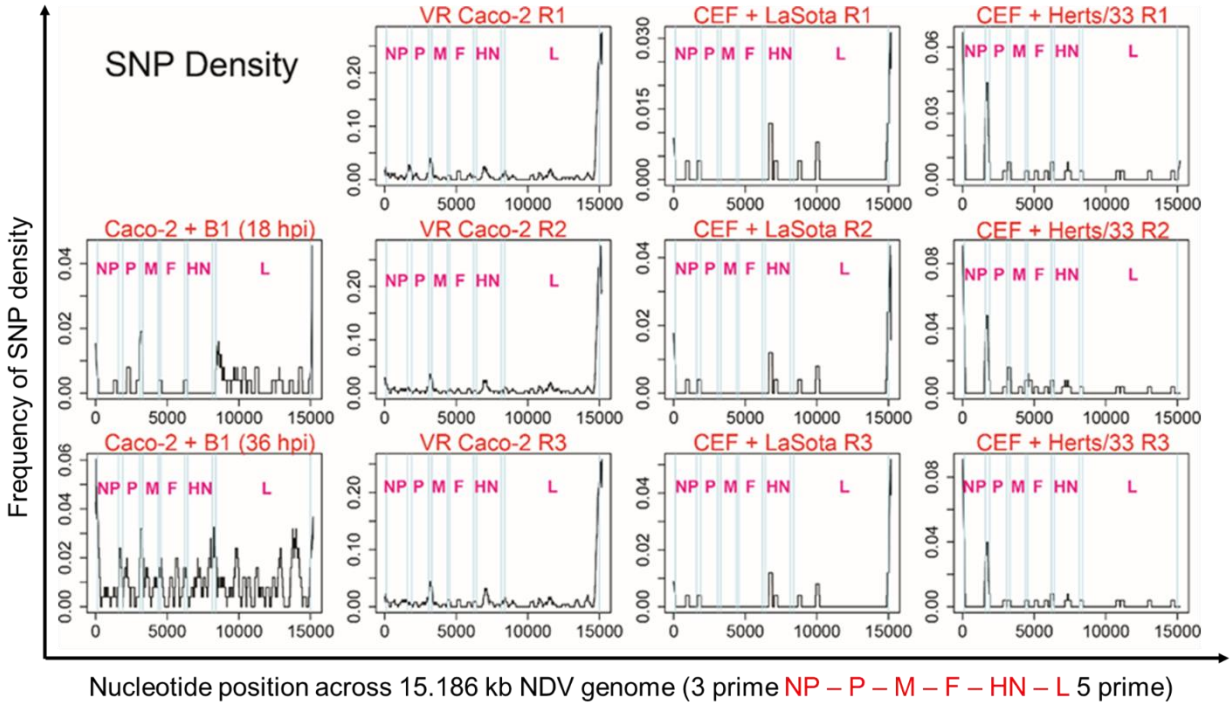

Figure 6.3. Local SNP density estimation along the NDV genome across all samples. The blue vertical lines represent the NDV gene boundaries (NP, P, M, F, HN, and L) in all samples, where R1, R2, and R3 represents three different biological replicates of infected VR Caco-2 or CEF cells with different NDV strains (All samples have running averages of 250 bases, reading depth ≥400, and all variants with frequency ≥0.005).

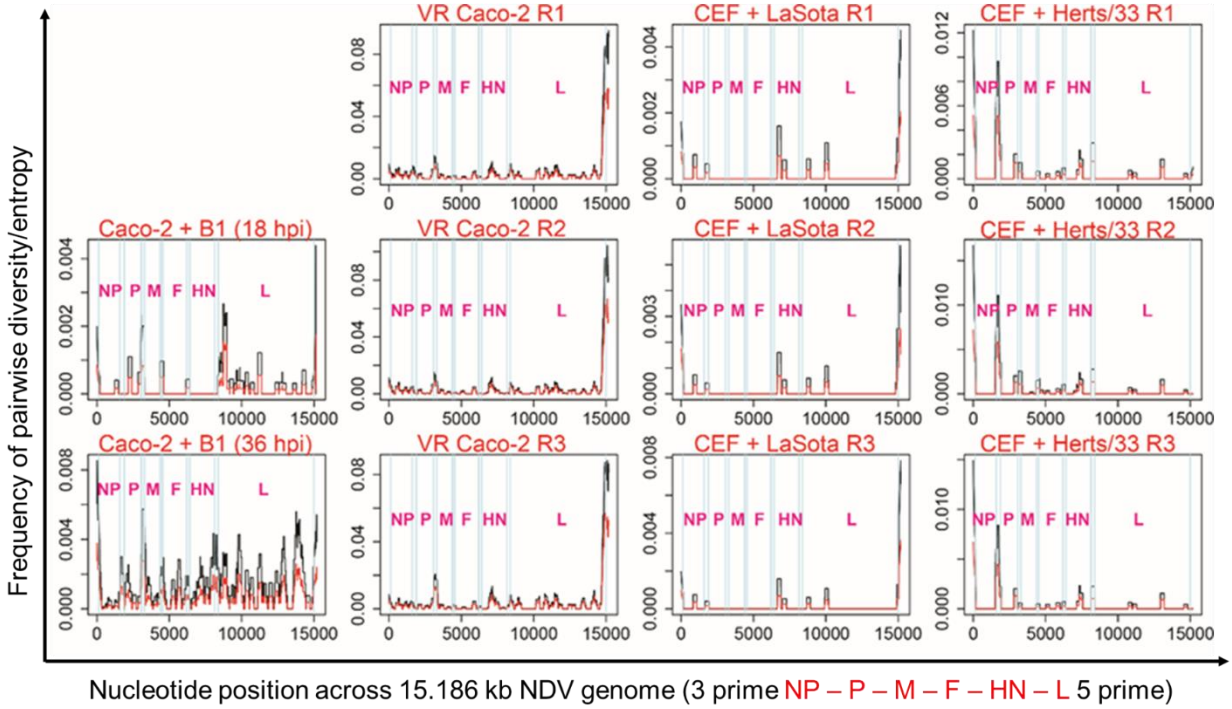

Figure 6.4. Measures of nucleotide diversity along the NDV genome across all the samples. The blue vertical lines represent the NDV gene boundaries (NP, P, M, F, HN, and L) in all samples, where R1, R2, and R3 represents three different biological replicates of infected VR Caco-2 or CEF cells with different NDV strains (All samples have running averages of 250 bases, reading depth ≥400, and all variants with frequency ≥0.005). Pairwise diversity showed in red colour and entropy in black colour.

The patterns of SNP density along the genome differ clearly across samples and genes **(Figure 6.3)**. There is a strong excess of SNPs at the 3 prime end for acute infections (B1 36 hpi in Caco-2 cells and Herts/33 12 hpi in CEF cells) contrasted by an excess at the 5 prime end for the other samples (B1 18 hpi in Caco-2 cells, persistent NDV in VR Caco-2 cells, and LaSota 12 hpi in CEF cells). Some general features are the concentration of SNPs in noncoding regions (between two genes and 3 prime/5 prime ends). Although with different patterns depending on the sample: for example, mutations in Caco-2 samples lie mostly between P and M genes, while in Herts/33 infected CEF cells they are concentrated between NP and P genes. Among coding regions, only the HN gene shows peaks systematically in SNP density.

The same different patterns are visible in nucleotide diversity and entropy across different samples and genes **(Figure 6.4).** There is a strong excess of pairwise diversity at the 3 prime endfor acute infections (B1 36 hpi in Caco-2 cells and Herts/33 12 hpi in CEFcells) contrasted by an excess at the 5 prime end for the other samples (B1 18hpi in Caco-2 cells, persistent NDV in VR Caco-2 cells, and LaSota 12 hpi in CEFcells). Some general features are the concentration of pairwise diversity in noncoding regions of B1-infected Caco-2 cells at 36 hpi (between two genes and 3 prime/5 prime ends). These differences could be due to mutational patterns or different selection pressures.

6.2.2. The frequency spectrum of mutations of NDV cultured in Caco-2 and CEF cells

The frequency distribution of mutations hints at dynamic, demographic and selective processes within the viral population (290, 291). Most of the distributions illustrated in **Figure 6.5** for all samples show a spectrum strongly concentrated around low frequencies. This is expected for viral swarms generated by a large number of slightly deleterious mutations. It is also expected for rapidly expanding populations, such as viral ones during acute infections. Even the spectrum of Herts/33 virus-infected CEF cells, despite some amount of common mutations, is strongly skewed towards rare mutations.

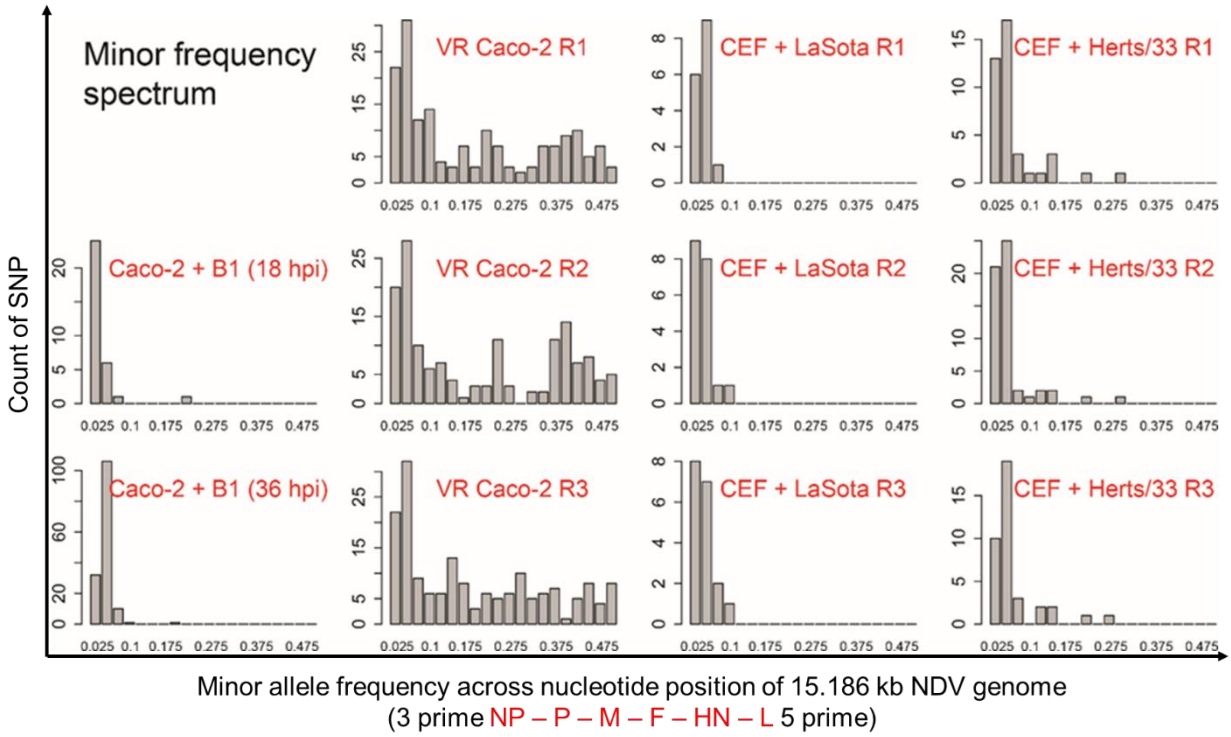

Figure 6.5. Mutation site frequency spectrum for SNPs across all samples. They are shown as histograms of the number of SNPs with a given minor allele frequency. All these spectra are concentrated around low frequencies, as expected from population genetics and quasi-species theory (All samples have running averages of 250 bases, reading depth ≥400, and all variants with frequency ≥0.005).

A simple way to visualise and quantify such an effect is the Tajima's D statistics, which is defined as the relative difference of pairwise nucleotide diversity and SNP density after the latter is normalised by a factor of |*log (minimum frequency)*| to account for the different scale of the two statistics (290, 291). Tajima's D statistic illustrates the deviations from the equilibrium between common variants (which contribute positively) and rare variants (which contribute negatively), and it is about 0 in neutrally evolving populations of constant size. The values for all datasets are illustrated in **Figure 6.6**.

The viral populations in VR Caco-2 cells clearly contain many common variants. This excess cannot be explained purely by the fact that the population is stable as the value of Tajima's D is positive for all VR Caco-2 samples (from passage 25) (**Figure 6.6**). Such an abundance of common variants suggests that the quasi-species in VR Caco-2 cells have a strong subpopulation structure with multiple possibly interacting components. These subpopulations could be maintained by complex selective pressures, ecological interactions or multiple niches in persistently-infected VR Caco-2 cells. These results suggest that a pool of complex viral population is present in the persistently NDV-infected VR Caco-2 cells.

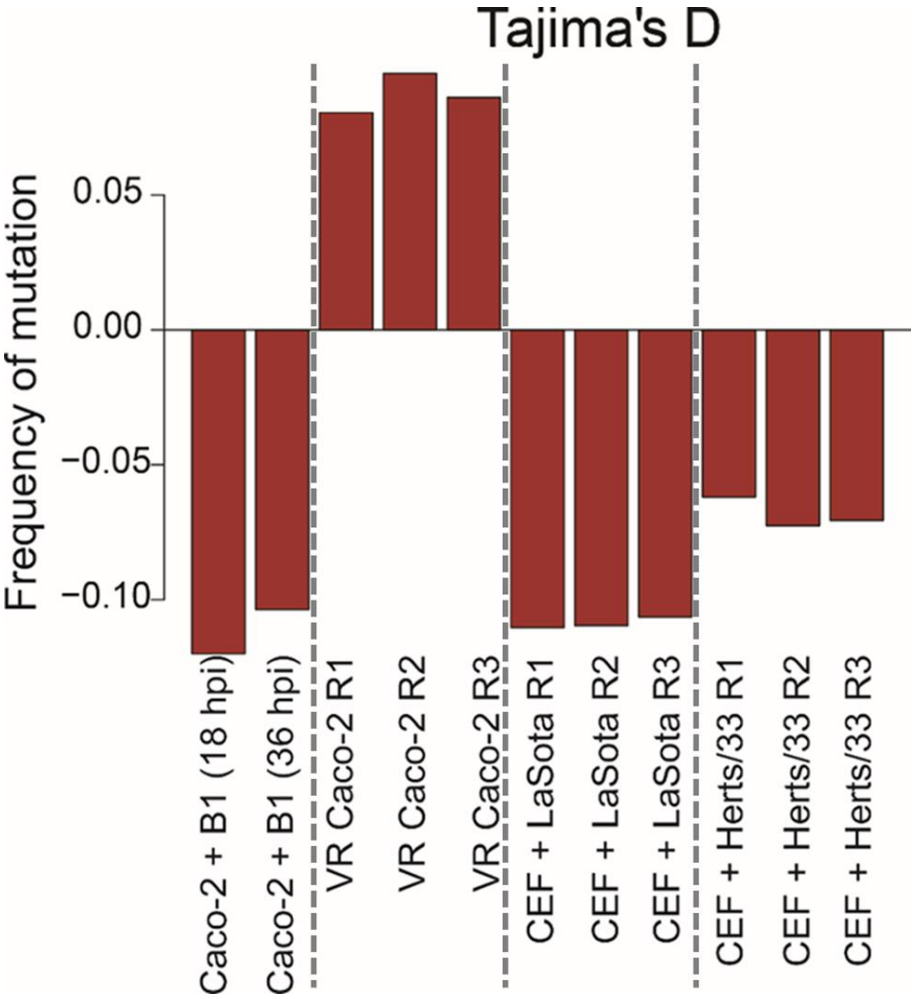

Figure 6.6. Tajima's D (a measure of the relative abundance of common vs rare alleles) across all samples. Most values are negative, i.e. variants are mostly rare. The exception is VR Caco-2 samples, which displayed many common variants at intermediate frequencies. Herts/33 also showed a slightly higher number of common variants.

6.2.3. Selection pressure on polymorphisms in coding sequences

The location represents a key feature to understand selection pressure on polymorphisms – and by extension of the functional role – of the variants. **Figure 6.7** show the frequency, location, and annotation of all variants in terms of whether coding or noncoding of the general location and the specific location within a codon.

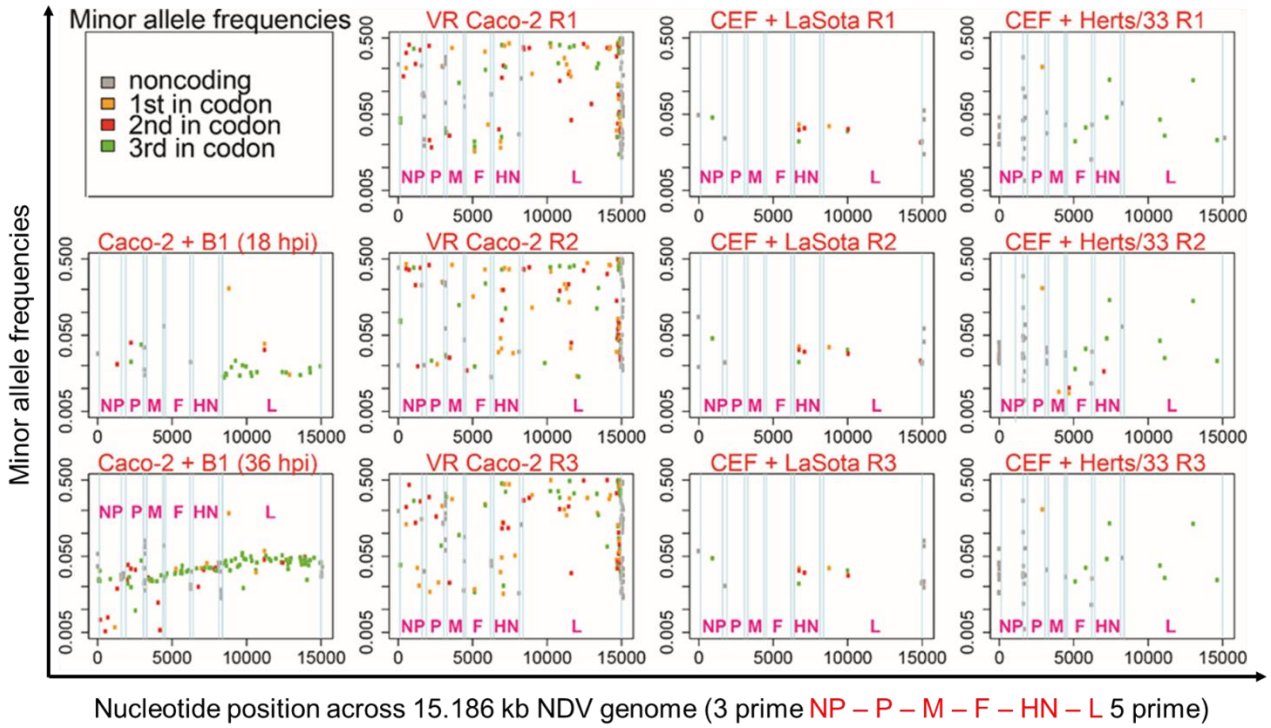

Figure 6.7. Location, frequency and classification of all SNPs across all samples. The blue vertical lines represent the NDV gene boundaries (NP, P, M, F, HN, and L) in all samples, where R1, R2, and R3 represents three different biological replicates of infected VR Caco-2 or CEF cells with different NDV strains (All samples have running averages of 250 bases, reading depth ≥400, and all variants with frequency ≥0.005).

In particular, the comparison of 1st and 2nd base of each codon with the 3rd one has made to estimate if selection acts at coding and noncoding region of the nucleotide sequence. Since mutations in 1st and 2nd bases are most often nonsynonymous and mutation in 3rd bases are most often synonymous, the comparison 1st/2nd versus 3rd base is a good proxy for nonsynonymous/synonymous comparisons and therefore for selection at the level of the protein sequence. The selection at the nucleotide level on coding sequences (3rd base only) and noncoding ones compared to estimate if selection acts on the nucleotide sequence as well. To do so, bases that are contained in the mRNA but usually not involved in the determination of the protein sequence are compared (i.e. the 3rd base of each codon) with bases that are not contained in the coding sequence at all (bases in noncoding regions). This approach would reveal the selection on the coding vs non-coding RNA.

A summary of the comparisons can be seen in **Figure 6.8**. Purifying selection appears to be quite strong for acute infections, but weak for persistent or milder infections. On the other hand, most samples show a strong purifying selection on the 3rd base. The latter signal could be spurious and related to hypermutability at some of the noncoding sites as

variants tend to be highly localised in small regions at 3 prime or 5 prime end of the genome (**Figure 6.7**).

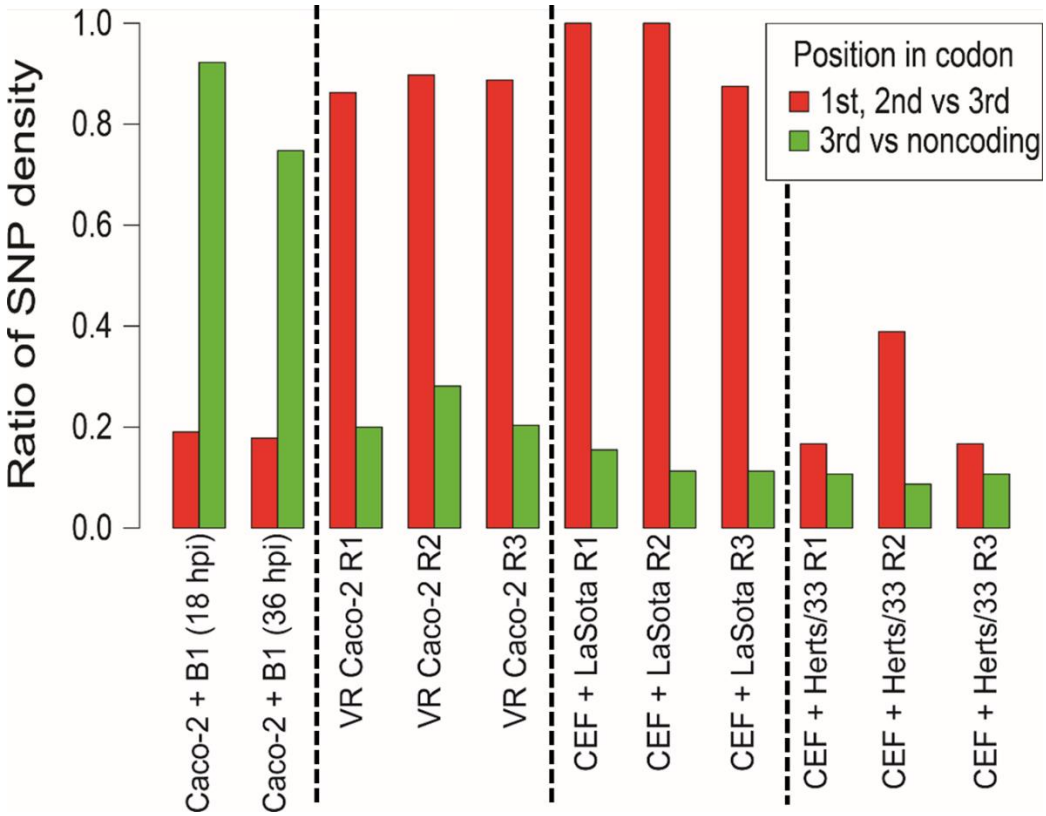

Figure 6.8. Measures of selection related to comparison of nonsynonymous to synonymous variants ratio. When these ratios are close to 1, selective pressures are similar for the two classes. In a red, relative number of SNPs located in 1st and 2nd base of codons versus 3rd base. This is a measure of selection on amino acid (protein) sequences. Purifying selective pressures appear to be present in acute virulent infections (acute B1 in Caco-2 cells and Herts/33 in CEF cells). In green, SNPs in 3rd base of codons versus noncoding SNPs. This is a measure of selective pressure on gene sequences at the RNA level. Note that hypermutability in specific noncoding regions between two genes or at 3 prime or 5 prime end of the genome could be affecting this measure.

6.2.4. Comparison between phylogenetic divergence and within-sample polymorphisms divergence between different NDV sequences from the same genotype

The comparison of the amount of polymorphic (synonymous or nonsynonymous) sites within and between populations – i.e. the analysis of polymorphisms versus divergence - is a popular tool to find regions of the genome under selection (290, 291). This comparison is useful because it is not affected by mutational biases favouring mutations at specific

locations in the genome: such biases would affect polymorphisms and divergence equally, and therefore disappear in the comparison

Patterns of NDV polymorphisms in Herts/33 virus-infected CEF cells differed from patterns of divergence in genotype IV (sequences in red in the tree in **Figure 6.9**). The divergence is quite homogeneous among coding regions and peaks in noncoding ones, while polymorphisms are skewed towards the noncoding 3 prime end of the genome and the noncoding region between the NP and P genes (**Figure 6.11**). Patterns of NDV polymorphisms in VR Caco-2 cells also bear little resemblance to the patterns of divergence in genotype II (**Figure 6.12**). A high level of polymorphisms in the L gene (which is quite conserved at the phylogenetic level) was observed possibly due to purifying selection pressure. The relatively low levels of noncoding polymorphism observed in the region between the NP and P genes. Also, relatively low levels of polymorphisms in coding regions of P gene. A relatively high levels of polymorphisms observed in noncoding region between P and M genes, and high polymorphisms at the 5 prime end of the genome of genotype II samples (**Figure 6.10**).

These results point to strong differences in the patterns of within-culture selection and the selective pressures between host cells. These differences could be related to the complex interactions between the different components of the quasi-species in VR Caco-2 cells and the related selective pressures. Sequences other than B1, LaSota, and Hets/33 from the genotype II and genotype IV were chosen randomly and were enough to represent selection pressure within multiple transmission within cultures in correspondence with polymorphism.

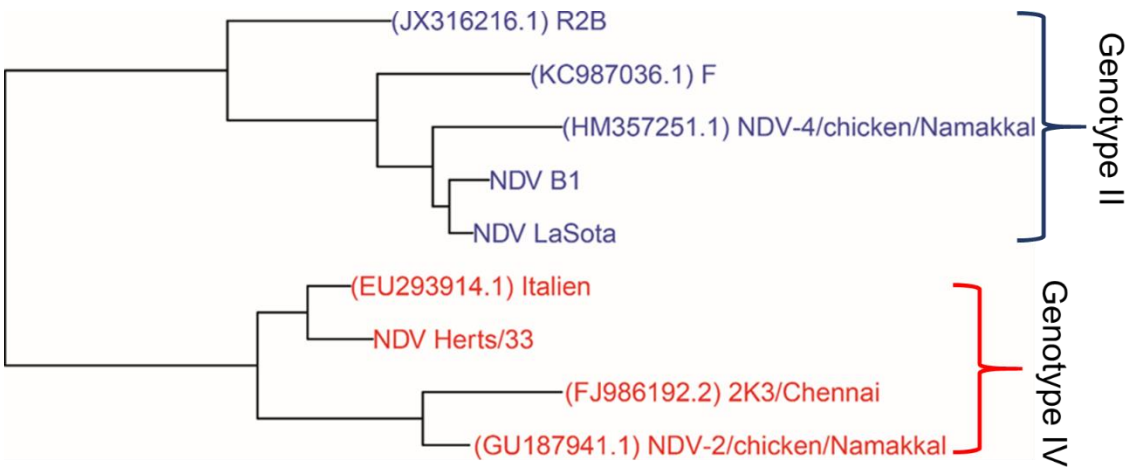

Figure 6.9. Neighbour-joining tree of avirulent NDV strains (genotype II, including LaSota and B1) and highly pathogenic strains (genotype IV, including Herts/33) used for the estimates of within-genotype divergence.

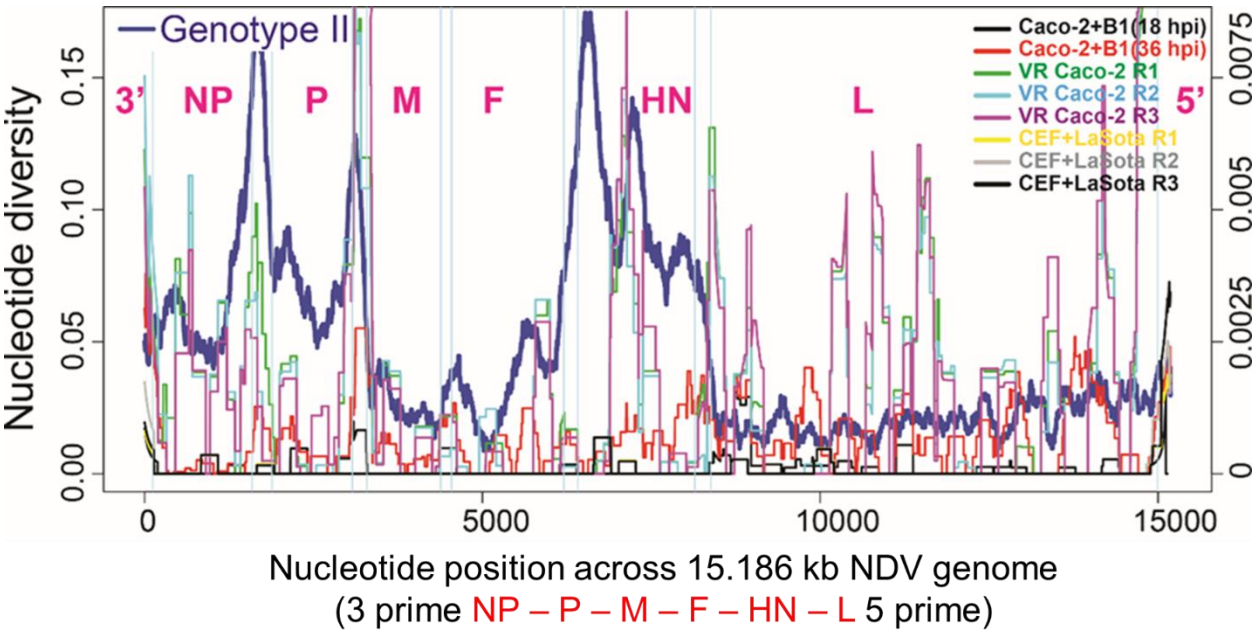

Figure 6.10. Comparison between patterns of divergence (scale on the left) and polymorphisms (nucleotide diversity, right) along the NDV genome for all samples in genotype II. (All samples have running averages of 250 bases, reading depth ≥400, and all variants with frequency ≥0.005).

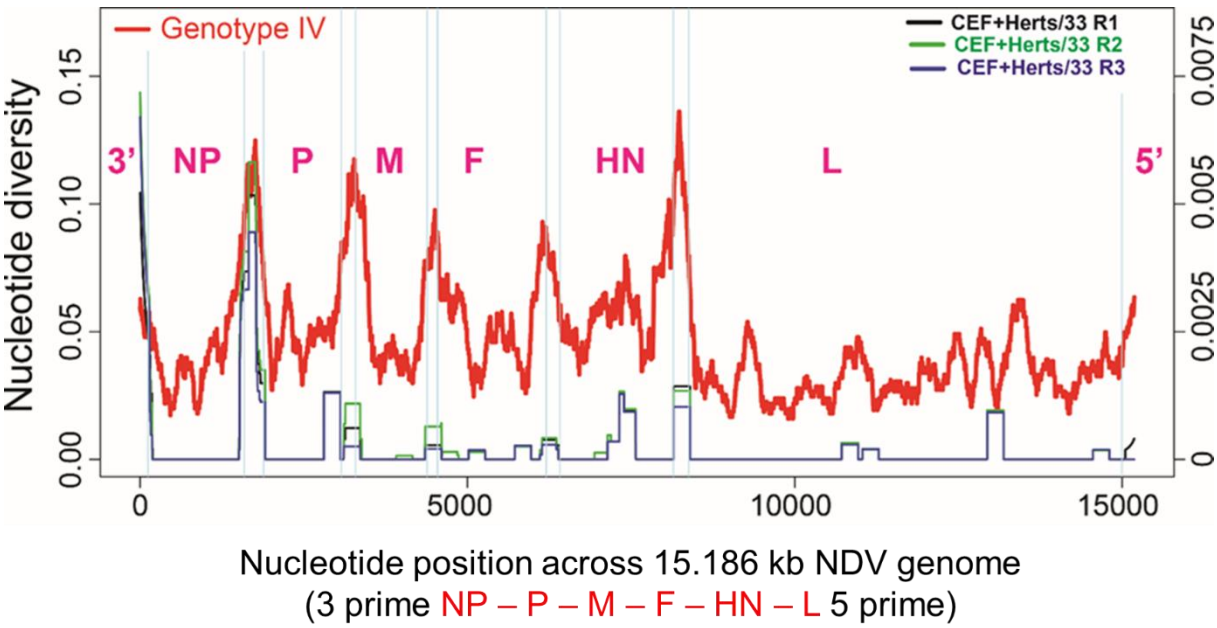

Figure 6.11. Comparison between patterns of divergence (scale on the left) and polymorphisms (nucleotide diversity, right) along the NDV genome for all samples in genotype IV. (All samples have running averages of 250 bases, reading depth ≥400, and all variants with frequency ≥0.005).

For VR Caco-2 cells, the patterns of nonsynonymous/synonymous mutations compared in coding regions. More precisely the average within-sample polymorphism or divergence

among genotype II sequences computed across the 1st and 2nd base in codons compared with the same quantities computed for the 3rd base in codons **(Figure 6.12)**.

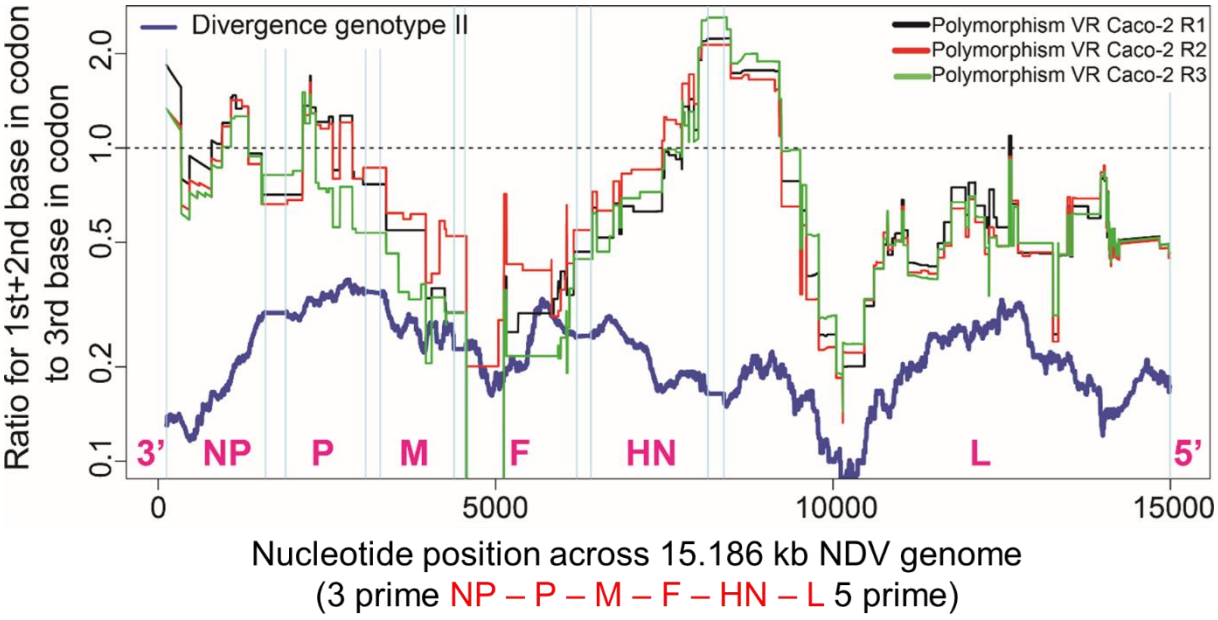

Figure 6.12. The ratio between polymorphisms (pairwise nucleotide diversity) or divergence estimated across the 1st and 2nd base of each codon versus the same quantities estimated for the 3rd base. (All samples have running averages of 250 bases, reading depth ≥400, and all variants with frequency ≥0.005).

Comparison between genotype divergence demonstrated that protein sequences are under strong purifying selection between cell lines derived from different hosts. On the other hand, polymorphisms show a trend towards positive selection (especially in NP and between HN and L genes) in VR Ccao-2 cells **(Figure 6.12)**. It is contrasting with strong purifying selection between M and F regions as well as in a region of the L gene located about 10000 bases from the 3 prime end of the genome which is also under strong between-host negative selection. This has confirmed significant differences in selection patterns within VR Caco-2 cells and highlights the functional role of NP, P and HN/L genes in quasi-species in persistent infections. The divergence genotype II analysis of VR Caco-2 cells demonstrated that high levels of polymorphism in HN gene where tail region of HN protein was found more conserved than globular head. The receptor binding avidity assay and comparative HN protein structure analysis of VR Caco-2 with B1 strain have confirmed mutation 10 mutation sites in globular head (discussed in details in **Figure 3.8** of chapter 3).

6.3. Conclusion

The presence of nucleotide variants and viral swarms is a common feature of RNA viruses, due to the error-prone nature of RNA polymerases. However, the structure and the selective forces on these swarms depend on the virus and the details of virus-host interactions. In this chapter, the patterns of nucleotide variants have shown within NDV samples. NDV viral swarms with a significant number of variants observed within all samples. This illustrates that NDV is also prone to generating viral swarms.

A limitation of this study is that the samples (presented in this chapter) were extracted from cell lines and therefore, do not necessarily share the same dynamics of viral populations from host tissues. Nevertheless, our findings suggest that such swarms could be found within NDV natural hosts as well. They could play a role both in the infection process and in the evolution of the virus, as happens for other RNA viruses.

It is already well known that variants in the NDV F (fusion) protein cleavage site can create a mixed population of lentogenic and velogenic viruses, which has a strong impact on the pathogenicity of the virus, but we do not observe any variant of significant frequency in that region (285, 292).

Purifying selection on viral swarms is likely to be partially shared at the within-host and between-host scales, because of structural constraints on proteins and RNA. Purifying selection could be weaker within hosts because of the lack of transmissibility constraints on viral sequences. A surprising amount of purifying selection was observed within the cell cultures: polymorphic bases were concentrated in small regions of the genome, most often in the noncoding areas, suggesting strong selection on the coding sequences. A possible alternative explanation for these findings could be hypermutability at some (noncoding) sites or even recombination hotspots, but there is no direct evidence of any of these phenomena.

The strongest signals of purifying selection on protein sequences were found in the samples from highly pathogenic infections. Viral populations in these samples are expected to have experienced recent rapid expansion, reducing the impact of any form of selection, which is in contrast with the above observation. More samples and longer times post-infection, or longitudinal studies, would be needed to clarify the relevance of this effect.

Intra-host variants are often shaped by selective forces that act within host tissues or cell cultures and can be extremely different from the ones observed between hosts. In fact, a comparison between the genomic distribution of polymorphisms and substitutions revealed a mismatch among selection pressures in cultures and between hosts. However, the

number of variants was often not large enough to enable these patterns to be studied in detail.

Variants in viral swarms may interact, for example via complementation or positive selection on viral diversity itself. Such complex interactions represent the hallmarks of the so-called “quasi-species” dynamics. Rare variants characterise the quasi-species structure observed in NDV populations from acute infections, and it is typical of expanding viral swarms. No evidence was found of complex quasi-species structure or interactions, although it would be difficult to observe them in the early phase of acute infections, because of the small number of variants and their low frequency.

On the other hand, persistently infected VR Caco-2 cells revealed a rich and complex quasi-species structure. Variants at intermediate frequency suggest the presence of multiple subpopulations, possibly related to the heterogeneity of the host cell line or the complexity of the system and the different niches therein. These patterns suggest that these cells could harbour complex quasi-species dynamics in the proper sense. The profiles of variability observed here could indicate which genes are actually involved in these complex interactions. Variants in NP and HN were more abundant than expected based on the divergence between sequences belonging to genotype II, suggesting that those genes are involved in quasi-species dynamics. A nonsynonymous/synonymous polymorphism/divergence analysis of the quasi-species showed evidence of strong selection against amino acid polymorphisms in L, M and F, while amino acid polymorphisms in NP and P appear to be neutral on average, which is consistent with the potential role of these two genes in quasi-species interactions; amino acid variants in a region between HN and L was favoured by selection in VR Caco-2 cells, pointing to this genomic region as a further determinant of such interactions.

The role of quasi-species in the interaction between the viral population and Caco-2 cells is unclear, although the quasi-species structure could be related to the changes between naïve and persistently infected cells. Further deep sequence data from persistently infected Caco-2 cells could shed some light on the actual quasi-species dynamics.

Chapter 7

7 General Discussion

Oncolytic viruses (OVs) are gaining augmented attraction as a modern-day cancer therapy and are being utilised in extensive clinical trials worldwide (293). The United States Food and Drug Administration and the European Union in 2015 have already approved IMLYGIC™ (T-VEC/Talimogene Laherparepvec), a genetically engineered live-attenuated HSV-1, to treat post-operative melanoma in an advanced state (38, 39). The Chinese Food and Drug Administration in 2005 has also approved the only adenovirus-based Oncorine vaccine for the treatment of advanced head and neck cancer with a combination of chemotherapy (31). There are more than 40 OVs such as adenoviruses, poxviruses, HSV-1, coxsackieviruses, poliovirus, measles virus, Newcastle disease virus (NDV), reovirus etc., belonging to over 10 different viral families are presently used in ongoing clinical trials either as a combination therapy or monotherapy to study various malignancies (26). NDV is an avian pathogen and known for its oncolytic properties over five decades. It has also demonstrated its potential to be an effective oncovirotherapeutic in several phase-I/-II clinical trials (154, 294).

This thesis set out to test the oncolytic properties of avirulent strains of NDV such as Hitchner B1, B1-GFP, LaSota, LaSota-GFP, and Ulster in various human cancer cell lines (Caco-2, A549, HeLa, Hep G2, and PC3). The Hitchner B1, B1-GFP, and LaSota strains demonstrated effective oncolysis in a heterogenous colorectal Caco-2 cell line. The oncolytic potential of naturally occurring Hitchner B1 and Ulster strains were demonstrated in several pancreatic cancer cell lines (295). The Hitchner B1 strain was genetically modified by altering the cleavage site in F protein to polybasic cleavage site of hyperfusogenic F protein and also by the addition of the gene for GFP and luciferase. A genetically engineered B1 strain demonstrated increased oncolytic potential in murine colon cancer cell line (CT26) *in vitro* as well as *in vivo* CT26 tumour bearing mouse model (163) and also in human pancreatic, breast, thyroid, head and neck, and gastric cancers, as well as human and murine malignant melanoma cell lines (168). Here, naturally occurring Hitchner B1 and genetically modified B1-GFP both have demonstrated induced significant cytotoxicity *in vitro* in Caco-2 cells.

Despite the high levels of NDV-induced cell cytotoxicity in Caco-2 cells, all avirulent strains (Hitchner B1, B1-GFP, LaSota, and LaSota-GFP) of NDV used in this PhD project were

able to establish persistent infection in small a proportion of Caco-2 cells. The isolated persistently NDV-infected Caco-2 cells were named VR Caco-2 (virus-resistant Caco-2) cells. VR Caco-2 cells (persistently NDV-infected Caco-2 cells) developed different behaviour compared to uninfected Caco-2 cells, which included 2-times slower cell proliferation, and continuous production of recoverable replicating NDV viral particles with lower virus titres. The persistent NDV infection of cell lines is not a novel phenomenon, and it already has been demonstrated in infected with a highly pathogenic strain of NDV (Victoria) infected pancreatic mucinous cystic neoplasms (L(MCN)) cells (296), highly pathogenic AF2240 strain of NDV-infected colorectal cancer cell line SW480 (237), and moderately pathogenic strain 73T-GFP of NDV-infected ovarian cancer cell line OVCAR3 (238). Here, for the first time demonstrated that lentogenic/non-pathogenic strains of NDV established persistent infection in Caco-2 cells. All persistently NDV-infected cells (MCN, SW480, and OVCAR3) produced replicating NDV particles at lower viral titres than B1 and B1-GFP strains of NDV, and a similar outcome has been demonstrated in VR Caco-2 cells. The resistance to heterologous viruses such as VSV (vesicular stomatitis virus) and homologous viruses (NDV) superinfection have been demonstrated in persistently NDV-infected L(MCN) cells, and the resistance was potentially explained by non-infectious viral particles and IFN production in L(MCN) cells (296). A similar trend of resistance to superinfection with heterologous or homologous viruses has been demonstrated in persistently NDV-infected OVCAR3 cells, and the acquired resistance was demonstrated to be due to the production of IFN-β but not because of defective interfering viral particles. Persistently NDV-infected OVCAR3 cells have achieved an antiviral immune status by constitutive expression of type-I IFN and IFN-induced antiviral proteins such as RIG-I, MDA5, and Mx1 (238).

In contrast, the susceptibility of VR Caco-2 cells to other viruses such as AIV (avian influenza-H9N2) and VSV infections demonstrated while maintaining specific resistance to re-infection with NDV. The VSV infection has resulted in increased cell cytotoxicity of VR Caco-2 cells. Both Caco-2 and VR Caco-2 cells were demonstrated inefficient in the induction of *IFN-β* and *ISG15* mRNAs in response to various stimuli (viruses and synthetic mimic of dsRNA), suggesting that VR Caco-2 cells lacked the active type-I IFN-mediated antiviral immune response. The establishment of persistent NDV infection was investigated in A549 cells. The A549 cells were moderately susceptible to NDV-induced cytotoxicity only at higher viral doses. The persistent infection was not observed in A549 cells, potentially explained by active type-I IFN responses recorded as a significant induction of *IFN-β* and *ISG15* mRNAs upon NDV infection. Perhaps it suggests that the active type-I IFN pathways prevents NDV from establishing persistent infection in A549 cells.

In studies using VSV infection of BHK cell cultures, next-generation sequencing (NGS) approach has been utilised to characterise VSV defective interfering particles (DIPs) in BHK cell cultures and validated by quantitative reverse transcription-PCR (256). A similar approach can be used in future to examine the role of DIPs in VR Caco-2 cells to study its impact on persistent NDV infection.

The NDV in persistently infected OVCAR3 cells has confirmed the hyperfusogenic nature because of reported mutation in the cleavage site of NDV F protein at $F117_S$ and altered receptor binding of HN protein due to mutation in the second sialic acid binding site at $HN169_R$ (238). Also recently a switch from lytic to persistent infection of parainfluenza virus type 5 (PIV5) has been demonstrated in A549 cells due to the single mutation in one of the phosphorylation sites of P protein of PIV5 (253). The sequence analysis of F, HN, and P mRNA transcripts of NDV produced in VR Caco-2 cells have not identified any of the reported mutations in either of the protein. However, I have identified several mutations surrounding the antigenic site 23, HA, and NA active sites of HN protein as well as several sites in P protein of NDV produced from VR Caco-2 cells, which need further investigation to detect the effect of each mutation on persistent NDV infection in VR Caco-2 cells. I have also demonstrated that NDV from VR Caco-2 cells have 6-times higher receptor binding avidity to partially sialic acid depleted cRBCs than B1-GFP strain of NDV.

The integrated approach using RNA-seq and proteomic data was employed to estimate the impact of persistent NDV infection in VR Caco-2 cells in comparison with uninfected Caco-2 cells. The integrated analysis has shown the activation of p53-independent G1/S DNA damage checkpoint, p53-Dependent G1 DNA damage response, and regulation of apoptosis in VR Caco-2 cells. The DNA damage response (DDR) pathways activation have been reported in various RNA virus-infected cells responsible for the instigation of inflammatory responses, activation of apoptotic cell death, and promotion of genomic instability leading to the increased risk of tumourigenesis (138). The activation of apoptotic cell death has been demonstrated in highly pathogenic NDV AF2240 strain infected GBM cells, which was identified by the loss in DNA in treated cells in G1, S and G2/M phases of the cell cycle, and shrinkage and blebbing of the membrane (140). The RNA-seq data from acutely NDV-infected Caco-2 and CEF cells have also confirmed the activation of DNA damage pathways. The PIV5 virus mutant P/V-CPI has demonstrated to establish persistent infection in human laryngeal cancer HEp-2 cells, and persistently infected cells have demonstrated an increase in sensitivity to cisplatin-induced DNA damage and cell death. The persistently infected HEp-2 cells have also shown the increased basal caspase activation, and cell viability was dependent on the activity of cellular inhibitors of apoptosis

(IAPs) such as survivin and XIAP. Also, cisplatin-induced cell death was found to be associated with DNA damage signalling pathways such as Chk1 phosphorylation and nuclear translocation of damage-specific DDB1 protein (DNA damage binding protein 1) (297). Likewise, the investigation of various DDR pathways in acute and persistent NDV-infected Caco-2 cells is required to understand the mechanism of NDV-induced oncolysis as well as to identify pathways exploited by the virus in order to survive persistent NDV infection.

The RNA-seq data analysis of persistently NDV-infected VR Caco-2 cells has demonstrated extensive changes in the regulation of 10039 genes while maintaining 50-times lower viral burden compared to acute NDV-infection 36 hpi at 0.1 MOI in Caco-2 cells. The transcriptomic analysis has revealed the upregulation of antiviral responses associated with ISGs such as *IL15*, *OASL*, *IFIT1*, *C3*, *CASP1*, *DDX60* etc., and pathways included IFN-signalling, cytokine regulation and TLR activation by endogenous ligands in VR Caco-2 cells compared to uninfected and acutely NDV-infected Caco-2 cells. These pathways and ISGs need to be validated in both persistently and acutely NDV- infected Caco-2 cells. Caco-2 cells are heterogeneous cell line and when grown as a 3D (3-Dimensional) culture in rotating wall culture vessel attains multicellular complexity by an intestinal cell differentiation to the intestinal epithelium, with apical-basolateral polarity, brush borders, the formation of well-developed tight junctions (249). The RNA-seq data analysis has shown that VR Caco-2 cells have attained more complexity by regulating intestinal differentiation markers such as *MUC 17, SLC10A1, MS4A10, Orm2, SLC38A4*, and *ALB* compared to the acutely NDV-infected and uninfected Caco-2 cells. It seems that the complexity of Caco-2 and VR Caco-2 cells with or without NDV need to be investigated further by culturing in the 3D model. The heterogeneity of Caco-2 cells and NDV infection seems to play a role in persistent infection apart from its inefficient *IFN-β* mRNA induction. The heterogeneity of Caco-2 cells and NDV population can be investigated further by considering the single-cell sequencing and epigenomics study.

NDV is also known to induce autophagy upon infection and activates several signalling pathways leading to cell death. SQSTM1/p62 is a multifunctional and multidomain signalling adapter molecule required for selective autophagy. The induction of autophagic cell death has been demonstrated in human cancer cells (141, 265, 277) and chicken cells (266, 278) by observing the fluctuation in SQSTM1/p62 protein along with the conversion of LC3-II with or without NDV infection. I have demonstrated degradation of SQSTM1/p62 in NDV-infected Caco-2 cells, and detailed investigation is required to identify the importance of autophagy in NDV-infected Caco-2 cells.

According to the International Agency for Research on Cancer (IARC) 2018 report, colorectal cancer was the second most common cause of cancer death worldwide. The Caco-2 cells can be an excellent model to study virotherapy, given its heterogeneous complexity and confirmed susceptibility to NDV-induced oncolysis. However, to understand the mechanism of NDV-induced oncolysis in Caco-2 cells the persistent infection and its impacts on NDV-induced oncolysis need to be addressed *in vitro* as well as *in vivo* studies before considering the development of NDV vaccines for clinical trials. The results generated in this PhD project strongly suggest that NDV establish not only persistent infection but also reduce NDV-induced cytotoxicity while regulating thousands of genes in Caco-2 cells.

In this PhD project, the main focus was on identifying the immune response and antiviral mechanisms underlying the persistence of the NDV in VR-Caco-2 cells. However, persistent infection in Caco-2 cells resulted only from a small population of surviving cells. It opens up the possibility to investigate the role of cancer stem cells (CSCs) in Caco-2 cells for the establishment of persistent NDV infection. The CSCs are class of self-renewing pluripotent cancer cells having an ability to participate in tumour development, cell proliferation, metastatic dissemination, drug resistance, and tumour recurrence in various types of cancers such as breast, brain, liver, lung, gastric, colon, prostate etc. (298). Several cell surface markers have been identified for colorectal CSCs such as CD44, CD133, CD24, EpCAM, LGR5 and ALDH (299). Recently the expression profiles of all identified surface markers of colorectal CSCs in 8 different colorectal cancer cell lines including Caco-2 cells, demonstrating the heterogeneous population of Caco-2 cells expressing different CSCs markers from large $CD133^{+}CD26^{high}$ and $CD133^{high}/CD26^{high}$ subsets (300). In future, the availability of detailed data on the transcriptome of Caco-2 and VR-Caco-2 cells will allow in-depth analysis of expression of CSC markers and metabolic pathways that can throw light as to whether the VR-Caco-2 cells have a distinct profile that has enabled them to overcome the NDV-induced cytotoxic killing, leading to different virus-host interaction resulting in viral persistence.

Chapter 8- Appendix

The data generated from the mass spectrometry (MS) analysis of persistently NDV-infected VR Caco-2 and uninfected Caco-2 cells is shown in this Appendix. Here **Figure 8.1** and **Figure 8.2** represents the heat maps of MS analysis in both samples, whereas **Table 8.1** represents most differentially expressed proteins in VR Caco-2 in comparison with the uninfected Caco-2 cells. Table contains proteins sharing the same set or subset of peptides as a protein group, protein identifier (protein ID), protein accession name (accession), the confidence score, (-10Log(P)), the percentage of protein sequence covered by identified peptides (Coverage %), the total number of distinct peptide sequences identified in the protein group (peptides), the number of peptide sequences that are unique to the protein group (the peptides that are common to the proteins of a protein group and which do not occur in the proteins of any other group-Unique peptides), any post-translational modifications found on the peptides (PTM) and description of the protein (description). For each protein, the confidence score was calculated (-10lgP), which is the cumulative value of p; the probability of the identified peptide sequence occurring randomly, for each unique peptide identified. The higher the confidence score, the higher the confidence in protein identification. Scores above 20 ($p< 0.01$) were seen as high confidence, and anything below was eliminated. The data was further filtered by setting the coverage percentage to 1% to reduce false discovery. The results were also filtered for the data to only include proteins with 2 or more unique peptides to increase confidence further.

Viral proteins (P, F, and W) overexpressed in VR Caco-2 cells are highlighted in **Figure 8.1** and **Table 8.1**.

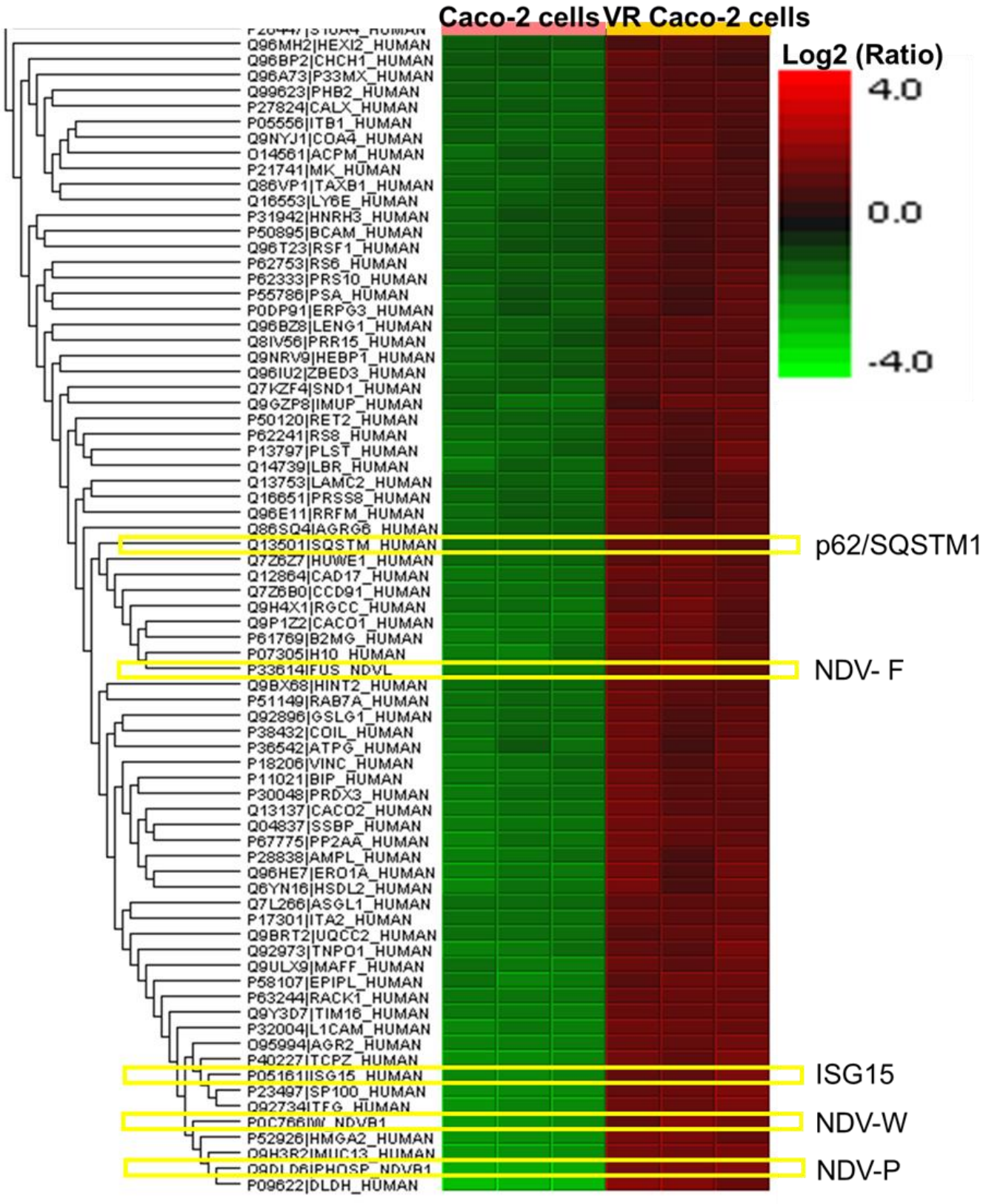

Figure 8.1. The sets and subsets of highly overexpressed proteins in VR Caco-2 cells. The proteins are shown in dark brown colour are significantly abundant in VR Caco-2 cells in comparison with the uninfected Caco-2 cells.

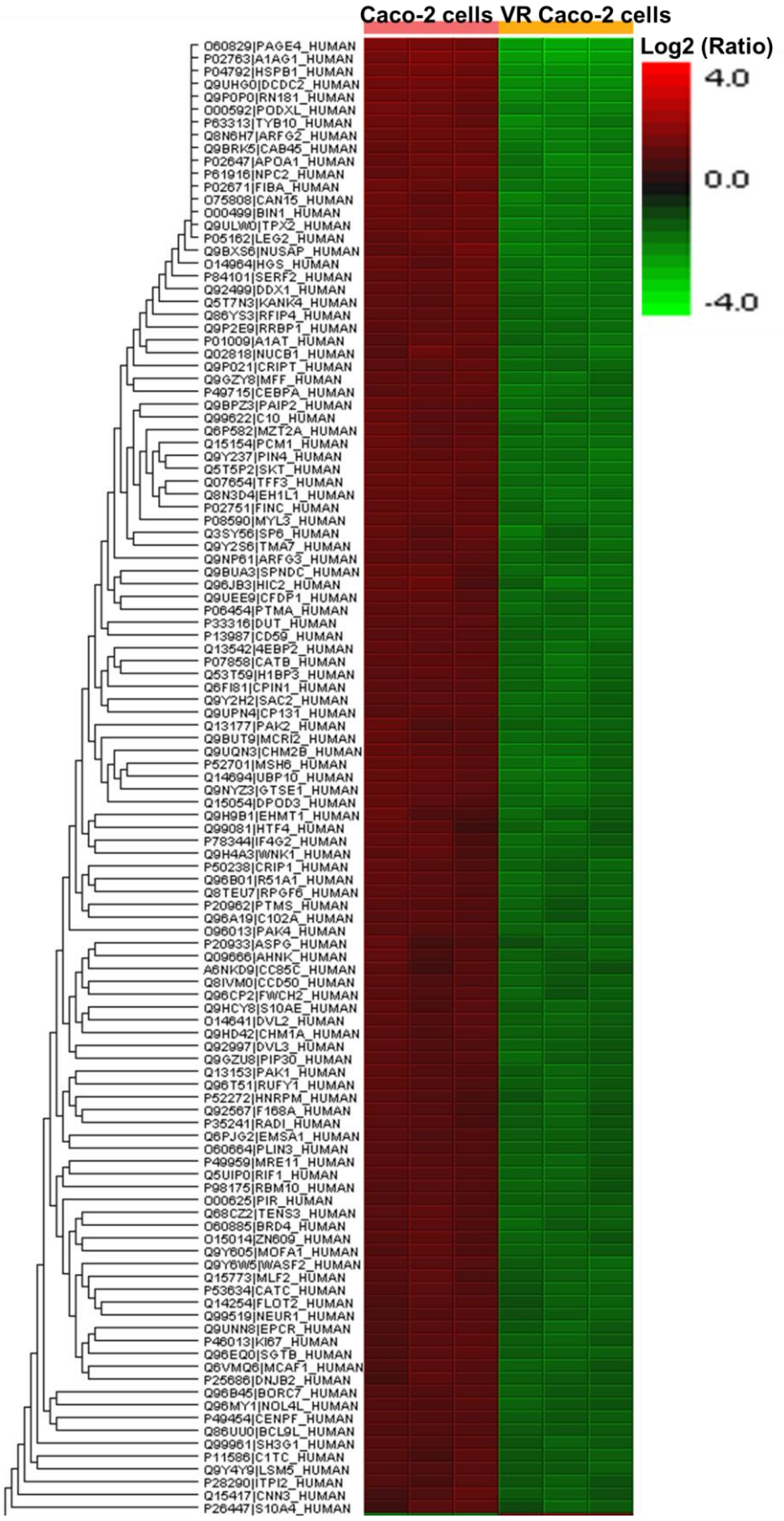

Figure 8.2. The sets and subsets of highly underexpressed proteins in VR Caco-2 cells. The proteins are shown in green colour are significantly lower in abundance in VR Caco-2 cells in comparison with the uninfected Caco-2 cells. There are more proteins significantly under-expressed in VR Caco-2 cells.

Table 8.1. List of significantly under- or over-expressed proteins in VR Caco-2 cells in comparison with uninfected Caco-2 cells.

Sr. No.	Protein Group	Protein ID	Accession	-10lgP	Coverage (%)	Peptides	Unique peptides	PTM	Description
1	156	136225	P09622|DLDH_HUMAN	320.52	50	27	27	Carbamidomethylation; TMT6plex; Oxidation (M)	Dihydrolipoyl dehydrogenase mitochondrial OS=Homo sapiens OX=9606 GN=DLD PE=1 SV=2
2	642	136774	Q9DLD6|PHOSP_NDVB1	214.12	13	11	6	Carbamidomethylation; TMT6plex	Phosphoprotein OS=Newcastle disease virus (strain Chicken/United States/B1/48) OX=652953 GN=P PE=3 SV=1
3	683	137357	Q9H3R2|MUC13_HUMAN	190.16	13	4	4	TMT6plex	Mucin-13 OS=Homo sapiens OX=9606 GN=MUC13 PE=1 SV=3
4	392	136859	P52926|HMGA2_HUMAN	250.89	82	15	13	TMT6plex	High mobility group protein HMGI-C OS=Homo sapiens OX=9606 GN=HMGA2 PE=1 SV=1
5	901	137190	P0C766|W_NDVB1	176.01	10	7	2	TMT6plex	Protein W OS=Newcastle disease virus (strain Chicken/United States/B1/48) OX=652953 GN=W PE=3 SV=1
6	246	136707	P23497|SP100_HUMAN	219.75	7	14	5	Carbamidomethylation; TMT6plex	Nuclear autoantigen Sp-100 OS=Homo sapiens OX=9606 GN=SP100 PE=1 SV=3
7	958	137741	Q92734|TFG_HUMAN	146.65	8	4	4	TMT6plex	Protein TFG OS=Homo sapiens OX=9606 GN=TFG PE=1 SV=2
8	705	137143	P40227|TCPZ_HUMAN	210.36	15	8	8	TMT6plex	T-complex protein 1 subunit zeta OS=Homo sapiens OX=9606 GN=CCT6A PE=1 SV=3
9	1986	138146	P05161|ISG15_HUMAN	95.5	15	3	3	TMT6plex	Ubiquitin-like protein ISG15 OS=Homo sapiens OX=9606 GN=ISG15 PE=1 SV=5
10	225	136520	O95994|AGR2_HUMAN	276.94	66	25	25	Carbamidomethylation; TMT6plex; Oxidation (M)	Anterior gradient protein 2 homolog OS=Homo sapiens OX=9606 GN=AGR2 PE=1 SV=1
11	2613	139770	P32004|L1CAM_HUMAN	48.02	2	2	2	TMT6plex	Neural cell adhesion molecule L1 OS=Homo sapiens OX=9606 GN=L1CAM PE=1 SV=2

Sr. No.	Protein Group	Protein ID	Accession	-10lgP	Coverage (%)	Peptides	Unique peptides	PTM	Description
12	850	137352	P33614|FUS_NDVL	166.87	9	7	7	TMT6plex	Fusion glycoprotein F0 OS=Newcastle disease virus (strain Chicken/United States/LaSota/46) OX=11184 GN=F PE=3 SV=1
13	850	137353	P33613|FUS_NDVH4	166.87	9	7	7	TMT6plex	Fusion glycoprotein F0 OS=Newcastle disease virus (strain B1-Hitchner/47) OX=11181 GN=F PE=3 SV=1
14	2414	138157	Q96HE7|ERO1A_HUMAN	91.08	5	2	2	TMT6plex	ERO1-like protein alpha OS=Homo sapiens OX=9606 GN=ERO1A PE=1 SV=2
15	1659	138387	P58107|EPIPL_HUMAN	62.19	1	3	2	TMT6plex	Epiplakin OS=Homo sapiens OX=9606 GN=EPPK1 PE=1 SV=3
16	1394	137989	Q9Y3D7|TIM16_HUMAN	151.08	37	3	3	TMT6plex	Mitochondrial import inner membrane translocase subunit TIM16 OS=Homo sapiens OX=9606 GN=PAM16 PE=1 SV=2
17	1835	138077	Q92973|TNPO1_HUMAN	98.28	3	3	2	Carbamidomethylation; TMT6plex	Transportin-1 OS=Homo sapiens OX=9606 GN=TNPO1 PE=1 SV=2
18	1949	138130	P67775|PP2AA_HUMAN	68.56	7	3	3	TMT6plex	Serine/threonine-protein phosphatase 2A catalytic subunit alpha isoform OS=Homo sapiens OX=9606 GN=PPP2CA PE=1 SV=1
19	2247	140533	Q6YN16|HSDL2_HUMAN	80.5	6	2	2	TMT6plex	Hydroxysteroid dehydrogenase-like protein 2 OS=Homo sapiens OX=9606 GN=HSDL2 PE=1 SV=1
20	2614	139994	Q9ULX9|MAFF_HUMAN	59.88	10	2	2	Carbamidomethylation; TMT6plex	Transcription factor MafF OS=Homo sapiens OX=9606 GN=MAFF PE=1 SV=2
21	1165	137645	P63244|RACK1_HUMAN	89.91	14	4	4	Carbamidomethylation; TMT6plex	Receptor of activated protein C kinase 1 OS=Homo sapiens OX=9606 GN=RACK1 PE=1 SV=3
22	2332	138135	Q9P1Z2|CACO1_HUMAN	92.73	4	2	2	TMT6plex	Calcium-binding and coiled-coil domain-containing protein 1 OS=Homo sapiens OX=9606 GN=CALCOCO1 PE=1 SV=2
23	469	136964	Q04837|SSBP_HUMAN	224.38	63	10	10	TMT6plex; Oxidation (M)	Single-stranded DNA-binding protein mitochondrial OS=Homo sapiens OX=9606 GN=SSBP1 PE=1 SV=1

Sr. No.	Protein Group	Protein ID	Accession	-10lgP	Coverage (%)	Peptides	Unique peptides	PTM	Description
24	125	136406	P07305|H10_HUMAN	280.74	55	28	28	TMT6plex; Oxidation (M); Acetylation (N-term)	Histone H1.0 OS=Homo sapiens OX=9606 GN=H1F0 PE=1 SV=3
25	1596	137421	P28838|AMPL_HUMAN	128.65	8	4	4	TMT6plex	Cytosol aminopeptidase OS=Homo sapiens OX=9606 GN=LAP3 PE=1 SV=3
26	1508	137905	P61769|B2MG_HUMAN	116.89	30	4	4	Carbamidomethylation; TMT6plex	Beta-2-microglobulin OS=Homo sapiens OX=9606 GN=B2M PE=1 SV=1
27	1710	137848	Q13137|CACO2_HUMAN	117.46	10	3	3	Carbamidomethylation; TMT6plex; Oxidation (M)	Calcium-binding and coiled-coil domain-containing protein 2 OS=Homo sapiens OX=9606 GN=CALCOCO2 PE=1 SV=1
28	1161	137616	P17301|ITA2_HUMAN	132.11	5	4	4	TMT6plex	Integrin alpha-2 OS=Homo sapiens OX=9606 GN=ITGA2 PE=1 SV=1
29	29	136151	P11021|BIP_HUMAN	424.26	72	64	60	Carbamidomethylation; TMT6plex; Oxidation (M)	Endoplasmic reticulum chaperone BiP OS=Homo sapiens OX=9606 GN=HSPA5 PE=1 SV=2
30	2514	139105	Q9BRT2|UQCC2_HUMAN	75.22	16	2	2	TMT6plex	Ubiquinol-cytochrome-c reductase complex assembly factor 2 OS=Homo sapiens OX=9606 GN=UQCC2 PE=1 SV=1
31	299	136312	Q12864|CAD17_HUMAN	292.38	30	23	22	Carbamidomethylation; TMT6plex; Oxidation (M)	Cadherin-17 OS=Homo sapiens OX=9606 GN=CDH17 PE=2 SV=3
32	2611	139471	Q9H4X1|RGCC_HUMAN	117.64	37	2	2	TMT6plex	Regulator of cell cycle RGCC OS=Homo sapiens OX=9606 GN=RGCC PE=1 SV=1
33	652	136342	P18206|VINC_HUMAN	258.91	19	17	17	Carbamidomethylation; TMT6plex	Vinculin OS=Homo sapiens OX=9606 GN=VCL PE=1 SV=4
34	724	137456	P30048|PRDX3_HUMAN	165.37	22	5	5	TMT6plex	Thioredoxin-dependent peroxide reductase mitochondrial OS=Homo sapiens OX=9606 GN=PRDX3 PE=1 SV=3
35	1128	137056	Q7Z6B0|CCD91_HUMAN	147.48	17	8	8	Carbamidomethylation; TMT6plex	Coiled-coil domain-containing protein 91 OS=Homo sapiens OX=9606 GN=CCDC91 PE=1 SV=2

Sr. No.	Protein Group	Protein ID	Accession	-10lgP	Coverage (%)	Peptides	Unique peptides	PTM	Description
36	2533	138271	Q7L266|ASGL1_HUMAN	73.91	6	2	2	Carbamidomethylation; TMT6plex	Isoaspartyl peptidase/L-asparaginase OS=Homo sapiens OX=9606 GN=ASRGL1 PE=1 SV=2
37	605	136766	P51149|RAB7A_HUMAN	214.33	40	8	8	Carbamidomethylation; TMT6plex	Ras-related protein Rab-7a OS=Homo sapiens OX=9606 GN=RAB7A PE=1 SV=1
38	1236	137399	P38432|COIL_HUMAN	104.11	6	4	4	TMT6plex	Coilin OS=Homo sapiens OX=9606 GN=COIL PE=1 SV=1
39	574	136974	Q14739|LBR_HUMAN	158.64	15	13	13	TMT6plex	Delta (14)-sterol reductase OS=Homo sapiens OX=9606 GN=LBR PE=1 SV=2
40	2001	137946	Q7Z6Z7|HUWE1_HUMAN	128.37	2	3	3	TMT6plex	E3 ubiquitin-protein ligase HUWE1 OS=Homo sapiens OX=9606 GN=HUWE1 PE=1 SV=3
41	1277	137918	Q9GZP8|IMUP_HUMAN	133.28	42	3	3	TMT6plex; Oxidation (M); Acetylation (N-term)	Immortalization up-regulated protein OS=Homo sapiens OX=9606 GN=IMUP PE=1 SV=1
42	1964	138117	P36542|ATPG_HUMAN	84.66	11	3	3	TMT6plex	ATP synthase subunit gamma mitochondrial OS=Homo sapiens OX=9606 GN=ATP5F1C PE=1 SV=1
43	728	136539	Q92896|GSLG1_HUMAN	205.32	10	9	9	Carbamidomethylation; TMT6plex	Golgi apparatus protein 1 OS=Homo sapiens OX=9606 GN=GLG1 PE=1 SV=2
44	328	136746	Q9BX68|HINT2_HUMAN	256.77	61	14	13	Carbamidomethylation; TMT6plex	Histidine triad nucleotide-binding protein 2 mitochondrial OS=Homo sapiens OX=9606 GN=HINT2 PE=1 SV=1
45	864	137064	Q13501|SQSTM_HUMAN	175.15	20	7	7	Carbamidomethylation; TMT6plex	Sequestosome-1 OS=Homo sapiens OX=9606 GN=SQSTM1 PE=1 SV=1
46	990	136776	P13797|PLST_HUMAN	179.52	12	8	5	Carbamidomethylation; TMT6plex	Plastin-3 OS=Homo sapiens OX=9606 GN=PLS3 PE=1 SV=4
47	1095	137921	P62241|RS8_HUMAN	124.72	21	4	4	Carbamidomethylation; TMT6plex	40S ribosomal protein S8 OS=Homo sapiens OX=9606 GN=RPS8 PE=1 SV=2
48	2065	138098	Q13753|LAMC2_HUMAN	78.44	4	3	2	TMT6plex; Oxidation (M)	Laminin subunit gamma-2 OS=Homo sapiens OX=9606 GN=LAMC2 PE=1 SV=2

Sr. No.	Protein Group	Protein ID	Accession	-10lgP	Coverage (%)	Peptides	Unique peptides	PTM	Description
49	1418	137615	Q86SQ4|AGRG6_HUMAN	100.47	4	5	5	TMT6plex	Adhesion G-protein coupled receptor G6 OS=Homo sapiens OX=9606 GN=ADGRG6 PE=1 SV=3
50	1940	137827	Q16651|PRSS8_HUMAN	112.49	14	4	4	Carbamidomethylation; TMT6plex	Prostasin OS=Homo sapiens OX=9606 GN=PRSS8 PE=1 SV=1
51	1282	138388	O14561|ACPM_HUMAN	91.82	15	2	2	TMT6plex; Oxidation (M)	Acyl carrier protein mitochondrial OS=Homo sapiens OX=9606 GN=NDUFAB1 PE=1 SV=3
52	2604	139043	Q96E11|RRFM_HUMAN	72.25	7	2	2	TMT6plex	Ribosome-recycling factor mitochondrial OS=Homo sapiens OX=9606 GN=MRRF PE=1 SV=1
53	2587	143378	P50120|RET2_HUMAN	73.89	7	2	2	TMT6plex	Retinol-binding protein 2 OS=Homo sapiens OX=9606 GN=RBP2 PE=1 SV=3
54	342	137360	Q9NYJ1|COA4_HUMAN	220.65	76	8	7	Carbamidomethylation; TMT6plex; Oxidation (M)	Cytochrome c oxidase assembly factor 4 homolog mitochondrial OS=Homo sapiens OX=9606 GN=COA4 PE=1 SV=2
55	677	136590	P05556|ITB1_HUMAN	230.65	14	12	12	Carbamidomethylation; TMT6plex	Integrin beta-1 OS=Homo sapiens OX=9606 GN=ITGB1 PE=1 SV=2
56	1700	137765	Q7KZF4|SND1_HUMAN	98.59	5	3	3	TMT6plex	Staphylococcal nuclease domain-containing protein 1 OS=Homo sapiens OX=9606 GN=SND1 PE=1 SV=1
57	1347	137779	Q99623|PHB2_HUMAN	130.18	11	3	3	TMT6plex	Prohibitin-2 OS=Homo sapiens OX=9606 GN=PHB2 PE=1 SV=2
58	649	137524	P21741|MK_HUMAN	173.3	36	6	6	Carbamidomethylation; TMT6plex	Midkine OS=Homo sapiens OX=9606 GN=MDK PE=1 SV=1
59	1253	137729	Q16553|LY6E_HUMAN	136.91	40	7	7	Carbamidomethylation; TMT6plex	Lymphocyte antigen 6E OS=Homo sapiens OX=9606 GN=LY6E PE=2 SV=1
60	2169	138486	Q96IU2|ZBED3_HUMAN	83	11	2	2	Carbamidomethylation; TMT6plex	Zinc finger BED domain-containing protein 3 OS=Homo sapiens OX=9606 GN=ZBED3 PE=1 SV=1
61	1869	137915	Q86VP1|TAXB1_HUMAN	79.31	4	3	3	TMT6plex	Tax1-binding protein 1 OS=Homo sapiens OX=9606 GN=TAX1BP1 PE=1 SV=2

Sr. No.	Protein Group	Protein ID	Accession	-10lgP	Coverage (%)	Peptides	Unique peptides	PTM	Description
62	424	136551	P27824|CALX_HUMAN	248.86	25	13	13	Carbamidomethylation; TMT6plex	Calnexin OS=Homo sapiens OX=9606 GN=CANX PE=1 SV=2
63	2252	140661	Q9NRV9|HEBP1_HUMAN	78.53	10	2	2	TMT6plex	Heme-binding protein 1 OS=Homo sapiens OX=9606 GN=HEBP1 PE=1 SV=1
64	2443	138177	Q8IV56|PRR15_HUMAN	88.58	22	2	2	TMT6plex	Proline-rich protein 15 OS=Homo sapiens OX=9606 GN=PRR15 PE=2 SV=1
65	1330	137269	P0DP91|ERPG3_HUMAN	150.67	5	4	4	Carbamidomethylation; TMT6plex	Chimeric ERCC6-PGBD3 protein OS=Homo sapiens OX=9606 GN=CSB-PGBD3 PE=1 SV=1
66	1330	137279	Q03468|ERCC6_HUMAN	150.67	4	4	4	Carbamidomethylation; TMT6plex	DNA excision repair protein ERCC-6 OS=Homo sapiens OX=9606 GN=ERCC6 PE=1 SV=1
67	543	136836	Q96BZ8|LENG1_HUMAN	167.96	35	8	8	TMT6plex	Leukocyte receptor cluster member 1 OS=Homo sapiens OX=9606 GN=LENG1 PE=1 SV=1
68	2651	140530	Q96BP2|CHCH1_HUMAN	92.21	21	2	2	Carbamidomethylation; TMT6plex	Coiled-coil-helix-coiled-coil-helix domain-containing protein 1 OS=Homo sapiens OX=9606 GN=CHCHD1 PE=1 SV=1
69	1937	137595	P62333|PRS10_HUMAN	128.46	11	4	4	TMT6plex	26S proteasome regulatory subunit 10B OS=Homo sapiens OX=9606 GN=PSMC6 PE=1 SV=1
70	1412	138008	Q96A73|P33MX_HUMAN	124.9	11	3	3	TMT6plex	Putative monooxygenase p33MONOX OS=Homo sapiens OX=9606 GN=KIAA1191 PE=1 SV=1
71	1135	137090	P62753|RS6_HUMAN	147.31	20	7	7	TMT6plex	40S ribosomal protein S6 OS=Homo sapiens OX=9606 GN=RPS6 PE=1 SV=1
72	337	136370	P50895|BCAM_HUMAN	305.43	31	18	18	Carbamidomethylation; TMT6plex	Basal cell adhesion molecule OS=Homo sapiens OX=9606 GN=BCAM PE=1 SV=2
73	2314	138006	P55786|PSA_HUMAN	108.22	3	2	2	TMT6plex	Puromycin-sensitive aminopeptidase OS=Homo sapiens OX=9606 GN=NPEPPS PE=1 SV=2

Sr. No.	Protein Group	Protein ID	Accession	-10lgP	Coverage (%)	Peptides	Unique peptides	PTM	Description
74	468	136670	Q96MH2|HEXI2_HUMAN	211.06	29	10	8	Carbamidomethylation; TMT6plex	Protein HEXIM2 OS=Homo sapiens OX=9606 GN=HEXIM2 PE=1 SV=1
75	366	136303	Q96T23|RSF1_HUMAN	274.16	16	20	20	Carbamidomethylation; TMT6plex; Oxidation (M)	Remodeling and spacing factor 1 OS=Homo sapiens OX=9606 GN=RSF1 PE=1 SV=2
76	1082	137254	P31942|HNRH3_HUMAN	200.45	13	5	5	TMT6plex; Oxidation (M)	Heterogeneous nuclear ribonucleoprotein H3 OS=Homo sapiens OX=9606 GN=HNRNPH3 PE=1 SV=2
77	635	136353	Q86UU0|BCL9L_HUMAN	260.63	14	17	17	TMT6plex; Oxidation (M)	B-cell CLL/lymphoma 9-like protein OS=Homo sapiens OX=9606 GN=BCL9L PE=1 SV=1
78	1535	137835	P28290|ITPI2_HUMAN	120.76	3	3	3	TMT6plex	Protein ITPRID2 OS=Homo sapiens OX=9606 GN=ITPRID2 PE=1 SV=3
79	791	137330	Q99519|NEUR1_HUMAN	145.28	12	7	7	Carbamidomethylation; TMT6plex	Sialidase-1 OS=Homo sapiens OX=9606 GN=NEU1 PE=1 SV=1
80	134	136352	P52272|HNRPM_HUMAN	316.7	35	42	42	Carbamidomethylation; TMT6plex; Oxidation (M)	Heterogeneous nuclear ribonucleoprotein M OS=Homo sapiens OX=9606 GN=HNRNPM PE=1 SV=3
81	2359	138357	A6NKD9|CC85C_HUMAN	91.51	7	2	2	TMT6plex	Coiled-coil domain-containing protein 85C OS=Homo sapiens OX=9606 GN=CCDC85C PE=1 SV=1
82	2095	139407	P20933|ASPG_HUMAN	75.33	5	2	2	Carbamidomethylation; TMT6plex	N (4) - (beta-N-acetylglucosaminyl)-L-asparaginase OS=Homo sapiens OX=9606 GN=AGA PE=1 SV=2
83	1193	137045	Q15417|CNN3_HUMAN	154.77	18	5	5	TMT6plex; Oxidation (M)	Calponin-3 OS=Homo sapiens OX=9606 GN=CNN3 PE=1 SV=1
84	2605	139122	P26447|S10A4_HUMAN	61.71	17	2	2	TMT6plex	Protein S100-A4 OS=Homo sapiens OX=9606 GN=S100A4 PE=1 SV=1
85	1928	138287	O00625|PIR_HUMAN	57.38	6	2	2	TMT6plex	Pirin OS=Homo sapiens OX=9606 GN=PIR PE=1 SV=1
86	157	136259	O60664|PLIN3_HUMAN	334.64	64	28	28	Carbamidomethylation; TMT6plex; Oxidation (M)	Perilipin-3 OS=Homo sapiens OX=9606 GN=PLIN3 PE=1 SV=3
87	1185	138269	Q6PJG2|EMSA1_HUMAN	111.99	3	2	2	TMT6plex	ELM2 and SANT domain-containing protein 1 OS=Homo sapiens OX=9606 GN=ELMSAN1 PE=1 SV=2

Sr. No.	Protein Group	Protein ID	Accession	-10lgP	Coverage (%)	Peptides	Unique peptides	PTM	Description
88	476	136359	P35241|RADI_HUMAN	246.92	26	20	15	Carbamidomethylation; TMT6plex; Oxidation (M)	Radixin OS=Homo sapiens OX=9606 GN=RDX PE=1 SV=1
89	607	136646	Q99961|SH3G1_HUMAN	178.73	31	14	14	TMT6plex	Endophilin-A2 OS=Homo sapiens OX=9606 GN=SH3GL1 PE=1 SV=1
90	2190	138550	Q92567|F168A_HUMAN	108.87	11	2	2	TMT6plex; Oxidation (M); Acetylation (N-term)	Protein FAM168A OS=Homo sapiens OX=9606 GN=FAM168A PE=1 SV=2
91	1343	137335	P11586|C1TC_HUMAN	96.23	7	5	5	Carbamidomethylation; TMT6plex	C-1-tetrahydrofolate synthase cytoplasmic OS=Homo sapiens OX=9606 GN=MTHFD1 PE=1 SV=3
92	2139	138735	P25686|DNJB2_HUMAN	88.07	6	2	2	TMT6plex	DnaJ homolog subfamily B member 2 OS=Homo sapiens OX=9606 GN=DNAJB2 PE=1 SV=3
93	1592	138547	Q9Y4Y9|LSM5_HUMAN	116.07	46	3	3	TMT6plex; Oxidation (M)	U6 snRNA-associated Sm-like protein LSm5 OS=Homo sapiens OX=9606 GN=LSM5 PE=1 SV=3
94	581	136585	Q8IVM0|CCD50_HUMAN	202.21	37	11	11	Carbamidomethylation; TMT6plex	Coiled-coil domain-containing protein 50 OS=Homo sapiens OX=9606 GN=CCDC50 PE=1 SV=1
95	2413	138137	Q92997|DVL3_HUMAN	79.52	3	2	2	TMT6plex	Segment polarity protein dishevelled homolog DVL-3 OS=Homo sapiens OX=9606 GN=DVL3 PE=1 SV=2
96	412	136348	P49454|CENPF_HUMAN	252.72	9	25	25	Carbamidomethylation; TMT6plex	Centromere protein F OS=Homo sapiens OX=9606 GN=CENPF PE=1 SV=3
97	1214	137764	P53634|CATC_HUMAN	208.66	7	7	7	Carbamidomethylation; TMT6plex	Dipeptidyl peptidase 1 OS=Homo sapiens OX=9606 GN=CTSC PE=1 SV=2
98	1474	138047	Q96B45|BORC7_HUMAN	110.38	32	3	3	TMT6plex	BLOC-1-related complex subunit 7 OS=Homo sapiens OX=9606 GN=BORCS7 PE=3 SV=2
99	1758	137864	Q14254|FLOT2_HUMAN	88.64	8	3	3	TMT6plex	Flotillin-2 OS=Homo sapiens OX=9606 GN=FLOT2 PE=1 SV=2

Sr. No.	Protein Group	Protein ID	Accession	-10lgP	Coverage (%)	Peptides	Unique peptides	PTM	Description
100	1230	137324	Q96MY1|NOL4L_HUMAN	128.94	10	6	6	TMT6plex	Nucleolar protein 4-like OS=Homo sapiens OX=9606 GN=NOL4L PE=1 SV=2
101	755	136818	P98175|RBM10_HUMAN	182.81	9	10	8	TMT6plex	RNA-binding protein 10 OS=Homo sapiens OX=9606 GN=RBM10 PE=1 SV=3
102	2131	137945	Q96T51|RUFY1_HUMAN	84.83	6	3	3	Carbamidomethylation; TMT6plex	RUN and FYVE domain-containing protein 1 OS=Homo sapiens OX=9606 GN=RUFY1 PE=1 SV=2
103	57	136196	P46013|KI67_HUMAN	399.28	31	94	93	Carbamidomethylation; TMT6plex; Oxidation (M)	Proliferation marker protein Ki-67 OS=Homo sapiens OX=9606 GN=MKI67 PE=1 SV=2
104	1143	137109	Q9HD42|CHM1A_HUMAN	131.31	27	7	7	TMT6plex; Oxidation (M); Acetylation (N-term)	Charged multivesicular body protein 1a OS=Homo sapiens OX=9606 GN=CHMP1A PE=1 SV=1
105	2357	138263	Q6VMQ6|MCAF1_HUMAN	94.11	2	2	2	Carbamidomethylation; TMT6plex	Activating transcription factor 7-interacting protein 1 OS=Homo sapiens OX=9606 GN=ATF7IP PE=1 SV=3
106	1421	140563	Q9UNN8|EPCR_HUMAN	66.66	8	2	2	TMT6plex	Endothelial protein C receptor OS=Homo sapiens OX=9606 GN=PROCR PE=1 SV=1
107	759	136658	P49959|MRE11_HUMAN	211.47	15	11	11	TMT6plex; Oxidation (M)	Double-strand break repair protein MRE11 OS=Homo sapiens OX=9606 GN=MRE11 PE=1 SV=3
108	1	136172	Q09666|AHNK_HUMAN	614.81	59	338	337	Carbamidomethylation; TMT6plex; Oxidation (M); Acetylation (N-term)	Neuroblast differentiation-associated protein AHNAK OS=Homo sapiens OX=9606 GN=AHNAK PE=1 SV=2
109	798	137356	Q96CP2|FWCH2_HUMAN	164.56	64	7	7	Carbamidomethylation; TMT6plex	FLYWCH family member 2 OS=Homo sapiens OX=9606 GN=FLYWCH2 PE=1 SV=1
110	1680	138062	Q9Y605|MOFA1_HUMAN	142.52	38	3	3	TMT6plex	MORF4 family-associated protein 1 OS=Homo sapiens OX=9606 GN=MRFAP1 PE=1 SV=1

Sr. No.	Protein Group	Protein ID	Accession	-10lgP	Coverage (%)	Peptides	Unique peptides	PTM	Description
111	1573	137643	Q15773|MLF2_HUMAN	114.64	16	4	4	TMT6plex	Myeloid leukemia factor 2 OS=Homo sapiens OX=9606 GN=MLF2 PE=1 SV=1
112	529	137528	Q9HCY8|S10AE_HUMAN	172.95	46	4	4	Carbamidomethylation; TMT6plex	Protein S100-A14 OS=Homo sapiens OX=9606 GN=S100A14 PE=1 SV=1
113	1073	137101	O60885|BRD4_HUMAN	144.02	4	6	6	TMT6plex	Bromodomain-containing protein 4 OS=Homo sapiens OX=9606 GN=BRD4 PE=1 SV=2
114	1402	137814	Q96EQ0|SGTB_HUMAN	99.9	11	4	3	TMT6plex	Small glutamine-rich tetratricopeptide repeat-containing protein beta OS=Homo sapiens OX=9606 GN=SGTB PE=1 SV=1
115	1274	138101	Q96A19|C102A_HUMAN	109.5	7	3	3	TMT6plex	Coiled-coil domain-containing protein 102A OS=Homo sapiens OX=9606 GN=CCDC102A PE=1 SV=2
116	777	136500	Q5UIP0|RIF1_HUMAN	197.26	5	11	11	Carbamidomethylation; TMT6plex	Telomere-associated protein RIF1 OS=Homo sapiens OX=9606 GN=RIF1 PE=1 SV=2
117	119	137036	P20962|PTMS_HUMAN	248.97	90	17	17	TMT6plex	Parathymosin OS=Homo sapiens OX=9606 GN=PTMS PE=1 SV=2
118	260	136355	Q9GZU8|PIP30_HUMAN	291.63	65	24	23	Carbamidomethylation; TMT6plex; Oxidation (M); Acetylation (N-term)	PSME3-interacting protein OS=Homo sapiens OX=9606 GN=FAM192A PE=1 SV=1
119	1686	137420	O96013|PAK4_HUMAN	135.72	7	4	4	TMT6plex	Serine/threonine-protein kinase PAK 4 OS=Homo sapiens OX=9606 GN=PAK4 PE=1 SV=1
120	656	136638	Q68CZ2|TENS3_HUMAN	193.6	8	11	11	Carbamidomethylation; TMT6plex	Tensin-3 OS=Homo sapiens OX=9606 GN=TNS3 PE=1 SV=2
121	1444	137660	Q13153|PAK1_HUMAN	120.59	4	3	2	TMT6plex	Serine/threonine-protein kinase PAK 1 OS=Homo sapiens OX=9606 GN=PAK1 PE=1 SV=2
122	1546	137307	O15014|ZN609_HUMAN	116.6	3	5	5	Carbamidomethylation; TMT6plex	Zinc finger protein 609 OS=Homo sapiens OX=9606 GN=ZNF609 PE=1 SV=2

Sr. No.	Protein Group	Protein ID	Accession	-10lgP	Coverage (%)	Peptides	Unique peptides	PTM	Description
123	615	138055	P50238|CRIP1_HUMAN	174.82	52	9	9	Carbamidomethylation; TMT6plex	Cysteine-rich protein 1 OS=Homo sapiens OX=9606 GN=CRIP1 PE=1 SV=3
124	1356	137942	Q9H9B1|EHMT1_HUMAN	87.83	2	3	3	TMT6plex	Histone-lysine N-methyltransferase EHMT1 OS=Homo sapiens OX=9606 GN=EHMT1 PE=1 SV=4
125	2361	138429	Q99081|HTF4_HUMAN	74.18	6	2	2	TMT6plex	Transcription factor 12 OS=Homo sapiens OX=9606 GN=TCF12 PE=1 SV=1
126	1960	138007	O14641|DVL2_HUMAN	65.85	5	4	4	TMT6plex	Segment polarity protein dishevelled homolog DVL-2 OS=Homo sapiens OX=9606 GN=DVL2 PE=1 SV=1
127	1703	138250	Q8TEU7|RPGF6_HUMAN	59.66	1	3	2	TMT6plex	Rap guanine nucleotide exchange factor 6 OS=Homo sapiens OX=9606 GN=RAPGEF6 PE=1 SV=2
128	1851	137753	Q9H4A3|WNK1_HUMAN	101.88	1	3	3	TMT6plex	Serine/threonine-protein kinase WNK1 OS=Homo sapiens OX=9606 GN=WNK1 PE=1 SV=2
129	787	137068	Q9Y6W5|WASF2_HUMAN	158.25	10	7	7	TMT6plex	Wiskott-Aldrich syndrome protein family member 2 OS=Homo sapiens OX=9606 GN=WASF2 PE=1 SV=3
130	2090	138549	P78344|IF4G2_HUMAN	77.69	2	2	2	TMT6plex	Eukaryotic translation initiation factor 4 gamma 2 OS=Homo sapiens OX=9606 GN=EIF4G2 PE=1 SV=1
131	563	136763	Q13177|PAK2_HUMAN	235.97	23	11	10	TMT6plex	Serine/threonine-protein kinase PAK 2 OS=Homo sapiens OX=9606 GN=PAK2 PE=1 SV=3
132	1203	137833	Q9UPN4|CP131_HUMAN	120.17	3	3	3	TMT6plex	Centrosomal protein of 131 kDa OS=Homo sapiens OX=9606 GN=CEP131 PE=1 SV=3
133	1775	137909	Q96B01|R51A1_HUMAN	63.32	12	4	4	TMT6plex	RAD51-associated protein 1 OS=Homo sapiens OX=9606 GN=RAD51AP1 PE=1 SV=1
134	694	137443	P13987|CD59_HUMAN	181.37	39	7	7	Carbamidomethylation; TMT6plex	CD59 glycoprotein OS=Homo sapiens OX=9606 GN=CD59 PE=1 SV=1
135	865	137133	Q6FI81|CPIN1_HUMAN	182.19	20	5	5	Carbamidomethylation; TMT6plex	Anamorsin OS=Homo sapiens OX=9606 GN=CIAPIN1 PE=1 SV=2

Sr. No.	Protein Group	Protein ID	Accession	-10lgP	Coverage (%)	Peptides	Unique peptides	PTM	Description
136	578	136532	Q9NP61|ARFG3_HUMAN	229.45	27	10	10	Carbamidomethylation; TMT6plex; Oxidation (M)	ADP-ribosylation factor GTPase-activating protein 3 OS=Homo sapiens OX=9606 GN=ARFGAP3 PE=1 SV=1
137	2658	140599	Q9BUT9|MCRI2_HUMAN	85.57	22	2	2	TMT6plex	MAPK regulated corepressor interacting protein 2 OS=Homo sapiens OX=9606 GN=MCRIP2 PE=1 SV=2
138	714	137047	P33316|DUT_HUMAN	218.46	38	10	10	Carbamidomethylation; TMT6plex; Oxidation (M)	Deoxyuridine 5'-triphosphate nucleotidohydrolase mitochondrial OS=Homo sapiens OX=9606 GN=DUT PE=1 SV=4
139	2064	137999	Q15054|DPOD3_HUMAN	90.43	6	3	3	TMT6plex	DNA polymerase delta subunit 3 OS=Homo sapiens OX=9606 GN=POLD3 PE=1 SV=2
140	1855	138649	Q53T59|H1BP3_HUMAN	119.83	5	2	2	TMT6plex	HCLS1-binding protein 3 OS=Homo sapiens OX=9606 GN=HS1BP3 PE=1 SV=1
141	2089	138298	Q9Y2H2|SAC2_HUMAN	74.72	2	2	2	TMT6plex	Phosphatidylinositide phosphatase SAC2 OS=Homo sapiens OX=9606 GN=INPP5F PE=1 SV=3
142	1050	137231	Q9P021|CRIPT_HUMAN	174.36	44	8	8	Carbamidomethylation; TMT6plex	Cysteine-rich PDZ-binding protein OS=Homo sapiens OX=9606 GN=CRIPT PE=1 SV=1
143	390	136372	Q9UEE9|CFDP1_HUMAN	231.89	56	20	20	TMT6plex; Oxidation (M)	Craniofacial development protein 1 OS=Homo sapiens OX=9606 GN=CFDP1 PE=1 SV=1
144	195	137117	P06454|PTMA_HUMAN	271.36	47	15	15	TMT6plex	Prothymosin alpha OS=Homo sapiens OX=9606 GN=PTMA PE=1 SV=2
145	1154	137991	Q13542|4EBP2_HUMAN	179.8	43	5	4	Carbamidomethylation; TMT6plex; Oxidation (M)	Eukaryotic translation initiation factor 4E-binding protein 2 OS=Homo sapiens OX=9606 GN=EIF4EBP2 PE=1 SV=1
146	1006	137402	Q9Y2S6|TMA7_HUMAN	135.17	58	8	7	TMT6plex; Oxidation (M)	Translation machinery-associated protein 7 OS=Homo sapiens OX=9606 GN=TMA7 PE=1 SV=1
147	1620	137917	Q99622|C10_HUMAN	135.41	40	3	3	TMT6plex	Protein C10 OS=Homo sapiens OX=9606 GN=C12orf57 PE=1 SV=1

Sr. No.	Protein Group	Protein ID	Accession	-10lgP	Coverage (%)	Peptides	Unique peptides	PTM	Description
148	722	137785	Q9UQN3|CHM2B_HUMAN	111.83	17	4	4	TMT6plex	Charged multivesicular body protein 2b OS=Homo sapiens OX=9606 GN=CHMP2B PE=1 SV=1
149	381	136666	P07858|CATB_HUMAN	276.88	27	25	25	Carbamidomethylation; TMT6plex	Cathepsin B OS=Homo sapiens OX=9606 GN=CTSB PE=1 SV=3
150	945	137053	P08590|MYL3_HUMAN	171.48	23	6	4	TMT6plex	Myosin light chain 3 OS=Homo sapiens OX=9606 GN=MYL3 PE=1 SV=3
151	3	136167	Q9P2E9|RRBP1_HUMAN	532.22	69	185	177	Carbamidomethylation; TMT6plex; Oxidation (M)	Ribosome-binding protein 1 OS=Homo sapiens OX=9606 GN=RRBP1 PE=1 SV=5
152	1089	137692	Q5T7N3|KANK4_HUMAN	105.19	3	3	2	TMT6plex	KN motif and ankyrin repeat domain-containing protein 4 OS=Homo sapiens OX=9606 GN=KANK4 PE=1 SV=1
153	1828	137533	Q86YS3|RFIP4_HUMAN	112.97	5	3	3	TMT6plex	Rab11 family-interacting protein 4 OS=Homo sapiens OX=9606 GN=RAB11FIP4 PE=1 SV=1
154	2469	138285	Q9NYZ3|GTSE1_HUMAN	64.93	3	2	2	Carbamidomethylation; TMT6plex	G2 and S phase-expressed protein 1 OS=Homo sapiens OX=9606 GN=GTSE1 PE=1 SV=3
155	1134	137054	P01009|A1AT_HUMAN	146.6	16	6	6	Carbamidomethylation; TMT6plex; Oxidation (M)	Alpha-1-antitrypsin OS=Homo sapiens OX=9606 GN=SERPINA1 PE=1 SV=3
156	1323	138089	Q9BPZ3|PAIP2_HUMAN	99.71	35	3	3	TMT6plex; Oxidation (M)	Polyadenylate-binding protein-interacting protein 2 OS=Homo sapiens OX=9606 GN=PAIP2 PE=1 SV=1
157	2425	138592	Q6P582|MZT2A_HUMAN	58.9	15	2	2	Carbamidomethylation; TMT6plex; Oxidation (M)	Mitotic spindle organizing protein 2A OS=Homo sapiens OX=9606 GN=MZT2A PE=1 SV=2
158	620	136833	Q14694|UBP10_HUMAN	201.07	22	7	7	Carbamidomethylation; TMT6plex	Ubiquitin carboxyl-terminal hydrolase 10 OS=Homo sapiens OX=9606 GN=USP10 PE=1 SV=2
159	1997	140617	Q9BUA3|SPNDC_HUMAN	63.27	4	2	2	TMT6plex	Spindlin interactor and repressor of chromatin-binding protein OS=Homo sapiens OX=9606 GN=SPINDOC PE=1 SV=3

Sr. No.	Protein Group	Protein ID	Accession	-10lgP	Coverage (%)	Peptides	Unique peptides	PTM	Description
160	2510	138997	Q96JB3|HIC2_HUMAN	58.52	2	2	2	TMT6plex	Hypermethylated in cancer 2 protein OS=Homo sapiens OX=9606 GN=HIC2 PE=1 SV=2
161	828	136870	P49715|CEBPA_HUMAN	147.18	19	9	8	TMT6plex	CCAAT/enhancer-binding protein alpha OS=Homo sapiens OX=9606 GN=CEBPA PE=1 SV=3
162	1702	137842	P52701|MSH6_HUMAN	103.72	4	3	3	TMT6plex	DNA mismatch repair protein Msh6 OS=Homo sapiens OX=9606 GN=MSH6 PE=1 SV=2
163	1215	138374	Q3SY56|SP6_HUMAN	111.94	7	2	2	Carbamidomethylation; TMT6plex	Transcription factor Sp6 OS=Homo sapiens OX=9606 GN=SP6 PE=2 SV=1
164	2442	138147	Q9GZY8|MFF_HUMAN	60.07	17	2	2	TMT6plex	Mitochondrial fission factor OS=Homo sapiens OX=9606 GN=MFF PE=1 SV=1
165	207	136302	Q02818|NUCB1_HUMAN	295.24	39	26	24	TMT6plex; Oxidation (M)	Nucleobindin-1 OS=Homo sapiens OX=9606 GN=NUCB1 PE=1 SV=4
166	22	136210	P02751|FINC_HUMAN	446.54	39	98	97	Carbamidomethylation; TMT6plex; Oxidation (M)	Fibronectin OS=Homo sapiens OX=9606 GN=FN1 PE=1 SV=4
167	1112	137021	Q8N3D4|EH1L1_HUMAN	185.17	5	5	5	Carbamidomethylation; TMT6plex	EH domain-binding protein 1-like protein 1 OS=Homo sapiens OX=9606 GN=EHBP1L1 PE=1 SV=2
168	871	140557	Q07654|TFF3_HUMAN	93.1	27	4	4	Carbamidomethylation; TMT6plex	Trefoil factor 3 OS=Homo sapiens OX=9606 GN=TFF3 PE=1 SV=2
169	2516	139154	Q9Y237|PIN4_HUMAN	100.93	18	2	2	TMT6plex; Oxidation (M)	Peptidyl-prolyl cis-trans isomerase NIMA-interacting 4 OS=Homo sapiens OX=9606 GN=PIN4 PE=1 SV=1
170	1692	138178	Q92499|DDX1_HUMAN	70.59	4	2	2	Carbamidomethylation; TMT6plex	ATP-dependent RNA helicase DDX1 OS=Homo sapiens OX=9606 GN=DDX1 PE=1 SV=2
171	1027	137080	Q15154|PCM1_HUMAN	130.32	2	6	5	Carbamidomethylation; TMT6plex	Pericentriolar material 1 protein OS=Homo sapiens OX=9606 GN=PCM1 PE=1 SV=5
172	455	137473	P84101|SERF2_HUMAN	126.79	63	7	7	TMT6plex; Oxidation (M)	Small EDRK-rich factor 2 OS=Homo sapiens OX=9606 GN=SERF2 PE=1 SV=1

Sr. No.	Protein Group	Protein ID	Accession	-10lgP	Coverage (%)	Peptides	Unique peptides	PTM	Description
173	88	136235	Q5T5P2|SKT_HUMAN	338.48	20	45	45	Carbamidomethylation; TMT6plex; Oxidation (M); Acetylation (N-term)	Sickle tail protein homolog OS=Homo sapiens OX=9606 GN=KIAA1217 PE=1 SV=2
174	2212	138039	O14964|HGS_HUMAN	86.7	4	3	3	Carbamidomethylation; TMT6plex	Hepatocyte growth factor-regulated tyrosine kinase substrate OS=Homo sapiens OX=9606 GN=HGS PE=1 SV=1
175	1007	137495	P05162|LEG2_HUMAN	165.57	57	7	7	Carbamidomethylation; TMT6plex; Oxidation (M)	Galectin-2 OS=Homo sapiens OX=9606 GN=LGALS2 PE=1 SV=3
176	306	136230	Q9ULW0|TPX2_HUMAN	297.98	35	23	23	Carbamidomethylation; TMT6plex	Targeting protein for Xklp2 OS=Homo sapiens OX=9606 GN=TPX2 PE=1 SV=2
177	183	136277	O00499|BIN1_HUMAN	317.85	43	28	28	Carbamidomethylation; TMT6plex; Oxidation (M)	Myc box-dependent-interacting protein 1 OS=Homo sapiens OX=9606 GN=BIN1 PE=1 SV=1
178	2426	138625	Q9BXS6|NUSAP_HUMAN	76.54	4	2	2	TMT6plex	Nucleolar and spindle-associated protein 1 OS=Homo sapiens OX=9606 GN=NUSAP1 PE=1 SV=1
179	1334	137285	P02671|FIBA_HUMAN	146.7	8	5	5	TMT6plex; Oxidation (M)	Fibrinogen alpha chain OS=Homo sapiens OX=9606 GN=FGA PE=1 SV=2
180	1131	137198	Q9BRK5|CAB45_HUMAN	156.72	19	6	6	TMT6plex	45 kDa calcium-binding protein OS=Homo sapiens OX=9606 GN=SDF4 PE=1 SV=1
181	560	137589	P61916|NPC2_HUMAN	197.79	56	8	8	Carbamidomethylation; TMT6plex; Oxidation (M)	NPC intracellular cholesterol transporter 2 OS=Homo sapiens OX=9606 GN=NPC2 PE=1 SV=1
182	2138	138581	O75808|CAN15_HUMAN	100.5	2	2	2	Carbamidomethylation; TMT6plex	Calpain-15 OS=Homo sapiens OX=9606 GN=CAPN15 PE=1 SV=1
183	189	136289	P02647|APOA1_HUMAN	296.8	72	39	39	TMT6plex; Oxidation (M)	Apolipoprotein A-I OS=Homo sapiens OX=9606 GN=APOA1 PE=1 SV=1

Sr. No.	Protein Group	Protein ID	Accession	-10lgP	Coverage (%)	Peptides	Unique peptides	PTM	Description
184	442	137673	P63313|TYB10_HUMAN	181.5	57	11	7	TMT6plex	Thymosin beta-10 OS=Homo sapiens OX=9606 GN=TMSB10 PE=1 SV=2
185	536	136677	Q8N6H7|ARFG2_HUMAN	213.19	17	10	10	TMT6plex	ADP-ribosylation factor GTPase-activating protein 2 OS=Homo sapiens OX=9606 GN=ARFGAP2 PE=1 SV=1
186	1384	137591	O00592|PODXL_HUMAN	128.14	10	5	5	TMT6plex	Podocalyxin OS=Homo sapiens OX=9606 GN=PODXL PE=1 SV=2
187	1636	138114	Q9P0P0|RN181_HUMAN	82.02	15	3	3	Carbamidomethylation; TMT6plex	E3 ubiquitin-protein ligase RNF181 OS=Homo sapiens OX=9606 GN=RNF181 PE=1 SV=1
188	1479	137555	Q9UHG0|DCDC2_HUMAN	147.2	17	5	5	TMT6plex	Doublecortin domain-containing protein 2 OS=Homo sapiens OX=9606 GN=DCDC2 PE=1 SV=2
189	602	136797	P04792|HSPB1_HUMAN	249.99	53	14	14	TMT6plex	Heat shock protein beta-1 OS=Homo sapiens OX=9606 GN=HSPB1 PE=1 SV=2
190	1175	138181	P02763|A1AG1_HUMAN	132	16	3	3	TMT6plex	Alpha-1-acid glycoprotein 1 OS=Homo sapiens OX=9606 GN=ORM1 PE=1 SV=1
191	636	137596	O60829|PAGE4_HUMAN	141.4	44	6	6	Carbamidomethylation; TMT6plex; Oxidation (M)	P antigen family member 4 OS=Homo sapiens OX=9606 GN=PAGE4 PE=1 SV=1

References

1. Foster I. 2008. **Cancer: A cell cycle defect.** *Radiography* 14:144-149.
2. Bower JJ, Vance LD, Psioda M, Smith-Roe SL, Simpson DA, Ibrahim JG, Hoadley KA, Perou CM, Kaufmann WK. 2017. **Patterns of cell cycle checkpoint deregulation associated with intrinsic molecular subtypes of human breast cancer cells.** *NPJ Breast Cancer* 3:9.
3. Hunt T, Nasmyth K, Novák B. 2011. **Introduction: The cell cycle.** *Philosophical Transactions: Biological Sciences* 366:3494-3497.
4. Schafer KA. 1998. **The Cell Cycle: A Review.** *Veterinary Pathology* 35:461-478.
5. Williams GH, Stoeber K. 2012. **The cell cycle and cancer.** *The Journal of Pathology* 226:352-364.
6. Hanahan D, Weinberg RA. 2000. **The Hallmarks of Cancer.** *Cell* 100:57-70.
7. Hanahan D, Weinberg RA. 2011. **Hallmarks of Cancer: The Next Generation.** *Cell* 144:646-674.
8. Nevins JR. 2001. **The Rb/E2F pathway and cancer.** *Human Molecular Genetics* 10:699-703.
9. Fulda S. 2009. **Tumor resistance to apoptosis.** *International Journal of Cancer* 124:511-515.
10. Negrini S, Gorgoulis VG, Halazonetis TD. 2010. **Genomic instability--an evolving hallmark of cancer.** *Nature Reviews Molecular Cell Biology* 11:220-8.
11. Pardoll DM. 2012. **The blockade of immune checkpoints in cancer immunotherapy.** *Nature Reviews Cancer* 12:252-64.
12. Sivanandam V, LaRocca CJ, Chen NG, Fong Y, Warner SG. 2019. **Oncolytic Viruses and Immune Checkpoint Inhibition: The Best of Both Worlds.** *Molecular therapy oncolytics* 13:93-106.
13. Granier C, De Guillebon E, Blanc C, Roussel H, Badoual C, Colin E, Saldmann A, Gey A, Oudard S, Tartour E. 2017. **Mechanisms of action and rationale for the use of checkpoint inhibitors in cancer.** *ESMO Open* 2:e000213.
14. Cooper GM. **The Cell: A Molecular Approach. 2nd edition.** Sunderland (MA): Sinauer Associates;
2000.
Available from: https://www.ncbi.nlm.nih.gov/books/NBK9839/
15. Edge SB BD, Compton CC, Fritz AG, Greene FL, Trotti A. 2010. **AJCC cancer staging manual, 7th ed.** New York, NY: Springer. 1–648.
16. Izuo M. 2004. **Medical history: Seishu Hanaoka and his success in breast cancer surgery under general anesthesia two hundred years ago.** *Breast Cancer* 11:319-24.
17. Connell PP, Hellman S. 2009. **Advances in Radiotherapy and Implications for the Next Century: A Historical Perspective.** *Cancer Research* 69:383-392.
18. DeVita VT, Jr., Chu E. 2008. **A history of cancer chemotherapy.** *Cancer Research* 68:8643-53.
19. Heller JR. 1962. **Cancer chemotherapy, history and present status.** *Bulletin of the New York Academy of Medicine* 38:348-63.

20. Bluming A, Ziegler J. 1971. **Regression of Burkitt's lymphoma in association with measles infection.** *The Lancet* 298:105-106.

21. Sinkovics JG, Horvath JC. 2008. **Natural and genetically engineered viral agents for oncolysis and gene therapy of human cancers.** *Archivum Immunologiae et Therapiae Experimentalis* 56:1-59.

22. Lin E, Nemunaitis J. 2004. **Oncolytic viral therapies.** *Cancer Gene Therapy* 11:643-664.

23. Kelly E, Russell SJ. 2007. **History of oncolytic viruses: genesis to genetic engineering.** *Molecular Therapy* 15:651-9.

24. Parato KA, Senger D, Forsyth PAJ, Bell JC. 2005. **Recent progress in the battle between oncolytic viruses and tumours.** *Nature Reviews Cancer* 5:965-976.

25. Garofalo M, Villa A, Rizzi N, Kuryk L, Mazzaferro V, Ciana P. 2018. **Systemic Administration and Targeted Delivery of Immunogenic Oncolytic Adenovirus Encapsulated in Extracellular Vesicles for Cancer Therapies.** *Viruses* 10:558.

26. Kaufman HL, Kohlhapp FJ, Zloza A. 2015. **Oncolytic viruses: a new class of immunotherapy drugs.** *Nature Reviews Drug Discovery* 14:642.

27. Donina S, Strele I, Proboka G, Auzins J, Alberts P, Jonsson B, Venskus D, Muceniece A. 2015. **Adapted ECHO-7 virus Rigvir immunotherapy (oncolytic virotherapy) prolongs survival in melanoma patients after surgical excision of the tumour in a retrospective study.** *Melanoma Research* 25:421-6.

28. Alberts P, Olmane E, Brokāne L, Krastiņa Z, Romanovska M, Kupčs K, Isajevs S, Proboka G, Erdmanis R, Nazarovs J, Venskus D. 2016. **Long-term treatment with the oncolytic ECHO-7 virus Rigvir of a melanoma stage IV M1c patient, a small cell lung cancer stage IIIA patient, and a histiocytic sarcoma stage IV patient-three case reports.** *APMIS* 124:896-904.

29. Babiker HM, Riaz IB, Husnain M, Borad MJ. 2017. **Oncolytic virotherapy including Rigvir and standard therapies in malignant melanoma.** *Oncolytic virotherapy* 6:11-18.

30. Wei D, Xu J, Liu X-Y, Chen Z-N, Bian H. 2017. **Fighting Cancer with Viruses: Oncolytic Virus Therapy in China.** *Human Gene Therapy* 29:151-159.

31. Garber K. 2006. **China approves world's first oncolytic virus therapy for cancer treatment.** *Journal of the National Cancer Institute* 98:298-300.

32. Ries S, Korn WM. 2002. **ONYX-015: mechanisms of action and clinical potential of a replication-selective adenovirus.** *British Journal of Cancer* 86:5-11.

33. Harada JN, Berk AJ. 1999. **p53-Independent and -dependent requirements for E1B-55K in adenovirus type 5 replication.** *Journal of Virology* 73:5333-44.

34. Goodrum FD, Ornelles DA. 1998. **p53 Status Does Not Determine Outcome of E1B 55-Kilodalton Mutant Adenovirus Lytic Infection.** *Journal of Virology* 72:9479-9490.

35. Xia ZJ, Chang JH, Zhang L, Jiang WQ, Guan ZZ, Liu JW, Zhang Y, Hu XH, Wu GH, Wang HQ, Chen ZC, Chen JC, Zhou QH, Lu JW, Fan QX, Huang JJ, Zheng X. 2004. **[Phase III randomized clinical trial of intratumoral injection of E1B gene-deleted adenovirus (H101) combined with cisplatin-based chemotherapy in treating squamous cell cancer of head and neck or esophagus].** *Ai Zheng Chinese Journal of Cancer* 23:1666-70.

36. Zhang S, Huang W, Zhou X, Zhao Q, Wang Q, Jia B. 2013. **Seroprevalence of neutralizing antibodies to human adenoviruses type-5 and type-26 and**

chimpanzee adenovirus type-68 in healthy Chinese adults. *Journal of Medical Virology* 85:1077-84.

37. Nwanegbo E, Vardas E, Gao W, Whittle H, Sun H, Rowe D, Robbins PD, Gambotto A. 2004. **Prevalence of neutralizing antibodies to adenoviral serotypes 5 and 35 in the adult populations of The Gambia, South Africa, and the United States.** *Clinical and Diagnostic Laboratory Immunology* 11:351-7.

38. EMA. 2015. **First oncolytic immunotherapy medicine recommended for approval.** https://www.ema.europa.eu/en/news/first-oncolytic-immunotherapy-medicine-recommended-approval

39. USFDA. 2015. **FDA Approves IMLYGIC™ (Talimogene Laherparepvec) as first oncolytic viral therapy in the US.** https://www.amgen.com/media/news-releases/2015/10/fda-approves-imlygic-talimogene-laherparepvec-as-first-oncolytic-viral-therapy-in-the-us/

40. Andtbacka RHI, Kaufman HL, Collichio F, Amatruda T, Senzer N, Chesney J, Delman KA, Spitler LE, Puzanov I, Agarwala SS, Milhem M, Cranmer L, Curti B, Lewis K, Ross M, Guthrie T, Linette GP, Daniels GA, Harrington K, Middleton MR, Miller WH, Zager JS, Ye Y, Yao B, Li A, Doleman S, VanderWalde A, Gansert J, Coffin RS. 2015. **Talimogene Laherparepvec Improves Durable Response Rate in Patients With Advanced Melanoma.** *Journal of Clinical Oncology* 33:2780-2788.

41. Greig SL. 2016. **Talimogene Laherparepvec: First Global Approval.** *Drugs* 76:147-154.

42. Liu BL, Robinson M, Han ZQ, Branston RH, English C, Reay P, McGrath Y, Thomas SK, Thornton M, Bullock P, Love CA, Coffin RS. 2003. **ICP34.5 deleted herpes simplex virus with enhanced oncolytic, immune stimulating, and anti-tumour properties.** *Gene Therapy* 10:292-303.

43. Ribas A, Dummer R, Puzanov I, VanderWalde A, Andtbacka RHI, Michielin O, Olszanski AJ, Malvehy J, Cebon J, Fernandez E, Kirkwood JM, Gajewski TF, Chen L, Gorski KS, Anderson AA, Diede SJ, Lassman ME, Gansert J, Hodi FS, Long GV. 2017. **Oncolytic Virotherapy Promotes Intratumoral T Cell Infiltration and Improves Anti-PD-1 Immunotherapy.** *Cell* 170:1109-1119 e10.

44. Khuri FR, Nemunaitis J, Ganly I, Arseneau J, Tannock IF, Romel L, Gore M, Ironside J, MacDougall RH, Heise C, Randlev B, Gillenwater AM, Bruso P, Kaye SB, Hong WK, Kirn DH. 2000. **A controlled trial of intratumoral ONYX-015, a selectively-replicating adenovirus, in combination with cisplatin and 5-fluorouracil in patients with recurrent head and neck cancer.** *Nature Medicine* 6:879-885.

45. Nemunaitis J, Cunningham C, Tong AW, Post L, Netto G, Paulson AS, Rich D, Blackburn A, Sands B, Gibson B, Randlev B, Freeman S. 2003. **Pilot trial of intravenous infusion of a replication-selective adenovirus (ONYX-015) in combination with chemotherapy or IL-2 treatment in refractory cancer patients.** *Cancer Gene Therapy* 10:341-352.

46. Galanis E, Okuno SH, Nascimento AG, Lewis BD, Lee RA, Oliveira AM, Sloan JA, Atherton P, Edmonson JH, Erlichman C, Randlev B, Wang Q, Freeman S, Rubin J. 2005. **Phase I–II trial of ONYX-015 in combination with MAP chemotherapy in patients with advanced sarcomas.** *Gene Therapy* 12:437-445.

47. Xia ZJ, Chang JH, Zhang L, Jiang WQ, Guan ZZ, Liu JW, Zhang Y, Hu XH, Wu GH, Wang HQ, Chen ZC, Chen JC, Zhou QH, Lu JW, Fan QX, Huang JJ, Zheng X. 2004. **Phase III randomized clinical trial of intratumoral injection of E1B gene-deleted adenovirus (H101) combined with cisplatin-based chemotherapy in treating**

squamous cell cancer of head and neck or esophagus. *Aizheng Chinese Journal of Cancer* 23:1666-1670.

48. Freytag SO, Stricker H, Pegg J, Paielli D, Pradhan DG, Peabody J, DePeralta-Venturina M, Xia X, Brown S, Lu M, Kim JH. 2003. **Phase I Study of Replication-Competent Adenovirus-Mediated Double-Suicide Gene Therapy in Combination with Conventional-Dose Three-Dimensional Conformal Radiation Therapy for the Treatment of Newly Diagnosed, Intermediate- to High-Risk Prostate Cancer.** *Cancer Research* 63:7497-7506.

49. Ranki T, Pesonen S, Hemminki A, Partanen K, Kairemo K, Alanko T, Lundin J, Linder N, Turkki R, Ristimäki A, Jäger E, Karbach J, Wahle C, Kankainen M, Backman C, von Euler M, Haavisto E, Hakonen T, Heiskanen R, Jaderberg M, Juhila J, Priha P, Suoranta L, Vassilev L, Vuolanto A, Joensuu T. 2016. **Phase I study with ONCOS-102 for the treatment of solid tumors - an evaluation of clinical response and exploratory analyses of immune markers.** *Journal for immunotherapy of cancer* 4:17-17.

50. Harrington KJ, Hingorani M, Tanay MA, Hickey J, Bhide SA, Clarke PM, Renouf LC, Thway K, Sibtain A, McNeish IA, Newbold KL, Goldsweig H, Coffin R, Nutting CM. 2010. **Phase I/II study of oncolytic HSV GM-CSF in combination with radiotherapy and cisplatin in untreated stage III/IV squamous cell cancer of the head and neck.** *Clinical Cancer Research* 16:4005-4015.

51. Puzanov I, Milhem MM, Minor D, Hamid O, Li A, Chen L, Chastain M, Gorski KS, Anderson A, Chou J, Kaufman HL, Andtbacka RHI. 2016. **Talimogene Laherparepvec in Combination With Ipilimumab in Previously Untreated, Unresectable Stage IIIB-IV Melanoma.** *Journal of Clinical Oncology* 34:2619-2626.

52. Markert JM, Razdan SN, Kuo H-C, Cantor A, Knoll A, Karrasch M, Nabors LB, Markiewicz M, Agee BS, Coleman JM, Lakeman AD, Palmer CA, Parker JN, Whitley RJ, Weichselbaum RR, Fiveash JB, Gillespie GY. 2014. **A Phase 1 Trial of Oncolytic HSV-1, G207, Given in Combination With Radiation for Recurrent GBM Demonstrates Safety and Radiographic Responses.** *Molecular Therapy* 22:1048-1055.

53. Karapanagiotou EM, Roulstone V, Twigger K, Ball M, Tanay M, Nutting C, Newbold K, Gore ME, Larkin J, Syrigos KN, Coffey M, Thompson B, Mettinger K, Vile RG, Pandha HS, Hall GD, Melcher AA, Chester J, Harrington KJ. 2012. **Phase I/II trial of carboplatin and paclitaxel chemotherapy in combination with intravenous oncolytic reovirus in patients with advanced malignancies.** *Clinical cancer research : an official journal of the American Association for Cancer Research* 18:2080-2089.

54. Lampreht Tratar U, Horvat S, Cemazar M. 2018. **Transgenic Mouse Models in Cancer Research.** *Frontiers in oncology* 8:268-268.

55. Chavan A. 2013. **Animal models of cancer: a review.** *International Journal of Pharmaceutical Sciences and Research* 4:19-28.

56. House CD, Hernandez L, Annunziata CM. 2014. **Recent technological advances in using mouse models to study ovarian cancer.** *Frontiers in oncology* 4:26-26.

57. Clemens MJ. 2004. **Targets and mechanisms for the regulation of translation in malignant transformation.** *Oncogene* 23:3180-8.

58. Guo ZS, Liu Z, Bartlett DL. 2014. **Oncolytic Immunotherapy: Dying the Right Way is a Key to Eliciting Potent Antitumor Immunity.** *Frontiers in oncology* 4:74-74.

59. Fountzilas C, Patel S, Mahalingam D. 2017. **Review: Oncolytic virotherapy, updates and future directions.** *Oncotarget* 8:102617-102639.

60. You Z, Fischer DC, Tong X, Hasenburg A, Aguilar-Cordova E, Kieback DG. 2001. **Coxsackievirus–adenovirus receptor expression in ovarian cancer cell lines is associated with increased adenovirus transduction efficiency and transgene expression.** *Cancer Gene Therapy* 8:168-175.

61. Sanchala DS, Bhatt LK, Prabhavalkar KS. 2017. **Oncolytic Herpes Simplex Viral Therapy: A Stride toward Selective Targeting of Cancer Cells.** *Frontiers in pharmacology* 8:270-270.

62. Andtbacka RH, Kaufman HL, Collichio F, Amatruda T, Senzer N, Chesney J, Delman KA, Spitler LE, Puzanov I, Agarwala SS, Milhem M, Cranmer L, Curti B, Lewis K, Ross M, Guthrie T, Linette GP, Daniels GA, Harrington K, Middleton MR, Miller WH, Jr., Zager JS, Ye Y, Yao B, Li A, Doleman S, VanderWalde A, Gansert J, Coffin RS. 2015. **Talimogene Laherparepvec Improves Durable Response Rate in Patients With Advanced Melanoma.** *Journal of Clinical Oncology* 33:2780-8.

63. Varghese S, Rabkin SD, Liu R, Nielsen PG, Ipe T, Martuza RL. 2006. **Enhanced therapeutic efficacy of IL-12, but not GM-CSF, expressing oncolytic herpes simplex virus for transgenic mouse derived prostate cancers.** *Cancer Gene Therapy* 13:253-265.

64. Fukuhara H, Ino Y, Todo T. 2016. **Oncolytic virus therapy: A new era of cancer treatment at dawn.** *Cancer science* 107:1373-1379.

65. Ilan Y, Sauter B, Chowdhury NR, Reddy BV, Thummala NR, Droguett G, Davidson A, Ott M, Horwitz MS, Chowdhury JR. 1998. **Oral tolerization to adenoviral proteins permits repeated adenovirus-mediated gene therapy in rats with pre-existing immunity to adenoviruses.** *Hepatology* 27:1368-76.

66. Ricca JM, Oseledchyk A, Walther T, Liu C, Mangarin L, Merghoub T, Wolchok JD, Zamarin D. 2018. **Pre-existing Immunity to Oncolytic Virus Potentiates Its Immunotherapeutic Efficacy.** *Molecular Therapy* 26:1008-1019.

67. Kim J, Hall RR, Lesniak MS, Ahmed AU. 2015. **Stem Cell-Based Cell Carrier for Targeted Oncolytic Virotherapy: Translational Opportunity and Open Questions.** *Viruses* 7:6200-6217.

68. Brown VR, Bevins SN. 2017. **A review of virulent Newcastle disease viruses in the United States and the role of wild birds in viral persistence and spread.** *Veterinary research* 48:68-68.

69. Alexander DJ. 1988. **Historical Aspects. In: Alexander D.J. (eds) Newcastle Disease.** *Developments in Veterinary Virology*, vol 8. Springer, Boston, MAHistorical Aspects, pp1-10. doi:10.1007/978-1-4613-1759-3_1.

70. Walker PJ, Siddell SG, Lefkowitz EJ, Mushegian AR, Dempsey DM, Dutilh BE, Harrach B, Harrison RL, Hendrickson RC, Junglen S, Knowles NJ, Kropinski AM, Krupovic M, Kuhn JH, Nibert M, Rubino L, Sabanadzovic S, Simmonds P, Varsani A, Zerbini FM, Davison AJ. 2019. **Changes to virus taxonomy and the International Code of Virus Classification and Nomenclature ratified by the International Committee on Taxonomy of Viruses (2019).** *Archives of Virology* 164:2417-2429.

71. Fields BN, Knipe DM, Howley PM. 2007. **Fields virology.** Wolters Kluwer Health/Lippincott Williams & Wilkins, Philadelphia.

72. Nagai Y, Hamaguchi M, Toyoda T. 1989. **Molecular biology of Newcastle disease virus.** *Prog Vet Microbiol Immunol* 5:16-64.

73. Ganar K, Das M, Sinha S, Kumar S. 2014. **Newcastle disease virus: Current status and our understanding.** *Virus Research* 184:71-81.

74. Cattoli G, Susta L, Terregino C, Brown C. 2011. **Newcastle disease: a review of field recognition and current methods of laboratory detection.** *Journal of Veterinary Diagnostic Investigation* 23:637-56.

75. Fournier P, Schirrmacher V. 2013. **Oncolytic Newcastle Disease Virus as Cutting Edge between Tumor and Host.** *Biology (Basel)* 2:936-75.

76. Miller PJ, Decanini EL, Afonso CL. 2010. **Newcastle disease: Evolution of genotypes and the related diagnostic challenges.** *Infection, Genetics and Evolution* 10:26-35.

77. Diel DG, da Silva LHA, Liu H, Wang Z, Miller PJ, Afonso CL. 2012. **Genetic diversity of avian paramyxovirus type 1: Proposal for a unified nomenclature and classification system of Newcastle disease virus genotypes.** *Infection, Genetics and Evolution* 12:1770-1779.

78. Servan de Almeida R, Hammoumi S, Gil P, Briand F-X, Molia S, Gaidet N, Cappelle J, Chevalier V, Balança G, Traore A, Grillet C, Maminiaina OF, Guendouz S, Dakouo M, Samake K, Bezeid OEM, Diarra A, Chaka H, Goutard F, Thompson P, Martinez D, Jestin V, Albina E. 2013. **New avian paramyxoviruses type I strains identified in Africa provide new outcomes for phylogeny reconstruction and genotype classification.** *PLOS ONE* 8(10): e76413.

79. Harrison MS, Sakaguchi T, Schmitt AP. 2010. **Paramyxovirus assembly and budding: Building particles that transmit infections.** *The International Journal of Biochemistry & Cell Biology* 42:1416-1429.

80. Connaris H, Takimoto T, Russell R, Crennell S, Moustafa I, Portner A, Taylor G. 2002. **Probing the sialic acid binding site of the hemagglutinin-neuraminidase of Newcastle disease virus: identification of key amino acids involved in cell binding, catalysis, and fusion.** *Journal of Virology* 76:1816-24.

81. Lamb RA, Parks GD. 2013. **Paramyxoviridae: the viruses and their replication., 6 ed,** vol 1. Lippincott, Williams, and Wilkins, Philadelphia

82. Sánchez-Felipe L, Villar E, Muñoz-Barroso IJGJ. 2012. **α2-3- and α2-6- N-linked sialic acids allow efficient interaction of Newcastle Disease Virus with target cells.** *Glycoconjugate Journal* 29:539-549.

83. Ferreira L, Villar E, Munoz-Barroso I. 2004. **Gangliosides and N-glycoproteins function as Newcastle disease virus receptors.** *The International Journal of Biochemistry & Cell Biology* 36:2344-56.

84. Choppin PW, Compans RW. 1975. **Reproduction of Paramyxoviruses**, p 95-178. *In* Fraenkel-Conrat H, Wagner RR (ed), Comprehensive Virology: 4 Reproduction: Large RNA Viruses doi:10.1007/978-1-4684-2706-6_2. Springer US, Boston, MA.

85. Cantin C, Holguera J, Ferreira L, Villar E, Munoz-Barroso I. 2007. **Newcastle disease virus may enter cells by caveolae-mediated endocytosis.** *Journal of General Virology* 88:559-569.

86. Tan L, Zhang Y, Zhan Y, Yuan Y, Sun Y, Qiu X, Meng C, Song C, Liao Y, Ding C. 2016. **Newcastle disease virus employs macropinocytosis and Rab5a-dependent intracellular trafficking to infect DF-1 cells.** *Oncotarget* 7:86117-86133.

87. Peeters BP, Gruijthuijsen YK, de Leeuw OS, Gielkens AL. 2000. **Genome replication of Newcastle disease virus: involvement of the rule-of-six.** *Archives of Virology* 145:1829-45.

88. Parks GD, Alexander-Miller MA. 2013. **Paramyxovirus activation and inhibition of innate immune responses.** *Journal of Molecular Biology* 425:4872-92.

89. Yusoff K, Tan WS. 2001. **Newcastle disease virus: macromolecules and opportunities.** *Avian Pathology* 30:439-55.

90. Yan Y, Samal SK. 2008. **Role of intergenic sequences in newcastle disease virus RNA transcription and pathogenesis.** *Journal of Virology* 82:1323-31.

91. Mebatsion T, Verstegen S, De Vaan LT, Romer-Oberdorfer A, Schrier CC. 2001. **A recombinant newcastle disease virus with low-level V protein expression is immunogenic and lacks pathogenicity for chicken embryos.** *Journal of Virology* 75:420-8.

92. El Najjar F, Schmitt AP, Dutch RE. 2014. **Paramyxovirus glycoprotein incorporation, assembly and budding: a three way dance for infectious particle production.** *Viruses* 6:3019-54.

93. Sinkovics J. 1957. **Studies on the biological characteristics of the newcastle disease virus (NDV) adapted to the brain of newborne mice.** *Archiv für die gesamte Virusforschung* 7:403-411.

94. Cassel WA, Garrett RE. 1965. **Newcastle disease virus as an antineoplastic agent.** *Cancer* 18:863-868.

95. Russell SJ. 2002. **RNA viruses as virotherapy agents.** *Cancer Gene Therapy* 9:961-966.

96. Reichard KW, Lorence RM, Cascino CJ, Peeples ME, Walter RJ, Fernando MB, Reyes HM, Greager JA. 1992. **Newcastle disease virus selectively kills human tumor cells.** *Journal of Surgical Research* 52:448-453.

97. Fiola C, Peeters B, Fournier P, Arnold A, Bucur M, Schirrmacher V. 2006. **Tumor selective replication of Newcastle disease virus: association with defects of tumor cells in antiviral defence.** *International Journal of Cancer* 119:328-338.

98. Mansour M, Palese P, Zamarin D. 2011. **Oncolytic specificity of Newcastle disease virus is mediated by selectivity for apoptosis-resistant cells.** *Journal of Virology* 85:6015-6023.

99. Lazar I, Yaacov B, Shiloach T, Eliahoo E, Kadouri L, Lotem M, Perlman R, Zakay-Rones Z, Panet A, Ben-Yehuda D. 2010. **The Oncolytic Activity of Newcastle Disease Virus NDV-HUJ on Chemoresistant Primary Melanoma Cells Is Dependent on the Proapoptotic Activity of the Inhibitor of Apoptosis Protein Livin.** *Journal of Virology* 84:639-646.

100. Goodbourn S, Didcock L, Randall R. 2000. **Interferons: cell signalling, immune modulation, antiviral response and virus countermeasures.** *Journal of General Virology* 81:2341-2364.

101. Isaacs A, Lindenmann J. 1957. **Virus interference. I. The interferon.** *Proceedings of the Royal Society B: Biological Sciences* 147:258-267.

102. Horvath CM. 2004. **Weapons of STAT destruction. Interferon evasion by paramyxovirus V protein.** *European Journal of Biochemistry* 271:4621-4628.

103. Park M-S, Shaw ML, Munoz-Jordan J, Cros JF, Nakaya T, Bouvier N, Palese P, García-Sastre A, Basler CF. 2003. **Newcastle disease virus (NDV)-based assay demonstrates interferon-antagonist activity for the NDV V protein and the Nipah virus V, W, and C proteins.** *Journal of Virology* 77:1501-1511.

104. Krishnamurthy S, Takimoto T, Scroggs RA, Portner A. 2006. **Differentially regulated interferon response determines the outcome of Newcastle disease virus infection in normal and tumor cell lines.** *Journal of Virology* 80:5145-55.

105. Wilden H, Fournier P, Zawatzky R, Schirrmacher V. 2009. **Expression of RIG-I, IRF3, IFN-β and IRF7 determines resistance or susceptibility of cells to infection by Newcastle Disease Virus.** *International Journal of Oncology* 34:971-982.

106. Cheng J, Sun Y, Zhang X, Zhang F, Zhang S, Yu S, Qiu X, Tan L, Song C, Gao S, Wu Y, Ding C. 2014. **Toll-like receptor 3 inhibits Newcastle disease virus replication through activation of pro-inflammatory cytokines and the type-1 interferon pathway.** *Archives of Virology* 159:2937-2948.

107. Wilden H, Schirrmacher V, Fournier P. 2011. **Important role of interferon regulatory factor (IRF)-3 in the interferon response of mouse macrophages upon infection by Newcastle disease virus.** *International Journal of Oncology* 39:493-504.

108. Lorence RM, Katubig BB, Reichard KW, Reyes HM, Phuangsab A, Sassetti MD, Walter RJ, Peeples ME. 1994. **Complete Regression of Human Fibrosarcoma Xenografts after Local Newcastle Disease Virus Therapy.** *Cancer Research* 54:6017-6021.

109. Büll C, Stoel MA, den Brok MH, Adema GJ. 2014. **Sialic Acids Sweeten a Tumor's Life.** *Cancer Research* 74:3199-3204.

110. Santer UV, DeSantis R, Hard KJ, van Kuik JA, Vliegenthart JF, Won B, Glick MC. 1989. **N-linked oligosaccharide changes with oncogenic transformation require sialylation of multiantennae.** *European Journal of Biochemistry* 181:249-60.

111. Puhlmann J, Puehler F, Mumberg D, Boukamp P, Beier R. 2010. **Rac1 is required for oncolytic NDV replication in human cancer cells and establishes a link between tumorigenesis and sensitivity to oncolytic virus.** *Oncogene* 29:2205-16.

112. Schmitz AAP, Govek E-E, Böttner B, Van Aelst L. 2000. **Rho GTPases: Signaling, Migration, and Invasion.** *Experimental Cell Research* 261:1-12.

113. Taylor MP, Koyuncu OO, Enquist LW. 2011. **Subversion of the actin cytoskeleton during viral infection.** *Nature Reviews Microbiology* 9:427+.

114. Westover KM, Hughes AL. 2001. **Molecular Evolution of Viral Fusion and Matrix Protein Genes and Phylogenetic Relationships among the Paramyxoviridae.** *Molecular Phylogenetics and Evolution* 21:128-134.

115. Pecora AL, Rizvi N, Cohen GI, Meropol NJ, Sterman D, Marshall JL, Goldberg S, Gross P, O'Neil JD, Groene WS. 2002. **Phase I trial of intravenous administration of PV701, an oncolytic virus, in patients with advanced solid cancers.** *Journal of Clinical Oncology* 20:2251-2266.

116. Lorence RM, Roberts MS, Groene WS, Rabin H. 2001. **Replication-Competent, Oncolytic Newcastle Disease Virus for Cancer Therapy.** (Hernáiz Driever P, Rabkin SD (eds): Replication-Competent Viruses for Cancer Therapy). *Monographs in Virology*. Basel, Karger, vol 22, pp 160-182. doi:10.1159/000061724.

117. Hotte SJ, Lorence RM, Hirte HW, Polawski SR, Bamat MK, O'Neil JD, Roberts MS, Groene WS, Major PP. 2007. **An Optimized Clinical Regimen for the Oncolytic Virus PV701.** *Clinical Cancer Research* 13:977-985.

118. Alexander D. 2000. **Newcastle disease and other avian paramyxoviruses.** *Revue Scientifique et Technique-Office International des Epizooties* 19:443-455.

119. Fournier P, Wilden H, Schirrmacher V. 2012. **Importance of retinoic acid-inducible gene I and of receptor for type I interferon for cellular resistance to infection by Newcastle disease virus.** *International Journal of Oncology* 40:287-98.

120. Alexopoulou L, Holt AC, Medzhitov R, Flavell RA. 2001. **Recognition of double-stranded RNA and activation of NF-κB by Toll-like receptor 3.** *Nature* 413:732-738.

121. Zeng J, Fournier P, Schirrmacher V. 2002. **Induction of Interferon-α and Tumor Necrosis Factor-Related Apoptosis-Inducing Ligand in Human Blood Mononuclear Cells by Hemagglutinin-Neuraminidase but Not F Protein of Newcastle Disease Virus.** *Virology* 297:19-30.

122. Schirrmacher V, Ahlert T, Probstle T, Steiner HH, Herold-Mende C, Gerhards R, Hagmuller E, Steiner HH. 1998. **Immunization with virus-modified tumor cells.** *Seminars in Oncology* 25:677-96.

123. Schirrmacher V, Haas C, Bonifer R, Ahlert T, Gerhards R, Ertel C. 1999. **Human tumor cell modification by virus infection: an efficient and safe way to produce cancer vaccine with pleiotropic immune stimulatory properties when using Newcastle disease virus.** *Gene Therapy* 6:63-73.

124. Ertel C, Millar NS, Emmerson PT, Schirrmacher V, von Hoegen P. 1993. **Viral hemagglutinin augments peptide-specific cytotoxic T cell responses.** *European Journal of Immunology* 23:2592-6.

125. Lam K, Vasconcelos A, Bickford A. 1995. **Apoptosis as a cause of death in chicken embryos inoculated with Newcastle disease virus.** *Microbial Pathogenesis* 19:169-174.

126. Ravindra PV, Tiwari AK, Sharma B, Rajawat YS, Ratta B, Palia S, Sundaresan NR, Chaturvedi U, Gangaplara A, Chindera K, Saxena M, Subudhi PK, Rai A, Chauhan RS. 2008. **HN protein of Newcastle disease virus causes apoptosis in chicken embryo fibroblast cells.** *Archives of Virology* 153:749-54.

127. Molouki A, Hsu Y-T, Jahanshiri F, Abdullah S, Rosli R, Yusoff K. 2011. **The matrix (M) protein of Newcastle disease virus binds to human bax through its BH3 domain.** *Virology Journal* 8:385-385.

128. Ravindra PV, Tiwari AK, Ratta B, Chaturvedi U, Palia SK, Subudhi PK, Kumar R, Sharma B, Rai A, Chauhan RS. 2008. **Induction of apoptosis in Vero cells by Newcastle disease virus requires viral replication, de-novo protein synthesis and caspase activation.** *Virus Research* 133:285-290.

129. Szeberényi KJ, Fábián KZ, Töröcsik KB, Kiss KK, Csatary KL. 2003. **Newcastle Disease Virus-induced Apoptosis in PC12 Pheochromocytoma Cells.** *American Journal of Therapeutics* 10:282-288.

130. Molouki A, Hsu YT, Jahanshiri F, Rosli R, Yusoff K. 2010. **Newcastle Disease Virus Infection Promotes Bax Redistribution to Mitochondria and Cell Death in HeLa Cells.** *Intervirology* 53:87-94.

131. Ravindra PV, Tiwari AK, Ratta B, Bais MV, Chaturvedi U, Palia SK, Sharma B, Chauhan RS. 2009. **Time course of Newcastle disease virus-induced apoptotic pathways.** *Virus Research* 144:350-354.

132. Elankumaran S, Rockemann D, Samal SK. 2006. **Newcastle disease virus exerts oncolysis by both intrinsic and extrinsic caspase-dependent pathways of cell death.** *Journal of Virology* 80:7522-34.

133. Galluzzi L, Brenner C, Morselli E, Touat Z, Kroemer G. 2008. **Viral Control of Mitochondrial Apoptosis.** *PLOS Pathogens* 4:e1000018.

134. Baig S, Seevasant I, Mohamad J, Mukheem A, Huri HZ, Kamarul T. 2016. **Potential of apoptotic pathway-targeted cancer therapeutic research: Where do we stand?** *Cell Death & Disease* 7:e2058-e2058.

135. Fábián Z, Csatary CM, Szeberényi J, Csatary LK. 2007. **p53-Independent Endoplasmic Reticulum Stress-Mediated Cytotoxicity of a Newcastle Disease Virus Strain in Tumor Cell Lines.** *Journal of Virology* 81:2817.

136. Bian J, Wang K, Kong X, Liu H, Chen F, Hu M, Zhang X, Jiao X, Ge B, Wu Y, Meng S. 2011. **Caspase- and p38-MAPK-dependent induction of apoptosis in A549 lung cancer cells by Newcastle disease virus.** *Archives of Virology* 156:1335-1344.

137. Fabian Z, Torocsik B, Kiss K, Csatary LK, Bodey B, Tigyi J, Csatary C, Szeberenyi J. 2001. **Induction of apoptosis by a Newcastle disease virus vaccine (MTH-68/H) in PC12 rat phaeochromocytoma cells**. *Anticancer Research* 21:125-35.

138. Ryan EL, Hollingworth R, Grand RJ. 2016. **Activation of the DNA Damage Response by RNA Viruses.** *Biomolecules* 6:2.

139. Machida K, Cheng KT-H, Sung VM-H, Lee KJ, Levine AM, Lai MMC. 2004. **Hepatitis C Virus Infection Activates the Immunologic (Type II) Isoform of Nitric Oxide Synthase and Thereby Enhances DNA Damage and Mutations of Cellular Genes.** *Journal of Virology* 78:8835-8843.

140. Ali- Saeed R, Alabsi AM, Ideris A, Omar AR, Yusoff K, Ali AM. 2019. **Evaluation of Ultra-Microscopic Changes and Proliferation of Apoptotic Glioblastoma Multiforme Cells Induced by Velogenic Strain of Newcastle Disease Virus AF2240.** *Asian Pacific Journal of Cancer Prevention* 20:757-765.

141. Meng C, Zhou Z, Jiang K, Yu S, Jia L, Wu Y, Liu Y, Meng S, Ding C. 2012. **Newcastle disease virus triggers autophagy in U251 glioma cells to enhance virus replication.** *Archives of Virology* 157:1011-1018.

142. Koks CA, Garg AD, Ehrhardt M, Riva M, Vandenberk L, Boon L, De Vleeschouwer S, Agostinis P, Graf N, Van Gool SW. 2015. **Newcastle disease virotherapy induces long-term survival and tumor-specific immune memory in orthotopic glioma through the induction of immunogenic cell death.** *International Journal of Cancer* 136:E313-25.

143. Othman F, Ideris A, Motaleb GR, Eshak ZBT, Rahmat A. 2010. **Oncolytic effect of newcastle disease virus af2240 strain on the mcf-7 breast cancer cell line.** *Cell Journal (Yakhteh)* 12:17-24.

144. Schwaiger T, Knittler MR, Grund C, Roemer-Oberdoerfer A, Kapp J-F, Lerch MM, Mettenleiter TC, Mayerle J, Blohm U. 2017. **Newcastle disease virus mediates pancreatic tumor rejection via NK cell activation and prevents cancer relapse by prompting adaptive immunity.** *International Journal of Cancer* 141:2505-2516.

145. Schirrmacher V, Bai L, Umansky V, Yu L, Xing Y, Qian Z. 2000. **Newcastle disease virus activates macrophages for anti-tumor activity.** *International Journal of Oncology* 16:363-436.

146. Lorence RM, Rood PA, Kelley KW. 1988. **Newcastle Disease Virus as an Antineoplastic Agent: Induction of Tumor Necrosis Factor-α and Augmentation of Its Cytotoxicity3.** *JNCI: Journal of the National Cancer Institute* 80:1305-1312.

147. Umansky V, Shatrov VA, Lehmann V, Schirrmacher V. 1996. **Induction of NO synthesis in macrophages by Newcastle disease virus is associated with activation of nuclear factor-κB.** *International Immunology* 8:491-498.

148. Hrabák A, Csuka I, Bajor T, Csatáry LK. 2006. **The cytotoxic anti-tumor effect of MTH-68/H, a live attenuated Newcastle disease virus is mediated by the induction of nitric oxide synthesis in rat peritoneal macrophages *in vitro.*** *Cancer Letters* 231:279-289.

149. Washburn B, Weigand MA, Grosse-Wilde A, Janke M, Stahl H, Rieser E, Sprick MR, Schirrmacher V, Walczak H. 2003. **TNF-Related Apoptosis-Inducing Ligand Mediates Tumoricidal Activity of Human Monocytes Stimulated by Newcastle Disease Virus.** *The Journal of Immunology* 170:1814-1821.

150. Ni J, Galani IE, Cerwenka A, Schirrmacher V, Fournier P. 2011. **Antitumor vaccination by Newcastle Disease Virus Hemagglutinin–Neuraminidase plasmid DNA application: Changes in tumor microenvironment and activation of innate anti-tumor immunity.** *Vaccine* 29:1185-1193.

151. Jarahian M, Watzl C, Fournier P, Arnold A, Djandji D, Zahedi S, Cerwenka A, Paschen A, Schirrmacher V, Momburg F. 2009. **Activation of natural killer cells by newcastle disease virus hemagglutinin-neuraminidase.** *Journal of Virology* 83:8108-8121.

152. Washburn B, Schirrmacher V. 2002. **Human tumor cell infection by Newcastle Disease Virus leads to upregulation of HLA and cell adhesion molecules and to induction of interferons, chemokines and finally apoptosis.** *International Journal of Oncology* 21:85-93.

153. Koks CA, Garg AD, Ehrhardt M, Riva M, Vandenberk L, Boon L, Vleeschouwer SD, Agostinis P, Graf N, Van Gool SW. 2015. **Newcastle disease virotherapy induces long-term survival and tumor-specific immune memory in orthotopic glioma through the induction of immunogenic cell death.** *International Journal of Cancer* 136:E313-E325.

154. Schirrmacher V, van Gool S, Stuecker W. 2019. **Breaking Therapy Resistance: An Update on Oncolytic Newcastle Disease Virus for Improvements of Cancer Therapy.** *Biomedicines* 7:66.

155. Termeer CC, Schirrmacher V, Bröcker E-B, Becker JC. 2000. **Newcastle disease virus infection induces B7-1/B7-2-independent T-cell costimulatory activity in human melanoma cells.** *Cancer Gene Therapy* 7:316-323.

156. Zamarin D, Holmgaard RB, Subudhi SK, Park JS, Mansour M, Palese P, Merghoub T, Wolchok JD, Allison JP. 2014. **Localized Oncolytic Virotherapy Overcomes Systemic Tumor Resistance to Immune Checkpoint Blockade Immunotherapy.** *Science Translational Medicine* 6:226ra32-226ra32.

157. Howells A, Marelli G, Lemoine NR, Wang Y. 2017. **Oncolytic Viruses—Interaction of Virus and Tumor Cells in the Battle to Eliminate Cancer.** *Frontiers in Oncology* 7.

158. Peeters BPH, de Leeuw OS, Koch G, Gielkens ALJ. 1999. **Rescue of Newcastle Disease Virus from Cloned cDNA: Evidence that Cleavability of the Fusion Protein Is a Major Determinant for Virulence.** *Journal of Virology* 73:5001-5009.

159. Cardenas-Garcia S, Afonso CL. 2017. **Reverse Genetics of Newcastle Disease Virus,** p 141-158. *In* Perez DR (ed), Reverse Genetics of RNA Viruses: Methods and Protocols doi:10.1007/978-1-4939-6964-7_10. Springer New York, New York, NY.

160. Song KY, Wong J, Gonzalez L, Sheng G, Zamarin D, Fong Y. 2010. **Antitumor efficacy of viral therapy using genetically engineered Newcastle disease virus [NDV(F3aa)-GFP] for peritoneally disseminated gastric cancer.** *Journal of molecular medicine (Berlin, Germany)* 88:589-596.

161. Altomonte J, Marozin S, Schmid RM, Ebert O. 2010. **Engineered newcastle disease virus as an improved oncolytic agent against hepatocellular carcinoma.** *Molecular therapy : the journal of the American Society of Gene Therapy* 18:275-284.

162. Vigil A, Martinez O, Chua MA, García-Sastre A. 2008. **Recombinant Newcastle disease virus as a vaccine vector for cancer therapy.** *Molecular therapy: the journal of the American Society of Gene Therapy* 16:1883-1890.

163. Vigil A, Park M-S, Martinez O, Chua MA, Xiao S, Cros JF, Martínez-Sobrido L, Woo SLC, García-Sastre A. 2007. **Use of Reverse Genetics to Enhance the Oncolytic Properties of Newcastle Disease Virus.** *Cancer Research* 67:8285-8292.

164. Zamarin D, Palese P. 2012. **Oncolytic Newcastle disease virus for cancer therapy: old challenges and new directions.** *Future Microbiology* 7:347-367.

165. Zamarin D, Vigil A, Kelly K, García-Sastre A, Fong Y. 2009. **Genetically engineered Newcastle disease virus for malignant melanoma therapy.** *Gene Therapy* 16:796-804.

166. Park M-S, Steel J, García-Sastre A, Swayne D, Palese P. 2006. **Engineered viral vaccine constructs with dual specificity: avian influenza and Newcastle disease.** *Proceedings of the National Academy of Sciences of the United States of America* 103:8203-8208.

167. Elankumaran S, Chavan V, Qiao D, Shobana R, Moorkanat G, Biswas M, Samal SK. 2010. **Type I Interferon-Sensitive Recombinant Newcastle Disease Virus for Oncolytic Virotherapy.** *Journal of Virology* 84:3835-3844.

168. Zamarin D, Martínez-Sobrido L, Kelly K, Mansour M, Sheng G, Vigil A, García-Sastre A, Palese P, Fong Y. 2009. **Enhancement of oncolytic properties of recombinant newcastle disease virus through antagonism of cellular innate immune responses.** *Molecular therapy : the journal of the American Society of Gene Therapy* 17:697-706.

169. Wu Y, Zhang X, Wang X, Wang L, Hu S, Liu X, Meng S. 2012. **Apoptin Enhances the Oncolytic Properties of Newcastle Disease Virus.** *Intervirology* 55:276-286.

170. Pühler F, Willuda J, Puhlmann J, Mumberg D, Römer-Oberdörfer A, Beier R. 2008. **Generation of a recombinant oncolytic Newcastle disease virus and expression of a full IgG antibody from two transgenes.** *Gene Therapy* 15:371-383.

171. Maamary J, Array F, Gao Q, García-Sastre A, Steinman RM, Palese P, Nchinda G. 2011. **Newcastle Disease Virus Expressing a Dendritic Cell-Targeted HIV Gag Protein Induces a Potent Gag-Specific Immune Response in Mice.** *Journal of Virology* 85:2235-2246.

172. Bian H, Fournier P, Moormann R, Peeters B, Schirrmacher V. 2005. **Selective gene transfer in vitro to tumor cells via recombinant Newcastle disease virus.** *Cancer Gene Therapy* 12:295-303.

173. Bian H, Fournier P, Peeters B, Schirrmacher V. 2005. **Tumor-targeted gene transfer in vivo via recombinant Newcastle disease virus modified by a bispecific fusion protein.** *International Journal of Oncology* 27:377-84.

174. Bian H, Fournier P, Moormann R, Peeters B, Schirrmacher V. 2005. **Selective gene transfer to tumor cells by recombinant Newcastle Disease Virus via a bispecific fusion protein.** *International Journal of Oncology* 26:431-9.

175. Haas C, Lulei M, Fournier P, Arnold A, Schirrmacher V. 2006. **A tumor vaccine containing anti-CD3 and anti-CD28 bispecific antibodies triggers strong and durable antitumor activity in human lymphocytes.** *International Journal of Cancer* 118:658-67.

176. Fournier P, Aigner M, Schirrmacher V. 2010. **Transcriptome analysis and cytokine profiling of naive T cells stimulated by a tumor vaccine via CD3 and CD25.** *International Journal of Oncology* 37:1439-52.

177. Goto M, Okazaki M, Yazaki H. 1959. **Oncolytic effect of Newcastle disease virus on Yoshida sarcoma (1).** *Japanese Journal of Microbiology* 3:171-81.

178. Wheelock EF, Dingle JH. 1964. **Observations on the Repeated Administration of Viruses to a Patient with Acute Leukemia.** *New England Journal of Medicine* 271:645-651.

179. Cassel WA, Murray DR. 1992. **A ten-year follow-up on stage II malignant melanoma patients treated postsurgically with Newcastle disease virus oncolysate.** *Med Oncol Tumor Pharmacother* 9:169-71.

180. Batliwalla FM, Bateman BA, Serrano D, Murray D, Macphail S, Maino VC, Ansel JC, Gregersen PK, Armstrong CA. 1998. **A 15-year follow-up of AJCC stage III malignant melanoma patients treated postsurgically with Newcastle disease virus (NDV) oncolysate and determination of alterations in the CD8 T cell repertoire.** *Molecular Medicine* 4:783-94.

181. Schirrmacher V. (1989) **Successful Application of a Virus-Modified Tumor Vaccine for Anti-Metastatic Cancer Immunotherapy. In:** Drahovsky D., Kornhuber B. (eds) Human Malignancies. Springer, Berlin, Heidelberg

182. Shoham J, Hirsch R, Zakay-Rones Z, Osband ME, Brennert HJ. 1990. **Augmentation of tumor cell immunogenicity by viruses--an approach to specific immunotherapy of cancer.** *Natural immunity and cell growth regulation* 9:165-72.

183. Plaksin D, Porgador A, Vadai E, Feldman M, Schirrmacher V, Eisenbach L. 1994. **Effective anti-metastatic melanoma vaccination with tumor cells transfected with MHC genes and/or infected with newcastle disease virus (NDV).** *International Journal of Cancer* 59:796-801.

184. Schirrmacher V, Heicappell R. 1987. **Prevention of metastatic spread by postoperative immunotherapy with virally modified autologous tumor cells. II. Establishment of specific systemic anti-tumor immunity.** *Clinical & Experimental Metastasis* 5:147-56.

185. Schirrmacher V. 2005. **Clinical trials of antitumor vaccination with an autologous tumor cell vaccine modified by virus infection: improvement of patient survival based on improved antitumor immune memory.** *Cancer Immunology, Immunotherapy* 54:587-598.

186. Bohle W, Schlag P, Liebrich W, Hohenberger P, Manasterski M, Moller P, Schirrmacher V. 1990. **Postoperative active specific immunization in colorectal cancer patients with virus-modified autologous tumor-cell vaccine. First clinical results with tumor-cell vaccines modified with live but avirulent Newcastle disease virus.** *Cancer* 66:1517-23.

187. Schlag P, Manasterski M, Gerneth T, Hohenberger P, Dueck M, Herfarth C, Liebrich W, Schirrmacher V. 1992. **Active specific immunotherapy with Newcastle-disease-virus-modified autologous tumor cells following resection of liver metastases in colorectal cancer. First evaluation of clinical response of a phase II-trial.** *Cancer Immunol Immunother* 35:325-30.

188. Liang W, Wang H, Sun T-M, Yao W-Q, Chen L-L, Jin Y, Li C-L, Meng F-J. 2003. **Application of autologous tumor cell vaccine and NDV vaccine in treatment of tumors of digestive tract.** *World Journal of Gastroenterology* 9:495-498.

189. Steiner HH, Bonsanto MM, Beckhove P, Brysch M, Geletneky K, Ahmadi R, Schuele-Freyer R, Kremer P, Ranaie G, Matejic D, Bauer H, Kiessling M, Kunze S, Schirrmacher V, Herold-Mende C. 2004. **Antitumor Vaccination of Patients With Glioblastoma Multiforme: A Pilot Study to Assess Feasibility, Safety, and Clinical Benefit.** *Journal of Clinical Oncology* 22:4272-4281.

190. Csatary LK, Gosztonyi G, Szeberenyi J, Fabian Z, Liszka V, Bodey B, Csatary CM. 2004. **MTH-68/H oncolytic viral treatment in human high-grade gliomas.** *Journal of Neurooncology* 67:83-93.

191. Freeman AI, Zakay-Rones Z, Gomori JM, Linetsky E, Rasooly L, Greenbaum E, Rozenman-Yair S, Panet A, Libson E, Irving CS, Galun E, Siegal T. 2006. **Phase I/II**

Trial of Intravenous NDV-HUJ Oncolytic Virus in Recurrent Glioblastoma Multiforme. *Molecular Therapy* 13:221-228.

192. Csatary LK, Eckhardt S, Bukosza I, Czegledi F, Fenyvesi C, Gergely P, Bodey B, Csatary CM. 1993. **Attenuated veterinary virus vaccine for the treatment of cancer.** *Cancer Detection and Prevention* 17:619-27.

193. Laurie SA, Bell JC, Atkins HL, Roach J, Bamat MK, O'Neil JD, Roberts MS, Groene WS, Lorence RM. 2006. **A Phase 1 Clinical Study of Intravenous Administration of PV701, an Oncolytic Virus, Using Two-Step Desensitization.** *Clinical Cancer Research* 12:2555-2562.

194. Robert ML, Roberts MS, James DON, William SG, Jeffrey AM, Stephen NM, Michael KB. 2007. **Phase 1 Clinical Experience Using Intravenous Administration of PV701, an Oncolytic Newcastle Disease Virus.** *Current Cancer Drug Targets* 7:157-167.

195. Meng S, Zhou Z, Chen F, Kong X, Liu H, Jiang K, Liu W, Hu M, Zhang X, Ding C, Wu Y. 2012. **Newcastle disease virus induces apoptosis in cisplatin-resistant human lung adenocarcinoma A549 cells *in vitro* and *in vivo.*** *Cancer Letters* 317:56-64.

196. Jiang K, Li Y, Zhu Q, Xu J, Wang Y, Deng W, Liu Q, Zhang G, Meng S. 2014. **Pharmacological modulation of autophagy enhances Newcastle disease virus-mediated oncolysis in drug-resistant lung cancer cells.** *BMC Cancer* 14:551.

197. Bai Y, Chen Y, Hong X, Liu X, Su X, Li S, Dong X, Zhao G, Li Y. 2018. **Newcastle disease virus enhances the growth-inhibiting and proapoptotic effects of temozolomide on glioblastoma cells *in vitro* and *in vivo*.** *Scientific Reports* 8:11470.

198. Anonymous. 2013. **The Oncolytic Activity of Newcastle Disease Virus in Clear Cell Renal Carcinoma Cells in Normoxic and Hypoxic Conditions: The Interplay Between von Hippel-Lindau and Interferon-β Signaling.** *Journal of Interferon & Cytokine Research* 33:346-354.

199. Oseledchyk A, Ricca JM, Gigoux M, Ko B, Redelman-Sidi G, Walther T, Liu C, Iyer G, Merghoub T, Wolchok JD, Zamarin D. 2018. **Lysis-independent potentiation of immune checkpoint blockade by oncolytic virus.** *Oncotarget* 9:28702-28716.

200. Miller LT, Yates VJ. 1971. **Reactions of human sera to avian adenoviruses and Newcastle disease virus.** *Avian Diseases* 15:781-8.

201. Charan S, Mahajan VM, Agarwal LP. 1981. **Newcastle disease virus antibodies in human sera.** *The Indian Journal of Medical Research* 73:303-7.

202. Schirrmacher V. 2016. **Fifty Years of Clinical Application of Newcastle Disease Virus: Time to Celebrate!** *Biomedicines* 4:16.

203. Cattaneo R, Miest T, Shashkova EV, Barry MA. 2008. **Reprogrammed viruses as cancer therapeutics: targeted, armed and shielded.** *Nature Reviews Microbiology* 6:529-540.

204. Springfeld C, von Messling V, Frenzke M, Ungerechts G, Buchholz CJ, Cattaneo R. 2006. **Oncolytic efficacy and enhanced safety of measles virus activated by tumor-secreted matrix metalloproteinases.** *Cancer Research* 66:7694-700.

205. Peng KW, Vile R, Cosset FL, Russell S. 1999. **Selective transduction of protease-rich tumors by matrix-metalloproteinase-targeted retroviral vectors.** *Gene Therapy* 6:1552-7.

206. Dorer DE, Nettelbeck DM. 2009. **Targeting cancer by transcriptional control in cancer gene therapy and viral oncolysis.** *Advanced Drug Delivery Reviews* 61:554-71.

207. Khabar KS. 2010. **Post-transcriptional control during chronic inflammation and cancer: a focus on AU-rich elements.** *Cellular and Molecular Life Sciences* 67:2937-55.

208. Aurelian L. 2013. **Oncolytic virotherapy: the questions and the promise.** *Oncolytic Virotherapy* 2:19-29.

209. Mader EK, Maeyama Y, Lin Y, Butler GW, Russell HM, Galanis E, Russell SJ, Dietz AB, Peng KW. 2009. **Mesenchymal stem cell carriers protect oncolytic measles viruses from antibody neutralization in an orthotopic ovarian cancer therapy model.** *Clinical Cancer Research* 15:7246-55.

210. Nakashima H, Kaur B, Chiocca EA. 2010. **Directing systemic oncolytic viral delivery to tumors via carrier cells.** *Cytokine Growth Factor Reviews* 21:119-26.

211. Schirrmacher V, Bihari A-S, Stücker W, Sprenger T. 2014. **Long-term remission of prostate cancer with extensive bone metastases upon immuno- and virotherapy: A case report.** *Oncology Letters* 8:2403-2406.

212. Peggs KS, Quezada SA, Allison JP. 2009. **Cancer immunotherapy: co-stimulatory agonists and co-inhibitory antagonists.** *Clinical & Experimental Immunology* 157:9-19.

213. Hodi FS, O'Day SJ, McDermott DF, Weber RW, Sosman JA, Haanen JB, Gonzalez R, Robert C, Schadendorf D, Hassel JC, Akerley W, van den Eertwegh AJ, Lutzky J, Lorigan P, Vaubel JM, Linette GP, Hogg D, Ottensmeier CH, Lebbe C, Peschel C, Quirt I, Clark JI, Wolchok JD, Weber JS, Tian J, Yellin MJ, Nichol GM, Hoos A, Urba WJ. 2010. **Improved survival with ipilimumab in patients with metastatic melanoma.** *New England Journal of Medicine* 363:711-23.

214. Delyon J, Mateus C, Lefeuvre D, Lanoy E, Zitvogel L, Chaput N, Roy S, Eggermont AM, Routier E, Robert C. 2013. **Experience in daily practice with ipilimumab for the treatment of patients with metastatic melanoma: an early increase in lymphocyte and eosinophil counts is associated with improved survival.** *Annals of Oncology* 24:1697-703.

215. Kantoff PW, Higano CS, Shore ND, Berger ER, Small EJ, Penson DF, Redfern CH, Ferrari AC, Dreicer R, Sims RB, Xu Y, Frohlich MW, Schellhammer PF, Investigators IS. 2010. **Sipuleucel-T immunotherapy for castration-resistant prostate cancer.** *New England Journal of Medicine* 363:411-22.

216. Vijayakumar G, McCroskery S, Palese P. 2019. **Engineering Newcastle disease virus as oncolytic vector for intratumoral delivery of immune checkpoint inhibitors and immunocytokines.** *Journal of Virology* doi:10.1128/jvi.01677-19:JVI.01677-19.

217. Cox J, Mann M. 2008. **MaxQuant enables high peptide identification rates, individualized p.p.b.-range mass accuracies and proteome-wide protein quantification.** *Nature Biotechnology* 26:1367+.

218. https://github.com/FelixKrueger/TrimGalore.

219. Martin M. 2011. **Cutadapt removes adapter sequences from high-throughput sequencing reads.** EMBnetjournal; Vol 17, No 1: Next Generation Sequencing Data Analysis doi:10.14806/ej.17.1.200.

220. Marco-Sola S, Sammeth M, Guigó R, Ribeca P. 2012. **The GEM mapper: fast, accurate and versatile alignment by filtration.** *Nature Methods* 9:1185-1188.

221. Love MI, Huber W, Anders S. 2014. **Moderated estimation of fold change and dispersion for RNA-seq data with DESeq2.** *Genome Biology* 15:550.

222. Zhu A, Ibrahim JG, Love MI. 2019. **Heavy-tailed prior distributions for sequence count data: removing the noise and preserving large differences.** *Bioinformatics* 35:2084-2092.

223. R Core Team (2017). **R: A language and environment for statistical computing.** R Foundation for Statistical Computing V, Austria. .

224. Thomas PD, Kejariwal A, Guo N, Mi H, Campbell MJ, Muruganujan A, Lazareva-Ulitsky B. 2006. **Applications for protein sequence-function evolution data: mRNA/protein expression analysis and coding SNP scoring tools.** *Nucleic acids Research* 34:W645-W650.

225. Krämer A, Green J, Pollard J, Jr., Tugendreich S. 2014. **Causal analysis approaches in Ingenuity Pathway Analysis.** *Bioinformatics (Oxford, England)* 30:523-530.

226. Fiola C, Peeters B, Fournier P, Arnold A, Bucur M, Schirrmacher V. 2006. **Tumor selective replication of Newcastle disease virus: association with defects of tumor cells in antiviral defence.** *International Journal of Cancer* 119:328-38.

227. Amon R, Reuven EM, Leviatan Ben-Arye S, Padler-Karavani V. 2014. G**lycans in immune recognition and response.** *Carbohydrate Research* 389:115-22.

228. Pearce OM, Laubli H. 2016. **Sialic acids in cancer biology and immunity.** *Glycobiology* 26:111-28.

229. Iorio RM, Field GM, Sauvron JM, Mirza AM, Deng R, Mahon PJ, Langedijk JP. 2001. **Structural and Functional Relationship between the Receptor Recognition and Neuraminidase Activities of the Newcastle Disease Virus Hemagglutinin-Neuraminidase Protein: Receptor Recognition Is Dependent on Neuraminidase Activity.** *Journal of Virology* 75:1918-1927.

230. Zargar S, Tomar V, Shyamsundar V, Vijayalakshmi R, Somasundaram K, Karunagaran D. 2019. **A Feedback Loop between MicroRNA 155 (miR-155), Programmed Cell Death 4, and Activation Protein 1 Modulates the Expression of miR-155 and Tumorigenesis in Tongue Cancer.** *Molecular and Cellular Biology* 39:e00410-18.

231. Tili E, Croce CM, Michaille J-J. 2009. **miR-155: On the Crosstalk Between Inflammation and Cancer.** *International Reviews of Immunology* 28:264-284.

232. Liu J, Chen Z, Xiang J, Gu X. 2018. **MicroRNA-155 acts as a tumor suppressor in colorectal cancer by targeting CTHRC1 *in vitro.*** *Oncology Letters* 15:5561-5568.

233. Heuschele WP, Easterday BC. 1970. **Local Immunity and Persistence of Virus in the Tracheas of Chickens following Infection with Newcastle Disease Virus. I. Organ Culture Studies.** *The Journal of Infectious Diseases* 121:486-496.

234. Rodriguez JE. 1964. **Studies on Persistent Infections of Tissue Cultures: V. The Initial Stages of Infection of L(Mcn) Cells by Newcastle Disease Virus.** *Journal of Experimental Medicine* 119:895-922.

235. Liu H, Servan de Almeida R, Gil P, Albina E. 2018. **Cleavage site of Newcastle disease virus determines viral fitness in persistent infection cells.** *Veterinary Microbiology* 216:123-131.

236. Lawton P, Karimi Z, Mancinelli L, Seto JT. 1986. **Persistent infections with Sendai virus and Newcastle disease viruses.** *Archives of Virology* 89:225-33.

237. Chia S-L, Yusoff K, Shafee N. 2014. **Viral persistence in colorectal cancer cells infected by Newcastle disease virus.** *Virology Journal* 11:91.

238. Rangaswamy US, Wang W, Cheng X, McTamney P, Carroll D, Jin H. 2017. **Newcastle Disease Virus Establishes Persistent Infection in Tumor Cells *in vitro*:**

Contribution of the Cleavage Site of Fusion Protein and Second Sialic Acid Binding Site of Hemagglutinin-Neuraminidase. *Journal of Virology* 91.

239. Morrison TG, McGinnes LW. 1989. **Avian cells expressing the newcastle disease virus hemagglutinin-neuraminidase protein are resistant to newcastle disease virus infection.** *Virology* 171:10-17.

240. Melanson VR, Iorio RM. 2004. **Amino Acid Substitutions in the F-Specific Domain in the Stalk of the Newcastle Disease Virus HN Protein Modulate Fusion and Interfere with Its Interaction with the F Protein.** *Journal of Virology* 78:13053-13061.

241. Iorio RM, Melanson VR, Mahon PJ. 2009. **Glycoprotein interactions in paramyxovirus fusion.** *Future Virology* 4:335-351.

242. Yan Y, Liang B, Zhang J, Liu Y, Bu X. 2015. **Apoptotic induction of lung adenocarcinoma A549 cells infected by recombinant RVG Newcastle disease virus (rL-RVG) *in vitro.*** *Molecular Medicine Reports* 11:317-26.

243. Genoyer E, López CB. 2019. **Defective Viral Genomes Alter How Sendai Virus Interacts with Cellular Trafficking Machinery, Leading to Heterogeneity in the Production of Viral Particles among Infected Cells.** *Journal of Virology* 93:e01579-18.

244. Mura M, Combredet C, Najburg V, Sanchez David RY, Tangy F, Komarova AV. 2017. **Nonencapsidated 5' Copy-Back Defective Interfering Genomes Produced by Recombinant Measles Viruses Are Recognized by RIG-I and LGP2 but Not MDA5.** *Journal of Virology* 91.

245. Ten RM, Blank V, Le Bail O, Kourilsky P, Israel A. 1993. T**wo factors, IRF1 and KBF1/NF-kappa B, cooperate during induction of MHC class I gene expression by interferon alpha beta or Newcastle disease virus.** *Comptes Rendus de l'Académie des Sciences - Series III* 316:496-501.

246. Stark R, Grzelak M, Hadfield J. 2019. **RNA sequencing: the teenage years.** *Nature Reviews Genetics* 20:631-656.

247. Mutz K-O, Heilkenbrinker A, Lönne M, Walter J-G, Stahl F. 2013. **Transcriptome analysis using next-generation sequencing.** *Current Opinion in Biotechnology* 24:22-30.

248. Liu W, Qiu X, Song C, Sun Y, Meng C, Liao Y, Tan L, Ding Z, Liu X, Ding C. 2018. **Deep Sequencing-Based Transcriptome Profiling Reveals Avian Interferon-Stimulated Genes and Provides Comprehensive Insight into Newcastle Disease Virus-Induced Host Responses.** *Viruses* 10:162.

249. Drummond CG, Nickerson CA, Coyne CB. 2016. **A Three-Dimensional Cell Culture Model To Study Enterovirus Infection of Polarized Intestinal Epithelial Cells.** *mSphere 1* (1):e00030-15.

250. Munir S, Sharma JM, Kapur V. 2005. **Transcriptional response of avian cells to infection with Newcastle disease virus.** *Virus Research* 107:103-108.

251. Balogh A, Bator J, Marko L, Nemeth M, Pap M, Setalo G, Jr., Muller DN, Csatary LK, Szeberenyi J. 2014. **Gene expression profiling in PC12 cells infected with an oncolytic Newcastle disease virus strain.** *Virus Research* 185:10-22.

252. Karsunke J, Heiden S, Murr M, Karger A, Franzke K, Mettenleiter TC, Romer-Oberdorfer A. 2019. **W protein expression by Newcastle disease virus.** *Virus Research* 263:207-216.

253. Young DF, Wignall-Fleming EB, Busse DC, Pickin MJ, Hankinson J, Randall EM, Tavendale A, Davison AJ, Lamont D, Tregoning JS, Goodbourn S, Randall RE. 2019. **The switch between acute and persistent paramyxovirus infection caused by**

single amino acid substitutions in the RNA polymerase P subunit. PLoS Pathogens 15:e1007561.

254. Qiu X, Zhan Y, Meng C, Wang J, Dong L, Sun Y, Tan L, Song C, Yu S, Ding C. 2016. **Identification and functional analysis of phosphorylation in Newcastle disease virus phosphoprotein.** *Archives of Virology* 161:2103-16.

255. Manzoni TB, Lopez CB. 2018. **Defective (interfering) viral genomes re-explored: impact on antiviral immunity and virus persistence.** *Future Virology* 13:493-503.

256. Timm C, Akpinar F, Yin J. 2014. **Quantitative characterization of defective virus emergence by deep sequencing.** *Journal of Virology* 88:2623-32.

257. Bosma TJ, Karagiannis K, Santana-Quintero L, Ilyushina N, Zagorodnyaya T, Petrovskaya S, Laassri M, Donnelly RP, Rubin S, Simonyan V, Sauder CJ. 2019. **Identification and quantification of defective virus genomes in high throughput sequencing data using DVG-profiler, a novel post-sequence alignment processing algorithm.** PLOS One 14:e0216944.

258. Russell AB, Elshina E, Kowalsky JR, Te Velthuis AJW, Bloom JD. 2019. **Single-Cell Virus Sequencing of Influenza Infections That Trigger Innate Immunity.** *Journal of Virology* 93.

259. Kroemer G, Mariño G, Levine B. 2010. **Autophagy and the integrated stress response.** *Molecular Cell* 40:280-293.

260. Puissant A, Fenouille N, Auberger P. 2012. **When autophagy meets cancer through p62/SQSTM1.** *American Journal of Cancer Research* 2:397-413.

261. White E, Mehnert JM, Chan CS. 2015. **Autophagy, Metabolism, and Cancer.** *Clinical Cancer Research* 21:5037-46.

262. Fimia GM, Kroemer G, Piacentini M. 2013. **Molecular mechanisms of selective autophagy.** *Cell Death & Differentiation* 20:1-2.

263. Abdrakhmanov A, Gogvadze V, Zhivotovsky B. 2020. **To Eat or to Die: Deciphering Selective Forms of Autophagy.** *Trends in Biochemical Sciences* 45:347-364.

264. Johansen T, Lamark T. 2011. **Selective autophagy mediated by autophagic adapter proteins.** *Autophagy* 7:279-96.

265. Cheng JH, Sun YJ, Zhang FQ, Zhang XR, Qiu XS, Yu LP, Wu YT, Ding C. 2016. **Newcastle disease virus NP and P proteins induce autophagy via the endoplasmic reticulum stress-related unfolded protein response.** *Scientific Reports* 6:24721.

266. Kang Y, Yuan R, Xiang B, Zhao X, Gao P, Dai X, Liao M, Ren T. 2017. **Newcastle disease virus-induced autophagy mediates antiapoptotic signaling responses *in vitro* and *in vivo.*** *Oncotarget* 8.

267. Duran A, Amanchy R, Linares JF, Joshi J, Abu-Baker S, Porollo A, Hansen M, Moscat J, Diaz-Meco MT. 2011. **p62 is a key regulator of nutrient sensing in the mTORC1 pathway.** *Molecular Cell* 44:134-46.

268. Moscat J, Diaz-Meco MT. 2009. **p62 at the crossroads of autophagy, apoptosis, and cancer.** *Cell* 137:1001-4.

269. Mathew R, Karp CM, Beaudoin B, Vuong N, Chen G, Chen HY, Bray K, Reddy A, Bhanot G, Gelinas C, Dipaola RS, Karantza-Wadsworth V, White E. 2009. **Autophagy suppresses tumorigenesis through elimination of p62.** *Cell* 137:1062-75.

270. Shinoda H, Shannon M, Nagai T. 2018. **Fluorescent Proteins for Investigating Biological Events in Acidic Environments.** *International Journal of Molecular Sciences* 19:1548.

271. Hubbard V, Valdor R, Macian F, Cuervo A. 2012. **Selective autophagy in the maintenance of cellular homeostasis in aging organisms.** *Biogerontology* 13:21-35.

272. Sanz L, Diaz-Meco MT, Nakano H, Moscat J. 2000. **The atypical PKC-interacting protein p62 channels NF-kappaB activation by the IL-1-TRAF6 pathway.** *EMBO Journal* 19:1576-86.

273. Moscat J, Diaz-Meco MT, Albert A, Campuzano S. 2006. **Cell signaling and function organized by PB1 domain interactions.** *Molecular Cell* 23:631-40.

274. Jin Z, Li Y, Pitti R, Lawrence D, Pham VC, Lill JR, Ashkenazi A. 2009. **Cullin3-based polyubiquitination and p62-dependent aggregation of caspase-8 mediate extrinsic apoptosis signaling.** *Cell* 137:721-35.

275. Umemura A, He F, Taniguchi K, Nakagawa H, Yamachika S, Font-Burgada J, Zhong Z, Subramaniam S, Raghunandan S, Duran A, Linares JF, Reina-Campos M, Umemura S, Valasek MA, Seki E, Yamaguchi K, Koike K, Itoh Y, Diaz-Meco MT, Moscat J, Karin M. 2016. p62, **Upregulated during Preneoplasia, Induces Hepatocellular Carcinogenesis by Maintaining Survival of Stressed HCC-Initiating Cells.** *Cancer Cell* 29:935-948.

276. Nihira K, Miki Y, Ono K, Suzuki T, Sasano H. 2014. **An inhibition of p62/SQSTM1 caused autophagic cell death of several human carcinoma cells.** *Cancer Science* 105:568-75.

277. Jiang K, Li Y, Zhu Q, Xu J, Wang Y, Deng W, Liu Q, Zhang G, Meng S. 2014. **Pharmacological modulation of autophagy enhances Newcastle disease virus-mediated oncolysis in drug-resistant lung cancer cells.** *BMC Cancer* 14:551.

278. Sun Y, Yu S, Ding N, Meng C, Meng S, Zhang S, Zhan Y, Qiu X, Tan L, Chen H, Song C, Ding C. 2014. **Autophagy Benefits the Replication of Newcastle Disease Virus in Chicken Cells and Tissues.** *Journal of Virology* 88:525-537.

279. Vignuzzi M, Stone JK, Arnold JJ, Cameron CE, Andino R. 2006. **Quasispecies diversity determines pathogenesis through cooperative interactions in a viral population.** *Nature* 439:344-348.

280. Lauring AS, Andino R. 2010. **Quasispecies theory and the behavior of RNA viruses.** *PLOS Pathogen* 6:e1001005.

281. Domingo E, Perales C. 2019. **Viral quasispecies.** *PLOS Genetics* 15.

282. Jenkins GM, Rambaut A, Pybus OG, Holmes EC. 2002. **Rates of molecular evolution in RNA viruses: a quantitative phylogenetic analysis.** *Journal of Molecular Evolution* 54:156-65.

283. Miller PJ, Kim LM, Ip HS, Afonso CL. 2009. **Evolutionary dynamics of Newcastle disease virus.** *Virology* 391:64-72.

284. Kattenbelt JA, Stevens MP, Selleck PW, Gould AR. 2010. **Analysis of Newcastle disease virus quasispecies and factors affecting the emergence of virulent virus.** *Archives of Virology* 155:1607-1615.

285. Meng C, Qiu X, Yu S, Li C, Sun Y, Chen Z, Liu K, Zhang X, Tan L, Song C, Liu G, Ding C. 2015. **Evolution of Newcastle Disease Virus Quasispecies Diversity and Enhanced Virulence after Passage through Chicken Air Sacs.** *Journal of Virology* 90:2052-2063.

286. Braun T, Bordería AV, Barbezange C, Vignuzzi M, Louzoun Y. 2018. **Long-term context-dependent genetic adaptation of the viral genetic cloud.** *Bioinformatics* 35:1907-1915.

287. Ferretti L, Tennakoon C, Silesian A, Ribeca GFA. 2019. **SiNPle: Fast and Sensitive Variant Calling for Deep Sequencing Data.** *Genes (Basel)* 10.

288. Paradis E, Schliep K. 2019. **ape 5.0: an environment for modern phylogenetics and evolutionary analyses in R.** *Bioinformatics* 35:526-528.

289. Zhao L, Illingworth CJR. 2019. **Measurements of intrahost viral diversity require an unbiased diversity metric.** *Virus Evolution* 5:vey041.

290. Hartl DL, Clark AG, Clark AG. 1997. **Principles of population genetics**, vol 116. Sinauer associates Sunderland, MA.

291. Wills C. 2007. **Principles of Population Genetics**, 4th edition. Journal of Heredity 98:382-382.

292. Liu H, Servan de Almeida R, Gil P, Albina E. 2018. **Cleavage site of Newcastle disease virus determines viral fitness in persistent infection cells.** *Veterinary Microbiology* 216:123-131.

293. Ylösmäki E, Cerullo V. 2020. **Design and application of oncolytic viruses for cancer immunotherapy.** *Current Opinion in Biotechnology* 65:25-36.

294. Matveeva OV, Guo ZS, Senin VM, Senina AV, Shabalina SA, Chumakov PM. 2015. **Oncolysis by paramyxoviruses: preclinical and clinical studies.** *Molecular Therapy-Oncolytics* 2:15017.

295. Walter RJ, Attar BM, Rafiq A, Delimata M, Tejaswi S. 2012. **Two avirulent, lentogenic strains of Newcastle disease virus are cytotoxic for some human pancreatic tumor lines *in vitro.*** *Journal of the Pancreas* 13:502-13.

296. Rodriguez JE, Henle W. 1964. **Studies on persistent infections of tissue cultures. V. the initial stages of infection of l(mcn) cells by newcastle disease virus.** *The Journal of Experimental Medicine* 119:895-921.

297. Fox CR, Parks GD. 2018. **Parainfluenza Virus Infection Sensitizes Cancer Cells to DNA-Damaging Agents: Implications for Oncolytic Virus Therapy.** *Journal of Virology* 92(7): e01948-17.

298. Chang JC. 2016. **Cancer stem cells: Role in tumor growth, recurrence, metastasis, and treatment resistance.** *Medicine* 95:S20-S25.

299. Zhou Y, Xia L, Wang H, Oyang L, Su M, Liu Q, Lin J, Tan S, Tian Y, Liao Q, Cao D. 2017. **Cancer stem cells in progression of colorectal cancer.** *Oncotarget* 9:33403-33415.

300. Vázquez-Iglesias L, Barcia-Castro L, Rodríguez-Quiroga M, Páez de la Cadena M, Rodríguez-Berrocal J, Cordero OJ. 2019. **Surface expression marker profile in colon cancer cell lines and sphere-derived cells suggests complexity in CD26(+) cancer stem cells subsets.** *Biology Open* 8:bio041673.